DISS. ETH NO. 24407

Basin-wide assessment of the earthquake-triggered landslide- and tsunami hazard:

A conceptual approach and its application, tested in perialpine Lake Zurich (Switzerland)

A thesis submitted to attain the degree of

DOCTOR OF SCIENCES of ETH ZURICH

(Dr. sc. ETH Zurich)

presented by

Michael M. Strupler

MSc Physical Geography, University of Zurich
born on February 22, 1985
citizen of Frauenfeld (TG)

accepted on the recommendation of

Prof. Dr. Stefan Wiemer, Swiss Seismological Service at ETH Zurich, examiner
Prof. Dr. Michael Strasser, University of Innsbruck, co-examiner
Prof. Dr. Flavio S. Anselmetti, University of Bern, co-examiner
Prof. Dr. Marc De Batist, Ghent University, external co-examiner

2017

“*Science may be described as the art of systematic over-simplification — the art of discerning what we may with advantage omit.*”

Karl Popper

Table of Contents

Acknowledgements **I**

Abstract **III**

Zusammenfassung **V**

Abbreviations **VIII**

Chapter 1: **Introduction PhD Thesis** **1**

1.1 PhD Project 2

1.2 Current state of knowledge 2

1.3 Research motivation 3

1.4 Objectives of the thesis 5

1.5 Methodology 5

1.6 Regional setting of Lake Zurich 6

1.7 Outline of the PhD thesis 8

References 10

Chapter 2: Quantitative characterisation of subaqueous landslides in Lake Zurich (Switzerland) based on a high-resolution bathymetric dataset **13**

Abstract 14

2.1 Introduction 15

2.2 Study setting 16

2.3 Data and Methods 17

2.4 Results and Interpretation 18

2.5 Discussion 27

2.6 Conclusions 30

References 31

Chapter 3: Probabilistic stability evaluation and seismic triggering scenarios of submerged slopes in Lake Zurich (Switzerland) **33**

Abstract 34

3.1 Introduction 35

3.2 Physical setting and previous studies 36

3.3 Materials and methods 39

3.4 Results 42

3.5 Discussion 54

3.6 Conclusions 57

References 59

Chapter 4: A subaqueous hazard map for earthquake-triggered landslides in Lake Zurich, Switzerland 61

Abstract 62
4.1 Introduction 63
4.2 Setting of the study area and previous studies 64
4.3 Methods and Workflow 69
4.4 Results 73
4.5 Discussion 81
4.6 Conclusions 88
References 90

Chapter 5: Subaqueous landslide-triggered tsunami hazard for Lake Zurich, Switzerland 95

Abstract 96
5.1 Introduction 97
5.2 Setting of the study area and previous studies 98
5.3 Data and Methods 102
5.4 Results 103
5.5 Discussion 116
5.6 Conclusions 121
References 123

Chapter 6: Conclusions and Outlook 127

6.1 Overall conclusions 128
6.2 Specific conclusions 128
6.3 Outlook 130
References 133

Appendix A: Bathymetric dataset and sediment cores 135

A1 Bathymetric dataset 136
A2 Sediment coring locations and photos 137

Appendix B: Supplementary material chapter 2 161

B1 Uncertainty map of the bathymetric data 162

Appendix C: Supplementary material chapter 3 **163**

C1 Metadata of sediment cores and in-situ CPT 164
C2 Sedimentation model 166
C3 Sediment-mechanical stratigraphy 168
C4 Thicknesses of stratigraphic units converted from two-way-traveltime (TWT) 168
C5 Slope stability analysis 169
C6 Slope-stability assessment with SLIDE 172

Appendix D: Supplementary material chapter 4 **175**

D1 Sedimentation model 176
D2 Geotechnial data for core ZH15-K09 (Eastern lateral slopes) 179
D3 Depth of maximum PoF maps 180
D4 Mapped most probable slide areas and volumes 182
D5 Sensitivity test of the k*f coefficients 184
D6 Disaggregation plots for identifying predominant earthquake scenarios 185

Appendix E: Supplementary material chapter 5 **189**

E1 Back-analysed scenario Oberrieden ~2210 cal. yr BP landslide and tsunami 190
E2 Gauge plots 193

CURRICULUM VITAE **197**

Acknowledgements

First of all, I would like to thank my supervising committee: I would like to express my sincerest gratitude to Michi Strasser who guided me through this PhD journey yet giving me the space and freedom to develop my scientific and personal skills. Thank you for teaching me a lot and for your great physical and scientific efforts during fieldwork and during the writing process. I appreciated your always very detailed, motivating and on-schedule feedbacks either in person, via telephone or skype a lot.
I am very happy and grateful to have experienced such a broad spectrum of lake research, involving being a captain, planning and managing bathymetric, seismic and sediment-coring / CPT surveys, conducting lab work and interpreting the data. A summer school, national and international conferences, discussions with the supervising committee and specialists from other institutes helped a lot connecting the puzzle pieces of this PhD project.
Thank you Stefan Wiemer for taking over the formal dissertation lead after Michi got a full professorship in Innsbruck. The collaboration with the SED broadened my horizon. I want to thank Stefan a lot for extending my funding for an additional six months and for his scientific inputs concerning the landslide-hazard and tsunami manuscripts.
Flavio Anselmetti, thank you for your great help as a networker, during fieldwork, and as a co-author giving important reviews. I enjoyed being integrated in the Bernese group, including the participation on seminars and group retreats.
Apart from the supervising committee, I owe thanks to many other people:
Without the great support of Michi Hilbe, many problems of diverse nature would have remained unsolved in my thesis. Next to his technical help of enormous value, I really enjoyed on- and off-topic talks with Michi, who had a modest answer to almost any question. Michi always gave very exact and critical reviews on the manuscripts.
Katrina Kremer is gratefully acknowledged for her scientific and non-scientific support, and the many great discussions with or without coffee. Thanks for reading and commenting my texts and also for the very useful exchanges on family life ☺.
I could count on an awesome support from the whole Limnogeology community, thank you very much!
“Dank u wel” to Marc De Batist for agreeing on being member of the thesis committee.
“Merci beaucoup” à Nathalie Dubois for chairing my PhD Defense.
I am very grateful to have experienced the great technical support on fieldwork campaigns by Robert Hofmann, Reto Seifert, Stewart Bishop and Adi Gilli.
Also, all the co-authors of the manuscripts are kindly acknowledged: Michi Strasser, Flavio Anselmetti, Michi Hilbe, Achim Kopf, Timo Fleischmann, Katrina Kremer, Laurentiu Danciu and Stefan Wiemer.
The lake surveys and work on the acquired data were only possible due to the help of Michi Strasser, Flavio Anselmetti, Michi Hilbe, Anna Reusch, Stefano Fabbri, Toby Schwestermann, Achim Kopf, Timo Fleischmann, Christian Zöllner, Robert Hofmann, Reto Seifert, Stewart Bishop, Adi Gilli, Stefan Wiemer, Laurentiu Danciu, Andrea Wolter, Lukas Oesch, Utsav Mannu, Mohammed Usman, Rahel Liechti, Lina Tyroller, Markus Loher, Katrina Kremer, Nathalie Dubois, Yoann Charles, Stefanie Wirth, Jasper Moernaut, Beat Rick, Ralf Herzog, Andy Mäder, Christoph Schmied and the Lake Police crew.
Ursi Brupbacher is thanked a lot for the help with all the administrative stuff.
Thomas Löffler is thanked for the computer support.

All the members of the climate geology group are thanked for the great, fuelling coffee-breaks that included always lots of laughters.
Further, I would like to my former and actual office-mates for sharing a great time: Anna Reusch, Merle Gierga, Rui Bao, Stephan Wohlwend, Chia-Yu Chen, Yu Meng, Jia Juan, Lu Gang, and Jeremy Rugenstein.
Inigo Müller, Stephan Wohlwend, Katrina Kremer, Adam Hasenfratz, Lukas Oesch, Tessa van der Voort, Joep van Dijk, Franziska Lechleitner, Sascha Winterberg, Utsav Mannu, Reto Grischott, Nathan Looser is thanked for numerous lunch sessions in the Mensa, on the rooftop or in combination with swimming at the Letten. Werni from BQM is thanked for the awesome cappuchini.
A warm thanks goes also to all the former colleagues at Renard Centre of Marine Geology in Ghent. Special thanks go to my former office-mate Stan with whom I spent a lot of time in and out of the office.
Katrina Kremer, Anna Reusch, Samuel Weber, Marius Büchi and Dominik Behr are gratefully acknowledged for their constructive comments on the thesis introduction and conclusions. Adam Hasenfratz is acknowledged for finding typos in the last chapter.
I would also like to thank all my friends and my extended family for all your support.
Finally, I am very happy to travel through life together with Emilia and Cécilia. Thank you very much for all your support and inspiration!

Abstract

Geohazards can pose a severe threat to society and infrastructure. A quantitative understanding of geohazard magnitude, impact and recurrence rate is therefore crucial. In lacustrine or marine settings, subaqueous landslides that can be triggered by various factors including sediment overload, human activity, or earthquakes. As a direct consequence, subaqueous landslides can induce tsunamis. Due to its tectonic and topographic setting, Switzerland is prone to several geohazards. Numerous subaqueous landslides have occurred since deglaciation in Swiss lakes and many of them are assumed to be earthquake-triggered as they occur coevally on a basin-wide scale and because other potential triggers can be excluded. Previous studies have showed that such earthquake-triggered subaqueous landslides have induced tsunamis in various Swiss lakes. Although Switzerland's earthquake hazard can be considered moderate, strong earthquakes are expected to occur with a certain regularity. Hence, there is a need for assessing the earthquake-related subaqueous geohazards quantitatively. Slope-stability analyses build the basis for assessments of landslide hazards. So far, most of the subaqueous slope-stability assessments consist of a deterministic approach, which neglects the spatial variability of the geotechnical input data due to high efforts in costs and time. An efficient approach for assessing subaqueous slopes in a probabilistic manner, considering the spatial variabilty of the slope characteristics does not exist so far.

This PhD thesis aims at (i) conceptually advancing the assessment of the earthquake-triggered subaqueous landslide hazard and at (ii) quantifying and mapping the earthquake-triggered landslide and tsunami hazard on a basin-wide scale in Lake Zurich. The perialpine, glacially excavated Lake Zurich (Northern Switzerland) was selected for this study because a previous study assigned multiple basin-wide subaqueous landslide events along the slopes of the up to 136 m deep central basin to earthquakes as triggers. In addition, the shorelines of the lake are densely populated and could therefore be vulnerable to potential tsunamis. Despite such indications of past earthquakes and the potential vulnerability of the shorelines, no quantitative assessment of the earthquake-triggered subaqueous landslide and tsunami hazard exists for Lake Zurich.

The challenges are tackled with a multi-method approach by combining geophysical, sedimentological, geotechnical and modelling techniques at different scales. In a first step, a new high-resolution bathymetric dataset (1 m grid resolution) of Lake Zurich was acquired and therein documented mass-movement related morphologies identified and analysed quantitatively. In a further step, the lateral slopes of the case study site *Oberrieden* were characterised sedimentologically and mechanically by a combination of seven long Kullenberg-type sediment cores, 21 short gravity cores and in situ free-fall cone penetration testing (CPT) in consideration of an existing 3.5 kHz pinger seismic reflection dataset. Slope-stability under static and earthquake loading was calculated with a limit equilibrium equation on an infinite slope by implementing the spatial variability of the mechanical slope characteristics. Earthquake accelerations (for mean return periods of 475, 2475 and 9975 years) were considered from an existing probabilistic seismic hazard analysis for a spatial assessment of the earthquake-triggered landslide hazard. Finally the calculated slide volumes were used to estimate tsunami wave heights and the inundation on the shores, based on an existing approach of combining open source codes to model landslide mobility and tsunami propagation.

In this PhD thesis, novel and further developed concepts are presented that facilitate the efficient assessment of the subaqueous slope stabilities and the related landslide hazard. Furthermore, we demonstrate one of the first subaqueous earthquake-triggered landslide hazard evaluation.

The newly acquired, high-resolution bathymetric dataset of Lake Zurich revealed large- and small-scale morphological features that are related to subaqueous landslides at the bottom of Lake Zurich. Integration with previous studies showed that the landslides visible in the bathymetric dataset

date back to ~5000 cal. yr BP. A quantitative surface roughness analysis of landslide-translation areas combined with ages from an existing, well-dated catalogue of subaqueous landslides allowed the assignment of roughness to relative ages. Our findings suggest that surface-roughness analyses of subaqueous landslides should become a routine step in subaqueous hazard analyses.

Furthermore, based on the high-resolution subbottom analyses, we present a novel concept of a flexibly adaptable sediment-mechanical stratigraphy. The here presented methodology allows a simple inclusion of the subaqueous slope-characteristics into deterministic and probabilistic slope-stability assessments. The concept was tested at the Oberrieden study site in Lake Zurich and allowed a classification of the post-glacial sediment drape of the lateral slopes into four mechanical units with distinct characteristics. Slope-stability calculations and groundtruthing with sediment cores both showed that Late Glacial plastic muds form a weak layer. This is coherent with reports from other perialpine Lakes. Moreover, previously presumed earthquake-triggers hypothesized for two late Holocene landslide events occurring at ~2210 cal. yr BP and ~640 cal. yr BP were supported from back-analysed slope stabilities. For the present-day situation, certain patches of the lateral slopes were considered as failure-prone, even under static loading conditions. Slope-transversal undulations that correlate with high failure probabilities may be a first expression of slopes expected to fail in the near future.

We demonstrate one of the first subaqueous earthquake-triggered landslide hazard evaluation (delta collapse are excluded) that includes earthquake accelerations derived from a probabilistic seismic hazard assessment. Tested in Lake Zurich, this concept allows constraining future events in space and time: For earthquakes with a mean return period of 475 years, multiple yet very small landslides with a total volume of ~3 Mio m^3 are expected to occur on the lateral slopes of the central basin. Such landslides, however, are not expected to cause considerable tsunami waves. Earthquakes with a mean return period of 9975 years however, are expected to trigger landslides on all yet unfailed lateral slopes and may cause free surface waves of ~2 m and flow depths of up to ~4.6 m at selected locations. Even for such a worst-case scenario, the cities of Zurich and Rapperswil, located at the northern and southern ends of the Lake are expected to experience very little damage. In general, the tsunami hazard of Lake Zurich can be regarded as relatively low considering the large mean return periods for seismic events expected to cause tsunamigenic landslides. The hazard maps from this study may be further used to create a mitigation plan for such subaqueous hazards and to derive a risk zonation.

In summary, the here presented concepts and results demonstrate that an approach combining multiple state-of-the-art methods from the fields of limnogeology and earthquake engineering is essential for better quantitative understanding of subaqueous geohazards and their spatiotemporal impact. Finally, our approaches may also be transferred to the marine realm.

Zusammenfassung

Geologische Ereignisse können eine ernstzunehmende Gefährdung für Gesellschaft und Infrastruktur darstellen. Ein quantitatives Verständnis des Ausmasses, der Auswirkungen und der Wiederkehrperiode einer geologischen Gefährdung ist daher von grundlegender Wichtigkeit. Unterwasser-Hangrutschungen im Meer oder in Seen können durch verschiedene Faktoren ausgelöst werden, wie z.B. Sediment-Überlast, menschliche Aktivitäten oder Erdbeben. Als direkte Auswirkungen solcher Unterwasser-Hangrutschungen können Tsunamis entstehen. Aufgrund ihrer tektonischen und topographischen Lage, ist die Schweiz ein Land, indem Naturgefahren regelmässig auftreten. Mehrere Rutschungen ereigneten sich an den Unterwasserhängen von Schweizer Seen seit dem Gletscherrückzug nach der letzten Eiszeit. Bei einigen dieser Rutschungen wird angenommen, dass sie durch Erdbeben ausgelöst wurden, weil sie zeitgleich in Seebecken auftreten, und andere mögliche Auslöser ausgeschlossen werden können. Frühere Arbeiten haben gezeigt, dass in der Vergangenheit durch Erdbeben verursachte Hangrutschungen in verschiedenen Schweizer Alpenrandseen Tsunamis ausgelöst hatten. Auch wenn die Schweiz generell eine moderate Erdbebengefährdung aufweist, sind stärkere Erdbeben mit einer gewissen Regelmässigkeit zu erwarten. Daher ist es notwendig, die Gefährdung durch erdbebenverursachte Unterwasser-Hangrutschungen und potentiell darauffolgende Tsunamis in Schweizer Seen quantitativ abzuschätzen. Hangstabilitätsanalysen bilden die Grundlage für eine Beurteilung der Gefährdung durch Hangrutschungen. Die meisten Analysen von Unterwasser-Hangrutschungen basieren auf deterministischen Konzepten und vernachlässigen aufgrund von Zeit- und Kostengründen den Einfluss der räumlichen Variabilität der Einflussparameter. Zurzeit fehlt ein Ansatz für die effiziente, flächenhafte Beurteilung von Unterwasser-Hangstabilitäten, welcher die räumliche Variabilität der Einflussparameter berücksichtigt.

Die hier vorgestellte Doktorarbeit verfolgte das Ziel, (i) ein effizientes Konzept zur Beurteilung der Gefährdung durch erdbebenausgelöste Unterwasserrutschungen zu erstellen. Mit diesem Konzept soll (ii) im perialpinen Zürichsee (nördliche Schweiz) eine probabilistische Unterwasserrutschungs-Gefahrenkarte erstellt und eine Abschätzung von allfälligen, durch Rutschungen verursachten Tsunamis durchgeführt werden. Für dieses Projekt wurde der Zürichsee ausgewählt, weil eine frühere Studie aus mehreren beckenweiten Unterwasserrutschungen im bis zu 136 m tiefen mittleren Seebecken Rückschlüsse auf starke prähistorische Erdbeben gemacht hatte. Ausserdem ist das Zürichseeufer heute stark bebaut und könnte daher durch rutschungsverursachte Tsunamis gefährdet sein. Trotz Anzeichen von starken vergangenen Erdbeben und der potentiellen Verletzlichkeit des Seeufers existiert bis heute noch keine quantitative Beurteilung der erdbebenausgelösten Gefährdung durch Unterwasser-Rutschungen und Tsunamis für den Zürichsee.

Um die Ziele dieses Projektes zu erreichen werden verschiedene Methoden aus der Geophysik, der Sedimentologie, der Geotechnik und der Modellierung kombiniert. In einem ersten Schritt wurde ein neues, hochauflösendes Tiefenmodell des Zürichsees aufgenommen und darin abgebildete Spuren von Unterwasserrutschungen identifiziert und quantitativ analysiert. In einem weiteren Schritt wurde der Untergrund der lateralen Unterwasser-Hänge im Gebiet Oberrieden mit Laboranalysen an sieben Kullenberg-typ Langkernen, 21 Kurzkernen und mit in situ Cone Penetration Tests (CPT) unter Einbezug eines existierenden 3.5 kHz pinger-reflexionsseismischen Datensatzes sedimentologisch und mechanisch charakterisiert. Statische und erdbebenabhängige Hangstabilitäten wurden mit Kräftegleichgewichtsberechnungen unter Annahme eines unendlich langen Hanges durchgeführt, wobei die räumliche Variabilität der mechanischen Charakteristiken, die aus Sedimentkernen und CPT ermittelt wurden, berücksichtigt wurde. Für die Erstellung einer Gefahrenanalyse durch Erdbeben verursachter Unterwasser-Hangrutschungen wurden Erdbebenbeschleunigungen (für

mittlere Wiederkehrperioden von 475, 2475 und 9975 Jahren) aus einer existierenden probabilistischen seismischen Gefährdungsanalyse in die Berechnung der Rutschungswahrscheinlichkeit der Hänge einbezogen. Zuletzt wurden aus den errechneten Rutschungsvolumina Wellenhöhen und überschwemmte Gebiete abgeschätzt.

In dieser Doktorarbeit werden neue und weiterentwickelte Konzepte präsentiert, welche eine effiziente Beurteilung der Stabilität von Unterwasserhängen und damit verbundenen Gefahren durch Hangrutschungen ermöglichen. Im Weiteren wird eine der ersten Gefährdungskarte für durch Erdbeben ausgelöste Unterwasserhangrutschungen erstellt.

Das neue Tiefenmodell des Seebodens zeigt dank seiner hohen Auflösung (1 m) bisher unbekannte Unterwasser-Landschaftsformen, welche z.T. Unterwasserrutschungen mit Altern von bis zu ~5000 cal. yr BP zugeordnet werden können. Durch den Vergleich einer quantitativen Oberflächenrauhigkeitsanalyse der Rutschflächen mit den Rutschungsaltern eines existierenden Rutschungskataloges konnten im neuen Tiefenmodell identifizierte Rutschungen relativ zueinander datiert werden. Aufgrund der hier gewonnenen Erkenntnisse werden Oberflächenanalysen von Unterwasserrutschungen als ein Standardvorgehen im Prozess von Gefährdungsanalysen im subaquatischen Bereich empfohlen.

Zudem wird in dieser Arbeit ein neuartiges Konzept für eine flexibel anpassbare sediment-mechanischen Stratigraphie vorgestellt, die auf den hochauflösenden Untergrunduntersuchungen basiert. Geotechnische Eigenschaften von Unterwasserhängen können mit dieser Methode einfach in deterministische und probabilistische Hangstabilitätsanalysen einbezogen werden. Die lateralen Hänge des Zürichsees konnten in vier mechanische Einheiten mit klar abgrenzbaren Charakteristiken eingeteilt werden. Die Ergebnisse aus den Hangstabilitätsanalysen und Sedimentkernanalysen zeigen eine Schwachschicht, die aus spätglazialen Tonen besteht. Diese Erkenntnis deckt sich mit den Ergebnissen aus anderen perialpinen Seen. Unsere Hangstabilitätsanalysen unterstützen auch die Hypothese einer früheren Studie, wonach mehrere spätholozäne Hangrutschungen ~2210 und 640 cal. yr BP durch Erdbeben ausgelöst wurden. Einige relativ steile, mit mehreren Metern Sediment beladene Hangabschnitte sind heute rutschungsanfällig, auch ohne externe auslösende Faktoren. Undulationen, welche an Hangabschnitten mit einer berechneten hohen Rutschwahrscheinlichkeit auftreten, könnten Anzeichen einer Initialphase einer Rutschung darstellen.

Die in dieser Arbeit erstellte Gefährdungsbeurteilung von erdbebenverursachten Unterwasserrutschungen (Deltakollapse ausgeschlossen) ist eine der ersten ihrer Art, dadurch dass sie Erdbebenbeschleunigungen aus einer probabilistischen seismischen Gefährdungsanalyse in eine räumliche Hangstabilitätsmodellierung, einbaut. Angewandt am Zürichsee erlaubt die Gefährdungsanalyse eine räumliche und zeitliche Einordnung von zukünftigen Szenarien: Für Erdbeben mit einer mittleren Wiederkehrperiode von 475 Jahren wird erwartet, dass sie mehrere, hauptsächlich sehr kleine Hangrutschungen mit einem Gesamtvolumen von ~3 Mio m^3 auslösen. Für ein solches Szenario wird keine Tsunamiwelle erwartet. Ein Erdbeben mit einer mittleren Wiederkehrperioden von 9975 Jahren könnte allerdings Rutschungen an allen bisher stabil gebliebenen, mit Sediment-beladenen Hängen Rutschungen auslösen, welche Wellenamplituden von ~2 m auf der Seeoberfläche generieren und Fliesstiefen am Ufer von bis zu ~4.6 m bewirken könnten. Die grössten Städte im Untersuchungsgebiet, Zürich und Rapperswil wären allerdings auch bei einem solchen Extremszenario relativ ungefährdet. Insgesamt kann die Tsunamigefährdung für den Zürichsee als relativ gering eingestuft werden, in Anbetracht der langen Wiederkehrperioden von Erdbeben, welche tsunamigenerierende Hangrutschungen auslösen könnten. Die in dieser Studie erstellten Gefährdungskarten können als Grundlage für spezifischere Untersuchungen und für die Schadensverminderung und Risikokartierung verwendet werden.

Zusammengefasst wurden in dieser Arbeit Konzepte für die effiziente Analyse von Unterwasserhangrutschungen und deren Gefährdung vorgestellt. Dabei zeigte sich, dass ein Ansatz,

welcher aus verschiedenen, aktuellen Methoden aus den Bereichen der Limnogeologie und der Erdbeben-Ingenieurswissenschaften besteht, notwendig ist für ein besseres quantitatives Verständnis von geologischen Unterwassergefahren und deren raum-zeitlichen Auswirkungen. Die hier vorgestellten Konzepte können auch auf den marinen Bereich übertragen werden.

Abbreviations

AD	Anno Domini
BC	Before Christ
BP	Before Present
CPT	Cone penetration testing
DDM	Digital depth model
EP_{50}	Exceedance period in 50 years
FS	Factor of safety
GIS	Geographic information system / geographic information science
GPS	Global positioning system
LHN95	Landeshöhennetz 95
LiDAR	Light detection and ranging
LU	Lithological unit
LV03	Landesvermessung 03
LV95	Landesvermessung 95
MCS	Monte carlo simulation
MSCL	Multi sensor core logger
MTD	Mass transport deposit
M_w	Moment magnitude
PGA	Peak ground acceleration
PoF	Probability of failure (general)
PoF_{eo}	Probability of failure (conditional on earthquake occurrence)
PoF_g	Probability of failure (conditional on geotechnical properties)
PSA	Pseudostatic acceleration
RP	Return period
S1	1918 AD Oberrieden subaqueous landslide
S2	~2210 cal.yr BP Oberrieden subaqueous landslide
S3	~640 cal.yr BP Oberrieden subaqueous landslide
SMU	Sediment mechanical unit
SSA	Slope stability assessment
s_u	Undrained shear strength
TPI	Topographic position index
TWT	Two way travel time
Vs_{30}	average shear-wave velocity of the uppermost 30 m of the soil
wd	water depth
ρ_{bulk}	Sediment bulk density

Chapter 1

Introduction PhD Thesis

1.1 PhD Project

This PhD project was carried out from the beginning of 2014 until summer 2017 as part of the Swiss National Science Foundation (SNSF) founded Project (Project number: PP00P2-133481) entitled "Dynamic Nankai Trough (Japan) and Swiss Molasse Basin: Investigating NeoTectonics, Paleo-Earthquakes and associated Geohazards (DYNAMITE)". The overwhelming scientific objectives of this PhD thesis are (i) to conceptually advance the assessment of the earthquake-related subaqueous landslide hazard and (ii) to quantify and map the landslide and tsunami hazard on a basin-wide scale in Lake Zurich, Northern Switzerland.

1.2 Current state of knowledge

Geohazards, defined as the probability that damaging geological phenomena occur within a given period of time, are existing in many parts of the world (e.g. ISSMGE 2004; Hoffmann and Reicherter 2016). Geohazards include earthquakes, gravity-driven mass movements, tsunamis and flooding. In the subaqueous environment, landslides can occur as a consequence of slope instabilities and can be triggered by various factors such as earthquakes, wave loading, sediment overload, fluid flow or human activity (Locat and Lee 2002). Apart from a trigger mechanism, a favourable topography and the necessary amount of sediments need to be present for a subaqueous landslide to occur (Nadim et al. 1996). Subaqueous landslides can be classified according to various attributes, e.g. failure-mechanism or material involved and there is a broad use of nomenclature (Hampton et al. 1996; Mulder and Cochonat 1996; Masson et al. 2006). Many subaqueous landslides are translational slides, i.e. they have a distinct, planar glide plane and a low ratio between the depth to the length of the slide (Mulder and Cochonat 1996; De Blasio 2011). Throughout this thesis, the terms 'landslide' and 'subaqueous mass movement' are used for describing the gravity-driven processes resulting from slope failures.

As a consequence of subaqueous landslides, tsunamis may be produced (e.g. Jiang and Leblond 1992; Bardet et al. 2003; Masson et al. 2006). Typically, tsunamis are characterised by high travel speeds and long wavelengths. The elevation of landslide-generated waves on the free surface depends primarily upon the volume, initial acceleration, speed, water depth, and coherence of the mass movement (Watts 1998; Tappin et al. 2008; Bornhold and Thomson 2012). The understanding of these parameters is crucial because both subaqueous landslides and tsunamis can pose hazards to shore communities and infrastructure onshore and offshore (e.g. Prior et al. 1982; Tappin et al. 2001; Locat and Lee 2002; Schnellmann et al. 2002; Masson et al. 2006). Knowledge about subaqueous landslides and the related hazard greatly benefits from advances in surveying techniques. Multibeam echosounders allow the construction of high-resolution bathymetric datasets, which can be quantitatively analyzed (Lamarche et al. 2016; Lecours et al. 2016; Tappin 2017). Not only information about the existence or absence of a hazard, but also its quantitative assessment has gained more scientific attention in recent years (Lee and Jones 2014; Mueller et al. 2016). Internationally, a lot of research is conducted on subaqueous mass movements and their consequences, reflected by geoscience programmes such as SMMTC (Submarine Mass Movements

and Their Consequences) and S4slide (Significance of Modern and Ancient Submarine Slope LandSLIDEs).

A primary step in hazard assessment is the investigation of past occurrences. Sea- or lake bottom-sediments often act as excellent archives, because they are sensitive to geohazards and because the traces of such events are likely to be preserved due to continuous sedimentation. Compared to the marine environment, lakes have the advantage that they can be investigated on a basin-wide scale due to their relatively smaller size and depth (e.g. De Batist and Chapron 2008; Strasser et al. 2011). In the sedimentary record of many lakes, stacked landslide deposits can be found, indicating a repeated landslide activity through time. Long term records of past events are highly important for subaqueous hazard assessments (e.g. Schnellmann et al. 2006; Moernaut et al. 2007; Strasser and Anselmetti 2008; Waldmann et al. 2011; Kremer et al. 2015; Reusch et al. 2016; Praet et al. 2016). The coeval occurrence of mass movements over a large area is often interpreted as a proxy of past earthquakes (e.g. Jibson 1996). It is also assumed that strong earthquakes can trigger multiple basin-wide landslides at the lake bottoms.

1.3 Research motivation

1.3.1 Need for a slope-stability analysis that considers spatial variability of input parameters

The assessment of subaqueous slope stabilities is a crucial, yet complex step as it involves the consideration of many geomorphic, hydrological, and geotechnical factors. Due to this complexity, common approaches consider a broad combination of methods used in marine and lacustrine geology, such as geophysical surveying, sediment coring and analysis, geotechnical testing, and modelling. However, due to limitations in costs and time, many slope stability models are often treated as deterministic, i.e. they consider data from only a few sampling locations that are assumed to represent the characteristics of the entire slope. The spatial variability of slope geotechnical parameters thus often remains underexplored (Klaucke and Cochonat 1999; Leynaud and Sultan 2010). A high-resolution geomorphic and geotechnical characterisation of a study site and a stability assessment including the spatial variability of the slope characteristics is therefore needed to better understand the failure susceptibility of subaqueous slopes.

In most cases, the limit-equilibrium method is used for the assessment of slope stabilities. Slope stability of deterministic approaches is expressed with a factor of safety (FS), representing the ratio between resisting and downward driving forces. Slopes with an FS < 1 are considered unstable as the downward-driving stress exceeds the resisting strength of a landslide block (Kramer 1996; Abramson et al. 2002; Coduto et al. 2011; Johari and Javadi 2012). In a probabilistic approach, the stability of a slope is often expressed with a probability of failure (PoF) that ranges between 0 and 1 (Nadim 2006).

Strasser et al. (2011) proposed a concept for assessing the subaqueous slope-failure susceptibility with a deterministic limit-equilibrium approach on an infinite slope and tested it on perialpine Lake Lucerne (central Switzerland; Fig. 1.1). The infinite-slope model assumes slopes of infinite extent with a slope-parallel failure surface, and a failure-depth that is small compared to the length of the

slope (Craig 2004; Coduto et al. 2011). The concept of Strasser et al. (2011), which is based on geophysical and geotechnical methods, yielded valuable information on the past and present slope failure susceptibility. However, spatial variability was not considered, and the thickness of the sediment drape was assumed to be constant for the entire slope. A conceptual advancement of the approach presented by Strasser et al. (2011) towards a probabilistic, spatial assessment of slope-failure susceptibility is expected to contribute to a better understanding of slope failure processes in general, and for Swiss perialpine Lakes specifically.

1.3.2 Need for a conceptual approach to assess the subaqueous landslide- and tsunami hazard and its application in Lake Zurich

Switzerland is a 'geohazard country' (Raetzo et al. 2002; Wiemer et al. 2016) mostly because large parts of the country are located in an Alpine and perialpine setting. Earthquakes in this area are generally a result of the collision between the European and African plates. Although Switzerland has a moderate seismic hazard compared to the rest of Europe (Wiemer et al. 2016), several strong prehistoric, historic, and recent earthquakes have occurred in the Swiss Molasse basin and Northern Alpine realm (e.g. Strasser et al., 2013; Monecke et al., 2004; Fäh et al., 2011). 28 earthquake events with a Moment Magnitude (M_w) $\geq$ 5.5 have occurred in Switzerland during the past 800 years, and data from a recent probabilistic seismic hazard assessment suggest that a M_w 6 or larger event is expected in Switzerland and its immediate neighbourhood every 50 – 150 years (Wiemer et al. 2009; Wiemer et al. 2016).

Previous studies suggest that earthquakes have repeatedly caused multiple subaqueous landslides at the slopes of Swiss perialpine lakes (e.g. Schnellmann et al. 2002; Strasser et al. 2013; Kremer et al. 2014; Reusch et al. 2016). Some of these slides were even reported to have initiated tsunamis (Siegenthaler et al. 1987; Schnellmann et al. 2002; Kremer et al. 2015; Hilbe and Anselmetti 2015). In Lake Zurich, a catalogue of 149 subaqueous landslide deposits that are embedded in the lacustrine sediment succession was constructed by Strasser and Anselmetti (2008) and Strasser et al. (2013). These authors assigned coeval basin-wide events of generally translational landslides to assumedly strong earthquakes in the Lake Zurich Region, occurring at ~13760 cal. yr BP, ~11600 cal. yr BP and ~2210 cal. yr BP. Despite this indications of major impact of past earthquakes on the lake, no assessment of the earthquake-triggered subaqueous landslide and tsunami hazard exists for Lake Zurich so far. The city of Zurich, Switzerland's economic center with ~400'000 inhabitants (Statistik Stadt Zürich 2016), could, however, be particularly vulnerable. In addition, seismic reflection data (Strasser and Anselmetti 2008; Strasser et al. 2013) shows that parts of the lateral slopes in Lake Zurich are sediment-charged and thus potential sources for landslides. However, it is not known (i) which parts of the subaqueous slopes are failure-prone, (ii) what landslide-volumes are estimated for expected earthquake scenarios, and (iii) most importantly for the shore communities, whether potential future landslides are tsunamigenic. A quantitative assessment of the earthquake-triggered landslide and tsunami hazard is thus of great importance. Furthermore, despite the existence of well-developed seismic hazard assessments in Switzerland (e.g. Wiemer et al. 2016), there has been no integration of probabilistic seismic hazard outputs in subaqueous hazard analyses. A probabilistic, quantitative characterisation of the subaqueous landslide-hazard conditional on the earthquake occurrence may lead to an advanced characterisation and understanding of the subaqueous landslides.

Also, subaqueous landslide hazard assessments build the basis for landslide-triggered tsunami hazard assessments. Due to the spare observations of landslide generated tsunamis, physical and numerical modelling are important tools to improve our understanding on possible effects of such tsunamis (e.g. Assier-Rzadkiewicz et al. 1996; Fritz 2002; Masson et al. 2006; e.g. Bornhold and Thomson 2012; Hilbe and Anselmetti 2015). Hilbe and Anselmetti (2015) assessed landslide-triggered tsunamis in Lake Lucerne by combining two open source codes for the modelling of subaqueous landslide mobility and tsunami wave propagation and inundation. The application of the approach from Hilbe and Anselmetti (2015) combined with estimated slide volumes from a subaqueous landslide-hazard assessment may allow to quantitatively investigate the occurrence of past events, and to identify and assess locations potentially experiencing great tsunami impact.
Although it is not possible to prevent the occurrence of earthquake-related hazards, it is possible to mitigate the damage. A crucial step towards this end is the prediction and mapping of locations prone to such hazards (Kramer 1996; McAdoo 1999). Also, hazard assessments (e.g. investigating where a hazard will occur, how strong it will be, and how often it is expected to occur) are building the basis for risk assessments as risk is the product of hazard, exposure and vulnerability.

1.4 Objectives of the thesis

The aforementioned knowledge gaps lead to the objectives of this thesis. A first and fundamental step of this PhD project was the acquisition of a new high-resolution bathymetric dataset of Lake Zurich. Based on this and additional datasets the specific objectives of this thesis are:

- To map and characterise the morphologic features of the subaqueous landslides that are identifiable in the high-resolution bathymetric dataset
- To characterise the lateral slopes in Lake Zurich morphologically, sedimentologically and geotechnically
- To develop an efficient approach for probabilistically analysing the stability of the lateral, non-deltaic slopes under static and seismic loading, thereby accounting for the spatial variability of the sediment-mechanical properties
- To develop an approach for a basin-wide quantification of the earthquake-triggered subaquatic landslide hazard and to test it in Lake Zurich.
- To assess the basin-wide tsunami hazard for Lake Zurich quantitatively

1.5 Methodology

To address the aims of this thesis, a multi-method approach that combines geophysical, sedimentological, geotechnical, Geo Information Science (GIS), and modelling methods was used. Newly acquired data were combined with existing datasets. In spring 2014, a new high-resolution bathymetric dataset was acquired with a multibeam echosounder (Kongsberg EM2040, operating at 300 kHz). Within a GIS environment, traces of subaqueous landslides were identified, characterised

and quantified based on the newly acquired bathymetric dataset. During multiple lake surveys, seven Kullenberg-type cores (Kelts et al. 1986) and 21 short gravity sediment cores (14 cores/km^2) were taken at a case-study site in Oberrieden (~2 km^2; Figs. 1b and 2). In collaboration with MARUM (Bremen), free-fall in situ cone penetration testing (CPT), consisting of 39 tests (~20 CPT/km^2) was performed. Additionally, standard laboratory measurements were executed on the long and short sediment cores to characterise the lateral slopes sedimentologically and geotechnically. Core-to-seismic correlation was conducted with an existing 3.5 kHz pinger seismic reflection dataset from Strasser and Anselmetti (2008) complemented by a few additional seismic profiles acquired in this thesis. Probabilistic slope-stability analyses were conducted based on a limit-equilibrium equation for an infinite slope (e.g. Coduto et al. 2011) with Matlab. Earthquake shaking as input for the seismic slope stability analysis was derived from the Swiss Seismic Hazard Model (SUIHaz2015; Wiemer et al. 2016). Finally, modelling of the tsunami hazard was conducted with a combination of open-source codes following Hilbe and Anselmetti (2015).

1.6 Regional setting of Lake Zurich

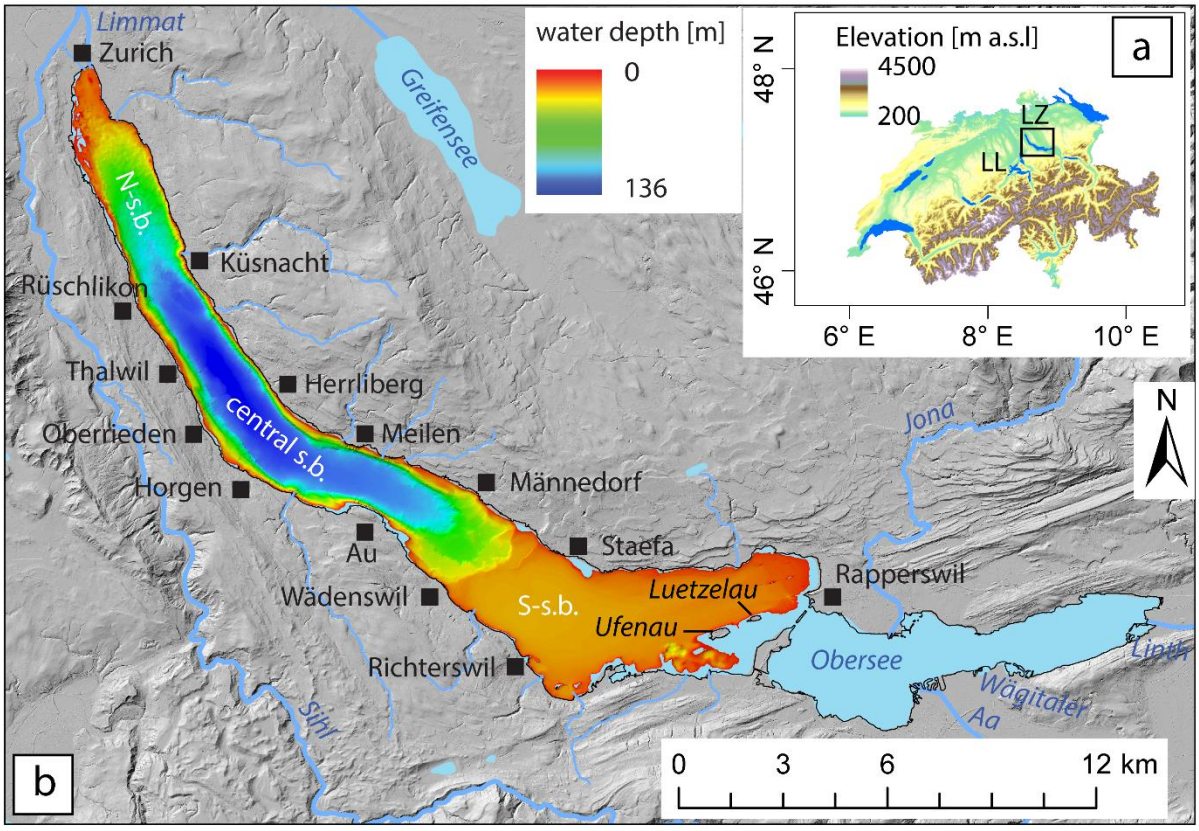


Figure 1. 1 Setting of the study area of this PhD Thesis. a) location of the study area within Switzerland. LZ = Lake Zurich, LL=Lake Lucerne b) Bathymetric dataset of Lake Zurich (Strupler et al. 2015). N-s.b.=Northern sub-basin, central s.b. = central sub-basin, S-s.b.=southern sub-basin. Geodata: Swisstopo.

Lake Zurich (~47° N, 8.5°E, 406 m a.s.l.) is located in a glacially overdeepened trough, incised in the Molasse, in Northern Switzerland. The main inflows are the Linth, Jona, and Wägitaler Aa. The Limmat river flows out of the lake at its northernmost tip, passing through the city of Zurich. The lake is split in two parts by the remnants of a terminal moraine emplaced during a last glacial retreat stage (e.g. Keller and Krayss 2005). The 'Lake Zurich' sensu stricto is located to the north and the 'Obersee' to the south of this moraine ridge.

The geographical focus of this thesis is on Lake Zurich sensu stricto, which shows three elongated sub-basins: A ~25 m deep, relatively flat W-E orientated basin connects via an escarpment structure with topographic steps in the Molasse bedrock to an up to 136 m deep, NW-SE orientated, central basin with steep lateral slopes. The northernmost sub-basin has an irregular bathymetry and shallows out progressively towards the city of Zurich (Figs. 1 and 2). Two islands, 'Ufenau' and 'Lützelau' exist in the southern sub-basin. The glacially excavated Molasse bedrock trough is overlain by a Quaternary infill consisting of glacial, glaciolacustrine and lacustrine deposits (Schindler, 1974; Schlüchter, 1984, Lister et al. 1984). The postglacial lithostratigraphic succession in the basin has been described by previous studies: the till-covered bedrock is overlain by Late Glacial muds that contain in the lower part some ice-rafted debris. During the Younger Dryas, iron sulphide muds were deposited. Lacustrine chalks and marls were subsequently deposited with further warming into the Holocene (Schindler 1974; Gyger et al. 1976; Giovanoli 1979). In contrast to this basinal sequence, the lithostratigraphic succession on the slopes has not been systematically analysed so far.

First settlements at the shores of Lake Zurich are dated to ~3000 yr BP (Primas 1981). Due to different societal and climatic factors, alternating colonization and de-colonization of the shorelines occurred during the following millennia. At present, almost a quarter million people are living within 1 km from the shorelines of Lake Zurich (Henriod et al. 2016).

On the lateral slopes of the central basin, multiple subaqueous mass-movements occurred repeatedly since deglaciation, assumedly triggered by sediment overloading, earthquakes, and human activity onshore (e.g. Heim 1876; Nipkow 1927; Schindler 1976; Kelts 1978; Giovanoli 1979; Kelts and Hsü 1980; Kuen 1999; Strasser and Anselmetti 2008; Strasser et al. 2013). Traces of subaqueous slides are known from previous mapping based a seismic-reflection survey and a single beam echosounder survey (Schlund 1972; Schindler 1974; Strasser and Anselmetti 2008). Due to the occurrence of distinct, well-dated traces of subaqueous mass movements, the slopes offshore Oberrieden (Fig. 1.1b and 2) constitute a prime site for a geotechnical characterisation.

In the last four decades, the instrumentally measured seismic activity in the larger region of Lake Zurich has been very low with the exception of two M_w 4.2 and M_w 3.5 earthquakes near Zug in 2012 (Swiss Seismological Service 2016).

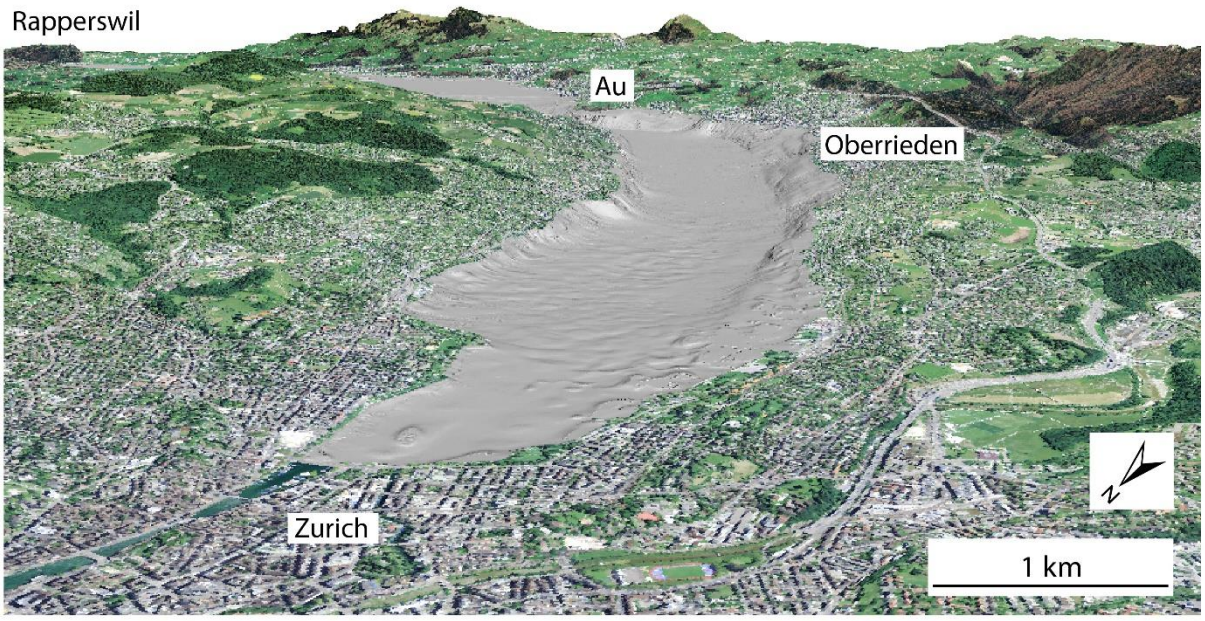


Figure 1. 2 Virtual aerial view from the city of Zurich to the northern and central Lake basin, displayed with the new high-resolution digital depth model (Strupler et al. 2015). *Swissalti3D digital elevation model and Swissimage orthophoto from Swisstopo. Vertical exaggeration: 2x. Due to perspective, the scale is only valid for the lower part of the image.*

1.7 Outline of the PhD thesis

After this introductory chapter 1, chapters 2 to 5 represent four individual scientific articles that are either published, in press, or submitted for publication in scientific journals.

The thesis-chapters are structured in the chronological order of the thesis-workflow:

Chapter 2 that was submitted to the "Geological Society Special Publication on Subaqueous Mass Movements and Their Consequences: Assessing Geohazards, Environmental Implications and Economic Significance of Subaqueous Landslides" quantitatively characterizes the landslide-related, morphologic features on the lake bottom, based on a new digital bathymetric model that was published in a short article in Swiss Bulletin for Applied Geology (Strupler et al. 2015; in german). Results demonstrated that morphometric analyses on a high-resolution DDM can contribute to a better understanding of the processes and timing of sublacustrine mass movements.

Chapter 3, published in "Geo-marine letters", presents a flexible approach for the sediment-mechanical characterisation of the lateral slopes of Lake Zurich by incorporating the spatial variability. The analyses were based on the new bathymetric dataset, an existing seismic reflection dataset (Strasser and Anselmetti 2008), and a newly acquired high-resolution geotechnical dataset. These geotechnical data acquired with laboratory and in situ measurements at a case-study site in Oberrieden (Figs. 1.1 and 1.2) were used as input for a Monte Carlo simulated limit-equilibrium model on an infinite slope to assess the past and present slope stability under static and seismic

loading. Results showed that the location of the modelled failure plane is consistent with stratigraphic analysis and failure-plane identification from sediment cores.

Chapter 4, in press for "Natural Hazards", presents a first subaqueous hazard map for earthquake-triggered landslides in Lake Zurich. The manuscript combines the high-resolution sediment-mechanical and geophysical input data (Chapter 3) with data from an existing probabilistic seismic hazard assessment. Probabilities of failure of the slopes, conditioning on earthquake occurrence were assessed with a limit-equilibrium approach on an infinite slope that was adapted for a grid-based application. Failure prone zones for earthquake accelerations estimated for mean return periods of 475, 2475 and 9975 years were mapped and their volumes calculated.

Chapter 5 (submitted to Swiss Journal of Geosciences), presents a first-order assessment of the tsunami hazard posed by subaqueous earthquake-triggered landslides. It was investigated (i) whether a Holocene earthquake-triggered landslide event may have caused tsunamis and (ii) whether a tsunami hazard exists for the present-day sediment drape. Tsunami modelling was conducted using an existing approach of combining two open source codes for the modelling of the landslide progression, wave propagation and run-up. Results implied that the tsunami hazard for Lake Zurich is relatively low and mainly affects the shorelines around the central basin.

Chapter 6 presents the main conclusions of this PhD thesis and recommendations for future work. In summary, this thesis presents a flexible approach for the quantitative assessment of slope stabilities by considering the spatial variability of the input data. This approach is subsequently included in a probabilistic assessment of the basin-wide subaqueous landslide hazard, and tested in perialpine Lake Zurich. Furthermore, a first-order assessment of the tsunami hazard in Lake Zurich is presented.

References

Abramson LW, Lee TS, Sharma S and Boyce GM (2002) Slope stability and stabilization methods, 2nd ed. Wiley, New York

Assier-Rzadkiewicz S, Mariotti C and Heinrich P (1996) Modelling of submarine landslides and generated water waves. Physics and Chemistry of the Earth 21:7–12. doi: 10.1016/S0079-1946(97)00002-5

Bardet JP, Synolakis CE, Davies HL, Imamura F and Okal EA (2003) Landslide Tsunamis: Recent findings and research directions. Pure and Applied Geophysics 160:1793–1809. doi: 10.1007/s00024-003-2406-0

Bornhold BD and Thomson RE (2012) Tsunami hazard assessment related to slope failures in coastal waters. In: Clague JJ, Stead D (eds) Landslides. Cambridge University Press, Cambridge, pp 108–120

Coduto DP, Yeung MR and Kitch WA (2011) Geotechnical Engineering: Principles and Practices, 2nd edn. Prentice Hall, Upper Saddle River

Craig RF (2004) Craig's Soil Mechanics, 7th edn. Spon Press, New York

De Batist M and Chapron E (2008) Lake systems: Sedimentary archives of climate change and tectonics. Palaeogeography, Palaeoclimatology, Palaeoecology 259:93–95. doi: 10.1016/j.palaeo.2007.10.016

De Blasio FV (2011) Introduction to the Physics of Landslides. Springer Netherlands, Dordrecht

Fritz HM (2002) Initial phase of landslide generated impulse waves. Mitteilungen der Versuchsanstalt fur Wasserbau, Hydrologie und Glaziologie an der Eidgenossischen Technischen Hochschule Zurich 1–253. doi: 10.3929/ethz-a-004443906

Giovanoli F (1979) Die remanente Magnetisierung von Seesedimenten. ETH Zürich, PhD Thesis Nr.6350

Gyger M, Müller-Vonmoos M and Schindler C (1976) Untersuchungen zur Klassifikation spät- und nacheiszeitlicher Sedimente aus dem Zürichsee. Schweizerische mineralogische und petrographische Mitteilungen 56:387–406.

Hampton MA, Lee HJ and Locat J (1996) Submarine Landslides. Reviews of Geophysics 34–1:33–59.

Heim A (1876) Bericht und Expertengutachten über die im Februar und September 1875 in Horgen am Zürichsee vorgekommenen Rutschungen. Die Eisenbahn 4:191–196.

Henriod S, Douard R, Ullmann D and Humbel R (2016) Statistik der Bevölkerung und Haushalte (STATPOP). Bundesamt für Statistik (BFS), Bern. BFS-Nummer: be-d-00.03-13-STATPOP-v16

Hilbe M and Anselmetti FS (2015) Mass Movement-Induced Tsunami Hazard on Perialpine Lake Lucerne (Switzerland): Scenarios and Numerical Experiments. Pure and Applied Geophysics 172:545–568. doi: 10.1007/s00024-014-0907-7

Hoffmann G and Reicherter K (2016) Geohazards: Coastal Disasters. In: Harff J, Meschede M, Petersen S, Thiede Jö (eds) Encyclopedia of Marine Geosciences. Springer Netherlands, Dordrecht, pp 276–283

ISSMGE (2004) Glossary of Risk Assessment Terms - Version 1. TC32 - Technical Committee on Risk Assessment and Management 66:1–7.

Jiang L and Leblond PH (1992) The Coupling of A Submarine Slide and The Surface. Journal of Geophysical Research 97:12731–12744.

Jibson RW (1996) Use of landslides for paleoseismic analysis. 43:291–323.

Johari A and Javadi AA (2012) Reliability assessment of infinite slope stability using the jointly distributed random variables method. Scientia Iranica 19:423–429. doi: 10.1016/j.scient.2012.04.006

Keller O and Krayss E (2005) Der Rhein-Linth-Gletscher im letzten Hochglazial. 1. Teil: Einleitung, Aufbau und Abschmelzen des Rhein-Linth-Gletschers im Oberen Würm. Verteljahrsschrift der Naturforschenden Gesellschaft in Zürich 150:19–32.

Kelts K (1978) Geological and sedimentary evolution of Lakes Zurich and Zug, Switzerland. ETH Zurich, PhD Thesis, Nr.6146

Kelts K, Briegel U, Ghilardi K and Hsu K (1986) The limnogeology-ETH coring system. Swiss Journal of Hydrology 48:104–115. doi: 10.1007/BF02544119

Kelts K and Hsü KJ (1980) Resedimented facies of 1875 Horgen slumps in Lake Zurich and a process model of longitudinal transport of turbidity currents. Eclogae geol Helv 73:271–281.

Kramer SL (1996) Geotechnical Earthquake Engineering. Prentice-Hall, Upper Saddle River

Kremer K, Hilbe M, Simpson G, Decrouy L, Wildi W and Girardclos S (2015) Reconstructing 4000 years of mass movement and tsunami history in a deep peri-Alpine lake (Lake Geneva, France-Switzerland). Sedimentology 1305–1327. doi: 10.1111/sed.12190

Kremer K, Marillier F, Hilbe M, Simpson G, Dupuy D, Yrro BJF, Rachoud-Schneider A-M, Corboud P, Bellwald B, Wildi W and Girardclos S (2014) Lake dwellers occupation gap in Lake Geneva (France–Switzerland) possibly explained by an earthquake–mass movement–tsunami event during Early Bronze Age. Earth and Planetary Science Letters 385:28–39. doi: 10.1016/j.epsl.2013.09.017

Kuen E (1999) Der Uferabbruch im Kusen. In: Küsnachter Jahrheft. Ortsgeschichtliche Kommission der Kulturellen Vereinigung Küsnacht, pp 44–50

Lamarche G, Mountjoy J, Bull S, Hubble T, Krastel S, Lane E, Micallef A, Moscardelli L, Mueller C, Pecher I and Woelz S (2016) Submarine Mass Movements and their Consequences. Springer International Publishing, Cham

Lecours V, Dolan MFJ, Micallef A and Lucieer VL (2016) A review of marine geomorphometry, the quantitative study of the seafloor. Hydrology and Earth System Sciences 20:3207–3244. doi: 10.5194/hess-20-3207-2016

Lee EM and Jones DKC (2014) Landslide Risk Assessment, 2nd edn. ICE Publishing, London

Locat J and Lee HJ (2002) Submarine landslides: advances and challenges. Canadian Geotechnical Journal 39:193–212. doi: 10.1139/t01-089

Masson DG, Harbitz CB, Wynn RB, Pedersen G and Løvholt F (2006) Submarine landslides: processes, triggers and hazard prediction. Philosophical transactions Series A, Mathematical, physical, and engineering sciences 364:2009–2039. doi: 10.1098/rsta.2006.1810

McAdoo BG (1999) Mapping Submarine Slope Failures. In: Wright D, Bartlett D (eds) Marine and Coastal Geographical Information Systems. Taylor & Francis Group, London, p 17

Moernaut J, De Batist M, Charlet F, Heirman K, Chapron E, Pino M, Brümmer R and Urrutia R (2007) Giant earthquakes in South-Central Chile revealed by Holocene mass-wasting events in Lake Puyehue. Sedimentary Geology 195:239–256. doi: 10.1016/j.sedgeo.2006.08.005

Mueller C, Mountjoy J, Power W, Lane E and Wang X (2016) Towards a Spatial Probabilistic Submarine Landslide Hazard Model for Submarine Canyons. In: Lamarche G, Mountjoy J, Bull S, et al. (eds) Submarine Mass Movements and their Consequences. Cham, pp 589–597

Mulder T and Cochonat P (1996) Classification of Offshore Mass Movements. Journal of Sedimentary Research 66:43–57. doi: 10.1306/D42682AC-2B26-11D7-8648000102C1865D

Nadim F (2006) Challenges to geo-scientists in risk assessment for sub-marine slides. Norsk Geologisk Tidsskrift 86:351–362.

Nadim F, Kalsnes B and Eide A (1996) Analysis of submarine slope stability under seismic action. In: Senneset K (ed) Landslides. Balkema, Rotterdam, pp 561–565

Nipkow F (1927) Über das Verhalten der Skelette planktischer Kieselalagen im geschichteten Tifenschlamm des Zürich- und Baldeggersees. ETH Zurich, PhD Thesis, Nr. 455

Praet N, Moernaut J, Van Daele M, Boes E, Haeussler PJ, Strupler M, Schmidt S, Loso MG and De Batist M (2016) Paleoseismic potential of sublacustrine landslide records in a high-seismicity setting (south-central Alaska). Marine Geology. doi: 10.1016/j.margeo.2016.05.004

Primas M (1981) Urgeschichte des Zürichseegebietes im Überblick: Von der Steinzeit bis zur Früheisenzeit. In: Degen R (ed) Zürcher Seeufersiedlungen - Von der Pfahlbau-Romantik zur modernen archäologischen Forschung. Basel, pp 5–18

Prior DB, Coleman JM and Bornhold BD (1982) Results of a known seafloor instability event. Geo-Marine Letters 2:117–122. doi: 10.1007/BF02462751

Raetzo H, Lateltin O, Bollinger D and Tripet JP (2002) Hazard assessment in Switzerland - Codes of practice for mass movements. Bulletin of Engineering Geology and the Environment 61:263–268. doi: 10.1007/s10064-002-0163-4

Reusch A, Moernaut J, Anselmetti FS and Strasser M (2016) Sediment mobilization deposits from

episodic subsurface fluid flow-A new tool to reveal long-term earthquake records? Geology 44:243–246. doi: 10.1130/G37410.1

Schindler C (1974) Zur Geologie des Zürichsees. Eclogae geol Helv 67:163–196.

Schindler C (1976) Eine geologische Karte des Zürichsees und ihre Deutung. Eclogae geol Helv 69:125–138.

Schlund RA (1972) Zürichsee: topogr. Plan 1:5 000. Meliorations- und Vermessungsamt des Kt. Zürich.

Schnellmann M, Anselmetti FS, Giardini D and McKenzie JA (2006) 15,000 Years of mass-movement history in Lake Lucerne: Implications for seismic and tsunami hazards. Eclogae Geologicae Helvetiae 99:409–428. doi: 10.1007/s00015-006-1196-7

Schnellmann M, Anselmetti FS, Giardini D, McKenzie JA and Ward SN (2002) Prehistoric earthquake history revealed by lacustrine slump deposits. Geology 30:1131–1134. doi: 10.1130/0091-7613(2002)030<1131:PEHRBL>2.0.CO;2

Siegenthaler C, Finger W, Kelts K and Wang S (1987) Earthquake and seiche deposits in Lake Lucerne, Switzerland. Eclogae Geologicae Helvetiae 80:241–260.

Statistik Stadt Zürich (2016) Bevölkerung. In: Statistisches Jahrbuch der Stadt Zürich 2016. Stadt Zürich, Präsidialdepartement, Statistik Stadt Zürich, Zürich, pp 24–79

Strasser M and Anselmetti FS (2008) Mass-movement event stratigraphy in Lake Zurich; A record of varying seismic and environmental impacts. Beiträge zur Geologie der Schweiz 95:23–41.

Strasser M, Hilbe M and Anselmetti FS (2011) Mapping basin-wide subaquatic slope failure susceptibility as a tool to assess regional seismic and tsunami hazards. Marine Geophysical Research 32:331–347. doi: 10.1007/s11001-010-9100-2

Strasser M, Monecke K, Schnellmann M and Anselmetti FS (2013) Lake sediments as natural seismographs: A compiled record of Late Quaternary earthquakes in Central Switzerland and its implication for Alpine deformation. Sedimentology 60:319–341. doi: 10.1111/sed.12003

Strupler M, Hilbe M, Anselmetti FS and Strasser M (2015) Das neue Tiefenmodell des Zürichsees: Hochauflösende Darstellung der geomorphodynamischen Ereignisse im tiefen Seebecken. Swiss Bull angew Geol 20:71–83.

Swiss Seismological Service (2016) Earthquakes Switzerland. http://www.seismo.ethz.ch/en/earthquakes/switzerland/all-earthquakes/index.html. Accessed 26 Apr 2017

Tappin DR (2017) The Generation of Tsunamis. In: Encyclopedia of Maritime and Offshore Engineering. John Wiley & Sons, Ltd, Chichester, UK, pp 1–10

Tappin DR, Watts P and Grilli ST (2008) The Papua New Guinea tsunami of 17 July 1998: anatomy of a catastrophic event. Nat Hazards Earth Syst Sci 8:243–266.

Tappin DR, Watts P, McMurtry GM, Lafoy Y and Matsumoto T (2001) The Sissano, Papua New Guinea tsunami of July 1998 - Offshore evidence on the source mechanism. Marine Geology 175:1–23. doi: 10.1016/S0025-3227(01)00131-1

Waldmann N, Anselmetti FS, Ariztegui D, Austin Jr J a., Pirouz M, Moy CM and Dunbar R (2011) Holocene mass-wasting events in Lago Fagnano, Tierra del Fuego (54°S): implications for paleoseismicity of the Magallanes-Fagnano transform fault. Basin Research 23:171–190. doi: 10.1111/j.1365-2117.2010.00489.x

Watts P (1998) Wavemaker curves for tsunamis generated. Journal of Waterway, Port, Coastal, and ocean engineering 127–137.

Wiemer S, Danciu L, Edwards B, Marti M, Fäh D, Hiemer S, Wössner J, Cauzzi C, Kästli P and Kremer K (2016) Seismic Hazard Model 2015 for Switzerland. 1–163. doi: 10.12686/a2

Wiemer S, Giardini D, Fäh D, Deichmann N and Sellami S (2009) Probabilistic seismic hazard assessment of Switzerland: best estimates and uncertainties. Journal of Seismology 13:449–478. doi: 10.1007/s10950-008-9138-7

Chapter 2

Quantitative characterisation of subaqueous landslides in Lake Zurich (Switzerland) based on a high-resolution bathymetric dataset

This chapter was submitted to the Geological Society Special Publication on Subaqueous Mass Movements and Their Consequences: Assessing Geohazards, Environmental Implications and Economic Significance of Subaqueous Landslides as Strupler, M., Anselmetti, F.S., Hilbe, M., Strasser M. Quantitative characterisation of subaqueous landslides in Lake Zurich (Switzerland) based on a high-resolution bathymetric dataset.

The bathymetric dataset, which this study builds on, was published in german in the Swiss Bulletin for applied geology as Strupler M., Hilbe, M., Anselmetti F.S., Strasser, M. 2015. Das neue Tiefenmodell des Zürichsees: Hochauflösende Darstellung der geomorphodynamischen Ereignisse im tiefen Seebecken.

Abstract

New high-resolution surveying techniques allow investigating the subaqueous geomorphology in great detail. Such analyses are important, as the morphologies are often witnesses of past processes, including mass movements. For perialpine Lake Zurich, a plenitude of mass-wasting events have occurred in the past millennia. While the ages of these events are known from past studies on the respective deposits in the lake basin, the surface expressions and distribution of the respective features on the slopes have not been extensively described. Here we quantitatively characterise the morphologic features on the entire lake floor: A total of 50 subaqueous landslides are morphologically identified in a high-resolution digital bathymetric model (DBM), mapped and characterised using a Geographic Information System (GIS). Many slides show relatively small erosion areas (< 0.05 km^2) and are located in shallow water (< 10 m water depth). The roughness of the individual landslide-translation areas is quantified using the standard deviation of a measure called topographic position index (TPI) and related to the slides ages. The DBM allows the detection of traces of mass-movements dating back to ~5000 cal. yrs. BP. Our results demonstrate that morphometric analyses on a high-resolution DBM can contribute to a better understanding of sublacustrine mass movements.

2.1 Introduction

In recent years, various high-resolution bathymetric surveys have been conducted on perialpine lakes located around the world or in Switzerland (Bini et al. 2007; Bozzano et al. 2009; Hilbe et al. 2011; Miller et al. 2013; Kremer et al. 2015; Reusch 2015; Wessels et al. 2015a; Wessels et al. 2015b). Bathymetric data document the lake-floor morphologies resulting from a broad variety of geological and hydrodynamic processes. Such processes include currents, subaqueous mass movements, fluid-flow and glacial activity. Subaqueous mass movements and potential landslide-triggered tsunamis can have catastrophic impacts on infrastructure and people living along the shorelines. Different natural (e.g. earthquakes, wave loading, sedimentation, fluid flow) and human factors (e.g. construction works on shore) can trigger subaqueous mass movements (e.g. Locat and Lee 2002).

Geophysical investigations have already started decades ago in Lake Zurich (Northern Switzerland). In particular, Hsü and Kelts (1970) investigated the evolution of Lake Zurich and its subbottom with seismic reflection data. A campaign with a single-beam echosounder (Krupp Atlas Deso 10) in 1972 led to a bathymetric dataset of Lake Zurich. From the datapoints, a bathymetric map with isobath spacing of 5 m in the deep zones and 2.5 m in the nearshore areas was constructed (Schlund 1972). This map, together with information from sediment cores, enabled Schindler (1976) to design a geological map of Lake Zurich's bottom, exhibiting many geomorphic structures of the lake floor, such as basin plain, deltas, and subaqueous landslides. The valuable information from these past studies provided knowledge about the formation of the lake and its morphology, establishing a solid basis for further investigations. Multiple subaqueous landslides have occurred on the lateral slopes of Lake Zurich since deglaciation. They were triggered by sediment overloading, earthquakes and, for the slides occurring in the last ~150 years, construction work on the shores (Schindler 1976; Kelts 1978; Strasser et al. 2013). Strasser et al. (2013) mapped and dated the mass-transport deposits of the past ~17'000 years in the central basin of Lake Zurich with reflection seismic data (3.5 kHz Pinger) and sediment cores. These authors documented a total of 21 event horizons, each comprising between 1 and 23 coeval mass movements on the subaqueous slopes. The extent of the glide planes, however, could not be systematically documented with the available data at the time.

For a better understanding of the gravitational mass-movement processes at the slopes, a digital terrain model (DTM) with a grid resolution in the range of the size of features to be investigated is needed (Glenn et al. 2006). State-of-the-art multibeam echosounders enable the acquisition of high-resolution bathymetric datasets that allow the identification of small-scale features. Such a dataset of Lake Zurich was acquired in 2014 with a multibeam echosounder (Kongsberg EM2040; 300 kHz; 1° x 1° beam width; Strupler et al. 2015). This new high-resolution DBM represents the lake floor with a horizontal grid resolution of 1 m. Vertical depth differences of less than 1 dm can be identified.

We analyse this high-resolution DBM of Lake Zurich in order to map the traces of subaquatic geomorphodynamic events in detail and to extract quantitative information concerning the causes, processes and timing of the sublacustrine mass movements. Here we focus on the identification of the geomorphic characteristics from the new DBM, which document past subaqueous slides. Quantitative analyses of slide areas, water depth of the headscarp and slide morphologies in a geographic information system (GIS) show how the high-resolution DBM can contribute to a better understanding of the sublacustrine landslides.

Specifically, the following research questions are answered:

- At what locations on the slopes do subaqueous slides occur and what is their extent?
- Can the frontal emplacement of landslides be distinguished based on detailed morphological features?
- How does the surface texture of the different glide planes vary with respect to their age?

2.2 Study setting

Lake Zurich is a perialpine, glacially excavated Lake in northern Switzerland (~47° N, 8.5° E, 406 m a.s.l.) with a basin volume of 3'900 Mio m^3 (BFS 2009). The main rivers inflowing the lake are the Linth, Jona and Wägitaler Aa. The only outflow is the Limmat river at the northern end of the lake (Fig. 2.1).

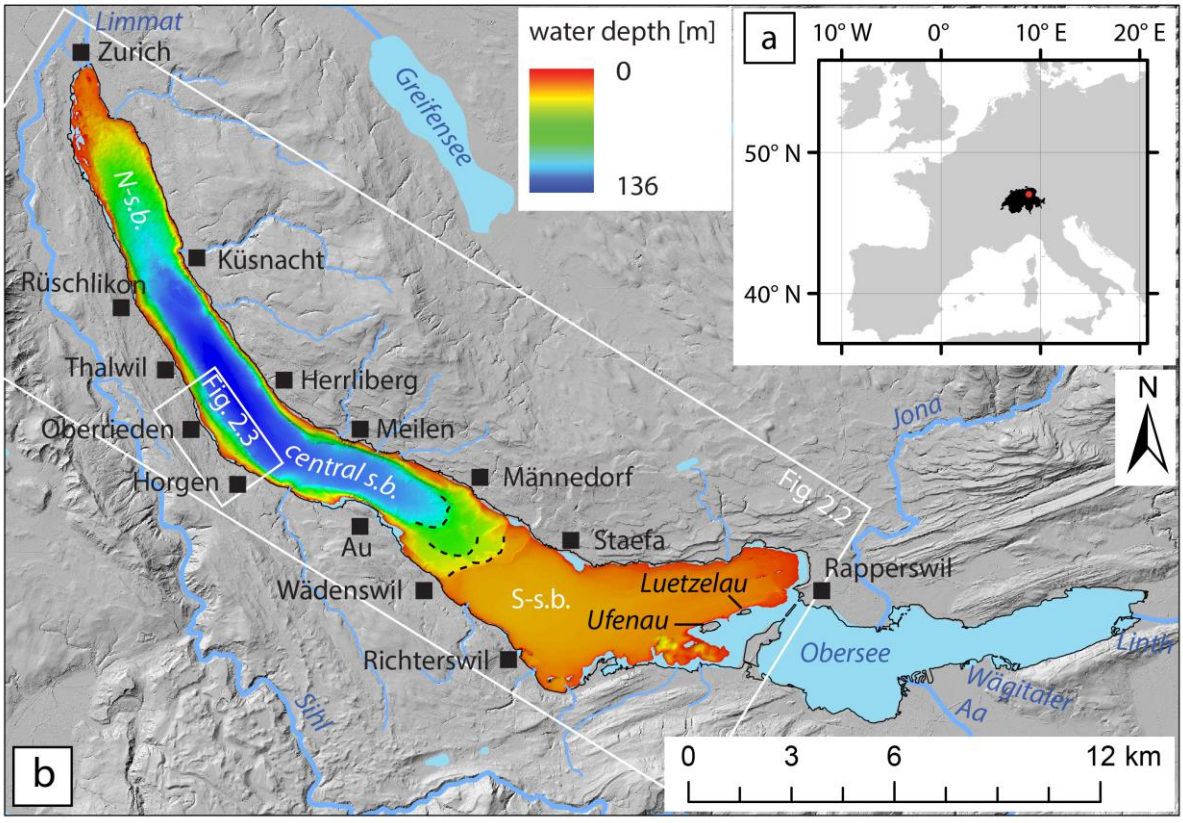


Figure 2. 1 (a) Location of Switzerland and Lake Zurich (red dot) within Europe. (b) Location of the sub-basins in Lake Zurich. Black dashed lines represent escarpment structure between the central and the southern sub-basins. N-sb=Northern sub-basin, central sb = central sub-basin, S-sb=southern sub-basin. Bathymetric dataset: Strupler et al. 2015. Digital elevation data: Swisstopo.

Lake Zurich is separated in two parts by remnants of an end moraine from the last glaciation (e.g. Keller and Krayss 2005), i.e. 'Lake Zurich' s. stricto to the North and the 'Obersee' to the South of the moraine. In this article we focus on Lake Zurich s. stricto (Fig. 2.1), which can be divided in three parts: A ~25 m deep, relatively flat W-E-orientated basin is connected via an escarpment structure with topographic steps in the molasse bedrock to an up to 136 m deep, NW-SE-orientated, central basin. Most of the documented subaqueous landslides occur in the central sub-basin (Strasser et al. 2013). The northernmost part of Lake Zurich is progressively getting shallower towards the city of Zurich. The lake floor on that part of the lake shows an irregular bathymetry that is interpreted as originating from glacial dumping of till (Schindler 1968; Schlund 1972; Schindler 1974).
The present-day lake morphology is a result from the glacially excavated bedrock structure and its infill with quaternary sediments. In the southern basin, various parallel throughs that are separated by narrow ridges (e.g. a ridge that hosts the two islands 'Ufenau' and 'Lützelau'; Fig. 2.1c) representing four generations of glacial erosion can be found. At the location of the escarpment structure (Fig. 2.1c), these troughs converge to a single, U-shaped trough. These excavations in the Molasse bedrock were filled with up to 120 m mostly glacial and glaciolacustrine sediments (Welti 1950; Hsü and Kelts 1970; Schindler 1976). During deglaciation, large amounts of Late Glacial clays were deposited. In a succeeding warmer period, iron sulphide mud, followed by lacustrine marls and chalks were deposited (Schindler 1974).

2.3 Data and Methods

Analysis of the DBM was conducted with a Geographic Information System (ArcGIS 10). To gain a better insight into the morphology and processes of the subaqueous landslides, existing 3.5 kHz Pinger-reflection seismic data from Strasser et al. (2013) were considered in addition to the bathymetric dataset. Based on a shaded relief of the DBM and a slope map, subaqueous slides were identified and mapped. Features of the landslides such as headscarps, lateral scars, translation and deposition areas were separated from the adjacent, undisturbed slopes. The parameters "area of the translation zone" (i.e. eroded area of a translational landslide), "depth of the headscarp below lake level", and "mean slope gradient of the translation zone" were calculated in ArcGIS. Ages of the translation areas were assigned by matching their spatial extent to the corresponding deposits in the seismic reflection data stratigraphically dated by Strasser et al. (2013).
The surface roughness of the translation areas was quantified by the zonal standard deviation of the Topographic Position Index (TPI; Weiss 2001). The TPI indicates the position of each pixel relative to its local neighbourhood, and thus can be used to describe landforms. We calculated the TPI following the method of Cooley (2015): Grids with minimal, maximal and mean elevation values of a local 5 x 5 cells neighbourhood were created (minDBM, maxDBM and meanDBM). Then, the TPI was calculated after Eq. 1:

$$TPI = \frac{(meanDBM - minDBM)}{(maxDBM - minDBM)} \qquad \text{(Equation 1)}$$

The result of Eq. 1 is a value between 0 and 1. A TPI value close to 0 means that the mean value of a neighbourhood is close to its minimum value, which is for instance the case a local highs. In contrast, a TPI value close to 1 means that the mean value of the neighbourhood is close to its maximum, which occurs e.g. in a local depression. In order to compare the variability of the surface of the individual translation areas of the landslides, which we interpret as the surface roughness, the standard deviation of the TPI was calculated for each translation area with the 'zonal statistics' tool in ArcGIS.

2.4 Results and Interpretation

2.4.1 Characteristics of the subaqueous landslides

The high-resolution bathymetric dataset allows the documentation of various characteristics of mass movements. Zones with a relatively higher surface roughness that are located at greater depths than the surrounding sediment are interpreted as glide planes of subaqueous mass-movements, constrained by headscarps and side scarps (hatched area in Fig. 2.2a). Recent sediment-coring and in situ geotechnical studies (Strupler et al. 2017) confirm these glide planes. A few of the glide planes are connected to distinct lobes in the basin, which are interpreted as deposition areas of the landslides (green outlined in Fig. 2.2a).

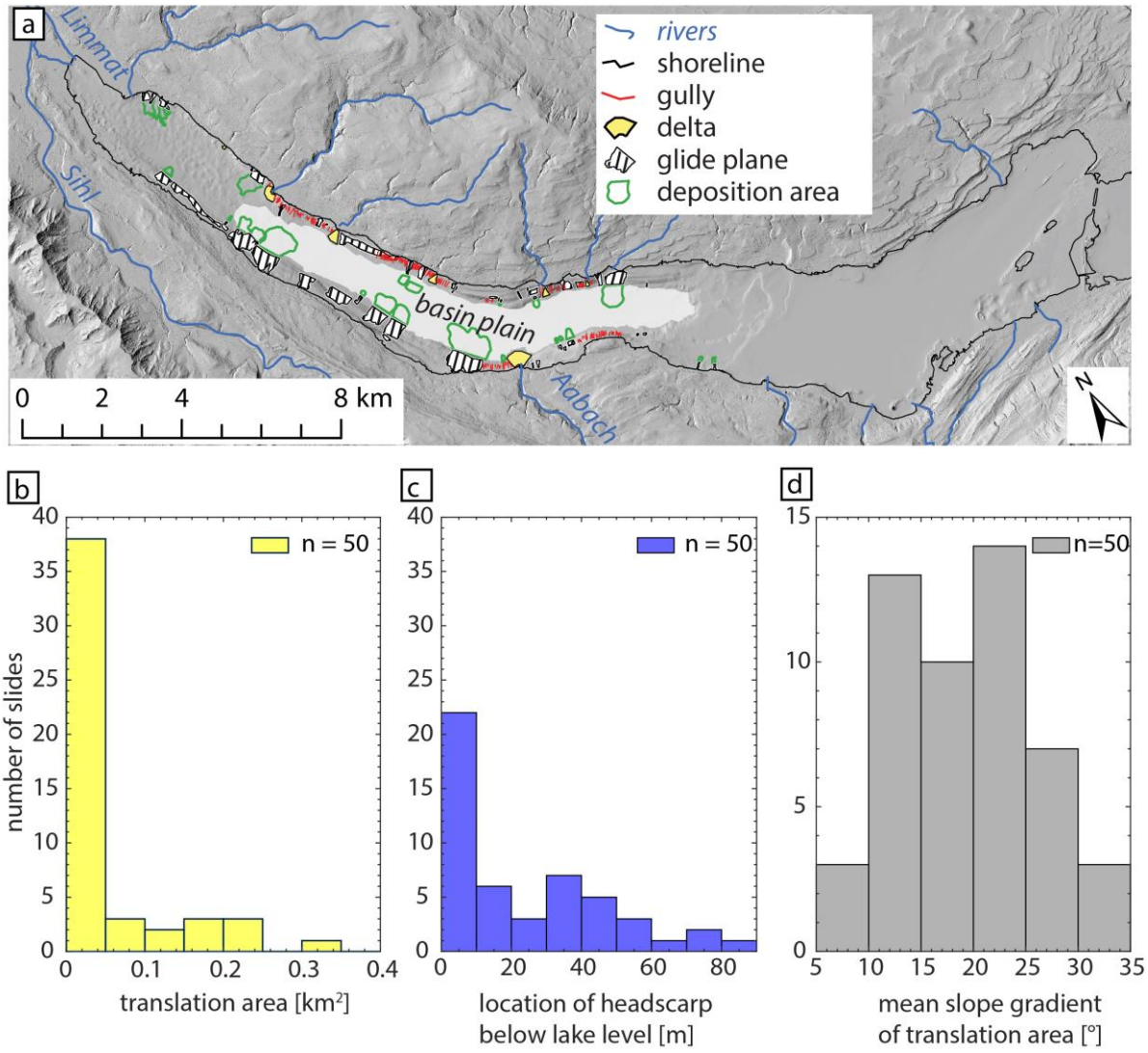


Figure 2. 2 (a) Mapped gravitative mass-transport-related features on the lakefloor. Bathymetric data: Strupler et al. 2015. Digital elevation model: Swisstopo. Frequency distributions are shown for the translation area (b), location of headscarp below lake level (c), and the mean slope gradient of the mapped translation areas (d) of the subaqueous landslides.

2.4.1.1 Characteristics of the translation area parameters

In total, 50 glide planes (hereafter called translation areas, as they all correspond to translational slides, i.e. occur on a planar slip surface; Cruden and Varnes 1996) were mapped (Fig. 2.2a). All except for two very small mapped subaqueous landslides are located in the central basin of Lake Zurich. The translation areas on the northeastern slopes could not always be mapped very precisely, as some slide areas are overprinted by gullies.

The frequency distribution of the translation area-size has a right-skewed character (Fig. 2.2b), showing that most of the mapped translation areas are smaller than 0.05 km^2. Only 7 slide areas are greater than 0.15 km^2. The extents of the mapped translation areas from the bathymetric dataset range between 0.001 km^2 and 0.33 km^2.

The frequency distribution of the water depth of the headscarp location is also right-skewed: 44% of the mapped headscarps are located in shallow water (< 10 m; Fig. 2.2c), and thus likely indicating shore loading as a trigger, as it is documented for the 1875 A.D Horgen slide and the 1955 A.D. Küsnacht slide (Heim 1876; Kuen 1999). Some of the slides, however, occurred in water depths of more than 50 m, indicating rather a natural trigger mechanism than anthropogenic shore loading.
The frequency distribution of the mean slope gradients of the translation areas is relatively symmetric. Fig. 2.2d shows the mean slope gradients of the translation areas; not the slope gradient at the position of the headscarps. Hence, a high mean slope gradient does not imply that the headscarp is located in a steep zone. Most of the translation areas are located on slopes with mean slope gradients of 10-25° (Fig. 2.2d), a gradient allowing enough sediment to be accumulated making them prone to failures. The data also show that some slope failures in Lake Zurich also occur on slopes with lower (i.e. 5-10°) and steeper (i.e. 25-35°) gradients.

2.4.1.2 Examples of different frontal emplacement styles

The subaquatic slope between the villages Horgen and Oberrieden shows traces of subaqueous slides dated to 1875 AD, 1918 AD, and ~2210 cal. yr BP (Fig. 2.3; Nipkow 1927; Kelts 1978; Strasser et al. 2013).

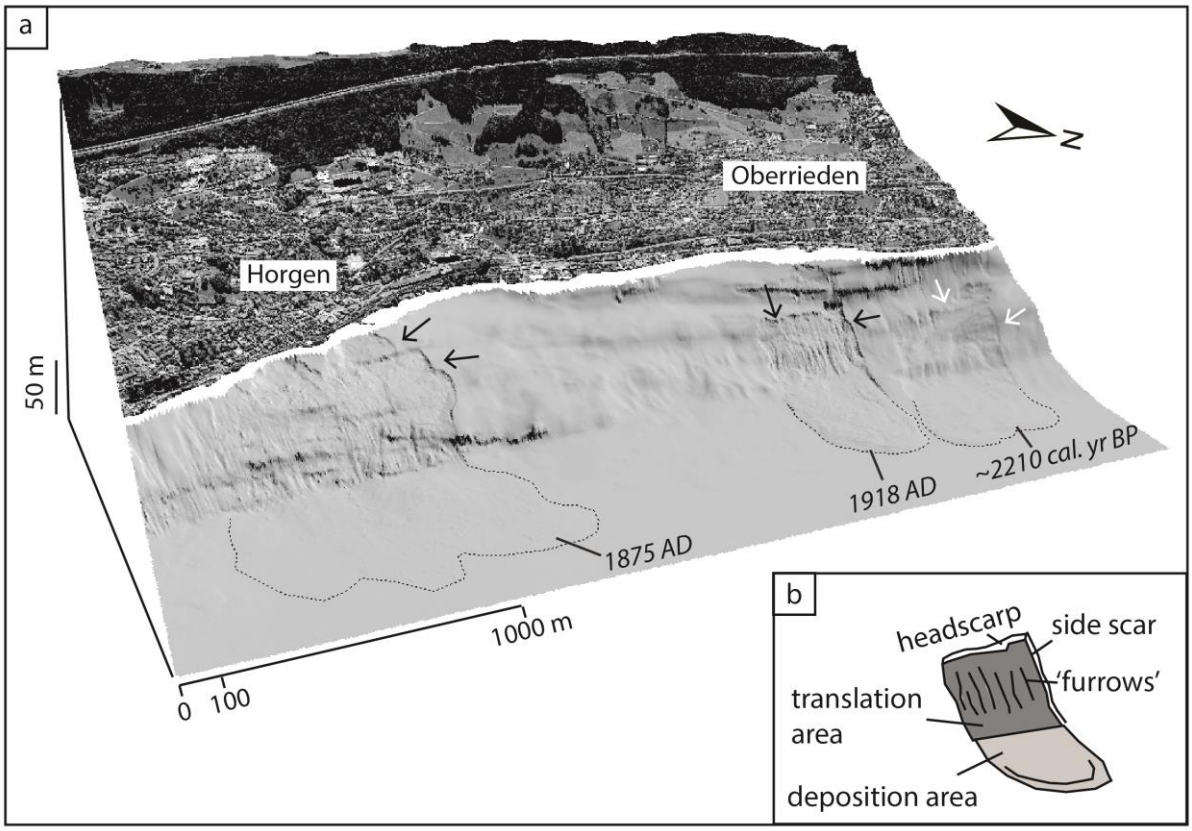


Figure 2. 3 (a) Subaqueous lateral slopes between Horgen and Oberrieden, showing slides 1, 2 and 4 from Fig. 2.5. Black arrows: crisp slide scars, white arrows: smooth slide scars. 3 times vertically exaggerated. SwissAlti3D digital elevation model and overlaying Swissimage50 orthophotos: Swisstopo. Location of the displayed slopes marked in Fig. 2.2a. (b) Sketch of a landslide with used landslide terminologies.

The 1875 AD Horgen slide, which was triggered as a consequence of construction works on the shore is one of the best-documented subaqueous slides in Lake Zurich (Heim 1876; Kelts 1978; Kelts and Hsü 1980). The slide, which occurred in multiple phases (i.e. the five main phases occurring within two days; Kelts and Hsü 1980), shows the largest translation area (0.33 km^2) of all the mapped slides in the DBM. In the hillshaded DBM, a plenitude of up to 20 m-wide outrunner blocks can be identified in the widespread deposition zone of the Horgen slide (Fig. 2.4a). No frontal bulges at the front of the deposition zone can be identified. The MTDs are characterised in the reflection seismic dataset by its chaotic-to-transparent facies (e.g. Schnellmann et al. 2005; Strasser et al. 2013; blue shading in Fig. 2.4) that can be distinguished from the undisturbed, continuously stratified sediments in the basin. The MTD of the 1875 AD Horgen slide is covering the undisturbed lake-floor strata at the time of the slide (Fig. 2.4a). Its maximum thickness is relatively small (~6 m). Both geomorphic and reflection seismic data (Fig. 2.4a) indicate thus a *frontally emergent* emplacement style (e.g. Frey-Martínez et al. 2006; Moernaut and De Batist 2011) of the Horgen 1875 AD slide. In contrast, the shaded relief of the 1918 AD and ~2210 cal. yr. BP slides near Oberrieden show no outrunner blocks but topographic bulges in the toe region, distinctly separating the MTD from the undisturbed basin-plain sediments. The MTD of the 1918 AD Oberrieden slide is characterised in the seismic reflection dataset by a relatively great thickness of ~15 m sediments (Fig. 2.4b). In the toe region, frontal thrusting structures can be identified. Such *frontally confined* emplacement styles are formed when the slide ploughs into the adjacent sediment, where it is decelerated and frontally thrusted (Frey-Martínez et al. 2006; Moernaut and De Batist 2011).

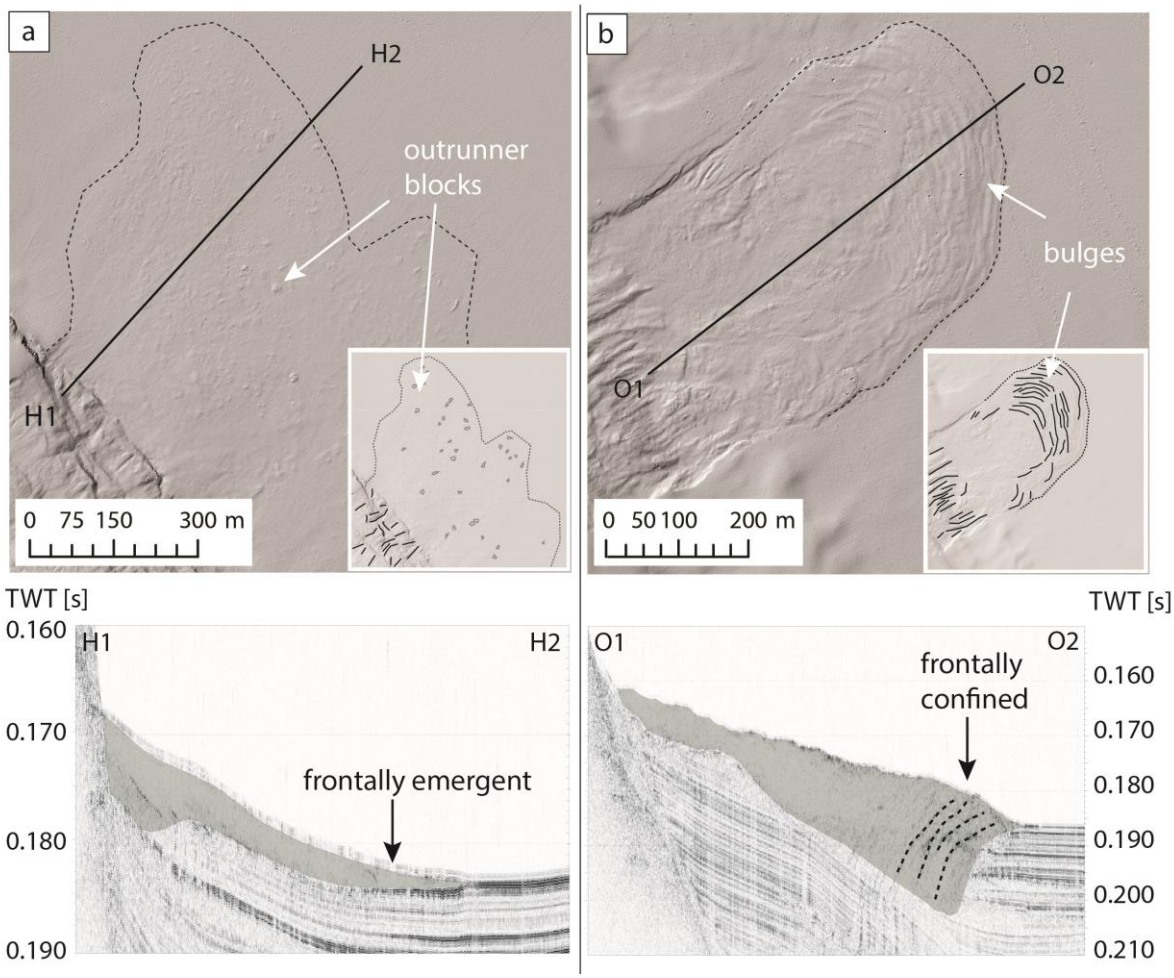


Figure 2. 4 (a) shaded relief (top) and seismic reflection dataset (bottom) of the frontally emergent Horgen 1875 AD slide (Nr. 4 in Fig. 2.5). (b) shaded relief (top) and seismic reflection dataset (bottom) of the frontally confined Oberrieden 1918 AD slide (Nr. 1 in Fig. 2.5 and Tab. 2.2). Grey shading: landslide deposit. Black dashed lines indicate frontal thrusting. Seismic reflection dataset from Strasser et al. 2013.

According to Moernaut and De Batist (2011), the height drop between the headscarp and frontal ramp and the subsurface depth of the basal shear surface are mainly determining the frontal emplacement style of landslides: Great height drops and shallow basal shear surfaces often lead to emerging depositional fronts, while small height drops and deep shear surfaces often lead to emerging fronts. For the Oberrieden 1918 AD landslide, the height drop between the headscarp and frontal ramp accounts for 83 m and the headscarp-height is ~ 4-5 m (Tab. 2.1), while for the 1875 Horgen slide the height drop is 130 m and the headscarp height ~6-7 m. Because of the comparably insignificant difference between the headscarp heights, we assume that the ~35% smaller height drop of the Oberrieden slide is mainly responsible for its confined front.

*Table 2. 1 Comparison of selected characteristics of the Horgen 1875 AD and the Oberrieden 1918 AD slides. The total length and height drop were measured from the uppermost limit of the headscarp to the downslope limit of the landslide deposit (including outrunner blocks). Slide ages from Heim (1876), Nipkow (1927) and Kelts and Hsü (1980) **=derived from bathymetric dataset with GIS; ++ = derived from pinger reflection seismic dataset (Strasser et al. 2013)*

Location and slide age	Headscarp height [m] ++/**	Total height drop [m] **	Total length [m] **	Frontal emplacement ** / ++
Horgen 1875 AD	Not visible in seismic data/ 6-7	130	1180	emerging
Oberrieden 1918 AD	~ 5 / 4-5	83	865	confined

2.4.1.3 Surface roughness of recent and sub-recent landslides

Translation areas of the subaqueous landslides in the bathymetric dataset show a distinct texture with furrows that are mostly parallel to the slope-gradient (Figs. 2.3 and 2.4). The here applied approach of a topographic position index (TPI) approach allows quantifying the roughness of these surface-textures: Translation areas that are colored in blue shading show a high zonal standard deviation of the TPI values, representing a high surface roughness, while a green coloured shading represents a low zonal standard deviation of the TPI, representing a low surface roughness (Fig. 2.5, Tab. 2.2). Most of the landslides with a high surface roughness (Standard deviation of the TPI > ~0.05; blue shading in Fig. 2.5) that show distinct slide scars in the shaded relief have already been mapped in the geological map of Schindler (1976). Strasser et al. (2013) related these slides to human activity during the last 150 years as triggers. Slides with a high roughness of the translation area that occurred during the last two centuries are thus called 'recent landslides'. For the slides with a lower surface roughness (i.e. standard deviation of the TPI < ~0.05, Tab. 2.2), it is assumed that the slide scars were also "crisp" immediately after the slide event, and that the roughness of the translation area once had a similar value as the recent slides. We hypothesize that ongoing sedimentation and other slope processes smooth out the surface of the glide plane with time. These slides are hereafter referred to as 'sub-recent' slides. Most of these sub-recent slides correlate to the mass-transport deposits with a maximum age of ~5000 years (Fig. 2.5, Tab. 2.2; Strasser et al. 2013).

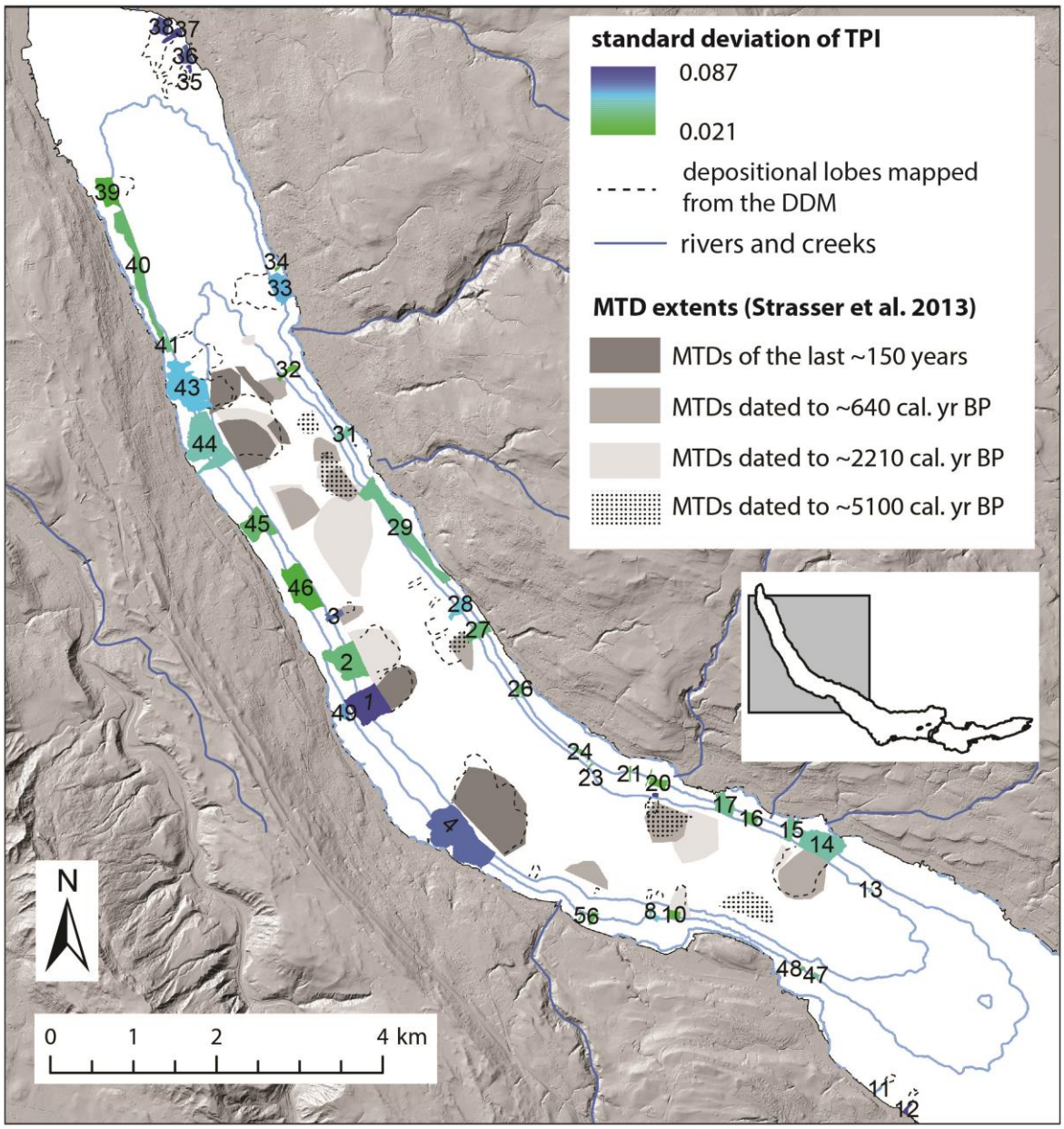


Figure 2. 5 Locations of the translation areas on the lateral slopes of the central and northern basins of Lake Zurich. Blue-shaded translation areas show high standard deviations of the TPI values within a single slide, thus indicate great roughness. Green shaded areas show low standard deviations of the TPI values within a single slide, indication low roughness. The extents of the Mass Transport Deposits (MTDs) of the past ~5000 years, mapped by Strasser et al. (2013) with seismic reflection data in the basin are shaded in different grey shading. Numbers of the translation areas refer to Obj. Nrs. in Tab 2.2. SwissAlti3D elevation model: Swisstopo

Only a few slides were not mapped out by Strasser et al. (2013) because (i) the acoustic signal did not penetrate into the subsurface in the northern and southern sub-basin (i.e. north of Küsnacht and south of Au; Fig. 2.1), and (ii) some slides were too small to be detected with the seismic reflection survey line spacing of ~100 to ~400 m.

Table 2. 2 Selected characteristics of the subaqueous landslides in Lake Zurich. slide ages from Strasser et al. 2013, Heim (1876), Nipkow (1927), Kelts and Hsü (1980) and Kuen (1999). b.l.l. = below lake level. Table continues on next page.

Object-Nr.	Translation area [m^2]	Water depth of headscarp [m b.l.l.]	Maximum water depth of deposition area [m b.l.l.]	Slide age (Strasser and Anselmetti, 2008)	Stdev of TPI	Slide age B.P. (i.e. before 1950 A.D)
1	159'975	51.3	134.7	1918 AD	0.0772	32
2	150'059	42.1	-	2210 cal. yr BP	0.0396	2210
3	16'846	75.9	133.3	640 cal. yr BP	0.0663	640
4	329'580	3.2	134.0	1875 AD	0.0675	75
5	2'803	3.5	-	?	0.0362	?
6	9'848	2.6	-	?	0.0352	?
7	2'119	54.2	-	?	0.0355	?
8	4'447	45.3	118.6	?	0.0458	?
9	3'901	31.8	117.7	?	0.0540	?
10	15'410	32.4	-	2210 cal. yr BP	0.0302	2210
11	5'220	2.9	-	?	0.0607	?
12	7'137	6.7	-	?	0.0875	?
13	1'655	82.0	-	?	0.0443	?
14	141'996	2.6	119.3	640 cal. yr BP	0.0468	640
15	27'190	4.6	-	2210 cal. yr BP	0.0437	2210
16	23'879	28.3	-	3330 cal.yr BP	0.0369	3330
17	49'928	4.1	-	2210 cal. yr BP	0.0429	2210
18	3'719	75.9	117.7	?	0.0842	?
19	3'484	21.8	-	?	0.0362	?
20	20'509	31.1	-	5100 cal. yr BP	0.0312	5100
21	4'746	32.2	-	?	0.0329	?
22	1'313	41.4	-	?	0.0409	?
23	1'677	58.9	-	?	0.0385	?
24	8'675	30.1	-	1430 cal. yr BP?	0.0378	1430
25	2'121	35.0	-	?	0.0404	?

Object-Nr.	Translation area [m^2]	Water depth of headscarp [m b.l.l.]	Maximum water depth of deposition area [m b.l.l.]	Slide age (Strasser and Anselmetti, 2008)	stdev of TPI	slide age B.P. (i.e. before 1950 A.D)
26	11'470	13.0	-	?	0.0375	?
27	45'468	7.3	-	2210 cal. yr BP or 640 cal. yr BP	0.0395	2210 or 640
28	34'752	6.2	-	1870 cal. yr BP	0.0543	1870
29	217'115	3.2	-	2210 cal. yr BP	0.0428	2210
30	982	14.4	-	?	0.0831	?
31	20'657	6.9	-	640 cal. yr BP	0.0455	640
32	15'982	26.4	-	?	0.0298	?
33	67'724	4.3	98.5	1955 AD	0.0583	-5
34	2'859	9.6	-	?	0.0230	?
35	5'021	17.9	-	1909 AD?	0.0861	41
36	24'718	4.1	-	1909 AD?	0.0687	41
37	18'226	5.8	-	1909 AD?	0.0788	41
38	34'301	8.4	-	1909 AD?	0.0692	41
39	72'565	13.1	-	?	0.0245	?
40	159'451	9.4	-	?	0.0379	?
41	13'854	13.2	-	?	0.0433	?
42	3'227	61.3	-	?	0.0480	?
43	220'731	3.2	109.1	1898 or 1900 AD	0.0565	50 or 52
44	240'870	2.3	128.9	1898 or 1900 AD	0.0480	50 or 52
45	99'193	4.8	-	2210 cal. yr BP or 640 cal. yr BP	0.0373	2210 or 640
46	148'793	13.9	-	3300 cal. yr BP	0.0211	3330
47	4'430	42.4	-	?	0.0430	?
48	2'680	36.0	-	?	0.0378	?
49	15'687	8.0	-	?	0.0605	?
50	2'291	47.0	-	3330 cal.yr BP ?	0.0291	3330

2.5 Discussion

In the following, we first discuss the advantages of a high resolution DBM for the identification and morphometric analysis of mass-movement related features at the lateral slopes and basin plain of Lake Zurich. Subsequently we discuss the knowledge gain on the basin-wide slope failures in the lake, derived from frequency distributions of various parameters.

2.5.1 Advantages of the new high-resolution DBM for geomorphometric analyses

The high-resolution digital depth model (DBM) of Lake Zurich allows the identification and geomorphometric analysis of mass-movement-related features on the lake floor with much greater detail than previous DBMs. Its spatial resolution (1 m) is comparable to existing subaerial LiDAR-Elevation data (e.g. SwissAlti3D with a grid resolution of 2 m; Swisstopo 2014). Although larger-scale features such as subaqueous landslides were already described on the bathymetric dataset of Schlund (1972) more than four decades ago, the new DBM allows the identification of small-scale features with dimensions of dm to a few meters that were previously not identifiable. For example, in the previous DBMs with a lower spatial resolution (Schlund 1972), gullies and features of subaqueous landslides, such as their headscarp and sidescars, surface texture and frontal emplacement style were either not at all or only vaguely identifiable. The mapping of these newly identified small-scale features in great detail and the analysis of extracted parameters leads to a better understanding of the subaquatic mass-transport processes, as discussed in the following paragraphs.

2.5.2 Information on subaqueous slope failures in Lake Zurich derived from morphometric analyses

The amount of mapped slides (n=50) in the DBM of Lake Zurich is a rather small number to make general conclusions on parameters affecting subaqueous landslides. However, the results still provide valuable first-order information on slope-failure processes in Lake Zurich. For example, the information that the greatest amount of the mapped slides are relatively small (i.e. smaller than 0.05 km^2) can be used for slide area assessments (McAdoo 1999). A similar frequency distribution of slide areas can also be observed for submarine slopes (e.g. Hühnerbach and Masson 2004). As on submarine slopes, landslides in Lake Zurich occur on a broad variety of gradients of the lateral slopes (e.g. Hühnerbach and Masson 2004). In contrast, in Lake Lucerne, no slides can be found on slopes > 22° (Strasser et al. 2011), where the authors assumed that on steeper slopes no sediment accumulates as permanent re-mobilization due to gravity removes the particles. In Lake Zurich, various 'terraces' occurring on the lateral slopes might be responsible for buttressing the sediment on steeper slopes (Strupler et al. 2017). The occurrence of gullies on the steepest parts of the slopes (i.e. > 25°) may indicate that in such steep zones, these gullies act as pathways for sediment transport (e.g. Field et al. 1999) where no considerable sediment can be accumulated.

The morphologic expressions related to the subaqueous landslides and the calculated results of landslide parameters complement the catalogue of sublacustrine landslides in Lake Zurich (Strasser et al. 2013), which is based on seismic reflection data. While a seismic reflection dataset allows the identification of multiple generations of subaqueous landslides, a bathymetric dataset often only shows traces of the youngest events. The combination of both methods allows an investigation of the

surface morphology of a slide and subsurface architecture, which can contribute to a better interpretation of a slide process. This is especially the case for analysing the MTDs: While the frontal emplacement style of the subaqueous landslides in Lake Zurich could be identified with the bathymetric dataset alone, a more detailed characterisation of the MTDs (e.g. maximum thickness, deformed basin sediments), requires complementary seismic reflection data. While most of the MTDs mapped in the DBM can be assigned to a slide from the reflection seismic dataset, not all MTDs from the reflection seismic data are visible in the bathymetric dataset. In general, slides older than ~5000 years cannot be mapped clearly in the new bathymetric dataset, as the corresponding morphologies have been smoothed out completely by sedimentation and slope processes. However, also for some slide deposits dated to younger ages, no corresponding translation area could be identified on the bathymetric dataset. Hence, the preservation of the geomorphic expression of a landslide deposit on the lake floor may also depend on the slide mechanism: frontally confined lobes of landslides may be longer preserved in the morphology of the lake floor over time due to their distinct outlines and bulges expressing frontal thrusting.

The age information of the slide deposits, combined with the calculated surface roughness, allowed assigning a high surface roughness with a recent slide age and a smooth surface roughness with a sub-recent slide age. Because of this successful relative dating of the subaqueous landslides with the surface roughness, expressed by the standard deviation of the TPI, an attempt of relating the absolute age of the slides to the standard deviation of the TPI was conducted (Fig. 2.6). We tested whether it is possible to calculate the slide age numerically as a function of the smoothing of the translation area, provided by the sedimentation. Results indicate that for sub-recent slides our approach may be indeed used to derive first-order ages of landslides, based on the surface-roughness of their translation area. Fig. 2.6 shows for these slides ranging in age between 150 and 5000 years, a correlation between the standard deviation of TPI and age can be quantified with a linear fit (R^2 of 0.64). However, a broad range of standard deviation values of the TPI for the recent slides (i.e. ~0.05 to 0.09; Fig. 2.6 and Tab. 2.2) makes it difficult to assign a roughness value to an absolute age for subaqueous slides of the last ~150 years. Reasons for the relatively broad variety of roughnesses of the recent slides may be related the reactivation of previous landslide scars and overriding of a pre-defined topography, or to different slide mechanisms.

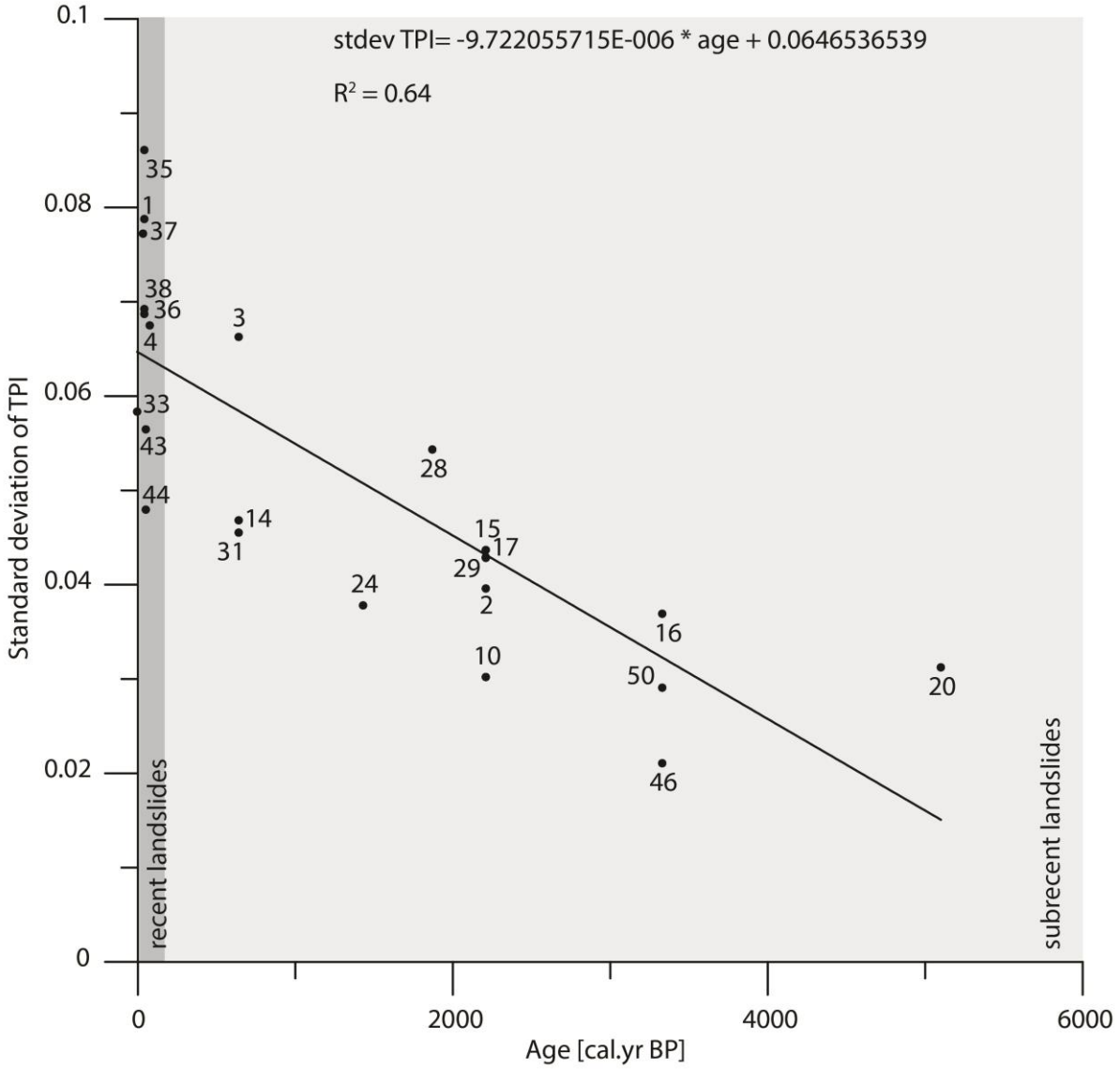


Figure 2. 6 Standard deviation of the Topographic Position Index (TPI) plotted vs. slide ages from Strasser et al. 2013. Translation areas Nr. 27 and 45 that may correspond to slide deposits of greatly differing ages (Tab. 2.2) were not plotted.

2.5.3 Outlook

The similar spatial resolution between the bathymetric dataset and publicly available elevation data (e.g. SwissAlti3D LiDAR data; Swisstopo 2014) may allow the investigation of processes in amphibious seamless topography models, allowing in particular new insights in processes crossing the terrestrial and lacustrine realms (e.g. subaerial slope failures) or vice versa (e.g. tsunamis, inundations). Such calculations, however, ideally require that no "white zone" (i.e. lack of data) occurs between the DBM and the DEM (e.g. Lecours et al. 2016). Areas of less than ~5 m water depth, however, are only inefficiently surveyed using swath bathymetric tools, so that high-resolution DBMs of these zones are often missing (as is the case of Lake Zurich). The missing data connecting the two DTMs can be acquired with airborne LIDAR techniques using a green laser allowing

penetration of a few meters below the lake level, as has been demonstrated in other perialpine lakes such as Lake Constance (Wessels et al. 2015a; Wessels et al. 2015b).
To further develop and calibrate our proposed concept of correlating relative and absolute landslide ages to the zonal standard deviation of the TPI, more high-resolution datasets containing information on ages morphologies of the translation areas from various lakes are desired. The here presented approach may lead to better results with more data and after a detailed selection of translation areas with similar preconditions (e.g. slope gradient, landslide-history, slide depth, occurrence in multiple phases, frontal emplacement style). A vision of our approach is to be able to estimate an age range of subrecent subaqueous landslides just based on a high-resolution bathymetric dataset and knowledge about the sedimentation rate.

2.6 Conclusions

In this article, traces of subaqueous landslides identifiable in the high-resolution bathymetric dataset from Strupler et al. (2015) were mapped and quantitatively characterised. The main outcomes are:

- A total of 50 landslide translation areas on the lateral slopes were mapped with a Geographic Information System.
- Most of the mapped slides have a size of the translation area of <0.05 km^2 and headscarps in shallow water depths (<10 m below lake level).
- Ages of subrecent slides, 150-5000 years in age, can be quantitatively estimated with the standard deviation of the ‘topographic postion index (TPI)' derived from high-resolution bathymetric data using a linear equation with an R^2 of 0.64.
- The standard deviation of the TPI of recent slides (i.e. younger than ~150 years) varies substantially, so that with existing bathymetry data alone, their ages cannot be discerned.
- Even with a high-resolution digital bathymetric model, only the last generations of overlapping subaqueous landslides can be identified. Slides that occurred more than ~5000 years at the slopes of Lake Zurich and whose translation area was smoothed by sedimentation and other slope processes, can only be investigated with seismic reflection analyses.

Acknowledgements

This work was supported by the Swiss National Foundation Grant Nr. 133481. Swisstopo geodata was reproduced with the authorisation JA100120. We acknowledge Robert Hofmann, Reto Seifert, Stefano Fabbri and Tobias Schwestermann for their efforts during the bathymetric data acquisition. Katrina Kremer is acknowledged for her comments on the manuscript.

References

BFS (2009) Die grössten Seen und höchsten Berge. https://www.bfs.admin.ch/bfs/de/home/statistiken/kataloge-datenbanken/tabellen.assetdetail.104833.html. Accessed 10 Mar 2017

Bini A, Corbari D, Falletti P, Fassina M, Perotti CR and Piccin A (2007) Morphology and geological setting of Iseo Lake (Lombardy) through multibeam bathymetry and high-resolution seismic profiles. Swiss Journal of Geosciences 100:23–40. doi: 10.1007/s00015-007-1204-6

Bozzano F, Mazzanti P, Anzidei M, Esposito C, Floris M, Fasani GB and Esposito A (2009) Slope dynamics of Lake Albano (Rome, Italy): insights from high resolution bathymetry. Earth Surface Processes and Landforms 34:1469–1486. doi: 10.1002/esp.1832

Cooley SW (2015) GIS4Geomorphology. http://www.gis4geomorphology.com. Accessed 28 Aug 2015

Cruden DM and Varnes DJ (1996) Landslide Types and Processes. In: A.K. T, Shuster RL (eds) Landslides Investigation and Mitigation; Transportation Research Board. National Research Council, Special Report 247, Washington DC, pp 36–75

Field ME, Gardner J V. and Prior DB (1999) Geometry and significance of stacked gullies on the northern California slope. Marine Geology 154:271–286. doi: 10.1016/S0025-3227(98)00118-2

Frey-Martínez J, Cartwright J and James D (2006) Frontally confined versus frontally emergent submarine landslides: A 3D seismic characterisation. Marine and Petroleum Geology 23:585–604. doi: 10.1016/j.marpetgeo.2006.04.002

Glenn NF, Streutker DR, Chadwick DJ, Thackray GD and Dorsch SJ (2006) Analysis of LiDAR-derived topographic information for characterizing and differentiating landslide morphology and activity. Geomorphology 73:131–148. doi: 10.1016/j.geomorph.2005.07.006

Heim A (1876) Bericht und Expertengutachten über die im Februar und September 1875 in Horgen am Zürichsee vorgekommenen Rutschungen. Die Eisenbahn 4:191–196.

Hilbe M, Anselmetti FS, Eilertsen RS, Hansen L and Wildi W (2011) Subaqueous morphology of Lake Lucerne (Central Switzerland): Implications for mass movements and glacial history. Swiss Journal of Geosciences 104:425–443. doi: 10.1007/s00015-011-0083-z

Hsü KJ and Kelts K (1970) Seismic investigation of Lake Zurich: Part II Geology. Eclogae geol Helv 63:525–538.

Hühnerbach V and Masson DG (2004) Landslides in the North Atlantic and its adjacent seas: An analysis of their morphology, setting and behaviour. Marine Geology 213:343–362. doi: 10.1016/j.margeo.2004.10.013

Keller O and Krayss E (2005) Der Rhein-Linth-Gletscher im letzten Hochglazial. 1. Teil: Einleitung, Aufbau und Abschmelzen des Rhein-Linth-Gletschers im Oberen Würm. Verteljahrsschrift der Naturforschenden Gesellschaft in Zürich 150:19–32.

Kelts K (1978) Geological and sedimentary evolution of Lakes Zurich and Zug, Switzerland. ETH Zurich, PhD Thesis, Nr.6146

Kelts K and Hsü KJ (1980) Resedimented facies of 1875 Horgen slumps in Lake Zurich and a process model of longitudinal transport of turbidity currents. Eclogae geol Helv 73:271–281.

Kremer K, Hilbe M, Simpson G, Decrouy L, Wildi W and Girardclos S (2015) Reconstructing 4000 years of mass movement and tsunami history in a deep peri-Alpine lake (Lake Geneva, France-Switzerland). Sedimentology 1305–1327. doi: 10.1111/sed.12190

Kuen E (1999) Der Uferabbruch im Kusen. In: Küsnachter Jahrheft. Ortsgeschichtliche Kommission der Kulturellen Vereinigung Küsnacht, pp 44–50

Lecours V, Dolan MFJ, Micallef A and Lucieer VL (2016) A review of marine geomorphometry, the quantitative study of the seafloor. Hydrology and Earth System Sciences 20:3207–3244. doi: 10.5194/hess-20-3207-2016

Locat J and Lee HJ (2002) Submarine landslides: advances and challenges. Canadian Geotechnical Journal 39:193–212. doi: 10.1139/t01-089

McAdoo BG (1999) Mapping Submarine Slope Failures. In: Wright D, Bartlett D (eds) Marine and Coastal Geographical Information Systems. Taylor & Francis Group, London, p 17

Miller H, Bull JM, Cotterill CJ, Dix JK, Winfield IJ, Kemp AES and Pearce RB (2013) Lake bed

geomorphology and sedimentary processes in glacial lake Windermere, UK. Journal of Maps 9:299–312. doi: 10.1080/17445647.2013.780986

Moernaut J and De Batist M (2011) Frontal emplacement and mobility of sublacustrine landslides: Results from morphometric and seismostratigraphic analysis. Marine Geology 285:29–45. doi: 10.1016/j.margeo.2011.05.001

Nipkow F (1927) Über das Verhalten der Skelette planktischer Kieselalagen im geschichteten Tifenschlamm des Zürich- und Baldeggersees. ETH Zurich, PhD Thesis, Nr. 455

Reusch A (2015) Sublacustrine paleoseismology and fluid flow in the Western Swiss Molasse Basin: New constraints from the sedimentary archive of Lake Neuchâtel. PhD Thesis ETH Zurich, Nr. 232131.

Schindler C (1968) Zur Quartärgeologie zwischen dem untersten Zürichsee und Baden. Eclogae geol Helv 61:395–433.

Schindler C (1974) Zur Geologie des Zürichsees. Eclogae geol Helv 67:163–196.

Schindler C (1976) Eine geologische Karte des Zürichsees und ihre Deutung. Eclogae geol Helv 69:125–138.

Schlund RA (1972) Zürichsee: topogr. Plan 1:5000. Meliorations- und Vermessungsamt des Kt. Zürich.

Schnellmann M, Anselmetti FS, Giardini D and McKenzie JA (2005) Mass movement-induced fold-and-thrust belt structures in unconsolidated sediments in Lake Lucerne (Switzerland). Sedimentology 52:271–289. doi: 10.1111/j.1365-3091.2004.00694.x

Strasser M, Hilbe M and Anselmetti FS (2011) Mapping basin-wide subaquatic slope failure susceptibility as a tool to assess regional seismic and tsunami hazards. Marine Geophysical Research 32:331–347. doi: 10.1007/s11001-010-9100-2

Strasser M, Monecke K, Schnellmann M and Anselmetti FS (2013) Lake sediments as natural seismographs: A compiled record of Late Quaternary earthquakes in Central Switzerland and its implication for Alpine deformation. Sedimentology 60:319–341. doi: 10.1111/sed.12003

Strupler M, Hilbe M, Anselmetti FS, Kopf AJ, Fleischmann T and Strasser M (2017) Probabilistic stability evaluation and seismic triggering scenarios of submerged slopes in Lake Zurich (Switzerland). Geo-Marine Letters 37:241–258. doi: 10.1007/s00367-017-0492-8

Strupler M, Hilbe M, Anselmetti FS and Strasser M (2015) Das neue Tiefenmodell des Zürichsees: Hochauflösende Darstellung der geomorphodynamischen Ereignisse im tiefen Seebecken. Swiss Bull angew Geol 20:71–83.

Swisstopo (2014) Das hoch aufgelöste Terrainmodell der Schweiz. Detaillierte Produktinformation. Bundesamt für Landestopografie swisstopo, Wabern

Weiss A (2001) Topographic position and landforms analysis. Poster Presentation. ESRI User Conference, San Diego, CA.

Welti G (1950) Flugbild und subaquatische Geomorphologie : Beobachtungen bei Rapperswil. Geographica Helvetica 5:293–295. doi: 10.5194/gh-5-293-1950

Wessels M, Anselmetti F, Artuso R, Baran R, Daut G, Gaide S, Geiger A, Groeneveld JD, Hilbe M, Möst K, Klauser B, Niemann S, Roschlaub R, Steinbacher F, Wintersteller P and Zahn E (2015a) Bathymetry of Lake Constance - A high-resolution survey in a large, deep lake. ZFV - Zeitschrift fur Geodasie, Geoinformation und Landmanagement 140:203–210. doi: 10.12902/zfv-0079-2015

Wessels M, Anselmetti F, Artuso R, Baran R, Daut G, Roschlaub R, Steinbacher F, Wintersteller P and Zahn E (2015b) Bathymetry of Lake Constance State-of-the-art in surveying a large lake. Hydrographische Nachrichten 100:6–11.

Chapter 3

Probabilistic stability evaluation and seismic triggering scenarios of submerged slopes in Lake Zurich (Switzerland)

This chapter was published as: Strupler, M., Hilbe, M., Anselmetti, F.S., Kopf, A.J., Fleischmann, T., and Strasser, M. 2017. Probabilistic stability evaluation and seismic triggering scenarios of submerged slopes in Lake Zurich (Switzerland). Geo-Marine Letters 1–18. doi: 10.1007/s00367-017-0492-8.

Abstract

Subaqueous landslides and their consequences, such as tsunamis, can cause serious damage to offshore infrastructure and coastal communities. Stability analyses of submerged slopes are therefore crucial, yet complex steps for hazard assessment, as many geotechnical and morphological factors need to be considered. Typically, deterministic models with data from a few sampling locations are used for the evaluation of slope stabilities, as high efforts are required to ensure high spatial data coverage. This study presents a simple but flexible approach for the probabilistic stability assessment of subaqueous slopes that takes into account the spatial variability of geotechnical data. The study area (~2 km^2) in Lake Zurich (northern Switzerland) shows three distinct subaquatic landslides with well-defined headscarps, translation areas (i.e. the zone where translational sliding occurred) and mass transport deposits. The ages of the landslides are known (~2210 and ~640 cal. yr BP, and 1918 AD), and their triggers have been assigned to different mechanisms by previous studies. A combination of geophysical, geotechnical, and sedimentological methods served to analyse the subaquatic slope in great spatial detail: 3.5 kHz pinger seismic reflection data and a 300 kHz multibeam bathymetric dataset (1 m grid) were used for the detection of landslide features and for the layout of a coring and an in situ cone penetration testing campaign. The assignment of geotechnical data to lithological units enabled the construction of a sediment-mechanical stratigraphy that consists of four units, each with characteristic profiles of bulk density and shear strength. The thickness of each mechanical unit can be flexibly adapted to the local lithological unit thicknesses identified from sediment cores and seismic reflection profiles correlated to sediment cores. The sediment-mechanical stratigraphy was used as input for a Monte Carlo simulated limit-equilibrium model on an infinite slope for the assessment of the present slope stability and for a back analysis of past landslides in the study area, both for static and earthquake-triggered scenarios. The results show that the location of failure initiation in the model is consistent with stratigraphic analysis and failure-plane identification from sediment cores. Furthermore, today's sediment-charged slopes are failure-prone, even for a static case. This approach of including an adaptable sediment-mechanical stratigraphy into a limit-equilibrium slope stability analysis may be applied as well to the marine realm.

3.1 Introduction

Slope instabilities can have serious consequences in the marine and the lacustrine environment. As a consequence of unstable slopes, subaquatic landslides can occur, which in turn can produce tsunamis (Jiang and Leblond 1992). Both subaqueous landslides and landslide-triggered tsunamis can pose hazards to shore communities and to infrastructure onshore and at the sea/lake bottom (e.g. Prior et al. 1982; Tappin et al. 2001; Locat and Lee 2002; Schnellmann et al. 2002; Masson et al. 2006; Dan et al. 2007). Stability evaluations of submerged slopes are thus crucial steps for assessing such hazards.

Various approaches for slope stability assessments (SSAs) exist, depending on the purpose and scale. Reflected in extensive documentation in the geotechnical literature, the limit-equilibrium method is used in most cases (Johari and Javadi 2012). With this method, a slope is considered unstable if the downward-driving shear stress exceeds the resisting shear strength (e.g. Kramer 1996; Abramson et al. 2002). Changes in stress and shear strength may result from various geological, physical and human-induced processes (e.g. erosion, rapid sedimentation, earthquakes, wave loading, water level changes and fluid escape; e.g. Locat and Lee 2002; Chapron et al. 2004). In many cases, the presence of a weak layer in the sedimentary succession facilitates slope failures (e.g. Craig 2004; Leynaud et al. 2004; Biscontin and Pestana 2006; Dan et al. 2007).

For earthquake-triggered landslides, back analyses are a valuable tool for estimating the intensities of past earthquakes (Leynaud et al. 2004; Strasser et al. 2007, 2011). The greatest uncertainties for SSAs are often associated with the soil properties (Craig 2004). Due to limitations in cost and time, slope stability models are often treated as deterministic models, considering data from a few sampling locations that are assumed to represent the characteristics of the entire slope. Hence, the spatial variability of slope geotechnical parameters often remains underexplored (Klaucke and Cochonat 1999; Leynaud and Sultan 2010). A probabilistic SSA is needed, however, to account for the spatial variation of the geotechnical properties and uncertainties (Chandler 1996; Lacasse and Nadim 1996; Leynaud and Sultan 2010; Johari and Javadi 2012). In many approaches, gradients of geotechnical parameters (e.g. density, shear strength) are used to estimate values with depth, providing acceptable results in areas where the thickness of lithological units shows little spatial variation (e.g. Strasser et al. 2011). However, the use of only a few gradients describing the geotechnical parameters within lithological units often ignores variations. Additionally, for locally very thick lithological units, extrapolation of data with gradients can lead to an overestimation of values.

The main aim of this study is to design a simple, powerful concept for a quantitative SSA under static and seismic loading that accounts for the spatial variability of geotechnical parameters. Compared to a deterministic analysis, a probabilistic analysis has the advantages of incorporating parameter uncertainty and allows the quantification of that uncertainty (Wolff 1996). A high spatiotemporal understanding of the slope characteristics is a prerequisite for constructing a probabilistic slope stability concept. This study focuses on a well-constrained slope in Lake Zurich, Switzerland, where three distinct subaquatic landslides with known ages have occurred (two of them interpreted as earthquake-triggered; Strasser and Anselmetti 2008; Strasser et al. 2013). High-resolution geophysical, geotechnical and sedimentological data from the undisturbed slope adjacent to the

subaqueous landslides are used for a probabilistic SSA: Monte Carlo simulated (MCS) input data from a sediment-mechanical stratigraphy are integrated into a limit-equilibrium model. With this approach, the present study analyses (i) the location of failure initiation of the documented subaqueous landslides, (ii) the pseudostatic critical acceleration needed to create the two earthquake-triggered landslides in the study area and (iii) the current slope stability with the present sediment drape under static and possible earthquake-shaking conditions.

3.2 Physical setting and previous studies

Lake Zurich is a glacially overdeepened, perialpine lake in northern Switzerland (~47°N, 8.5°E, 406 m a.s.l.), which consists of Lake Zurich sensu stricto and the upstream Obersee (Fig. 3.1). The two parts of the lake are separated by an end moraine from the last glaciation. Within Lake Zurich, an escarpment in the molasse bedrock separates an up to 136 m deep northern basin with steep slopes and a flat basin plain from a ~25 m deep southern basin (Schindler 1974). The molasse bedrock is overlain by an up to ~154 m thick Quaternary infill, consisting of glacial, glaciolacustrine and lacustrine deposits (Schlüchter 1984; Lister et al. 1984). The permeability of the molasse bedrock in the study area has been described as very low (Bitterli et al. 2004).

The postglacial sedimentary succession in the deep basin (Table 3.1) is known from previous studies (Schindler 1974; Gyger et al. 1976; Giovanoli 1979; Strasser and Anselmetti 2008): The till-covered bedrock is overlain by a thick succession of late glacial bluish to light grey muds (with high plasticity), which originate from current-dispersed suspended sediment (Schindler 1974). The lower part of these plastic muds contains some ice-rafted debris, which disappear in the upper part (Gyger et al. 1976). The latter shows some cm-thick lamination, interpreted as produced by glacial cycles by Giovanoli (1979). The overlying sediments display a beige colour, which indicates aeolian input of sediment exposed to surface weathering (Giovanoli 1979). During the Younger Dryas, blackish iron sulphide muds, containing small organic particles and almost no carbonate, were deposited. With subsequent further warming into the Holocene, lacustrine chalks and marls were deposited (Schindler 1974; Gyger et al. 1976; Giovanoli 1979). In contrast to this basinal sequence, the sedimentary succession on the slopes has not been systematically analysed so far. Moreover, no publically available high-resolution geotechnical survey data exist for the slopes of Lake Zurich. Only some data on the mechanical behaviour of the postglacial sediments in the southern part of Lake Zurich are available (Gyger et al. 1976), where it was concluded that the physical characteristics of the different lithological units vary strikingly. A study by Strasser et al. (2008) classified the postglacial lithological succession in three lithological units (LUs) and dated them (Table 3.1). The present study refers to that classification.

Table 3. 1 *Postglacial lithological units and their ages* (Strasser et al. 2008)

Lithological unit	**Age**
LU3b: lacustrine marls	Present day to ~7,000 cal. yr BP
LU3a: lacustrine chalks	~7,000 to ~12,000 cal. yr BP
LU2: iron sulphide muds	~12,000 to ~14,500 cal. yr BP
LU1: late glacial plastic muds	~14,500 to ~17,600 cal. yr BP

Since deglaciation, subaquatic mass movements occurred repeatedly in Lake Zurich's deep basin, triggered by sediment overload, earthquakes or anthropogenic influence on the shores (Schindler 1976; Kelts and Hsü 1980; Strasser et al. 2006, 2013). Strasser and Anselmetti (2008) provide well-constrained ages for the landslides. For five events with simultaneously triggered subaquatic mass movements, earthquakes are the assumed trigger (Strasser and Anselmetti 2008). Synchronous basinwide landslide occurrences are a typical signature for earthquake-triggered landslides in perialpine lakes (e.g. Schnellmann et al. 2006; Strasser et al. 2013). In the last ~150 years, a few subaquatic landslides have occurred in the northern basin of Lake Zurich, all triggered by human activity (e.g. Heim 1876; Nipkow 1927; Kelts and Hsü 1980).

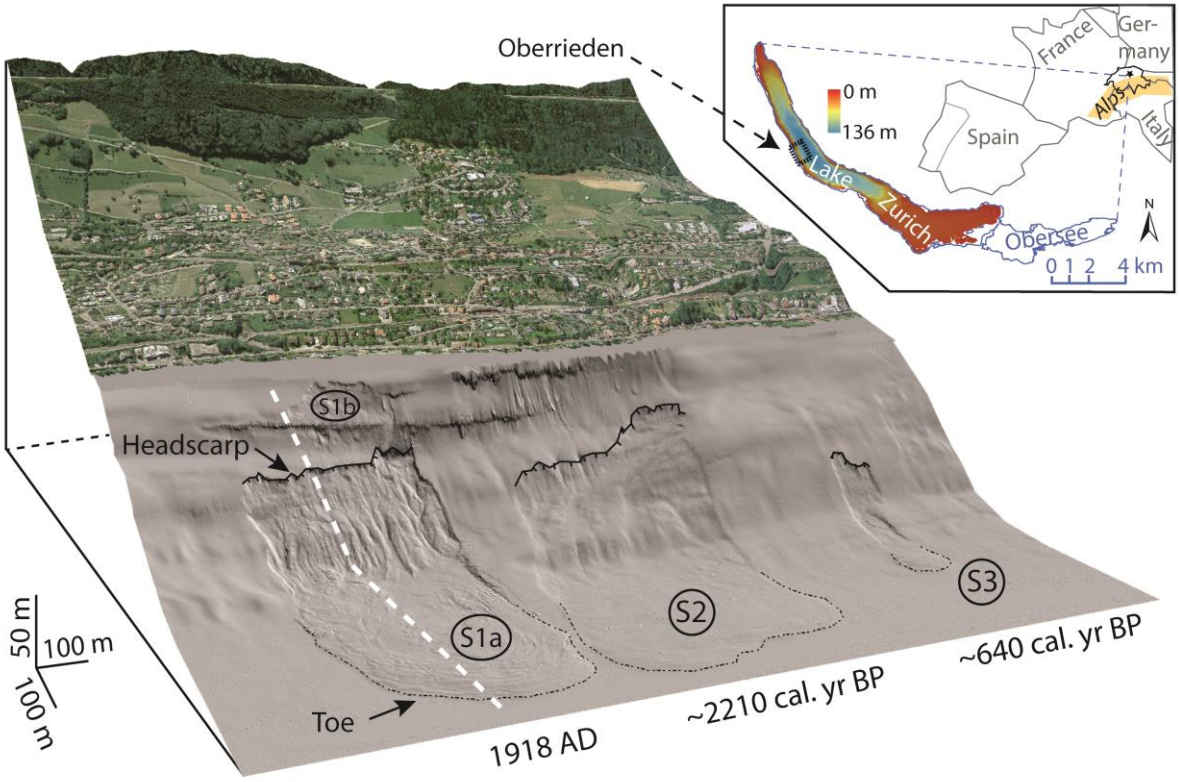


Figure 3. 1 *Three-dimensional representation of the DDM representing the study area. The southernmost landslide (S1a) occurred in 1918 AD, the slide in the centre (S2) ~2210 cal. yr BP, and the slide in the north (S3) ~640 cal. yr BP. Vertical exaggeration: 3×. View towards the west. Dashed white line: Seismic profile shown in Fig. 3.2. Subaqueous DDM: Strupler et al. (2015). Subaerial LiDAR-DEM and Orthophoto: Swisstopo*

The study site is located on the western flank of the northern basin, offshore the village of Oberrieden. In an area of ~2 km^2, the site comprises three distinct NE-facing translational, frontally confined subaquatic landslides (Fig. 3.1). The southernmost landslide (S1a in Fig. 3.1 and Table 3.2), dated to 1918 AD, was triggered by human activity onshore (Nipkow 1927). The slides in the middle sector (S2 in Fig. 3.1 and Table 3.2, ~2210 cal. yr BP) and in the north (S3 in Fig. 3.1 and Table 3.2, ~640 cal. yr BP) are assumed to have been triggered by earthquakes (Strasser and Anselmetti 2008). Because the slope is not affected by river inflows and shows no fluid-escape features in the bathymetric dataset, and because the bedrock has a very low permeability, the site is well suited for a simple SSA approach.

Upslope of S1a, in the shallow nearshore area (~10 m water depth; Fig. 3.1), a smaller eroded patch (S1b) with a ~4 m high headscarp and an areal coverage of ~15,000 m^2 can be found. No visible connection occurs between the main slide S1a and S1b. However, a part of the eroded material of the small, upper slide is deposited directly above the headscarp of S1a (Fig. 3.1). Between the extents of each slide, some patches of undisturbed sediment drape exist. The two slides S1a and S2 show similar outlines and dimensions and their eroded sediment volume is estimated at about 10^6 m^3 (Table 3.2). Their failure scars extend laterally to ~400 m.

Table 3. 2 Overview characteristics of the slides (Strupler et al. 2015)

	S1a	**S2**	**S3**
Age	1918 AD	~2210 cal. yr BP	~640 cal. yr BP
Erosion area (m^2)	~160’000	~150’000	~17’000
Depth headscarp (m below lake level)	51	42	76
Max. water depth of deposits (m below lake level)	135	135	133
Runout distance (m)	865	791	383
Height of headscarp (m)	~5	~5–7	~3–4
Landslide volume (m^3)[a]	~800’000	~750’000 to 105’0000	~51’000 to 68’000

[a]Estimated by multiplication of erosion area and headscarp height

Reflection seismic data from the slopes (Strasser and Anselmetti 2008) display a seismic-stratigraphic unit with continuous parallel reflections of alternating amplitudes that overlies a unit with a chaotic, high-amplitude facies, which, in turn, covers the acoustic basement. Fig. 3.2 shows a seismic reflection profile along S1a (cf. dashed white line in Fig. 3.1), revealing an irregular slope with an alternating gradient (Fig. 3.2a). Between ~40 and 70 ms TWT, a steep zone (>30°) can be identified where no significant sedimentation occurs. A closeup of the failure scar of S1a (~5 m high; Table 3.2) can be found in Fig. 3.2b. The area affected by mass transport deposits (MTDs), characterized by a typical chaotic-to-transparent seismic facies (e.g. Schnellmann et al. 2002; Strasser and Anselmetti 2008), is highlighted in blue. It shows deformation of the basin-plain sediment (‘frontal thrusting’) expressed by topographic bulges (e.g. Schnellmann et al. 2005).

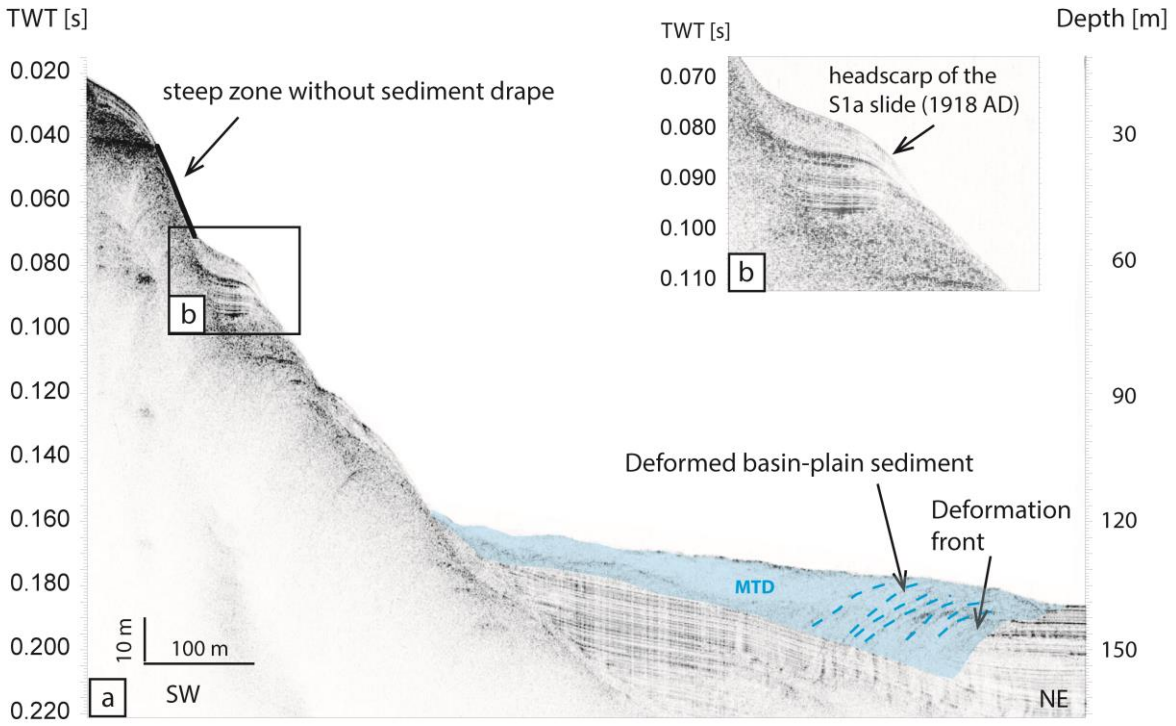


Figure 3. 2 Seismic profile of S1a (modified after Strasser and Anselmetti 2008). Seismic data are unmigrated, so that true geometries and sharp edges are masked by diffractions. Location of profile is shown on Fig. 3.1.

A short gravity core taken by Strasser et al. (2013) revealed that the glide plane of S1a consists of glacial deposits. This finding raises the question of whether the glide plane is located in the same lithological unit (or even in a specific weak layer within a unit) for all other subaqueous landslides in the study area and throughout each respective slide. A back analysis of the subaqueous landslides may support the seismic triggering with geotechnical arguments and quantitatively constrain pseudostatic critical accelerations needed to cause failure of these known occurrences.

3.3 Materials and methods

3.3.1 Geophysical data acquisition

A survey with a Kongsberg EM2040 multibeam echosounder (300 kHz) yielded a new high-resolution (1 m grid) digital depth model (DDM) of Lake Zurich (Strupler et al. 2015), enabling the investigation of the extent and geomorphic features of subaqueous landslides (Fig. 3.1). Slope gradient values derived from the DDM with a geographic information system (GIS) were used as input for the slope stability model. Calculations were done at a 5 m grid resolution.

An existing 3.5 kHz pinger seismic dataset (Strasser and Anselmetti 2008) was complemented by additional 3.5 kHz seismic data acquired in 2016 with the same equipment. No migration was applied to the seismic data. Conversion from two-way travel time to depth was conducted assuming a sonic

velocity of 1,500 m/s. The DDM and seismic dataset were used to determine locations for sediment coring and in situ cone penetration testing (CPT; Fig. 3.3).

3.3.2 Sediment coring and laboratory analysis

On the slopes offshore Oberrieden, seven Kullenberg-type piston cores (2.8 to 6 m long; Kelts et al. 1986) and 21 short gravity cores (maximum length: 1.3 m) were recovered from the floating platform ARARAT and from the research vessel ArETHuse respectively (Fig. 3.3). A handheld GPS device was used for positioning. The Kullenberg-type cores (except for ZH15-K13, which was taken in the translation area) were collected from the undisturbed slope sediments adjacent to the landslides to recover a continuous sedimentation record (Fig. 3.3). The short sediment cores were taken in the translation area to investigate the glide plane.

A sedimentological and geotechnical characterization of the cores was conducted in the laboratory. Bulk density ρ_{bulk} and magnetic susceptibility of the sediment core were logged with a multi-sensor core logger (MSCL; Geotek, Daventry, UK) using a sample interval of 1 cm. Subsequently, the sediment cores were split in two halves, photographed, and macroscopically described. Water content was measured by drying samples (sampling interval ~50 cm) in an oven for 24 h at 110 °C, following Blum (1997). Grain-size distribution was measured with a Malvern Mastersizer 2000s for selected cores (sampling interval ~50 cm). The undrained shear strength (s_u) was measured with a cone penetrometer at intervals of 5 cm. In addition, s_u was measured with laboratory vane tests at intervals of 50 cm.

3.3.3 CPT probing

In situ su profiles were measured using a free-fall CPT probe from Marum, Bremen (Stegmann et al. 2006a, 2006b) deployed from the ARARAT platform. The apparatus derives su from the measured resistance of the cone and the sleeve of the probe (Stegmann et al. 2006b). Configuration of the CPT length was adapted to thicknesses of seismic stratigraphic units, and varied between 2 and 6 m. For a more detailed information on CPT testing and processing, refer to Steiner et al. (2012) and Steiner (2013). Processing was conducted using a Nk value of 16. To cancel noise in the CPT su data, a 50 pt moving window filter was applied.

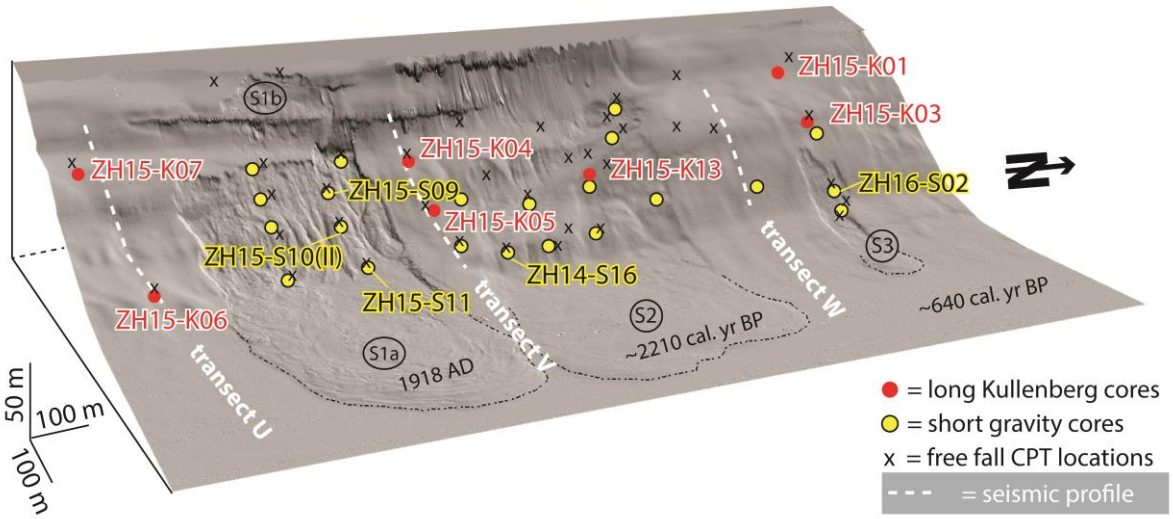


Figure 3. 3 Three-dimensional illustration of the study area with sediment core (red: Kullenberg-type cores, yellow: short gravity cores) and CPT locations. Vertical exaggeration: 3×. View towards the west. For coordinates, water depths and slope gradients of the core and CPT locations, refer to Tables C.1 and C.2 in the supplementary material in Appendix C.

3.3.4 Slope stability assessment

SSA was conducted with a limit-equilibrium model on an infinite slope for a static case and for earthquake-triggered scenarios. The infinite-slope model assumes planar slopes of infinite extent with a slope-parallel failure surface. Also, the failure depth is small compared to the length of the slope (Craig 2004; Coduto et al. 2011). An SSA was conducted along three transects on undisturbed sediment patches between the subaqueous slides. Each transect was analysed for reconstructed sediment drape thicknesses at the time of the S2 and S3 slides (with a sedimentation model; see Results section), and of the present-day conditions. The slope conditions (e.g. the slope gradient and thickness distribution of lithological units) are assumed to be similar to those in the neighbouring failed areas.

Water-saturated sediments with a low hydraulic conductivity are often assumed to be under undrained conditions when subjected to fast load changes, since water cannot flow into or out of the soil in a short time (Coduto et al. 2011). Therefore, the shear strength of Lake Zurich's slope sediments is described by s_u. The s_u data measured in situ by CPT were considered for the SSA. In a first step, the geotechnical data for ρ_{bulk} and s_u were assigned to lithological units, based on patterns of geotechnical parameters and visual core description. With these geotechnical data coupled to lithological units, a sediment-mechanical stratigraphy was constructed (see Results section).

The factor of safety (FS) on an infinite slope under undrained conditions was calculated according to Eq. 1 (Coduto et al. 2011):

$$\mathrm{FS} = \frac{s_u}{\gamma' * D * \sin\alpha * \cos\alpha} \qquad (1)$$

where γ' is the submerged unit weight, D the vertical depth below the lake bottom and α the slope gradient. Pore pressure is not considered in the equation, as the undrained shear strength is used.

A Matlab (Mathworks, Inc.) routine was used to calculate a deterministic FS-depth profile, the probability of failure (PoF) as well as the critical pseudostatic acceleration (a_c) needed to cause failure at selected model locations. The model conducts an independent SSA for each model location, assuming that each location is on an infinite slope with its respective slope gradient. The deterministic FS was calculated using the mean ρ_{bulk} and s_u from in situ CPT for each depth step from the sediment-mechanical stratigraphy.

For the probabilistic SSA in an MCS, 2500 FS-depth profiles were calculated for each model location with randomly sampled data from lognormal ρ_{bulk} and s_u distributions for each depth step. A lognormal distribution was used to avoid negative input values (e.g. Tobutt 1981; Lacasse and Nadim 1996; Abramson et al. 2002). The PoF results from the percentage of values in the FS distribution less than 1 (Chandler 1996).

The vertical error of the bathymetry (~0.5 m; Strupler et al. 2015) was simulated (MCS) in GIS after Zandbergen (2011) by adding a spatially auto-correlated error term to the original DDM. Subsequently, 2500 simulated slope maps were derived and implemented in the Matlab code.

a_c represents the effect of an earthquake by adding a constant acceleration to the failure mass (e.g. Kramer 1996). Therefore, it provides only approximate information on earthquake shaking (Jibson 2012). a_c, calculated with Eq. 2, assumes that the seismic force acts parallel to the slope (Newmark 1965; Jibson 1993):

$$a_c = (\mathrm{FS} - 1) * g * \sin\alpha \qquad (2)$$

To assess the quality of the results from the model, 2D profiles of the undisturbed slope with geotechnical data were used as an input for the professional SSA software SLIDE (Rocscience, Inc.). SLIDE conducts a 2D limit-equilibrium SSA to calculate a global mean FS with the Morgenstern and Price (1967) method.

3.4 Results

3.4.1 Slope characteristics

3.4.1.1 Geomorphic characteristics of the study area

Slope gradients vary between 0° and 58°, comprising alternating flat terraces (~5–10°) and steeper zones (~10–20°; Figs. 3.2, 3.4a). The headscarps of the three subaqueous slides are situated in the upper part of a steep zone (S1a and S2) or within a steep zone (S3). In the unfailed sediment patch between S1a and S2 (Fig. 3.1), a series of linear, isobath-parallel undulations with a width of ~5 m and an amplitude of ~10 cm can be identified in the shaded relief (~80–90 m water depth, ~20° slope gradient; Fig. 3.4b). These undulations cannot be identified in the reflection seismic dataset because the lateral dimension of the features is slightly lower than the lateral resolution (footprint) of the 3.5 kHz pinger seismic data at that depth.

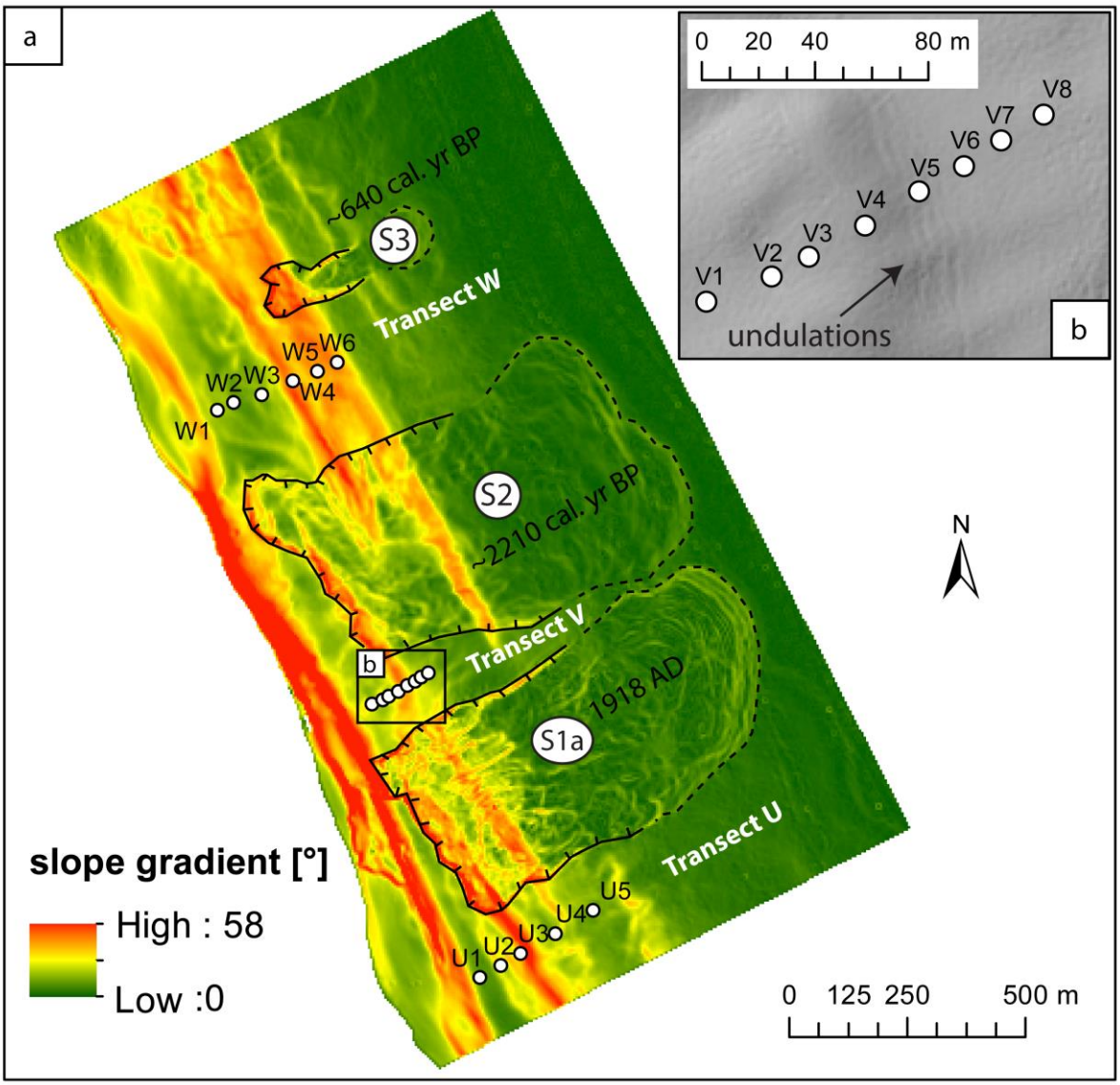


Figure 3. 4 *a) Slope gradient map and location of transects for modelling slope stability. B) Slope-transversal undulations on a shaded relief map*

3.4.1.2 Lithological units of the undisturbed slope

The six Kullenberg cores taken on the undisturbed slope (Fig. 3.3) enable a characterisation of the lithological succession on the slope. Core description and changes of geotechnical patterns allow the definition of different lithological units and subunits (Fig. 3.5; cf. Figs. 3.6 and 3.7), labelled in agreement with the postglacial lithological succession in Lake Zurich (Strasser et al. 2008). Depending on the water depth and slope gradient at the core locations, the individual unit thicknesses per core vary.

Describing from top to bottom, LU3c has a thickness of 10–60 cm and shows alternating organic and calcite couplets that represent varves, originating from lake eutrophication after the end of the 19th century (e.g. Kelts 1978; Giovanoli 1979). Due to the applied coring method, LU3c could not be recovered completely for some cores. Thickness of LU3c for those cores was estimated from

neighbouring short cores. LU3b (1.1–3 m thick) consists of dark-brown Holocene marls with a high silt content (~75–85%) and high water contents (more than 100% of dry weight). LU3a (0.7–1.4 m thick) shows a beige-white colour, a high sand content (up to 30%) and a high carbonate content. LU2 (0.15–0.5 m thick) is characterized by dark-grey to black clayey silts and low ρ_{bulk}. LU1 consists of a generally thin, beige-grey, homogeneous uppermost part with a strongly variable thickness amongst the cores (labelled as LU1b/c; subunits b and c described in Strasser et al. 2008 for the deep basin cannot be distinguished on the slopes). A bluish-grey, laminated part with densities of ~1.6 g/cm^3 (thickness: 0.1–2.9 m) in the middle (labelled as LU1a) can be distinguished from a lower part with dropstones. The occurrence of the dropstones is associated with an increase of ρ_{bulk} to >1.8 g/cm^3. LU1 is rich in clays (>25% clay content). Underneath the late glacial sediments of LU1, till occurs (Giovanoli 1979). Typically, the till shows poor sorting, no stratification, and the clasts are mostly angular (core ZH15-K13 in Fig. 3.6b) with ρ_{bulk} >2 g/cm^3.

3.4.1.3 Mechanical properties of the undisturbed slope

In all cores, the profiles of the sediment physical properties show characteristic patterns that generally correlate with the lithological units. Profiles of ρ_{bulk} and s_u show distinct changes at the boundaries between LU3b and LU3a, as well as at the boundaries between LU3a and LU2, between LU2 and LU1, and between the upper part of LU1 without clasts and the lower part with clasts (Fig. 3.5).

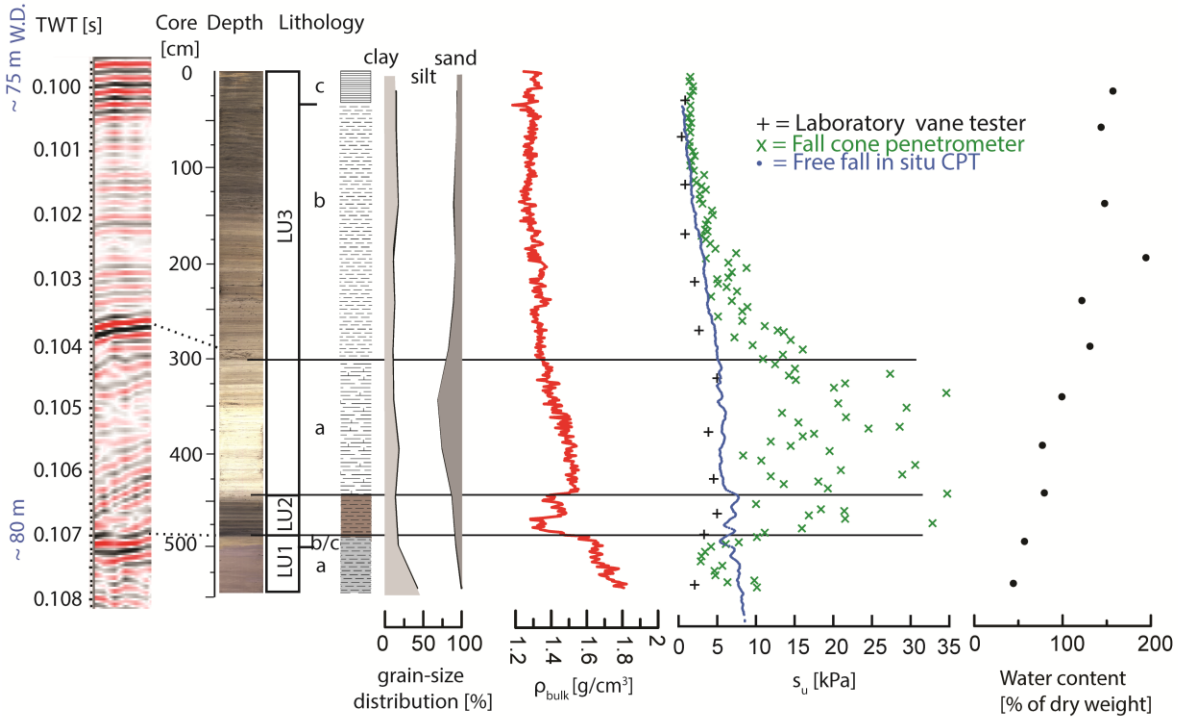


Figure 3. 5 Sediment-mechanical properties of the undisturbed slope, here at location ZH15-K04 (refer to Fig. 3.3 for core location)

ρ_{bulk} data show a slight linear increase with depth in LU3c and LU3b. In LU3a, the ρ_{bulk} profile has a convex shape that increases with depth to values of ~1.5 g/cm^3. It drops to a value of ~1.3 g/cm^3 in LU2 before it strongly increases to values exceeding 1.6 g/cm^3 in LU1.
The absolute values of s_u derived from different methods in situ and in the laboratory differ: results from the laboratory vane tests show the lowest values whereas the fall-cone tests show the highest values. In general, the three methods show a similar pattern: an increase of s_u with depth in the uppermost LU3b, roughly constant values in LU3a, fluctuations in LU2, and a decrease in values between LU2 and LU1. The s_u values measured with the fall cone are significantly higher for LU3a and LU2 when compared to LU1 and LU3b.
Generally, water content decreases linearly with depth. LU3c and LU3b have water contents between 194 and 122% of dry weight (mean: 148%), LU3a between 74 and 136% of dry weight (mean: 99%), LU2 between 88 and 168% (mean: 128%), and LU1 between 46 and 73% (mean: 56%).

3.4.1.4 Core-to-seismic correlation

The uppermost seismic stratigraphic unit with a facies of continuous parallel reflections is separated by two strong positive amplitude reflections. These reflections can be assigned from core-to-seismic correlation to the transition of LU1 to LU2 (slight increase in ρ_{bulk} and thus acoustic impedance) and the transition of LU3a to LU3b (distinct increase in ρ_{bulk}/impedance; Figs. 3.5 and 3.8). The transition between LU2 and LU3a cannot be differentiated with the reflection seismic data. The chaotic high-amplitude facies can be assigned to the till, and the acoustic basement to the molasse bedrock or till (distinction not always possible).

3.4.1.5 Lithological characteristics of the translation area

Results from the sediment cores taken in the translation areas of the subaquatic landslides show that Holocene marls (LU3b) and varves (LU3c) directly overlie late glacial plastic muds (LU1), and that LU3a and a large part of LU3b are missing (Fig. 3.6). These unconformities are also expressed in a sharp increase of ρ_{bulk} to ~1.6 g/cm^3. Fig. 3.6a shows three short cores taken along a depth transect of the slope eroded by S1a. In all three cores, a ~10 cm thick LU3c covers directly LU1a. For the topmost core in the transect (ZH15-S09), LU1a shows an undisturbed succession, whereas for the cores located more downslope (ZH15-S10(II) and ZH15-S11) LU1a is disturbed. Core ZH15-K13 from the translation area of S2 shows that most of LU1 has been eroded by the subaqueous landslide, as only ~70 cm of LU1a cover the underlying till (Fig. 3.6b). Core ZH14-S16, recovered near the toe of the slope, reveals the same stratigraphic depth of the glide plane. Thicknesses of LU3b and LU3c vary between 90 and 135 cm (see supplementary material in Appendix C Table C.3), depending on the water depth and slope gradient of the respective coring location. The core photograph and ρ_{bulk} profile of short core ZH16-S02 in the translation area of S3 (Fig. 3.6c) show that LU3b covers LU1b/c. Erosion of S3 does not reach as deep as for S1a and S2, where LU1b/c is missing in the cores in the translation areas.

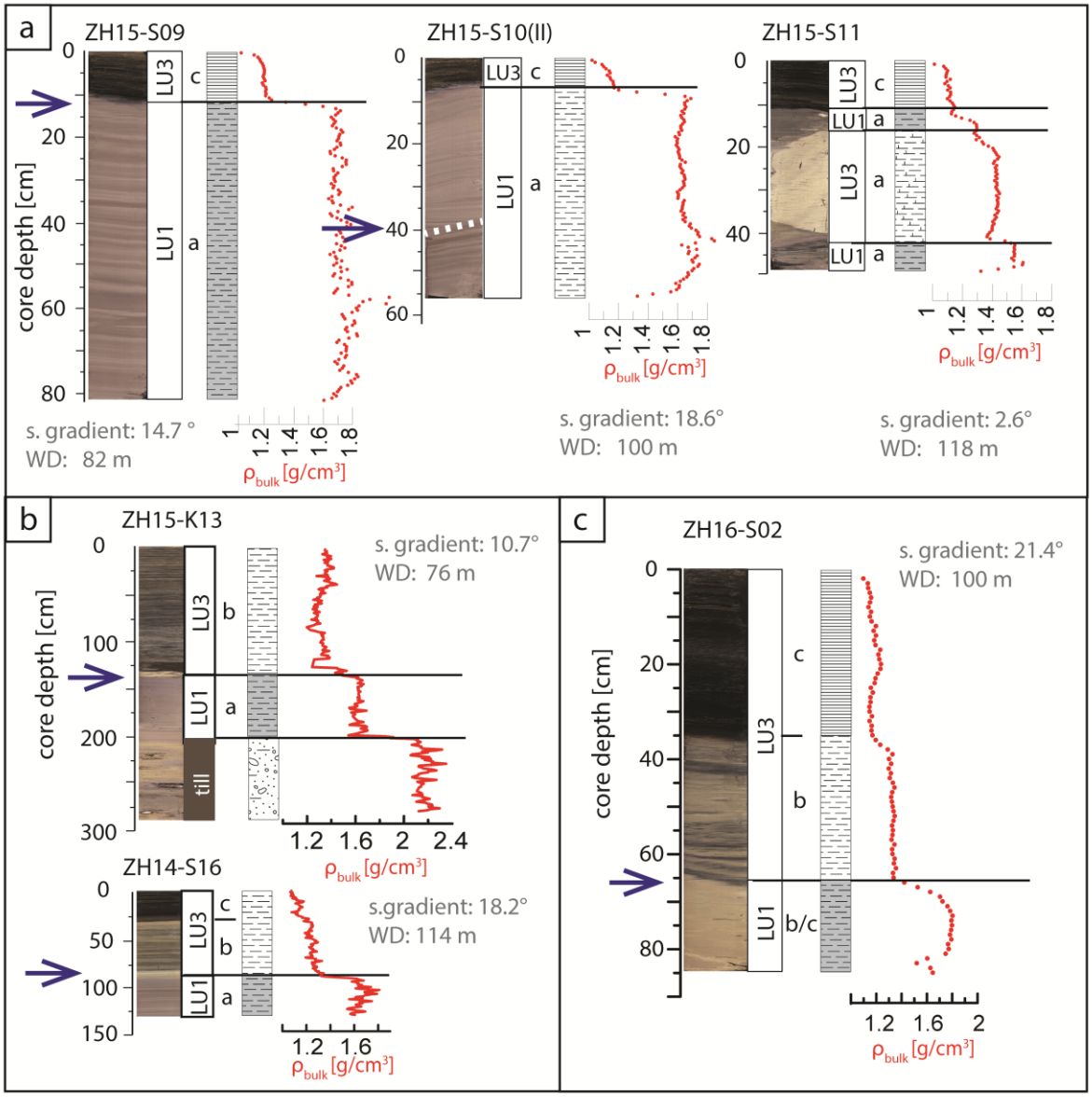


Figure 3. 6 Characteristics derived from sediment cores in the translation area of the three subaqueous landslides. a) Short cores taken on a transect in the translation area of the S1a slide. Dashed white line: Sharp change in lamination angles. b) Cores taken in the translation area of S2. c) Short core taken in the translation area of S3. Blue arrows: glide plane, S. gradient: slope gradient, WD: water depth. Refer to Fig. 3.3 for core locations.

3.4.2 Sediment-mechanical stratigraphy

The observation that s_u values from in situ CPT, laboratory fall-cone and vane-shear tests vary may be due to (1) s_u being significantly anisotropic (e.g. Craig 2004) or (2) different working concepts and calibration of the measuring devices. This study considers the s_u values from in situ CPT for the SSA, as the many data points obtained with this method qualify for statistical analysis (Lacasse and Nadim 1996). Furthermore, in situ CPT testing can be better than laboratory methods for assessing the

engineering properties of calcareous soils (such as lacustrine chalks; LU3a), due to difficulties in obtaining undisturbed samples for laboratory testing (Lunne et al. 2002).

The present study synthesizes a mechanical stratigraphy based on the fact that the profiles for ρ_{bulk} and CPT-derived s_u of each sediment core's lithological units show a similar pattern but different thicknesses, due to different sedimentation at the different coring locations (supplementary material in Appendix C, Table C.5). The geotechnical profiles per lithological unit amongst the sediment cores are stretched to a standard unit length (Eq. 3). By combining the geotechnical data per normalized unit from all the cores, the mean ρ_{bulk} and s_u profiles and their standard deviation per unit are calculated. For model simplicity reasons, stress history is neglected:

$$z_{\text{normalized}(i)} = \frac{z(i) - \min.(z(i))}{\text{length}(z(i))} * 100\,\text{cm} \qquad (3)$$

where $z(i)$ is the depth vector of lithological unit i (cm) and $z_{\text{normalized}(i)}$ is the normalized length of unit i (cm).

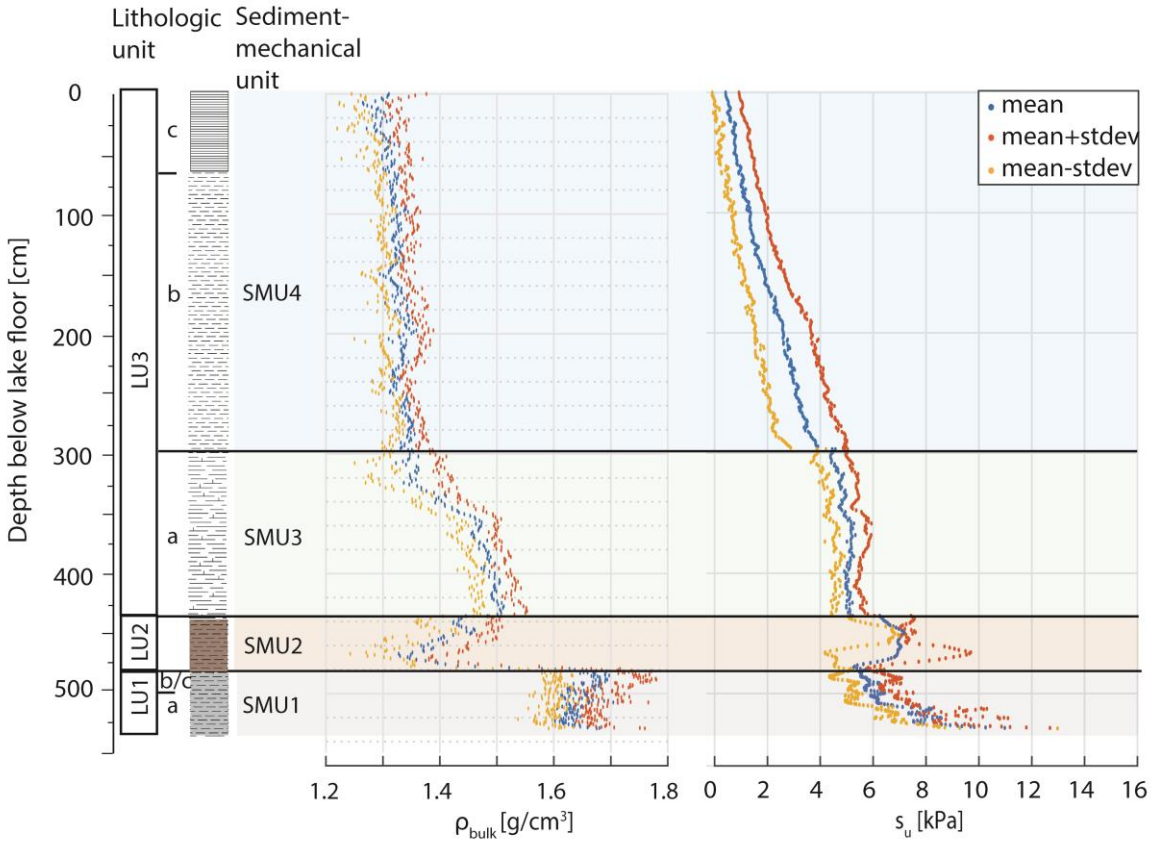


Figure 3. 7 Sediment-mechanical stratigraphy, showing mean ρbulk and mean su values from multiple Kullenberg-type cores and CPT locations respectively (blue). Yellow dots Mean values minus one standard deviation, red dots mean values plus one standard deviation. With this input, probability-density functions can be made for each depth step, and be used to select random values for each MCS run (here: mechanical units stretched to thicknesses of the lithological units at location K04)

The *sediment-mechanical stratigraphy*, consisting of four distinct sediment-mechanical units (SMUs), includes the spatial variability of the ρ_{bulk} and s_u data (Fig. 3.7). *SMU1* starts at the top of LU1 and ends where dropstones occur in the lower part of LU1a. Throughout the whole SMU1, density is greater than 1.6 g/cm^3. In situ s_u values from CPT increase from ~5 kPa at the unit top to ~10 kPa at the unit bottom.

SMU2 is defined as the part of the geotechnical profile containing LU2. Here, the ρ_{bulk} decreases sharply from ~1.5 to 1.35 g/cm^3 and the CPT s_u values fluctuate strongly.

SMU3 is defined by a convex shape in the ρ_{bulk} profile, which increases with depth from values of ~1.35 to ~1.5 g/cm^3, and by the constant s_u values of in situ CPT data (~5 kPa). SMU3 corresponds to LU3a.

SMU4 starts at the sediment surface and ends at the boundary between LU3b and LU3a. ρ_{bulk} at the unit top is ~1.3 g/cm^3 and increases linearly to ~1.35 g/cm^3 at the unit bottom. s_u increases downcore linearly from ~1 kPa at the top of the unit to ~4 kPa at the bottom.

While the amount of geotechnical input data for the mean ρ_{bulk} profile remains constant (n=6 cores) throughout the sediment-mechanical units (as ρ_{bulk} was measured in the laboratory on the cores), the amount of in situ CPT s_u profiles varies within the sediment-mechanical units, due to different penetration depths of the CPT device (n=8 for SMU4, n=6 for SMU3, n=4 for SMU2 and SMU1). The variability of the geotechnical data can be described by the coefficient of variation (CV, i.e. standard deviation divided by mean of a dataset). The CV of the ρ_{bulk} data is much smaller than that of the in situ CPT data (supplementary material in Appendix C, Table C.6). The highest variability in CPT s_u values is found in SMU4 (CV ~0.5) and the lowest variability in SMU3 (CV ~0.1).

3.4.2.1 Sedimentation model

From all the short cores taken in the translation areas, the thickness of the undisturbed sediment drape covering the glide plane (Fig. 3.6 and supplementary material in Appendix C, Table C.3) can be related to the slide age and water depth. A multivariate linear regression (supplementary material in Appendix C, Table C.4) leads to an empirical equation for estimating the sedimentary drape accumulation on the slope as a function of age and water depth (Eq. 4)—sediment drape accumulation (ΔZ, cm) since a landslide occurred at any location p:

$$\Delta Z_p(w,t) = 0.046 * t_p - 0.31 * w_p + 44.476 \quad (4)$$

where t_p is the age of landslide at location p (years) and w_p the water depth (m).

The reason for choosing this purely empirical model instead of one based on reconstructed sedimentation rates (dependent on water depth and slope gradient) is that the latter performs poorly. The presented linear regression provides good results for this particular slope for the thickness of the Holocene marls but should not be considered as valid for the whole basin.

3.4.2.2 Adapting sediment-mechanical units to local conditions

Using the core-to-seismic correlation, the thicknesses of SMU4 as well as the combined thickness of SMU2 and SMU3 can be calculated for any location where a reflection seismic profile exists

(Fig. 3.8). The thickness of SMU2 in the sediment cores of the present study is much smaller than the thickness of SMU3. With data from neighbouring sediment cores, the thickness of SMU2 is estimated and subtracted from the combined thickness of SMU3 and SMU2 to estimate the thickness of SMU3. The thickness of SMU1 can also be estimated from neighbouring cores.

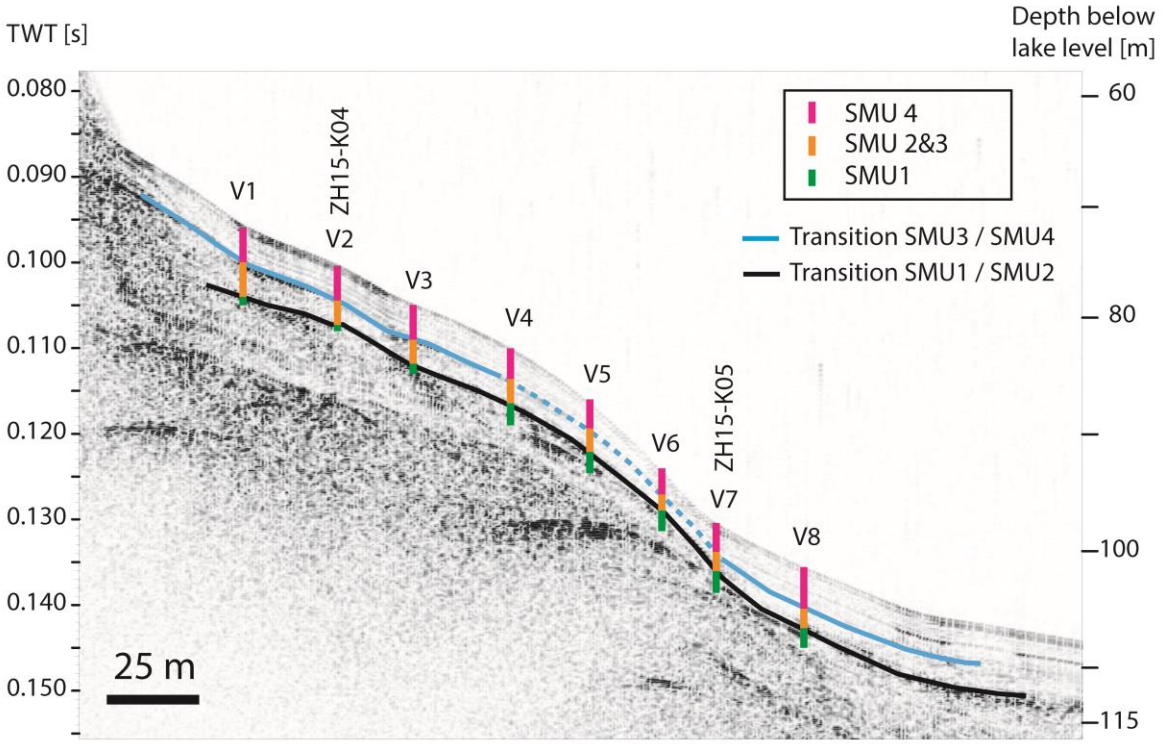


Figure 3. 8 Thicknesses of sediment-mechanical units according to core-to-seismic correlation. Black and blue horizons Strong reflections between SMU1 and 2 as well as SMU3 and 4 respectively. The dashed part of the blue horizon is interpreted, as the reflection was not visible in that part of the profile. Thicknesses of the individual units at the selected model locations V1–V8 can be found in the supplementary material (Appendix C, Table C.10). See Figs. 3.3 and 3.4 for locations of transects. Seismic profile modified after Strasser and Anselmetti (2008)

3.4.3 Slope stabilities

3.4.3.1 Static slope stability assessment

Thicknesses to subtract from the sediment drape for the model locations at the time of the S2 and S3 slides can be found in the supplementary material (Appendix C, Table C.11). Within the transects U, V and W, stabilities of the single modelled locations vary strongly (Figs. 3.9 and 3.10). Figure 3.9 shows PoF-depth and deterministic FS-depth profiles for a static scenario at two selected locations V5 and V7, both for the present situation and for the situation at the time of S2.

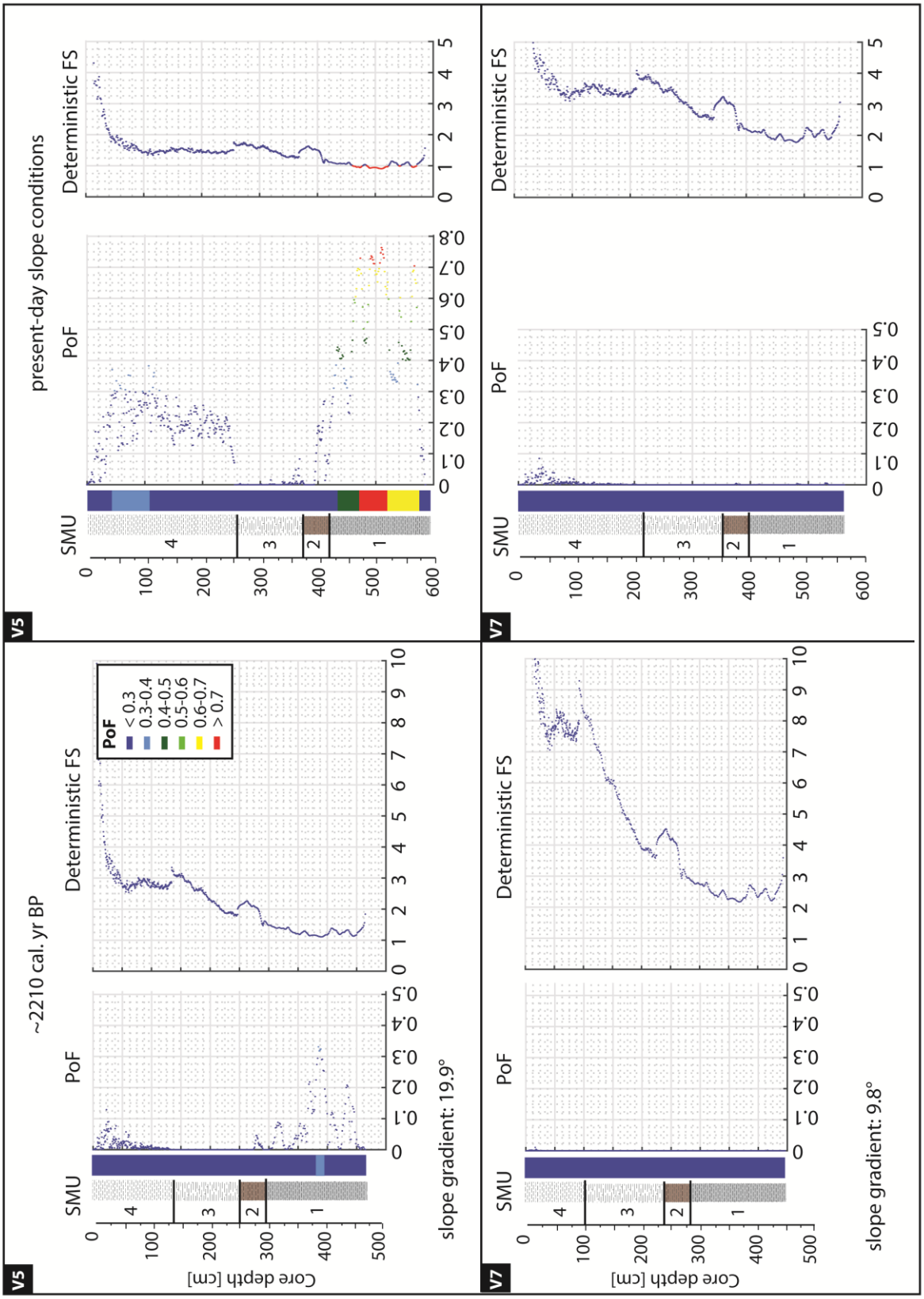


Figure 3. 9 PoF and deterministic FS for the back-calculated sedimentary drape ~2210 cal. yr BP (left) and for the present-day sedimentary drape at locations V5 (top) and V7 (bottom)

As the FS is directly proportional to s_u, a change in s_u with depth has a strong impact on the FS-depth profile. FS is also inversely proportional to the bulk density, slope gradient and thickness of the sediment drape covering the potential glide plane. This is demonstrated at the locations V5 and V7 (Figs. 3.9 and 3.10), which have similar SMU thicknesses: at V5, a slope gradient that is about twice as steep (~20° vs. ~10°) causes a decrease of the FS by a factor of 2 (minimum FS 1.1 vs. 2.2 for the FS-depth profiles of S2 and 0.9 vs. 1.8 for the present-day scenario). Generally, in the FS-depth profile, the FS decreases with depth. In SMU4, it decreases hyperbolically, in SMU3 linearly, and in SMU2 the FS increases again before decreasing smoothly in SMU1. Performing a back analysis of S2, i.e. reducing the sedimentary drape from the present-day situation by 122 cm (V5) and 119 cm (V7), increases the minimum FS of the FS-depth profiles towards a more stable situation by 0.2 for V5 and by 0.4 for V7.

Most of the PoF-depth profiles show PoF >0 in the uppermost part of SMU4, although the deterministic FS are much greater than 1 (Fig. 3.9). A high FS does not necessarily correspond to a low PoF (Nadim et al. 2005) as their relationship depends also on the uncertainties of the geotechnical factors involved. The high PoF in the uppermost part of SMU4, despite having a high FS, is related to the high variability of the geotechnical data in the top layer.Within the PoF-depth profiles V5 and V7, the highest PoFs is found in SMU1. For location V5, the additional load caused by sediment accumulation since ~2210 cal. yr BP increases the PoF from ~0.35 to 0.75. For location V7, the additional sediment load does not have a clear influence on the PoF. For all the model locations, the PoF remains close to zero in SMU3, even after an additional sediment load is applied.

Fig. 3.10 shows colour-coded static slope stability scenarios calculated for the sediment drape at ~2210 and ~640 cal. yr BP and for the present day on the three model transects. Generally, the highest PoF in the PoF-depth profile can be found in SMU1. Within a transect, PoFs are highest in steep zones (i.e. ~20°) with thick sediment cover on the potential failure plane. The minimum deterministic FS and maximum PoF of the FS-depth and PoF-depth profiles for each model location can be found in the supplementary material (Appendix C, Tables C.12 and C.13). For the scenario ~2210 cal. yr BP under static loading conditions, the deterministic FS is >1 for all model locations. Only some locations on the steep slope have a PoF slightly greater than 0.3 (U3: 0.38, V4: 0.43, V5: 0.33). For the ~640 cal. yr BP scenario under static loading conditions, locations U3, V4, V5 and W6 have a deterministic minimum FS of ≤1 in SMU1; for all the other model locations, the minimum FS is >1. On transect U, all PoFs except for U3 (0.63) are <0.2. On transect V, PoFs are <0.3 for all model locations except for V4 (PoF: 0.66) and V5 (PoF: 0.59). PoFs for transect W are <0.3 for SMU1 of all the locations except for W6 (PoF: 0.55). For the present-day situation, the minimum FS values range from 0.86 (V4) to 3.15 (U5). U3, V4, V5 and W6 have FS values <1, which implies that the slope is unstable at these locations in a deterministic analysis. In a probabilistic analysis, the maximum PoFs are 0.82 (U3), 0.83 (V4), 0.75 (V5) and 0.73 (W6), suggesting a high probability of static slope instability at these model locations for the present-day slope conditions. Locations W4 (PoF: 0.42) and W5 (PoF: 0.45) show medium probabilities of failure. The PoF of the relatively flat zones (slope gradient ~5–10°), however, is relatively low for the present-day sediment drape (i.e. <0.3). Since S2 occurred (~2210 cal. yr BP), additional sediment loading has doubled the PoF for the locations in the steep zones.

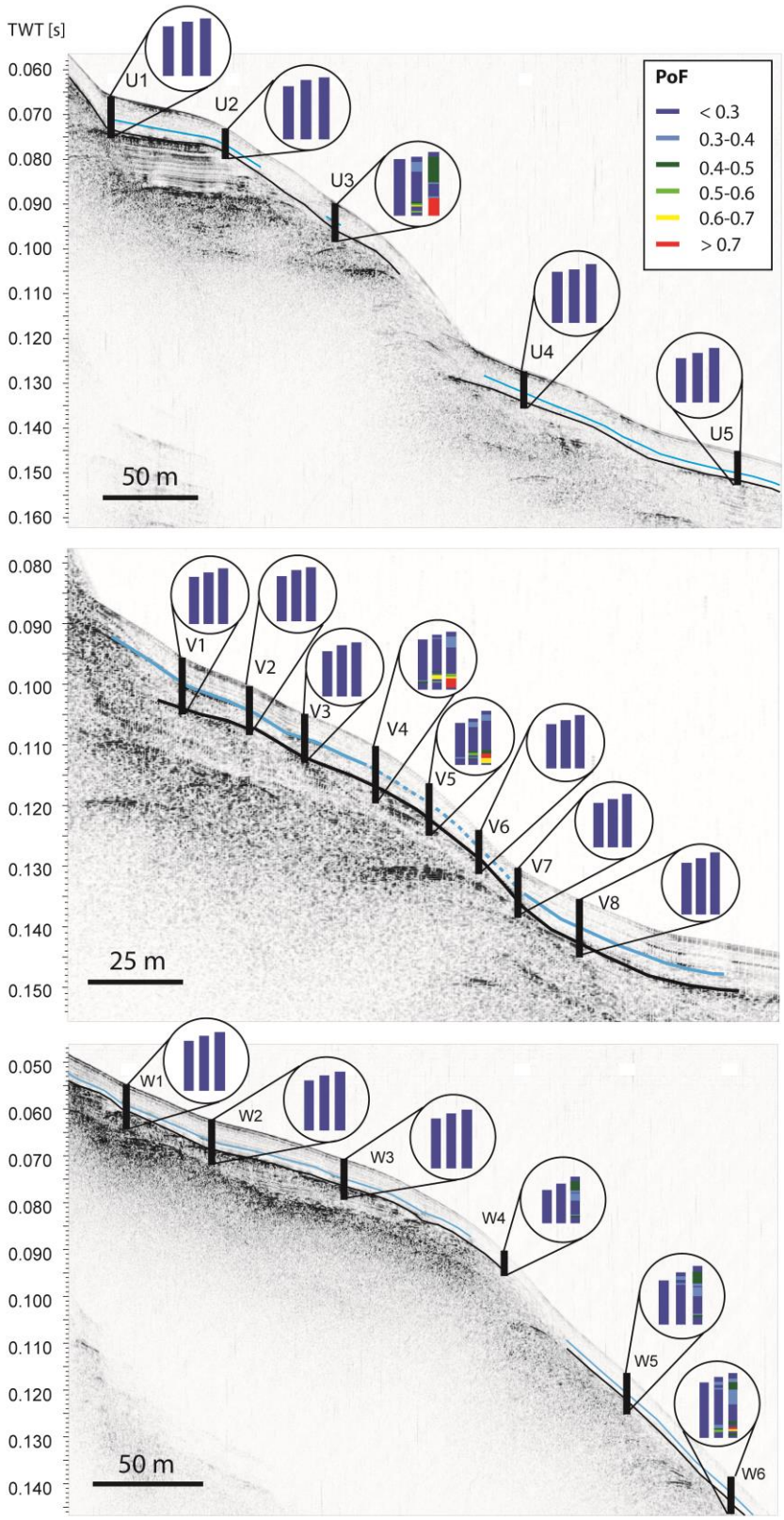


Figure 3. 10 Static slope stability for the three transects U, V and W (from top to bottom; see Figs. 3.3 and 3.4 for locations of transects; black vertical lines core locations). Magnified in circles, left: PoF for the scenario ~2210 cal. yr BP, middle: PoF for the scenario ~640 cal. yr BP, right: PoF for present-day slope conditions. Black and blue horizons Strong reflections between SMU1 and 2 as well as SMU3 and 4 respectively. Seismic profile of transect V modified after Strasser and Anselmetti (2008).

In summary, back analyses of S2 show low PoFs under static loading conditions, whereas back analyses of S3 reveal that some of the locations with steep slope gradients show a slightly increased PoF. Thus, within ~1,570 years between the two events, the static slope stability decreased. This implies a higher failure susceptibility when subjected to additional trigger mechanisms.

3.4.3.2 Critical pseudostatic accelerations for past subaqueous landslides

The a_c values required for the triggering of S2 and S3 are listed per model location in Table 3.3. For the sediment drape at ~2210 cal. yr BP, the minimum a_c is found at locations U3 and V4 (both 0.01*g*), V5 (0.04*g*) and W6 (0.05*g*). For the scenario ~640 cal. yr BP, the minimum a_c is 0 for U3, V4, V5 and W6, suggesting that no additional force is needed to cause failure at these model locations. Model location W5, situated in the same water depth as the failure scar of the slide, needs a minimum a_c of 0.04*g*.

Table 3. 3 Pseudostatic critical accelerations (ac) and depth of minimum ac for the model locations

Location	Slope gradient (°)	Min. a_c 2210 cal. yr BP (×*g*)	Depth of min. a_c in a_c-depth profile (m)	Min. a_c 640 cal. yr BP (×*g*)	Depth of min. a_c in a_c-depth profile (m)
U1	4.2	0.18	5.67	0.16	6.40
U2	11.2	0.16	4.58	0.13	4.57
U3	18.0	0.02	4.52	0	5.25
U4	10.1	0.13	4.90	0.10	5.62
U5	5.2	0.26	4.25	0.22	4.97
V1	9.1	0.11	4.92	0.08	5.64
V2	10.0	0.17	4.20	0.12	4.92
V3	10.0	0.16	4.14	0.12	4.86
V4	18.2	0.01	4.64	0	5.36
V5	19.9	0.04	3.88	0	4.60
V6	12.0	0.17	3.52	0.12	4.24
V7	9.8	0.20	3.67	0.16	4.39
V8	8.3	0.15	5.10	0.13	5.82
W1	8.1	0.13	5.66	0.11	6.38
W2	5.2	0.20	5.88	0.18	6.57
W3	6.0	0.24	4.76	0.21	5.48
W4	20.5	0.13	3.09	0.06	3.80
W5	18.3	0.10	3.77	0.04	4.49
W6	20.4	0.05	3.92	0	4.65

3.5 Discussion

3.5.1 Interpretation of glide-plane characteristics based on sediment core data

From the observations that LU3c (for S1a) and LU3b (for S2 and S3) directly overlie LU1, and from the geomorphic expression of slide translation areas, it is inferred that the glide plane (cf. blue arrow in Fig. 3.6) of the three landslides is located in LU1 (late glacial plastic muds). Macroscopic and geotechnical data indicate that the location of the glide planes within LU1 varies between the investigated subaqueous landslides. For S1a and S2, the glide plane is located in LU1a, whereas for S3 the glide plane is located in LU1b/c, close to the transition to LU2.

The cores taken along a transect on S1a (Fig. 3.6a) may contain some information about the slide mechanism: from the undisturbed part of LU1 in the topmost core, it is inferred that the original sediment cover (top of LU1, LU2, LU3a and large parts of LU3b) sled completely downslope, i.e. without parts of the slide being redeposited at that location. For core ZH15-S10(II), however, the change in lamination angles within the late glacial plastic muds (cf. dashed white line in Fig. 3.6a) may be interpreted as the location of the glide plane, which is covered by the 'tail' of the landslide. The succession in core ZH15-S11 is interpreted as being clasts of LU3 mixed with LU1 during the slide in the lower part of the slope.

3.5.2 Slope stability evaluation

3.5.2.1 Location of failure initiation

Lacustrine chalks, such as those found in LU3 (correlating with SMU3), are described in the literature as 'structure-sensitive' (i.e. their matrix can fall apart suddenly upon shaking; e.g. Huder 1963; Schindler 1996), and have been documented as 'weak layers' causing landslides that slide on a slurry rather than on a distinct glide plane (e.g. landslides of Zug; Schindler and Gyger 1989; Schindler 1996). On the slopes of Oberrieden, however, the modelled critical failure plane is found in SMU1 for the back-calculated and present-day scenarios. Lithologically, the modelled glide plane corresponds to the LU1 (late glacial plastic muds; Fig. 3.6). The modelled results thus coincide with the observed results from sediment cores taken on the failure planes. The reason why the failure develops in SMU1 (or, from a lithological point of view, why the late glacial plastic muds favour slope instability) may be found in the different mechanical behaviour of SMU1 in contrast to its covering mechanical units (i.e. the relatively low s_u compared to that of the covering SMU2). Such a different mechanical behaviour may be explained by the mineralogical composition (e.g. Hein and Longstaffe 1985; Stegmann et al. 2007). Mineralogical measurements by Gyger et al. (1976) on the late and postglacial sediments in Lake Zurich showed a much higher clay content in the late glacial clays compared to the overlying lithological units. Also for other lacustrine or marine slopes, clay often represents weak layers (Laberg et al. 2003; Solheim et al. 2005; Dan et al. 2007; Stegmann et al. 2007; Strasser et al. 2007; Sultan et al. 2010).

Interestingly, the modelled critical failure plane is not located at the transition between two SMUs, but rather within SMU1. The exact determination of whether the glide plane is located in LU1a or LUb/c is not possible in the model, as the two lithological subunits belong to the same SMU. The reason why slide S3 has its glide plane in a higher lithological subunit (LU1 b/c) than S1a and S2

(LU1a) may be related to the slope geometry: as the failure scar of S3 is located within a steep zone (and not at the top of a steep zone as for S1a and S2; cf. Results section), the additional downward-driving forces of the sediment columns in the upslope neighbourhood may be responsible for a slightly higher location of the weakest zone within the mechanic stratigraphy for S3.
The downslope position of the headscarp can be identified quite accurately: the location with the highest overall values in the PoF-depth profile corresponds to the position of the headscarp in the slope, identified from the DDM. This can be well identified at the locations U3, V4 and W5/W6. Kohv et al. (2009) concluded from an SSA on subaerial slopes that the critical slope angle for failure of groundwater-saturated glaciolacustrine clays is >10°. The locations of the failure scars in the present study area show similar results for the sublacustrine slopes in Lake Zurich. Also for Lake Lucerne, the majority of the slides in the late glacial clays occur on slopes >10° (Schnellmann et al. 2006; Strasser et al. 2011). The question why the patches between the three subaqueous landslides in the study area have not (yet) failed is of importance. The slope gradient of the potential glide plane and the spatial sediment-mechanical unit thicknesses distribution must influence the lateral extension of the slides. Although the present approach allows the determination of the glide plane and the identification of potential future headscarp locations, it is difficult to assess the lateral extension of the landslides.

3.5.2.2 Static and pseudostatic stability of the Oberrieden slopes

As for Lake Lucerne (Strasser et al. 2007), the static stability conditions of the Oberrieden slopes can change over short geological timescales. At the time of the occurrence of the past slides, the yet unfailed slopes were statically more stable than for the present-day situation. The more sediment accumulates with time, the higher the static load, and thus the lower an external force needed to create slope failure.
The results of the present study (Fig. 3.10) indicate that the Oberrieden slope was statically stable when S2 occurred. Hence, an external force must have triggered S2. This supports other evidence of that slide being earthquake-triggered, as suggested by Strasser and Anselmetti (2008) based on a geotechnical approach. a_c of 0.04 and 0.05g were needed to cause failure at the weakest model locations of the V and W transects. For Lake Lucerne, Strasser et al. (2011) approximate a minimum a_c of 0.034g for the ~2200 cal. yr BP event and relate this value to the probably strongest Holocene regional earthquake. The slightly higher a_c values of the present study indicate thus a marginally higher shaking intensity for Lake Zurich. For the scenario ~640 cal. yr BP, the model locations on steep slope gradients (i.e. ~20°) are statically slightly unstable both for the deterministic and probabilistic model, whereas the modelled locations on the smaller slope gradients (i.e. ~5–10°) are stable. On transect W, which is closest to S3, minimal a_c neighbouring the slide extent must be in the range between 0 (W6) and 0.04g (W5). S3 may be related to the historical 1356 AD Basel earthquake, which might have had a maximum intensity of VI in Zurich (Schwarz-Zanetti and Fäh 2011). It is assumed that the slope was already in a 'labile' situation, which might have allowed an earthquake intensity of <VI to trigger a failure. The back-analysed a_c should be used only as a first-order estimation, as the buttressing effect at the toe of the steep zones is not included. The steeper parts of the slope (~20°) with high PoFs are prone to failure, even without external trigger, as they are 'charged with sediment'.

The undulations that are located where the highest PoF in the V transect has been modelled (Fig. 3.4b) might be a geomorphic expression of a local instability, indicating some pre-failure movements as first stage of landslides (e.g. Leroueil et al. 1996; Shillington et al. 2012). The formation by waves can be ruled out, as the features are located between ~80 and ~90 m water depth, much deeper than the wave base. Sediment undulations have also been interpreted as formed by bottom currents or hyperpycnal flows (e.g. Bornhold and Prior 1990; Mosher and Thomson 2002; Urgeles et al. 2007). Bottom currents often create sediment waves that are oblique to the bathymetric contours (e.g. Flood et al. 1993). Here, the undulations are parallel to the bathymetric contours. Hyperpycnal flows are also unlikely, as there is no major river inflow nearby that could generate excess density by its sediment load (e.g. Parsons et al. 2001). As the undulations coincide with the location of the highest PoF in the transect, it is interpreted that the slope is unstable at some particular locations, which results in these features, yet it is not weak enough to slide completely. Little additional force may be needed to trigger a subaqueous landslide in the study area. However, as large parts of the slope have already failed, only relatively small undisturbed sediment patches may be mobilized.

The stability of the slope at the time of the S1a occurrence must have been very similar to the stability for the present-day situation, as in the ~100 years since the landslide occurrence only ~10–20 cm of sediment accumulated on the glide plane. In 1917, a wooden construction for changing booths of a new public bath was installed at the shore (pers. comm. I. Raimann, village of Oberrieden). The construction may have provided the extra load on the sediment to cause the slope to fail. As the translation areas of S1a and S1b are not connected, it is not clear whether these slides were triggered synchronously. S1b may have been triggered by construction activity onshore and, by adding its deposit on the slope above the main slide's headscarp, may have acted as an additional force for triggering S1a. Another explanation is that S1b was triggered independently in 1965, when a landfill occurred in the nearshore area (pers. comm. I. Raimann, village of Oberrieden) to extend the public baths (located in the immediate vicinity of the S1b failure scar). The exact slide mechanism, however, remains unknown.

3.5.2.3 Limitations and quality of the modelling approach

Considering the irregular geometry of the slope in the study area, the assumption of the infinite-slope model that the glide plane is planar is not strictly valid. However, for a SSA at single model locations, the model is not affected. If spatial SSAs are conducted, the buttressing effects of interslice forces need to be considered. Furthermore, the simple model of the present study does not include any considerations of hydrological effects. However, it is considered that this is not relevant in this case, as no rivers inflow the study area and no fluid flow evidence can be found in the geoacoustic datasets.

A linear increase in ρ_{bulk} and s_u values used in many SSAs may give reliable results for the investigation of slopes with homogeneous lithological units. For slopes with small-scale (i.e. decimetre) variations of mechanical properties with depth, as in the Oberrieden case, profiles instead of gradients might be more appropriate.

Although the present concept expresses slope stability quantitatively, the computed PoFs on the slopes in the study area should not be interpreted as absolute values but should rather be regarded

relative to other modelled PoFs. However, if interpreted with geological understanding, the concept yields valuable information. Formally, the calculated a_c on the unfailed slopes are to be regarded as maximum values. However, it is assumed that the stability conditions in the pre-failure areas were similar to the ones on the transects. This implies that values of minimal a_c must have been very close to the maximal a_c.

The comparison of the present results to those from calculations with SLIDE for transect V shows that the simple model of this study provides useful data for determination of the position of the failure plane within the sediment column (see supplementary material in Appendix C, Figs. C.1 and C.2): the potential glide plane modelled with SLIDE is also located in LU1. The global mean deterministic and probabilistic FS (1.36 and 1.47) does not exclude single locations in the transect with a smaller FS. By the use of gradients in the SLIDE model, variations in geotechnical parameters are smoothed out.

The present approach does not explain why the patches between the slides have not failed. A spatial analysis may help determining the lateral extent of the subaquatic landslides. Also, the limit-equilibrium approach does not give any results about the mechanism of the failure initiation. An approach that treats failure as a shear-band propagation process, such as applied by Puzrin and Germanovich (2005), would be necessary.

3.6 Conclusions

The presented concept provides a suitable tool for assessing the stability of subaqueous slopes. The high density of the sediment cores and CPT sites in a well-investigated area and the high-resolution measurement of the geotechnical parameters allow the inclusion of spatial variability in the model. To the authors' knowledge, the concept of including an adaptable sediment-mechanical stratigraphy into a limit-equilibrium SSA has not been applied on a larger scale. The concept thus might be an important contribution to the SSA for an entire lake basin or stretch of continental margin (excluding gas-rich littoral deposits or deltas). To this end, a bathymetric and seismic reflection dataset, and a grid of homogeneously distributed depth-profiles of bulk density and undrained shear strength on the undisturbed lateral slopes are needed. If the subsurface properties of a whole lake basin or stretch of the continental margin vary considerably (e.g. provoked by varying detrital input from major rivers), the slope may be divided into different zones, each with similar properties. Hence, if applied on a larger scale, as a first step, general patterns of geotechnical profiles taken at a low spatial sampling resolution (e.g. one core and one CPT profile per km^2) may be detected to construct zones. As a second step, the spatial sampling resolution can be increased and mechanical stratigraphies for the different zones can be constructed.

Extended from a 1D approach to a spatial basin-wide approach, the concept is expected to yield information on failure-prone zones with simple, time-efficient methods. Failure-prone zones can in a further step be analysed for their tsunamigenic potential. The main findings of this study can be summarised as follows:

1. The glide plane of the three investigated subaqueous slides in Lake Zurich can be assigned to late glacial plastic muds, both from modelled results and sedimentological groundtruthing. The glide

plane is thus located in the same lithostratigraphic unit as documented for nearby Lake Lucerne (Strasser et al. 2007).

2. The location of the headscarp of historical and pre-historical subaqueous landslides corresponds to the model locations in the transects with the highest probabilities of failure. This approach to assess slope stability should thus be able to determine the headscarp locations of future landslides.

3. The model supports the hypothesized earthquake triggers for the ~2210 and ~640 cal. yr BP events from a geotechnical point of view and adds first quantitative constraints for critical pseudostatic earthquake accelerations for Lake Zurich.

4. Today, sediment-charged, steeper (i.e. ~20°) slopes in the study area are prone to failure, even without the need of an additional trigger. Modelled results imply that future subaqueous landslides in Lake Zurich may glide in late glacial plastic muds (LU1)—hence, in the same lithological unit as the three investigated slides occurring in the past.

Acknowledgements

This work was supported by the Swiss National Foundation Grant Nr. 133481. We thank Anna Reusch, Katrina Kremer, Stefano Fabbri, Robert Hofmann, Reto Seifert, Stewart Bishop, Christian Zoellner, Tobias Schwestermann and Utsav Mannu for their efforts during the data acquisition, Andrea Wolter for her inputs with SLIDE Software, and Beat Rick (GeoVonMoos AG) for the access to additional Lake Zurich data.

References

Blum P (1997) Physical properties handbook, ODP Tech. Note 26. doi: 10.2973/odp.tn.26.1997.

Bornhold B. and Prior DB (1990) Morphology and sedimentary processes on the subacqueous Noeick River delta, British Columbia, Canada. In: Colella A, Prior DB (eds) Coarse-Grained Deltas. Blackwell, Oxford, pp 169–181

Chandler DS (1996) Monte Carlo Simulation to Evaluate slope Stability. In: Shakelford C., Nelson PP, Roth MJS (eds) Uncertainty in the geologic environment: from Theory to Practice. American Society of Civil Engineers, New York, pp 474–493

Coduto DP, Yeung MR and Kitch WA (2011) Geotechnical Engineering: Principles and Practices, 2nd edn. Prentice Hall, Upper Saddle River

Craig RF (2004) Craig's Soil Mechanics, 7th edn. Spon Press, New York

Dan G, Sultan N and Savoye B (2007) The 1979 Nice harbour catastrophe revisited: Trigger mechanism inferred from geotechnical measurements and numerical modelling. Marine Geology 245:40–64. doi: 10.1016/j.margeo.2007.06.011

Flood RD, Shor AN and Manley PL (1993) Morphology of abyssal mudwaves at project MUDWAVES sites in the Argentine Basin. Deep-Sea Research Part II 40:859–888. doi: 10.1016/0967-0645(93)90038-O

Giovanoli F (1979) Die remanente Magnetisierung von Seesedimenten. ETH Zürich, PhD Thesis Nr.6350

Hein FJ and Longstaffe FJ (1985) Sedimentologic, mineralogic, and geotechnical descriptions of fine-grained slope and basin deposits, Baffin Island Fiords. Geo-Marine Letters 5:11–16. doi: 10.1007/BF02629791

Huder J (1963) Bestimmung der Scherfestigkeit strukturempfindlicher Böden unter besonderer Berücksichtigung der Seekreide. Mitteilungen der Versuchsanstalt für Wasserbau und Erdbau an der Eidgenössischen Technischen Hochschule in Zürich 58:1–35.

Jibson RW (1993) Predicting Earthquake-Induced Landslide Displacements Using Newmark's Sliding Block Analysis. Transportation Research Record 1411:9–17.

Jibson RW (2012) Models of the triggering of landslides during earthquakes. Landslides 196–206. doi: 10.1017/CBO9780511740367.019

Kelts K (1978) Geological and sedimentary evolution of Lakes Zurich and Zug, Switzerland. ETH Zurich, PhD Thesis, Nr.6146

Kelts K, Briegel U, Ghilardi K and Hsu K (1986) The limnogeology-ETH coring system. Swiss Journal of Hydrology 48:104–115. doi: 10.1007/BF02544119

Kohv M, Talviste P, Hang T, Kalm V and Rosentau A (2009) Slope stability and landslides in proglacial varved clays of western Estonia. Geomorphology 106:315–323. doi: 10.1016/j.geomorph.2008.11.013

Kramer SL (1996) Geotechnical Earthquake Engineering. Prentice-Hall, Upper Saddle River

Laberg J., Vorren TO, Mienert J, Haflidason H, Bryn P and Lien R (2003) Preconditions Leading To the Holocene Trænadjupet Slide. Submarine Mass Movements and Their Consequences 19:247–254.

Lacasse S and Nadim F (1996) Uncertainties in characterising soil properties. In: Shackelford CD, Nelson PP, Roth MJS (eds) Uncertainty in the geologic environment: from Theory to Practice. American Society of Civil Engineers, New York, pp 49–75

Leroueil S, Vaunat J, Picarelli L, Locat J, Lee H and Faure R (1996) Geotechnical characterisation of slope movements. In: Senneset K (ed) Landslides, 1st edn. Balkema, Rotterdam, pp 53–74

Lunne T, Robertson PK and Powell JJM (2002) Cone penetration testing in geotechnical practice, 2nd edn. Spon Press, London

Morgenstern NR and Price VE (1967) A numerical method for solving the equations of stability of general slip surfaces. The Computer journal 9:388–393.

Mosher DC and Thomson RE (2002) The Foreslope Hills: Large-scale, fine-grained sediment waves in the Strait of Georgia, British Columbia. Marine Geology 192:275–295. doi: 10.1016/S0025-3227(02)00559-5

Nadim F, Einstein H and Roberds W (2005) Probabilistic stability analysis for individual slopes in

soil and rock. In: Hungr O, Fell R, Couture R, Eberhard E (eds) Landslide Risk Management. Taylor & Francis Group, Boca Raton, p 764

Newmark NM (1965) Effects of earthquakes on dams and embarkments. Geotechnique 2:139–160.

Parsons JD, Bush JWM and Syvitski JPM (2001) Hyperpycnal plume formation from riverine outflows with small sediment concentrations. Sedimentology 48:465–478. doi: 10.1046/j.1365-3091.2001.00384.x

Puzrin AM and Germanovich LN (2005) The growth of shear bands in the catastrophic failure of soils. Proceedings of the Royal Society A: Mathematical, Physical and Engineering Sciences 461:1199–1228. doi: 10.1098/rspa.2004.1378

Schindler C and Gyger M (1989) The landslides of Zug seen 100 years after the analysis of Albert Heim. In: Bonnard C (ed) Rutschungsphänomene im Gebiet des Alpenbogens. Balkema, Rotterdam, pp 123–126

Schindler CM (1996) Aussergewöhnliche Rutschungen, Felsstürze und Murgänge. In: Instabile Hänge und andere risikorelevante natürliche Prozesse. Birkhäuser, Basel, pp 73–84

Schnellmann M, Anselmetti FS, Giardini D and McKenzie JA (2006) 15,000 Years of mass-movement history in Lake Lucerne: Implications for seismic and tsunami hazards. Eclogae Geologicae Helvetiae 99:409–428. doi: 10.1007/s00015-006-1196-7

Schwarz-Zanetti G and Fäh D (2011) Grundlagen des Makroseismischen Erdbebenkatalogs der Schweiz Band 1: 1000-1680. vdf Hochschulverlag AG, Zürich

Shillington DJ, Seeber L, Sorlien CC, Steckler MS, Kurt H, Dondurur D, Çifçi G, Imren C, Cormier MH, McHugh CMG, Gürçay S, Poyraz D, Okay S, Atgin O and Diebold JB (2012) Evidence for widespread creep on the flanks of the sea of Marmara transform basin from marine geophysical data. Geology 40:439–442. doi: 10.1130/G32652.1

Solheim A, Bryn P, Sejrup HP, Mienert J and Berg K (2005) Ormen Lange - An integrated study for the safe development of a deep-water gas field within the Storegga Slide Complex, NE Atlantic continental margin; executive summary. Marine and Petroleum Geology 22:1–9. doi: 10.1016/j.marpetgeo.2004.10.001

Stegmann S, Strasser M, Anselmetti F and Kopf A (2007) Geotechnical in situ characterization of subaquatic slopes: The role of pore pressure transients versus frictional strength in landslide initiation. Geophysical Research Letters. doi: 10.1029/2006GL029122

Strasser M and Anselmetti FS (2008) Mass-movement event stratigraphy in Lake Zurich; A record of varying seismic and environmental impacts. Beiträge zur Geologie der Schweiz 95:23–41.

Strasser M, Hilbe M and Anselmetti FS (2011) Mapping basin-wide subaquatic slope failure susceptibility as a tool to assess regional seismic and tsunami hazards. Marine Geophysical Research 32:331–347. doi: 10.1007/s11001-010-9100-2

Strasser M, Schindler C and Anselmetti FS (2008) Late Pleistocene earthquake-triggered moraine dam failure and outburst of Lake Zurich, Switzerland. Journal of Geophysical Research: Earth Surface 113:1–16. doi: 10.1029/2007JF000802

Strasser M, Stegmann S, Bussmann F, Anselmetti FS, Rick B and Kopf A (2007) Quantifying subaqueous slope stability during seismic shaking: Lake Lucerne as model for ocean margins. Marine Geology 240:77–97. doi: 10.1016/j.margeo.2007.02.016

Sultan N, Savoye B, Jouet G, Leynaud D, Cochonat P, Henry P, Stegmann S and Kopf A (2010) Investigation of a possible submarine landslide at the Var delta front (Nice slope - SE France). Canadian Geotechnical Journal 47:486–496. doi: 10.1139/T09-105

Tobutt DC (1981) Monte Carlo Simulation Methods for Slope Stability. Computers & Geosciences 8:199–208.

Urgeles R, De Mol B, Puig P, De Batist M and Hughes-Clarke JE (2007) Sediment undulations on the Llobregat prodelta: Signs of early slope instability or sedimentary bedforms? Journal of Geophysical Research 112:1–12. doi: 10.1029/2005JB003929

Zandbergen PA (2011) Error Propagation Modeling for Terrain Analysis using Dynamic Simulation Tools in ArcGIS Modelbuilder. In: Hengl T, Evans IS, Wilson JP, Gould M (eds) Geomorphometry 2011. Redlands, pp 57–60

Chapter 4

A subaqueous hazard map for earthquake-triggered landslides in Lake Zurich, Switzerland

This chapter is in press as: Strupler, M., Danciu, L., Hilbe, M., Kremer, K., Anselmetti, F.S., Strasser, M., and Wiemer, S. A subaqueous hazard map for earthquake-triggered landslides in Lake Zurich, Switzerland. Natural Hazards. doi: 10.1007/s11069-017-3032-y

Abstract

The awareness of geohazards in the subaqueous environment has steadily increased in the past years and there is an increased need to assess these hazards in a quantitative sense. Prime examples are subaqueous landslides, which can be triggered by a number of processes including earthquakes or human activities, and which may impact offshore and onshore infrastructure and communities. In the literature, a plenitude of subaqueous landslide events are related to historical earthquakes, including cases from lakes in Switzerland. Here, we present an approach for a basin-wide earthquake-triggered subaquatic landslide hazard assessment for Lake Zurich, which is surrounded by a densely-populated shoreline. Our analysis is based on high-resolution sediment-mechanical and geophysical input data. Slope stabilities are calculated with a grid-based limit-equilibrium model on an infinite slope, which uses Monte Carlo sampled input data from a sediment-mechanical stratigraphy of the lateral slopes. Combined with probabilistic ground-shaking forecasts from a recent national seismic hazard analysis, subaquatic earthquake-triggered landslide-hazard maps are constructed for different mean return periods, ranging from 475 to 9975 years. Our results provide a first quantitative landslide-hazard estimation for the lateral slopes in Lake Zurich. Furthermore, a back-analysis of a case study site indicates that pseudostatic accelerations in the range between 0.04 and 0.08 g were needed to trigger a well-investigated subaqueous landslide, dated to ~2210 cal. years BP.

4.1 Introduction

A geohazard can be described as the ‘’probability that a geological state, which creates a particular threat to humans, property and their environment, occurs within a given period of time” (ISSMGE 2004; Hoffmann and Reicherter 2016). Geohazards are therefore mostly characterized by their intensity and recurrence rate (Bollinger 1996). In the subaqueous environment, the assessment of hazards has become more important in recent years (e.g. Lee and Jones, 2014; Mueller et al., 2016). Such hazards include subaqueous landslides and tsunamis, which may cause damage to infrastructure and loss of lives (e.g. Hoffmann and Reicherter, 2016; Lee and Jones, 2014). Subaqueous landslides can be triggered by various processes, such as earthquakes, wave loading or human activity. Apart from a trigger mechanism, a favourable topography and the necessary amount of sediments need to be present for a subaqueous landslide to occur (Nadim et al. 1996).

Landslide-hazard maps provide the database required to reduce damage, costs and other consequences of landsliding (Aleotti and Chowdhury 1999). For the construction of landslide-hazard maps, the failure-susceptibility of a slope and the probability of a specific trigger need to be assessed (e.g. Wang et al., 2005).

Sublacustrine landslides have been documented worldwide, and many of them were interpreted as earthquake-triggered (Chapron et al. 1999; e.g. Moernaut et al. 2007; Moernaut and De Batist 2011; Waldmann et al. 2011; Smith et al. 2013; Praet et al. 2016). In Switzerland, subaqueous landslides are common features in perialpine lakes. Also here, a plenitude of subaqueous landslide events have been related to past earthquakes, with various consequences (Schnellmann et al. 2002; Monecke et al. 2004; Strasser and Anselmetti 2008; Strasser et al. 2013; Kremer et al. 2015; Reusch et al. 2016). Evidence of tsunamis triggered by landslides has been documented for Lakes Lucerne (central Switzerland) and Lake Geneva (southwestern Switzerland) (Schnellmann et al. 2002; Kremer et al. 2012; Hilbe and Anselmetti 2015). The tectonics of Switzerland are strongly affected by the Alpine orogeny. In terms of overall crustal strain rate and seismicity rate, Switzerland is located in the transition zones between areas of high seismic activity (Greece, Italy) and areas of low seismic activity (Northern Europe). Damaging earthquakes occur on a regular basis and earthquakes are in fact the natural hazard with the highest risk potential (Wiemer et al. 2009). A well-established historical and paleoseismic catalogue of earthquakes exists (Fäh et al. 2011; Wiemer et al. 2009).

For Lake Zurich, a perialpine Lake in northern Switzerland, Strasser and Anselmetti (2008) identified and mapped a total of 149 landslide deposits in the postglacial sedimentary basin infill (past ~17’000 years) using reflection seismic data. The authors evaluated five landslide events as earthquake-triggered, as multiple mass-movement deposits occur simultaneously. A high-resolution bathymetric dataset of Lake Zurich (Strupler et al. 2015) allowed the identification, mapping and characterization of features related to landslides that occurred during the past ~5000 years. Apart from the landslides interpreted as earthquake triggered, a few subaquatic landslides with headscarps in shallow water depths (i.e. <10 m) have occurred in the past 150 years, triggered by onshore human activity (Heim 1876; Kuen 1999). Similar shore collapses leading to landslides have also been documented for the marine environment (e.g. Dan et al., 2007; L’Heureux et al., 2013). Today, ~247’000 people are living within 1 km distance from the shoreline of Lake Zurich (Henriod et al. 2016). The regular occurrence of subaqueous landslides in Swiss perialpine lakes, triggered by different mechanisms,

emphasizes the need for the assessment of the subaquatic landslide hazard. In this study we focus on the earthquake-triggered landslide hazard, as earthquakes represent the most common cause for large and multiple slide events on the slopes.
Strupler et al. (2017) constructed a sediment-mechanical stratigraphy of Lake Zurich's postglacial lateral slopes. This sediment-mechanical slope characteristics were used to assess the stability at a case-study site with a limit-equilibrium approach on an infinite slope for selected locations. The main objectives of this study are to develop a methodology for the mapping of the earthquake-triggered, subaqueous landslide-hazard, and to test it on Lake Zurich (Switzerland).
In particular, the following steps are performed and the respective research questions are answered:

Basin-wide modelling of sediment thicknesses

- How much potentially mobile sediment is available in which region of the lateral slopes?

Back-analysis of paleoseismic shaking

- What are the ranges of the back-calculated earthquake accelerations that were required to create the slope failures during known events?
- What limits the spatial extent of the pre-existing landslide features?

Basin-wide landslide susceptibility for the present-day situation

- Which lateral slopes in the basin are susceptible to failure for a static case (i.e. because of high sediment loading and without an external trigger)?

Subaqueous earthquake-induced landslide hazard map

What is the earthquake-induced landslide hazard for different ground-acceleration exceedance probabilities?

4.2 Setting of the study area and previous studies

4.2.1 Study site: Central basin of Lake Zurich, Switzerland

This study concentrates on the lateral slopes of the up to 136 m deep, central basin of Lake Zurich (Switzerland), as this is the region where most documented subaqueous landslides occurred (Nipkow 1927; Kelts 1978; Strasser et al. 2013). The major geomorphic characteristics (Fig. 4.1) are a flat basin plain and the relatively steep lateral slopes containing deltas, landslide features and gullies. Six relatively small deltas (cross-hatched in Fig. 4.1c) are formed by local creeks. Geomorphic expressions of subaqueous landslides can be identified on both lateral (i.e. NE and SW oriented) slopes. The landslide extents show translation areas (dashed areas) and deposition lobes expressing sediment removal, mobilisation and deposition. The observed gullies (i.e. small channels that are often parallel to one another and to the local slope gradient, with consistent width and spacing; Field et al., 1999) are located on the steepest slopes (i.e. > 25° slope gradient) and originate at the transition from the shallow shore platform to the steep slope. Because of a lack of understanding the processes leading to delta failures (e.g. Hilbe and Anselmetti 2014), we only consider non-deltaic lateral slopes

in the following earthquake-triggered landslide assessment. Also, zones, where the translation areas of past failures are still identifiable in the DDM (Strupler et al. 2015) are excluded from the calculations.

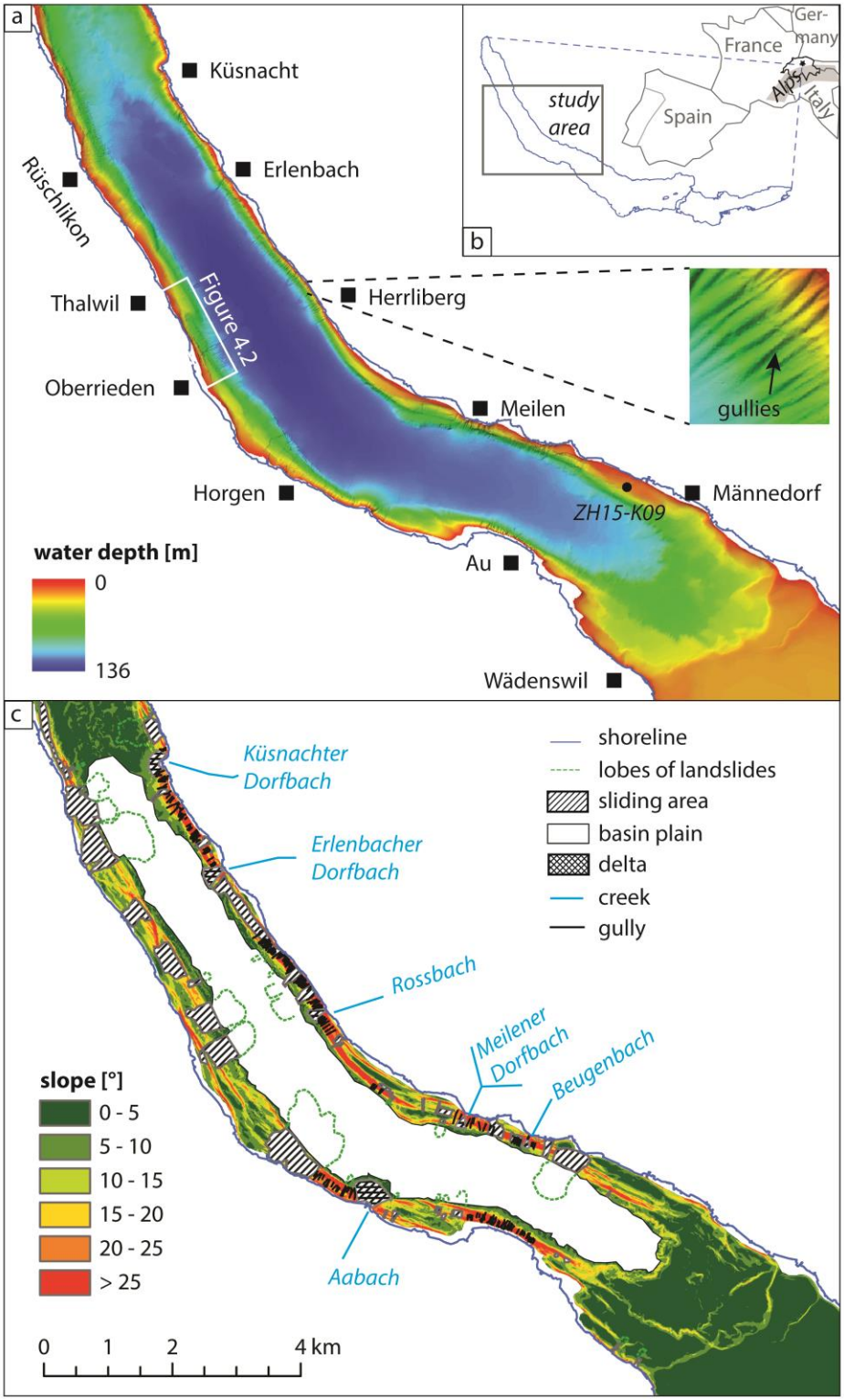


Figure 4. 1 a) Digital depth model (DDM) of Lake Zurich's deep basin as shaded relief with color-coded water depth. Data: Strupler et al., 2015. b) Location of the study area in Lake Zurich in the greater context. c) Slope gradient representation with mapped geomorphic features.

Various datasets available from previous work form the basis of the current study: We consider the landslide catalogue by Strasser and Anselmetti (2008), which was later included in a paleoseismic event catalogue for Central Switzerland (Strasser et al., 2013), outcomes of the probabilistic seismic hazard model of Switzerland (Wiemer et al. 2016), a bathymetric dataset and landslide extents from Strupler et al. (2015), and a mechanical stratigraphy of the postglacial sediment covering the lateral slopes of Lake Zurich (Strupler et al. 2017). The present-day lateral slopes of Lake Zurich show various prehistoric and historic slides, each with a different surface roughness of the translation area (Fig. 4.2), according to their ages (see Strupler et al. 2015).

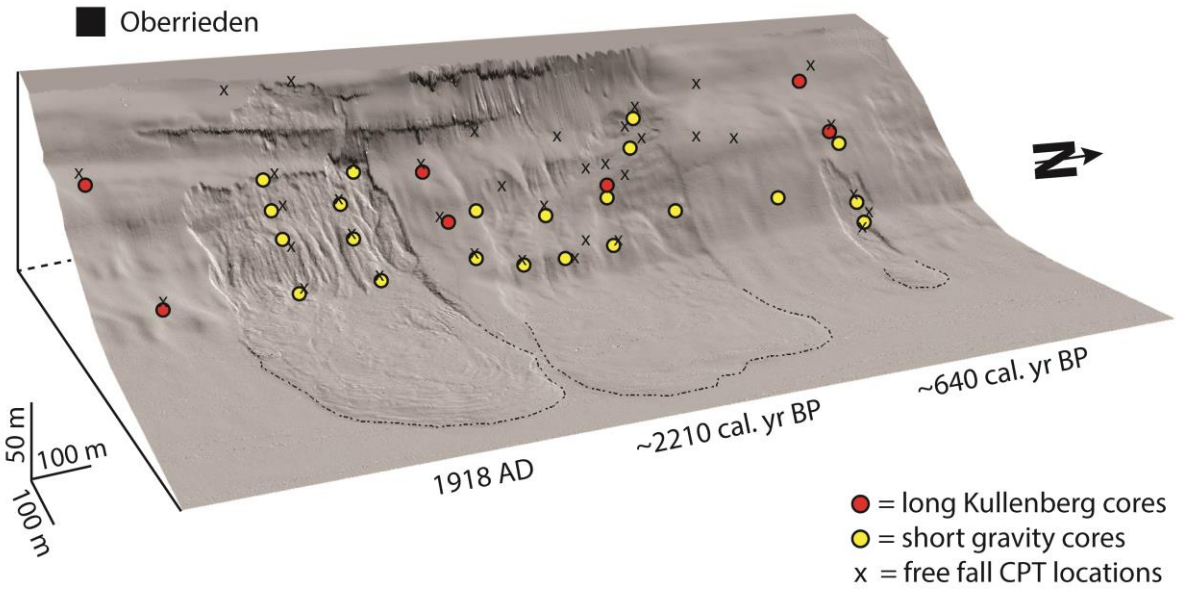


Figure 4. 2 Subaqueous landslides offshore the village of Oberrieden (location on Figure 4.1) with the positions of the retrieved sediment cores and CPT-sites. View towards Northwest. Modified from Strupler et al. 2017.

4.2.2 Late Quaternary earthquakes

As the historical seismic record of Switzerland spans only ~1000 years (Fäh et al. 2011), the inclusion of paleoseismological information from lake sediments is an important tool for extending the knowledge on the occurrence of earthquakes (e.g. Strasser et al. 2006; Strasser et al. 2013). Paleoseismic records indicate that the foreland region of Zurich may have experienced every few thousand years strong seismic events (with intensity (I) ≥ VII) that triggered basin-wide slope stabilities (Strasser et al. 2006). From the five assumedly earthquake-triggered events in Lake Zurich, Strasser et al. (2013) categorized three as 'major events' (~2210, ~11600 and ~13760 cal. years BP), which assumedly caused also slope instabilities in Lake Lucerne at a distance of ~40 km. The effect of earthquake shaking on lacustrine sediments has been quantified for Lake Lucerne by calculating a minimal critical pseudostatic acceleration of 0.034 g (Strasser et al. 2007 and 2011) to cause the slope to fail for a prehistoric earthquake (~2220 cal. years BP).

4.2.3 Sediment-mechanical stratigraphy on the postglacial, lateral slopes of Lake Zurich

The mechanical stratigraphy of the postglacial sediments on the lateral slopes of Lake Zurich (Strupler et al. 2017) is based on data from six up to 6 m long Kullenberg-type (Kelts et al. 1986) sediment cores and corresponding free fall CPT (Cone Penetrometer Testing) profiles that were taken on the case-study site offshore Oberrieden (Figs. 4.1a and 4.2). The Oberrieden site was used for the design of the conceptual model, since it shows three well-constrained subaqueous landslides with known ages that were assigned to different triggers (Strasser and Anselmetti 2008). Four sediment-mechanical units (SMU) were defined based on characteristic patterns of the bulk density (ρ_{bulk}) and undrained shear strength (s_u) (Table 4.1; Fig. 4.3a; Strupler et al. 2017).: The lowermost unit SMU1 shows typical ρ_{bulk}-values of > 1600 kg/m^3 and s_u-values that increase from ~5000 Pa at the unit top to ~10'000 Pa at the unit base. In SMU2, ρ_{bulk} decreases from ~1500 to 1350 kg/m^3 and the s_u-values fluctuate strongly. SMU3 is defined by a convex shape in the ρ_{bulk} profile, increasing with depth from values of ~1350 to ~1500 kg/m^3 and by constant s_u values of ~5000 Pa. The topmost sediment-mechanical unit shows linearly increasing profiles with depth of ρ_{bulk} and s_u (from ~1300 kg/m^3 to ~1350 kg/m^3 and from ~1000 Pa to ~4000 Pa, respectively).

The fact that SMU2 has relatively high s_u values despite its low bulk density has also been observed with laboratory measurements. This may be related to organic material found in that unit, which may keep the sediment together. However, the spatial variability in SMU2 is also relatively large (Strupler et al. 2017).

Table 4. 1 Postglacial lithologic units, their ages and corresponding sediment-mechanical units (Strasser & Anselmetti 2008; Strupler et al., 2017)

Lithologic Unit (LU)	**Corresponding sediment-mechanical unit (SMU)**
LU3b/c: lacustrine marls: present day to ~7'000 cal. years BP	SMU4
LU3a: lacustrine chalks: ~7'000 cal. years BP to ~12'000 cal. years BP	SMU3
LU2: iron sulphide muds: ~12'000 cal. years BP to ~ 14'500 cal. years BP	SMU2
LU1: Late Glacial plastic muds: ~14'500 cal. years BP to ~17'600 cal. years BP	SMU1

The thicknesses of the sediment mechanical units were derived based on information from core-to-seismic correlation, for locations with available reflection seismic data. The mechanical profiles per unit, including the spatial variability, were then adapted to local thicknesses of each mechanical unit.

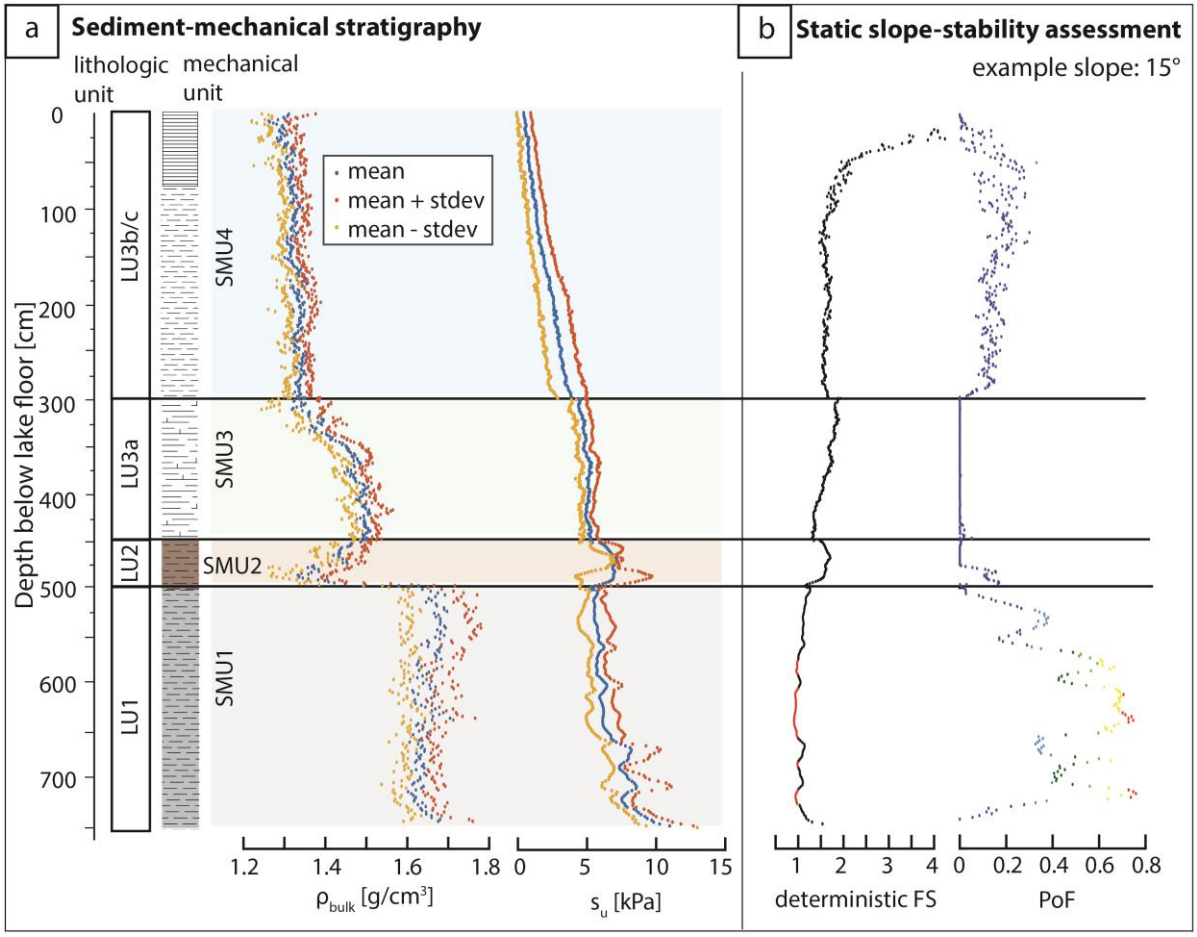


Figure 4. 3 a) Sediment-mechanical stratigraphy, showing characteristic patterns of the bulk density (ρ_{bulk}) and undrained shear strength (s_u) per mechanical unit. Modified from Strupler et al. (2017). b) deterministic FS vs. depth profile and PoF vs. depth profile for an example location with a slope gradient of 15°. Red stroke in the deterministic FS indicates depths with an FS <1. Modified from Strupler et al. 2017.

The spatial variability of the mechanical data from the input cores allowed to create log-normal distributions of the ρ_{bulk} and s_u for each depth step. To incorporate uncertainty due to the spatial variability of the ρ_{bulk} and s_u values, a Monte Carlo simulation (MCS) was carried out. Hereby, random values from the distributions were subsequently picked for each depth step. 1D-slope stabilities were then calculated probabilistically and deterministically (Fig. 4.3b): Probability of failure (PoF) vs. depth profiles were calculated for selected locations with a limit-equilibrium slope-stability assessment (SSA) on an infinite slope. The deterministic factor of safety (FS) was calculated by using the mean of the sediment-mechanical input data per depth step (for details see Strupler et al. 2017). The modelled data, as well as groundtruth data from short sediment cores (Fig. 4.2), showed that the glide plane of the three slides is located in a lithological unit consisting of Late Glacial plastic muds (LU1) corresponding to the sediment mechanical unit SMU1. The authors stated that future subaqueous slides on the lateral slopes are also expected to occur in this unit. The approach applied by Strupler et al. (2017) can only be used for single-model locations, along seismic reflection profiles. While the glide plane could be determined with a 1D model, the lateral extent of the slides could not be assessed. A grid-based SSA approach needed for a basin-wide subaqueous landslide

hazard-assessment does not exist so far for Lake Zurich. In this study, we are establishing such a hazard-assessment on a spatial scale. In doing so, we differentiate between the probability of failure conditional on geotechnical properties (PoF_g), representing the slope-failure susceptibility, and the probability of failure conditional on the earthquake occurrence (PoF_{eo}), representing the earthquake-triggered subaqueous landslide hazard. The latter one is calculated by including the seismic hazard in the geotechnical slope-failure probability calculation.

4.2.4 Probabilistic seismic hazard assessment of Switzerland

Wiemer et al. (2016) provide the latest probabilistic seismic hazard assessment (PSHA) for Switzerland incorporating updates of data, information and knowledge accumulated during the past three decades (e.g. Wiemer et al. 2009). These updates of the 2015 Swiss Seismic Hazard Model (SUIHaz2015) provide probabilistic estimates of horizontal ground motions, which can be coupled to the response of the local soil characteristics. The ground motions are calculated for a reference site condition with an average shear-wave velocity of the uppermost 30 m of the soil (V_{s30}) = 1100 ms^{-1}. The seismic hazard maps show the spatial distribution of ground motion values corresponding to a fixed probability of exceedance for each computational grid point (Wiemer et al. 2016).
According to Wiemer et al. (2016), earthquake events of magnitude 6 - 6.5 (hereafter, we refer to as moment magnitude – M_w) are believed to be possible everywhere in Switzerland, albeit they are most frequent in the Valais, the Basle region and the Grisons. A M_w 6 or larger event is expected in Switzerland and its immediate neighbourhood every 50 – 150 years, thus with an annual probability of about 1 %.

4.3 Methods and Workflow

From existing bathymetric, geotechnical and reflection seismic datasets (Strasser and Anselmetti 2008; Strupler et al. 2015; Strupler et al. 2017), as final results, back-analysed PoF_g scenarios for different earthquake acceleration scenarios and a basin-wide slope-failure susceptibility map for the present-day situation are calculated. Furthermore, a subaqueous earthquake-induced landslide hazard map is produced by including the expected ground shaking data from Wiemer et al. (2016) in the PoF_{eo} calculation (Fig. 4.4). Calculations are conducted on grids with 10 m spatial resolution in Matlab (Mathworks, Inc.) and visualized in ArcGIS (ESRI, Inc).

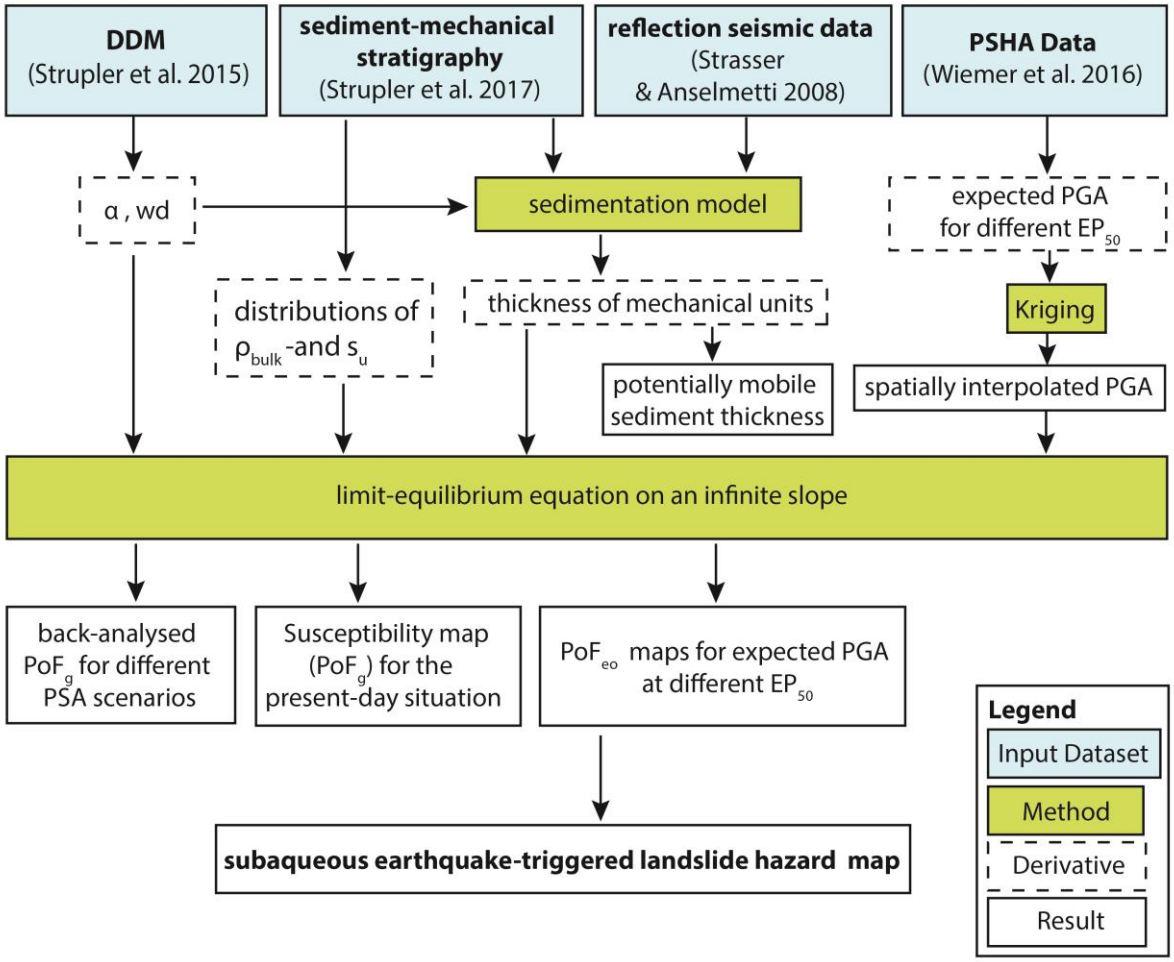


Figure 4. 4 Workflow for developing the earthquake-triggered, subaqueous landslide hazard map. DDM=digital depth model, PSHA = probabilistic seismic hazard analysis, α = slope gradient, wd = water depth, ρ_{bulk}= bulk density, s_u = undrained shear strength, EP_{50}= probability of exceedance in 50 years. PoF_g= probability of failure conditional on geotechnical parameters, PoF_{eo}=Probability of failure conditional on earthquake hazard, PSA=pseudostatic acceleration, see chap. 4.3.2., PGA=peak ground acceleration.

4.3.1 Sedimentation model

As the grid of the existing seismic reflection profiles (Strasser and Anselmetti 2008) has a spacing between ~100 and ~400 m, and as the topography on the lateral slopes of Lake Zurich is complex (Strupler et al. 2015), an interpolation of the sediment-mechanical unit-thicknesses, derived from reflection seismic data (Strupler et al. 2017) does not lead to realistic values. Therefore, to extend the thickness information of the mechanical units from locations where reflection seismic data is available to the whole study area, a sedimentation model is constructed (See Appendix D Figs. D.1 and D.2 for details). The sedimentation model assumes that slopes with comparable settings (e.g. slope gradients, stratigraphic succession) experienced similar sedimentation histories. For SMU3 and 4, the sedimentation rate (sr) at any pixel location (i) is calculated as a function of its water depth (wd) and slope gradient (α) (both derived from the DDM) with a linear regression (Eq.1, Table 4.2). The regression equation is calibrated with unit thicknesses from the seismic dataset (divided by the

unit age intervals from Strasser and Anselmetti, 2008; ~5 kyears and ~7 kyears for SMU3 and SMU4, respectively) on two undisturbed transects in the slope that show a wide variety of water depths and slope gradients (Appendix D, Figs. D.1 and D.2).

$$sr(i)[cm/yr] = a(i)\ [cm/yr] + b * wd(i)\ [m] - c * \alpha\ (i)\ [°] \quad (1)$$

Table 4. 2 Regression constants and factors for deriving the sedimentation rate sr(i) as a function of water depth and slope gradient.

	a	**b**	**c**
SMU4	0.047	0.000175	0.001305
SMU3	0.021	0.000104	0.000654

As unit thicknesses cannot be determined with seismic data, grids with constant values (250 and 40 cm for SMU1 and SMU2, respectively) that are estimated from sediment cores, are constructed for SMU1 and SMU2.

4.3.2 Limit-equilibrium equation on an infinite slope

The limit-equilibrium equation on an infinite slope has been applied spatially by several authors (e.g. Dimmock et al., 2012; Hammond et al., 1991; Jibson et al., 2000; Mulder et al., 1994; Terlien, 1996). Here, we extend the approach of Strupler et al. (2017), where values of log-normally distributed ρ_{bulk} and s_u were randomly sampled in an MCS for each depth step, and used in a limit-equilibrium equation on an infinite slope, to a spatial, grid-based model (Eq. 2). In comparison to other methods, where a pre-defined glide plane is assumed, our approach defines the depth of the glide plane as the depth of the maximum failure probability from all the PoFs per depth step of a PoF-depth profile (Fig. 4.3b). We assume that the sediment-mechanical conditions from Strupler et al. (2017) that are representing the Oberrieden area (Fig. 4.1) are also valid for all the slopes surrounding the deep basin. This may be an oversimplification, as the mechanical characteristics may locally vary. However, data from core ZH15-K09 taken at the eastern slope of the basin (Fig. 4.1) support this assumption, because the lithostratigraphy and the geotechnical profiles show the same patterns and ranges of values (Appendix D Fig. D.5).

The FS vs. depth (z [m]) profile at a pixel (i) for each of the 2500 MCS runs is calculated by dividing the resisting forces (dependent on the MCS-selected s_u [Pa] for an undrained case, such as in the water-saturated, fine-grained sediments in our study area) by the downward-driving forces (dependent on the submerged unit weight of the sediment γ' [$N*m^{-3}$] that itself depends on the MCS-selected ρ_{bulk}-value and the unit weight of water (γ_w [$N*m^{-3}$]), the vertical depth (z [m]) below the lake bottom, and the slope gradient (α). As the infinite-slope model does not account for 'interslice forces' (i.e. shear, compression and tension forces acting between adjacent elements of sediment) on the slope, a pixelwise FS calculation will typically lead to an underestimation of the FS and overestimation of PoF (Terlien 1996; Dimmock et al. 2012). Therefore, as applied by Dimmock et al. (2012), an additional model bias term (B) is added to the equation. We use B = 1.25, as it assigns a

deterministic FS of 1 to the pixel groups in the today stable slopes that were characterised by a FS below 1 without the inclusion of a bias term.

$$FS(i,z,MCS) = \frac{B * s_u(z,MCS)}{\left(\int_0^z (\gamma'(\mathrm{MCS}))dz\right) * \sin\alpha(i) * cos\alpha(i) + PSA(i) * \left(\int_0^z (\gamma'(MCS) + \gamma_w)dz\right) * cos^2\alpha(i)} \quad (2)$$

PSA represents the horizontal pseudostatic acceleration [in terms of g], which cannot be compared to the PGA directly, as it only represents a fraction of the PGA (Kramer 1996). Different pseudostatic coefficients *k* (ranging from 0.05 to 0.5; Melo and Sharma, 2004 and references therein) have been applied by different studies. Terzaghi (1951) recommended k-values of 0.1 and 0.2 for 'severe' and 'violent' earthquakes, respectively. Additionally, site amplification (*f*) for soft sediments (Vs_{30} <180 m/s) is ~ 3 times higher compared to rocks (Vs_{30} > 760 m/s; Dobry et al. 2000). As the PGA data from the PSHA is calculated for a Vs_{30}=1100 m/s, we multiply it in our study with a combined coefficient k*f=0.5, considering both the pseudostatic coefficient (*k*) and site amplification (*f*) (Eq.3).

PSA(soft soil(i))=k*f*PGA(rock(i)) (3)

To investigate the combined effects of *k* and *f* on the $POF_{eo,}$ a sensitivity test is conducted, assuming that the pseudostatic coefficient k and the PGA amplification by soft sediment (f) cancel each other out, hence *k*f*=1 (i.e. PSA=PGA; Grilli et al. 2009). The PoF of each depth step per pixel was calculated by dividing the amount of FS values < 1 (that were calculated for each MCS run) by the total amount of simulations (2500). Subsequently, maps showing the maximum PoF and corresponding depth of maximum PoF below lake bottom are calculated. Compared to the 1D-SSA approach applied by Strupler et al. (2017), two important changes are implemented in the spatial, grid-based approach: The sediment-thickness for the sediment-mechanical units at any pixel (i) in the study basin is estimated with the sedimentation model (section 4.3.1), and to reduce computation time, the depth sampling rate of the sediment-mechanical stratigraphy is reduced by a factor of 10.

4.3.3 Back-Analysis of the ~2210 cal. years BP event

To test the robustness of the model performance and to estimate the strength of the earthquake shaking, we conduct a back-analysis of the ~2210 cal. years BP slide in the Oberrieden area (Fig. 4.2). This slide, with a translation area of ~150'000 m^2 is assumed to be earthquake-triggered, as it occurs coevally with 9 other slides basin-wide (Strasser and Anselmetti 2008; Strupler et al. 2017). The sediment thickness of the drape at the time of failure is calculated with the sedimentation model (for the time ~2210 cal. years BP). In order to derive the slope gradient without post-slide morphological disturbances (i.e. channels, ridges), the extent of the eroded area is converted from raster to isobaths. The isobaths are smoothed and subsequently interpolated into a new grid, representing a homogenized slide plane. The PoF_g at each depth step at the time ~2210 cal. years BP is calculated from FS-distributions (Eq.2) for given PSA scenarios (i.e. 0, 0.02, 0.04, 0.06 0.08, and 0.1 g), and the failure plane assigned to the depth of the maximum PoF_g.

4.3.4 Assessment of the subaquatic earthquake-induced landslide hazard

The earthquake hazard potential is considered by using the probabilistic peak ground acceleration (PGA) for exceedance probabilities in 50 years (EP_{50}) of 10, 2, and 0.5% (i.e. mean return periods (RP) of 475, 2475, and 9975 years). Spatially distributed PGA values (Wiemer et al., 2016) are spatially interpolated in ArcGIS with the 'Kriging' algorithm, to converge from 10 km to 10 m grid resolution. Subsequently, the high-resolution PGA values corresponding to the different EP_{50} are converted to PSA with Eq. 3 and used in Eq. 2 to calculate PoF_{eo} maps. Finally, these maps are used to assess the subaquatic earthquake-triggered landslide hazard in Lake Zurich.

4.4 Results

This section provides first the potentially mobile sediment thickness, resulting from the sedimention model. Next, the results of the back analysed PoF_g for the ~2210 cal. years BP Oberrieden slide are presented. Finally, after showing a slope failure susceptibility map for the present-day sediment drape, we show the results of the earthquake-triggered subaquatic landslide hazard, given the input of a probabilistically estimated PGA.

4.4.1 Thickness of the potentially mobile sediment

The cumulative sediment thicknesses of the different SMU visualize the results of the sedimentation model (Fig. 4.5): In general, the greatest SMU thicknesses can be found in great water depths with gentle slope gradients (such as in the SE-corner of the study area). In shallow, steep zones, only little sediment accumulates, and consequently the smallest SMU thicknesses can be found there. For the basin-wide present-day situation (Fig. 4.5a), the cumulative thickness of most lateral slopes (gradient 5°-15°) ranges between 5 and 8 m. Basin-wide thicknesses of SMU3 and SMU4 vary between 0 and 1.8 m and 0 and 4.8 m, respectively (Appendix D, Fig. D.3). While at the time of the ~2210 cal. years BP slide, between ~4 and ~7 m of sediment was available on most parts of the slopes (Fig. 4.5b), up to ~1.5 m of sediment have been deposited on the slopes since that time (Appendix D, Fig. D.4).

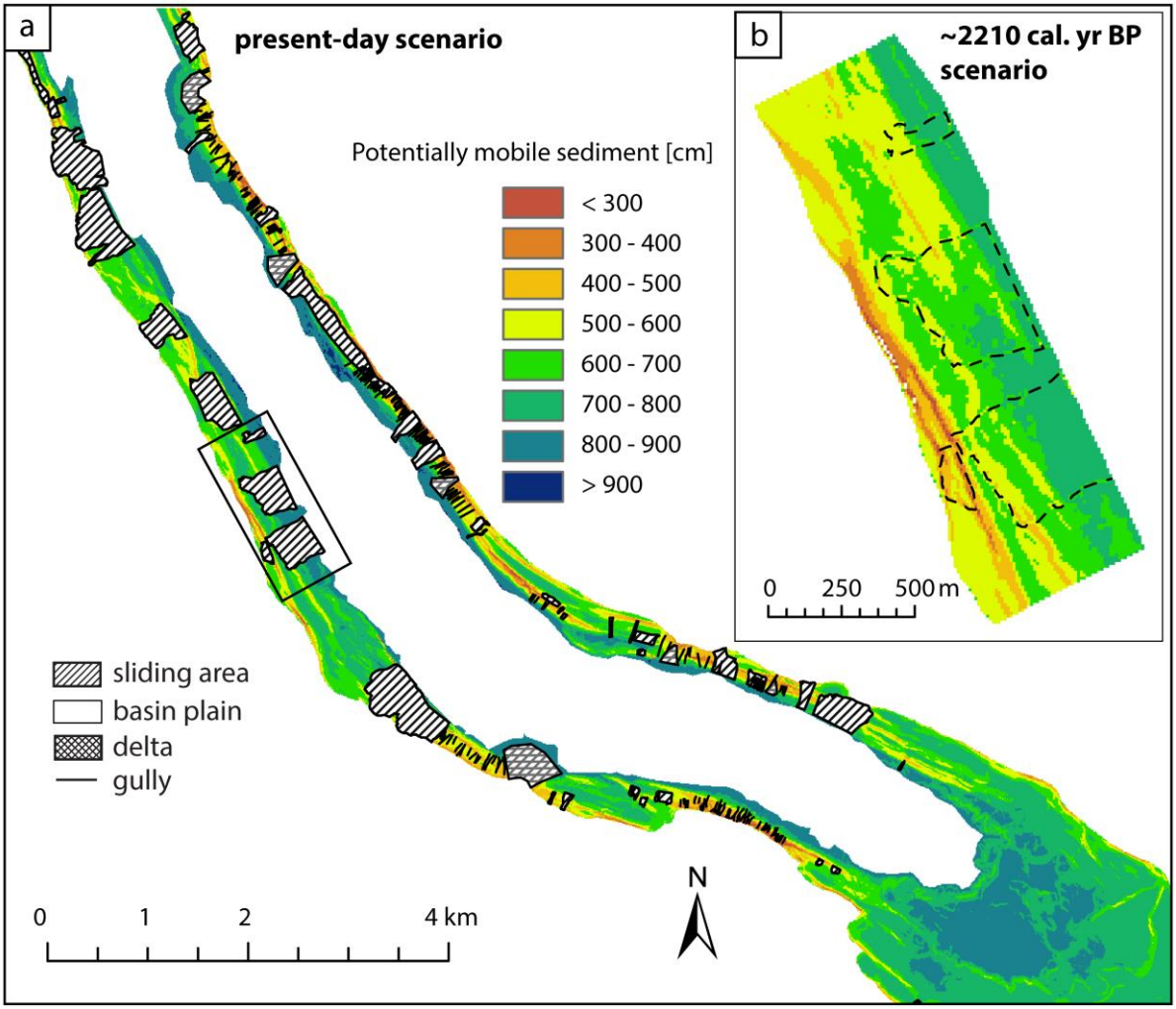


Figure 4. 5 Cumulative thickness of the potentially mobile sediment-mechanical units for the present-day situation (a) and the scenario ~2210 cal. years BP (b).

4.4.2 Back analysed PoF_g for the ~2210 cal. years BP landslide in Oberrieden

Grid-based PoF_g for the sediment drape at the time of the ~2210 cal. years BP event, calculated for different pseudostatic accelerations, are shown in Fig. 4.6. For a static situation (i.e. no external load) no major group of pixels with a PoF_g of greater than 0.2 can be found (Fig. 4.6a), indicating a generally stable slope. Whereas for PSA scenarios 0.2 and 0.4 g, a great part of the slope shows a low PoF_g (0-0.2) and only isolated zones have a PoF_g greater than 0.4, PoF_g become generally high (i.e. > 0.6) for PSA scenarios higher than 0.6 g (Figs. 4.6d-f). For a PSA of 0.08 g, the northern and southern parts of the Oberrieden slope shows a lower PoF_g towards the shore, while the central part of the slope shows high PoF_g (0.6-1) from nearshore to the toe of the basin. For a PSA scenario of 0.1 g, practically the whole slope has a PoF_g between 0.8 and 1.

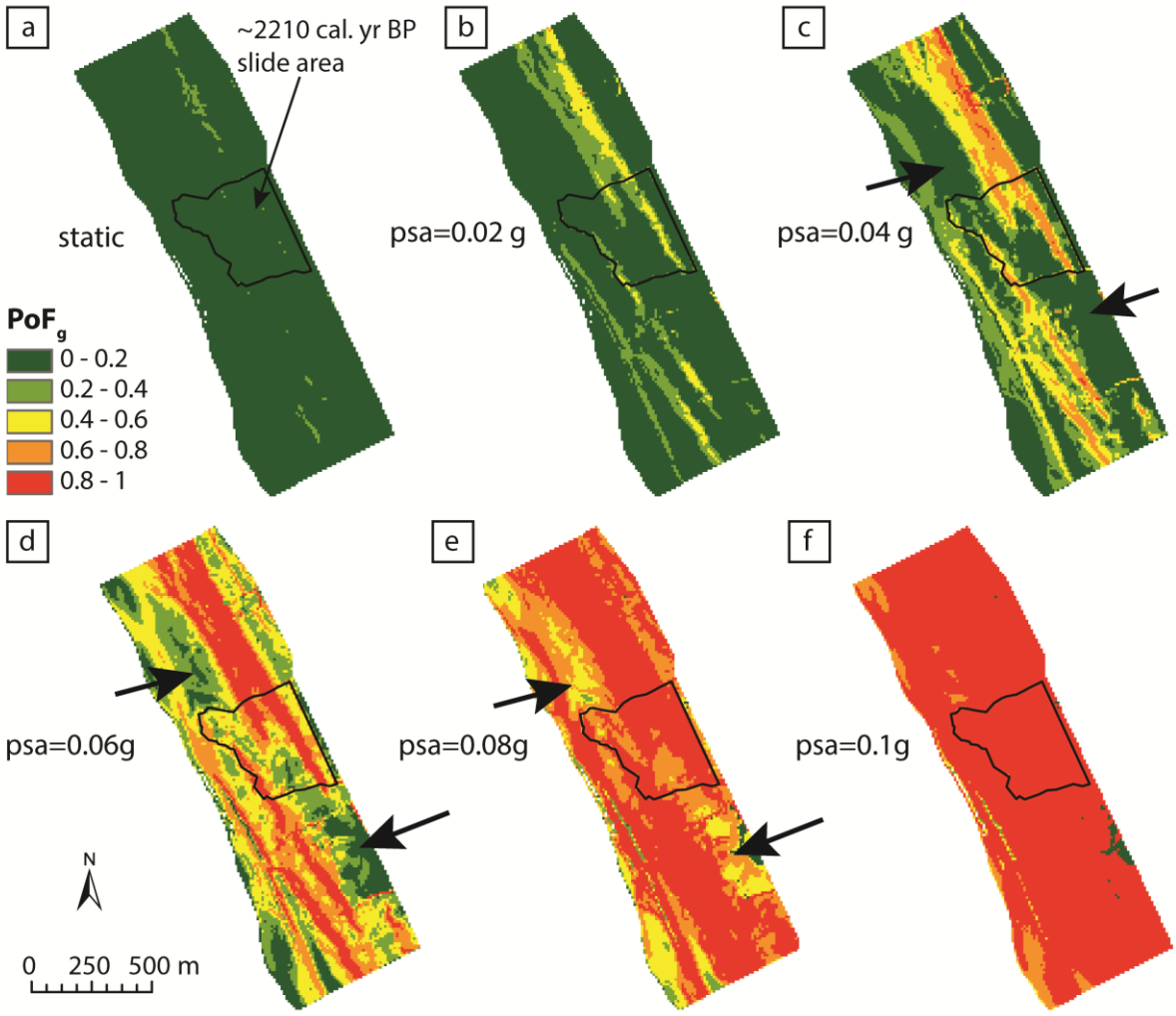


Figure 4. 6 Different pseudostatic earthquake acceleration scenarios (PSA=0, 0.02, 0.04, 0.06, 0.08 and 0.1g) for the Oberrieden slope at the time ~2210 cal. years BP resulting in different PoF. Black polygon shows extent of the ~2210 cal. years BP slide. Arrows mark isolated zones with a relatively low PoF compared to the surroundings.

A multiplication of the sum of the depth of the maximum PoF_g of all pixels (Appendix D, Fig. D.6.) with the cell size leads to a mobilized slide volume of the ~2210 cal. years BP slide in the range between ~583'000 and 818'000 m^3 (Table 4.3).

Table 4. 3 Modelled slide volumes for selected PSA scenarios presented in Fig. 4.6

PSA scenario [g]	Modelled slide volume [m^3]
0.04	582'900
0.06	803'900
0.08	817'500

4.4.3 Basin-wide slope-failure susceptibility of the static present-day situation

A basin-wide SSA for the present-day situation under static loading conditions show that 87 % of the studied slopes have a PoF_g of <0.2, 8% a PoF_g between 0.2 and 0.4, 4% a PoF_g between 0.4 and 0.6, and 0.5% have a PoF_g between 0.6 and 0.8 and 0.8 to 1, respectively (Fig. 4.7). Most of the pixel aggregations with a PoF_g > 0.4 occur on the steep slopes, where gullies occur. Only a few steep zones without gullies, located mostly in mid-slope or down-slope positions show a relatively high PoF_g (0.4-0.6). An interpretation of such relatively high static PoF_g is provided in the discussion section.

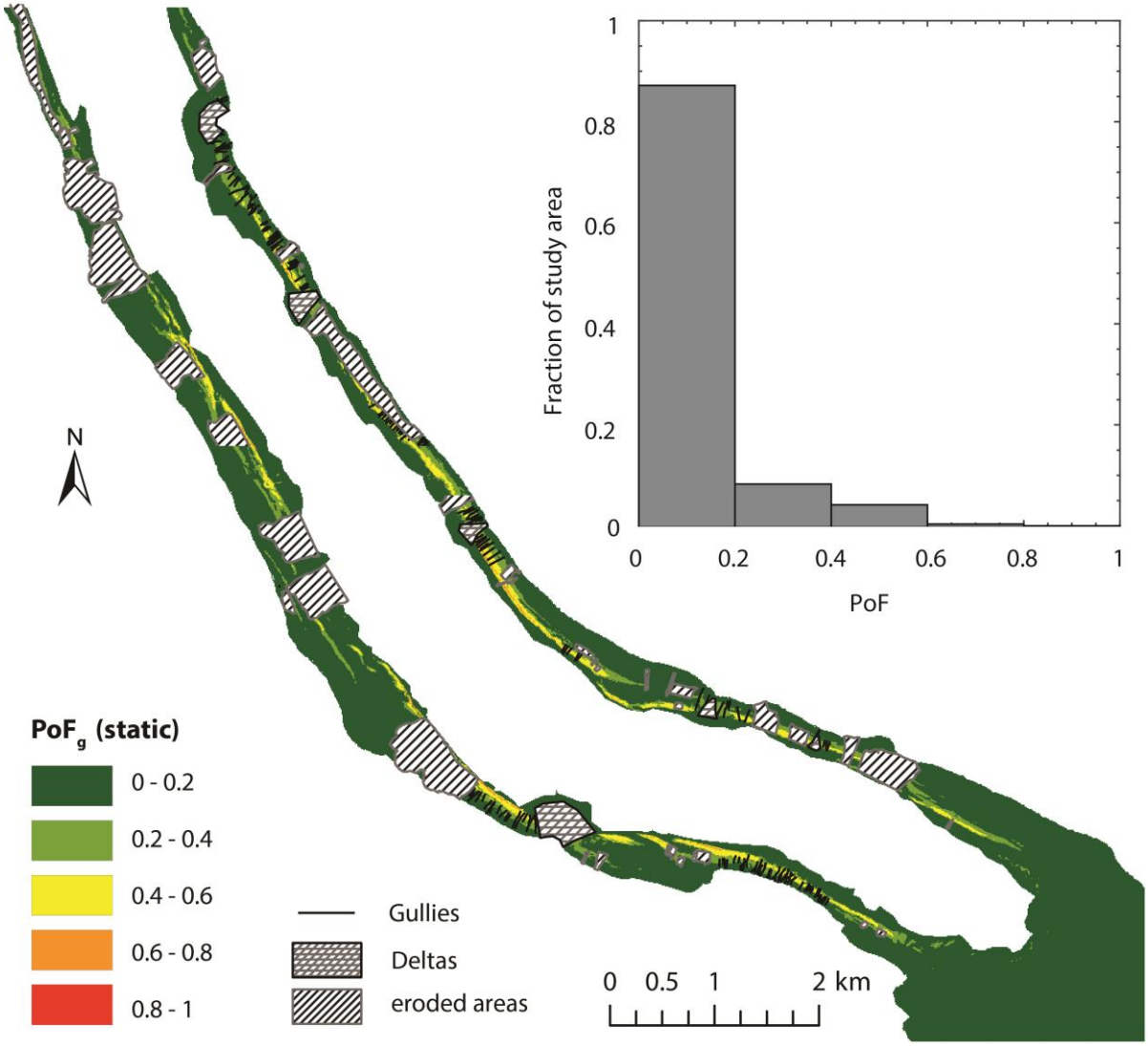


Figure 4. 7 Slope failure susceptibility map for the present-day situation for a static case (i.e. no external trigger)

4.4.4 Earthquake-triggered, basin-wide subaqueous landslide-hazard

4.4.4.1 Spatially interpolated ground-shaking values (PGA)

The reference hazard curve for Oberrieden gives the exceedance probabilities of various levels of PGA in 50 years. Median and two percentiles (5^{th} and 95^{th}) as provided by the 2015 updates of the Swiss Hazard Model (Wiemer et al. 2016) are illustrated in Fig. 4.8a. The horizontal black-dashed lines represent the considered EP_{50} and their corresponding PGA values (vertical black-dashed lines). Note, the smaller the EP_{50}, the greater the expected PGA values (Fig. 4.8).
In the whole study area, the median PGA values vary around ~0.05, ~0.1 and ~0.2 g for EP_{50} of 10, 2 and 0.5%, respectively. Values are slightly higher in the southeastern than in the northwestern part of the basin, due to proximity to the Alps (Wiemer et al. 2016).

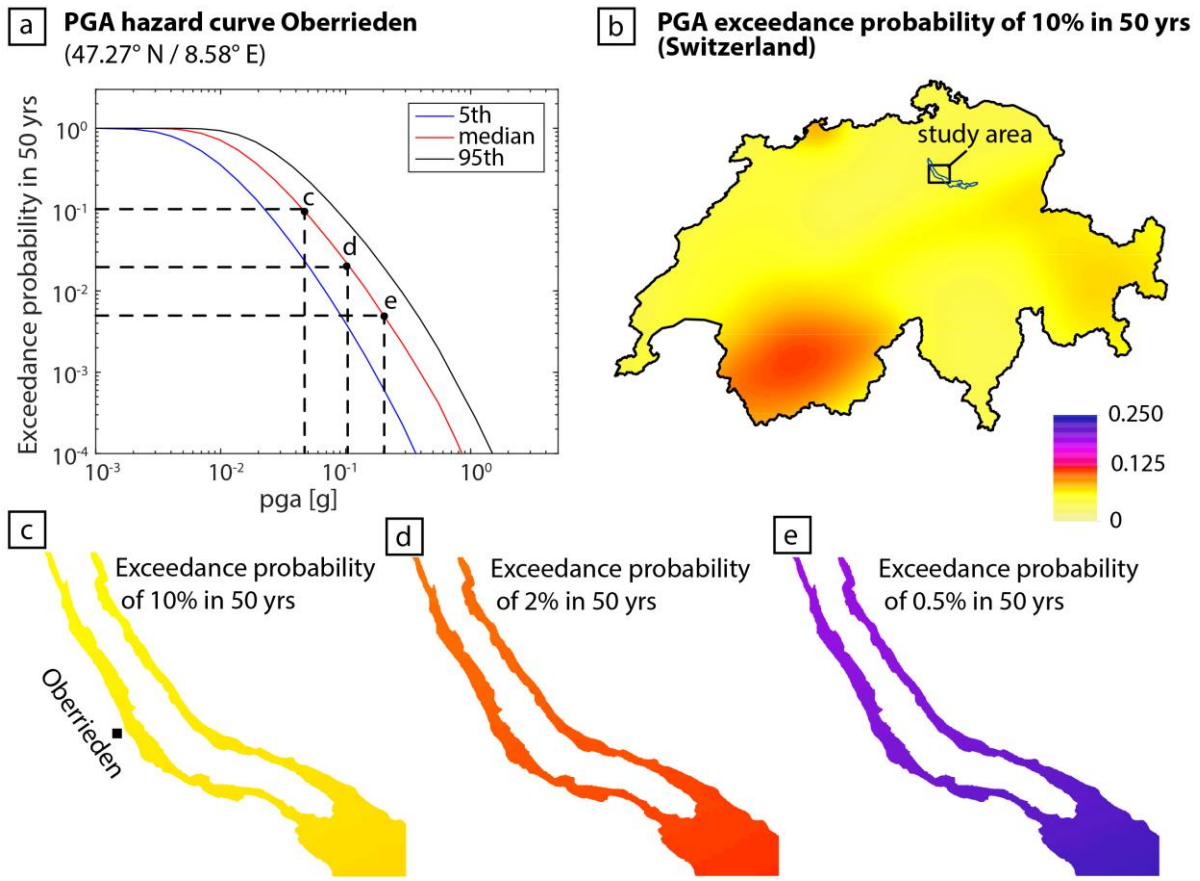


Figure 4. 8 a) Seismic hazard curves for Oberrieden as provided by the 2015 Swiss Seismic Hazard Model (Wiemer et al. 2016). b) Reference hazard map depicting PGA values for exceedance probabilities of 10% in 50 years. The study area is marked with a black rectangle. The spatial distributions of PGA for exceedance probabilities of 10, 2 and 0.5% in 50 years for the lateral slopes of Lake Zurich are shown in the subfigures c,d and e. Switzerland borders: swisstopo.

4.4.4.2 Basin-wide PoF_{eo} for PGA levels at different EP_{50}

In general, the PoF_{eo} increases with larger PGA values, which can be expected with smaller exceedance probabilities (Figs. 4.8 and 4.9). PGA values for an EP_{50} of 10% cause a high PoF (i.e. >0.6) at the steeper zones of the slope (~20°). Relatively gentle slopes (< 10°) show a low PoF (i.e. <0.2) for a PGA with an EP_{50} of 10% (Fig. 4.9a). For PGA values with an EP_{50} of 2%, only the gentle slopes (i.e. gradients < ~5°) show low to medium PoF_{eo} values (i.e. 0.4; Fig. 4.9b). For PGA values with an EP_{50} of 0.5%, all lateral slopes show a PoF between 0.8 and 1 (Fig 4.9c).

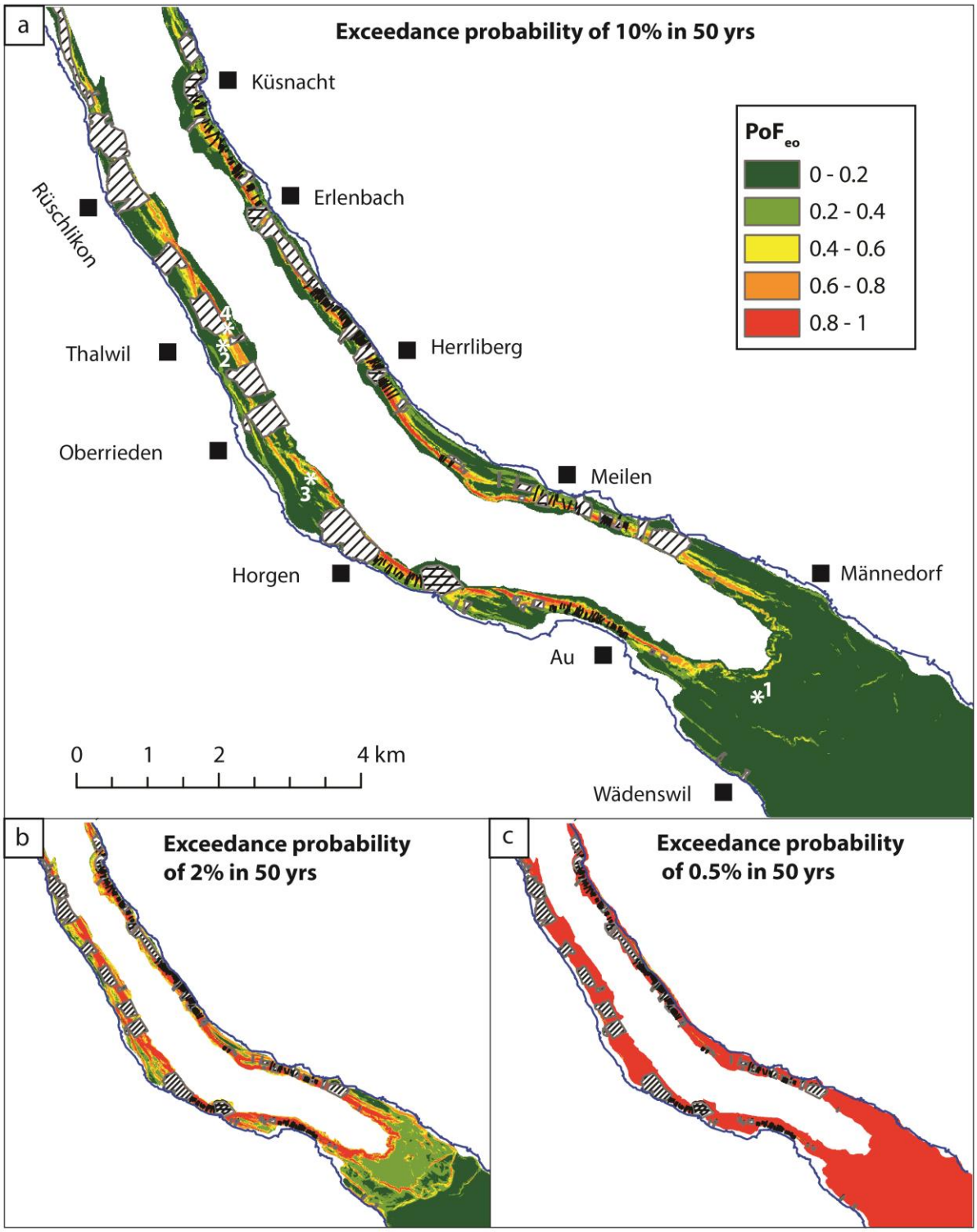


Figure 4. 9 PoF_{eo} *of each pixel given the forecasted, pixel-wise PGA (median) exceedance probabilities (c.f. Fig. 4.8) from the PSHA. Shorelines: swisstopo.*

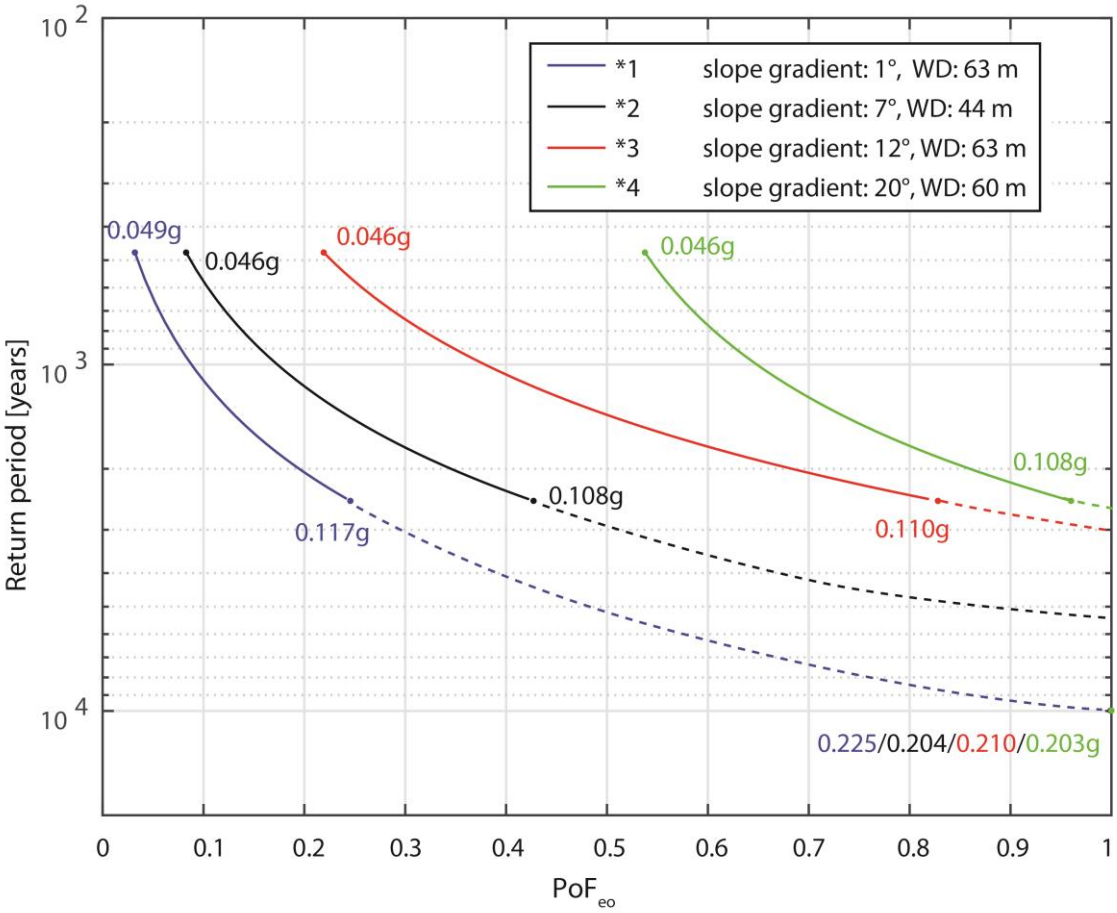


Figure 4. 10 PoF_{eo} vs. forecasted median PGA for different return periods at four selected locations with different slope gradients. The locations are indicated with white asterisks in Fig. 4.9. (dashed line is manually continued). Points are labelled with their local PGA values corresponding the respective EP_{50}.

The PoF_{eo} for selected locations with different slope gradients (indicated in Fig. 4.9 with white asterisks), plotted against median PGA for different mean RP are shown in Fig. 4.10. The blue and black curves, representing low slope gradients (of 1° and 7°, respectively) show a slower increase of PoF_{eo} with increasing mean RP than a medium slope gradient (12°, red curve). For slopes with steep gradients (~20°, green curve), however, the PoF_{eo}, increases slower with PGA values for higher mean return periods. This suggests a non-linearity between the involved factors slope gradient, water depth and thickness of the SMUs, which are also dependent on the slope gradient and water depth (c.f. sedimentation model), leading to the calculation of the PoF_{eo}. For steep slopes (20°, green curve), the slope gradient (and thus gravity) has a stronger influence on the PoF_{eo} than the PSA. This results from the applied limit equilibrium equation on an infinite slope, where the PSA is multiplied by the cosine of the slope, hence the steeper the slope, the smaller the influence of the PSA (i.e. cos 0° = 1 and cos 90°; scenario of a vertical slope = 0). Figure 4.10 also shows that for a mean RP of 9975 yrs (i.e. EP_{50} of 0.5%), the PoF_{eo} equals 1 for the selected locations. As the maximum PoF_{eq} is per definition 1 (i.e. 100%), the data points for a RP of 9975 yrs (i.e. EP_{50} of 0.5%) that show all a PoF_{eq}

of 1 are not following the expected linear fit for the same slope gradient, manually continued with a dashed line in the semi-logarithmic plot (Fig.4.10).

4.5 Discussion

In this section we discuss the results presented in the previous chapter in the context of the research questions posed in section 4.1.

4.5.1 Potentially mobile sediment on the lateral slopes

The water depth and slope gradient have a great influence on the estimated sedimentation rate: The greater the water depth, the more sediment, and the steeper the slope, the less sediment. This is consistent with dynamic processes along steep slopes, where hemipelagic sediment settled through the water column is not deposited but directly re-mobilized due to gravity and deposited at the foot of the slope. Due to the fact that the glide planes of the investigated slides in a previous study did not occur at a boundary between two sediment-mechanical units but rather within SMU1 (Strupler et al. 2017), the cumulative thickness of the sediment-mechanical units overestimates the potentially mobile sediment (as it accounts the whole SMU1 to the slide depth). Hence, we consider the potentially mobile sediment volume from the calculated depth of the modelled slide surface, characterised by the highest PoF value (Appendix D, Figs. D.6 and D.7.). The potentially mobile sediment volume is discussed for the back-analysis in section 4.5.2 and for the present-day hazard assessment in section 4.5.3.

4.5.2 Back-analysed PoF_g of the ~2210 cal. years BP slide for different PSA scenarios

The PoF_g < 0.2 for a static scenario (Fig. 4.6a) indicates a low probability of a spontaneous failure (i.e. without additional trigger) for the reconstructed sediment-drape thickness at the time of the ~2210 cal. years BP subaqueous landslide offshore Oberrieden. This supports the hypothesis by Strasser and Anselmetti (2008) of an earthquake as trigger for the ~2210 cal. years BP event. A PSA between 0.04 g (Fig. 4.6c) and 0.08 g (Fig. 4.6e) seems the most plausible for explaining the triggering of the 2210 cal. years BP event. The lower PSA limit can be constrained as many pixels in the area where the slide occurred show values with a PoF_g of between 0.6 and 1. The upper PSA limit can be constrained by the fact that a PSA of > 0.08 g would effect in a PoF_g of 0.8-1 for almost all pixels of the slope, which would most probably have resulted in a larger, slope-wide subaquatic slide. Converting the PSA values to PGA values with a k*f value of 0.5, PGA values between 0.08 and 0.16 g are suggested for the ~2210 cal. years BP event (Eq.3), approximating the expected PGA values for an earthquake with an EP_{50} of 2% (RP of 2475 yrs). The back-calculated values by Strasser et al. (2007) for the ~2220 cal. years BP event in neighbouring Lake Lucerne show a similar range (PGA = 0.06-0.16 g) as from our determination.

The modelled slide volume for a PSA scenario of 0.04 g (~583’000 m^3) is slightly lower than the first-order estimated volume (~750’000 to 1’050’000 m^3) by Strupler et al. (2017). This PSA scenario assigns a low depth of glide plane to the zones with a low PoF (Fig. 4.6 and Appendix D Fig. D.6) and might thus underestimate the slide volume. However, both calculated volumes of the slide for a

PSA of 0.06 and 0.08 g (Table 4.3) are within the range of the volume estimated by Strupler et al. (2017).

An exact determination of the lateral extents of the slides on the basis of the slope-stability modelling is not conclusive, because both high and low PoF_g values are calculated for the area inside and outside of the slope portion that failed during the ~2210 cal. years BP event. No clear pattern can be recognized from the PoF_g distribution that would allow to correctly predict the lateral extent of the landslide. However, it seems that the lateral extent of the ~2210 cal. years BP event is defined by a continuously high PoF throughout the slope (i.e. from the top to the toe of the slope), caused by local slope-gradient characteristics. The more gently inclined zones with a lower PoF to the north and south of the translation area of the slide (marked with arrows in Fig. 4.6) may have prevented the partially unstable zones of the slope to fail. A more sophisticated model would be needed to assess the exact slide extents (e.g. Bellugi et al. 2015). In conclusion, the back-analysis of the ~2210 cal.years BP slide offshore Oberrieden can be regarded as a proof of concept, as the estimated PSA values are in the range of similar events, the modelled slide volume is in the same range as estimations with other methods (Strupler et al. 2017), and as the slide occurred on areas with high calculated PoF_g values.

4.5.3 Subaqueous landslide hazard in Lake Zurich

4.5.3.1 Basin-wide subaquatic slope-failure susceptibility (PoF_g) for the present-day situation

Most parts of the slopes have a low PoF (i.e. < 0.2), indicating stable conditions for the present-day situation under static loading, i.e. without external trigger (Fig. 4.7). According to our model, the zones with steeper slope gradients (i.e. > 25° in Fig. 4.1) with a medium PoF_g (i.e. 0.4-0.6) are susceptible to failure for a static case. Due to the fact that gullies in Lake Zurich occur on most of these steep parts of the slope, and that no major landslide deposits can be found at the bottom of the lake below the gullied slopes, we assume that these gullies act as pathways of sediment transport (Field et al. 1999), as the slope is too steep for a considerable sediment accumulation. A subsequent failure of these parts of the slopes is thus very unlikely, suggesting the model is not valid on these steep slopes (>25°). Different mechanisms have been proposed for the formation of such gullies, e.g. slope-parallel bottom currents, sediment-gravity currents, among others (e.g. Field et al. 1999; Izumi 2004; Sultan et al. 2004; Fedele and García 2009; Micallef and Mountjoy 2011).

The assumption of constant SMU1 and SMU2 thicknesses may also contribute to the relatively high static PoF_g on the above mentioned slopes. For the few steep parts of the slopes, where no gullies occur, it cannot be excluded that spontaneous failures without an earthquake trigger occur. However, as their downslope length is often relatively short compared to the whole slope, they might be buttressed by the surrounding sediment. Also, landslides are mostly expected on slopes where greater accumulations of pixels with high PoF are found (Terlien 1996), thus such smaller zones with high PoF_g may not be enough to trigger landslides.

4.5.3.2 Earthquake-induced landslide hazard

While landslide-susceptibility maps show areas where future landslides are expected to occur, a landslide-hazard map includes the probability of their occurrence within a given observational time, e.g. described by the exceedance probability in 50 years (EP_{50}). The earthquake-triggered subaquatic landslide hazard has been assessed and discussed with different methods in the past (Urgeles et al. 2002; Grilli et al. 2009; Strasser et al. 2011; Dimmock et al. 2012). A novelty of our approach, which combines data from a high-resolution sediment-mechanical stratigraphy (Strupler et al. 2017) integrated in spatial PoF_g analyses with probabilistically estimated ground motions (Wiemer et al. 2016), is that the hazard is directly calculated as PoF_{eo} (Fig. 4.9). Plotting the PoF_{eo} as function of the mean return periods represents a novel tool to facilitate communicating the landslide hazard. To our knowledge, this constitutes one of the first sublacustrine earthquake-triggered landslide hazard maps (Fig. 4.9). The proposed methodological approach may also be applied for slopes in the marine realm.

For a forecasted median PGA for a EP_{50} of 10% (i.e. PGA values of ~0.05 g), slopes with gradients >20° become unstable ($PoF_{eq} > 0.6$; Figs. 4.9, 4.10 and 4.11). The comparably twice as high median PGA values expected for an EP_{50} of 2% (i.e. PGA values of ~0.1 g) would cause, under today's sediment load, most slopes greater than ~10° to fail. The ~2210 cal. years BP event mapped by Strasser and Anselmetti (2008) might represent such an event with an EP_{50} of 2% (RP 2245 years), as 10 basin-wide large mass failures are assigned to it, but not all lateral slopes failed coevally (which would rather suggest an earthquake with an EP_{50} of 0.5%). However, because of the up to ~1.5 m thinner sediment drape at that time, in general the Oberrieden slope was more stable ~2210 cal. years BP than it is at present. This means that some previously (i.e. 2210 cal. years BP) stable areas would fail at present for PGA scenarios with the same EP_{50}. Our model indicates that an earthquake with an EP_{50} of 0.5% (RP of 9975 years), would cause the simultaneous failure of all slopes (Figs. 4.9, 4.10, 4.11). We do not have any evidence for a coeval failure of all lateral slopes in the bathymetric nor in the seismic reflection datasets, covering timescales of the past 5'000 and ~17000 years, respectively (Strasser and Anselmetti 2008; Strupler et al. 2015). However we do not exclude such a strong earthquake with PGAs of an EP_{50} of 0.5% since deglaciation. As the lacustrine chalks (SMU3) and marls (SMU4) were only deposited in the last ~12'000 years (Strasser and Anselmetti 2008) and thus before then, no SMU3 and SMU4 were draping the Late Glacial plastic muds (SMU1). This means that the sediment load on today's weak layer (SMU1) must have been much lower back then. Therefore, the sublacustrine slopes might have stayed stable during a relatively strong earthquake in the beginning of the Holocene.

The absolute depth (within the sediment column) of the maximum PoF_{eo} for each pixel depends on the external load applied to the sediment column by the earthquake (Appendix D, Fig.D.7). For relatively gentle dipping slopes (<5°) with little earthquake loading, the maximum PoF_{eo} can be found in the uppermost dm of the sediment column, caused by the higher variability of the s_u-data in the uppermost layers (Strupler et al. 2017). For medium to steep slopes (> 15°), or for relatively gentle slopes with increased earthquake loading, this uppermost increased PoF_{eo} does not represent

the maximum PoF_{eo} of the PoF_{eo} vs. depth profile anymore, as the increasing horizontal component of gravity force and the resulting increased PSA value shift the maximum PoF_{eo} to SMU1. For moderate and steeper parts of the slope, the potential glide plane is always located in SMU1 (Late Glacial plastic muds). For the comprehensive SSA, we consider the fact that the maximum (albeit very low) PoF_{eo} on such gentle slopes is located in the uppermost dm of the sediment column as not relevant, as it is rarely greater than 0.2. Also, the maximum PoF_{eo} in the uppermost dm of the sediment column indicates that the PoF in SMU1 must be even smaller on such flat slopes. Based on the maps displaying the subaqueous earthquake-triggered landslide hazard, the individual zones of potential future landslides are mapped manually. In the following paragraphs we show and discuss potential landslide zones for a PoF_{eo} >0.6, excluding deltaic and zones and gullies (Fig. 4.11). This threshold value was selected in order to map the most probable areas of landslides. A pixel-wise multiplication of the zonal potential landslide area with the depth of the maximum PoF_{eo} for different EP_{50} leads to an estimation of potential landslide volumes.

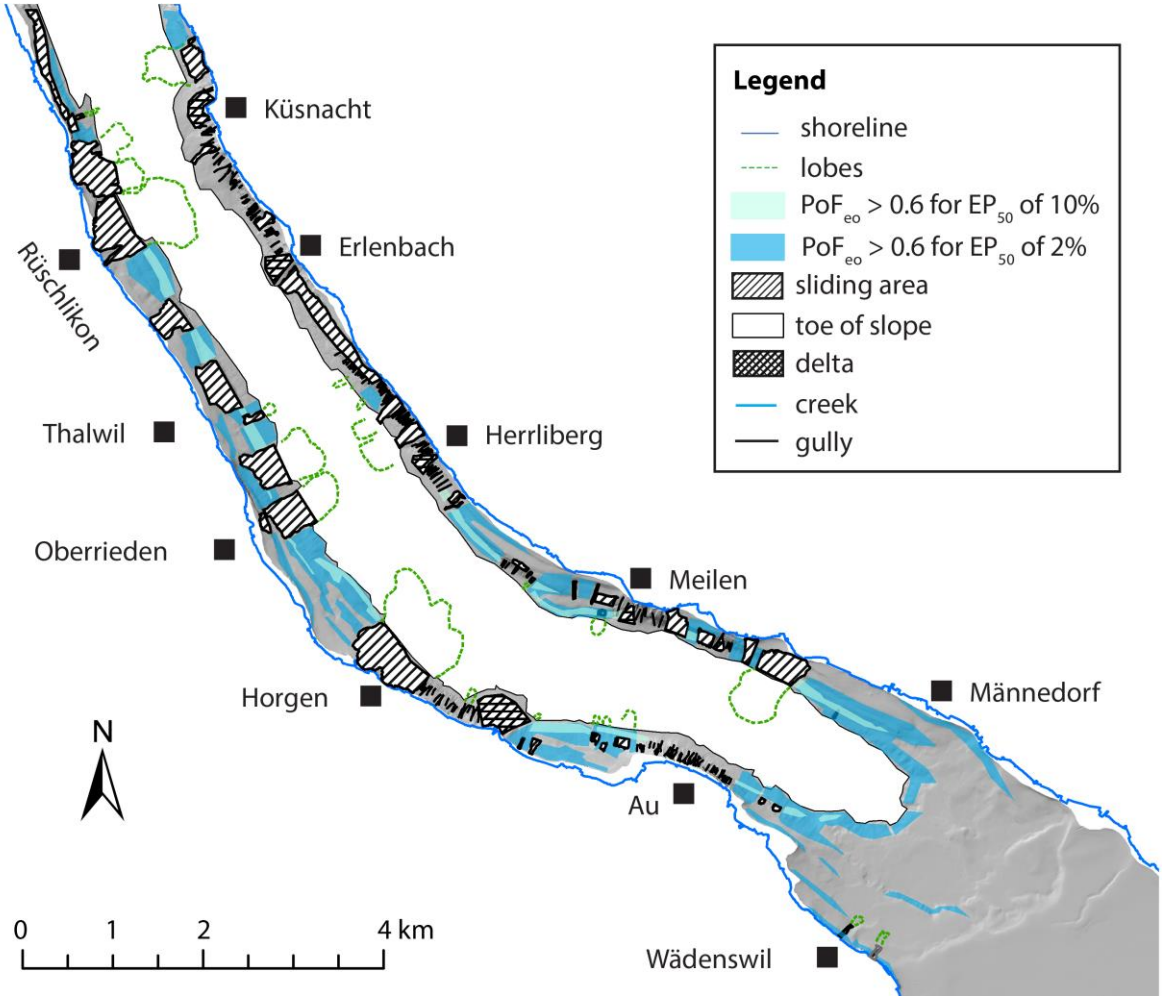


Figure 4. 11 Mapped most probable slide scenarios for EP50 of 10 (light blue) and 2% (dark blue): PoF_{eo} >0.6 for EP50 of 0.5% is not mapped for illustrating reasons, as it covers all yet unfailed slopes.

For an earthquake with an EP_{50} of 10%, a maximum basin-wide landslide area of ~600'000 m^2 and maximum volume of ~3 Mio m^3 is expected, if all considered slopes failed simultaneously ('worst

case scenario'; Appendix D, Table D.2). Most of the areas on the slopes presently prone to failure show potential translation areas that are smaller than the past slide areas, mapped in Strupler et al. (2015). These zones are mostly located midslope, especially on the northeast-facing slopes between the villages of 'Rüschlikon' and 'Thalwil' (potentially mobile volumes of ~540'000 m^3). The zone just north of the Horgen slide (Heim 1876; Kelts and Hsü 1980) is considered as relatively stable for an PGA with an EP_{50} of 10%. An earthquake with an EP_{50} of 2% (i.e. RP of 2475 yrs), may trigger landslides with a cumulative area and volume of ~2.2 Mio m^2 and ~12 Mio m^3, respectively. Especially failure-prone slopes are located between 'Rüschlikon' and 'Thalwil', in the zone south of the 1875 Horgen slide and north of Au (each with potentially mobile volumes of up to ~1.9 Mio m^3), and between 'Meilen' and 'Männedorf' (potentially mobile volumes of 4.3 Mio m^3; Appendix D, Fig. D.8 and Table D.3). For a scenario of an earthquake with an EP_{50} of 0.5%, a maximum cumulative sliding area and volume of ~13 Mio m^2 and ~70 Mio m^3, respectively, is estimated. The greatest potentially mobile sediment volumes for an EP_{50} of 0.5% are located at the geomorphic escarpment structure, separating the deep basin from the shallower basin to the south (Figure 4.1), where slope gradients are very low, indicating a low potential slide velocity.

Concluding, the slopes most prone to failure in Lake Zurich are the ones with a gradient between ~10° and ~25° (Fig. 4.11). This is also the slope range where most of the identifiable slides in the DDM occurred during the last ~5000 years (Strasser et al. 2013; Strupler et al. 2015). A similar range of slope gradients was identified as failure-prone by Strasser et al. (2011) for Lake Lucerne. The earthquake-induced landslide hazard should not be ignored, as most of the yet unfailed lateral slopes contain parts with a very high seismic landslide hazard. While for EP_{50} of 10 and 2% the amount of relatively small, individual slides is high, for EP_{50} of 0.5%, landslides with much greater extent and volumes are estimated. These maximum cumulative potential slide volumes for the different EP_{50} scenarios should be considered as worst-case scenarios, as all the mapped slides would occur coevally.

Disaggregation of seismic hazard at a given location provides the tool to identify controlling (i.e. most likely) scenarios for specific ground motion levels. We disaggregate the seismic hazard at the location of the deepest point of the central basin for the different mean return periods (i.e. 475 years, 2475 years and 9975 years). The controlling scenarios - defined by Mw and distance (R) in km, are: M_w = 4.7 and R 12.5 km for a mean return period of 475 years, Mw = 4.7 and R 7.5 km for a mean return period of 2475 years, and Mw = 5.1 and R 7.5 km for a mean return period of 9975 years (Appendix D, Figs. D.10-D.12).

4.5.4 Limitations and quality of our approach

Since the earliest attempts of slope-stability assessments (SSA), engineers have been plagued with discrepancies in the results obtained (Bertoldi 1988). The scope of this study was not to provide the absolute numbers of failure probability. Rather, we present a new approach for the assessment of the subaqueous, earthquake-induced landslide hazard in subaqueous settings. The results should thus be considered as a first-order estimation, due to the above mentioned limitations of the methods used in the analysis. However, the here presented subaquatic landslide-hazard map indicates parts of the slopes that are more prone to failure than others, which is valuable information, especially for estimating the consequences of potential slides.

Our results build on various datasets, each including uncertainties. The geotechnical uncertainties are considered by a Monte Carlo sampling of the input values, and the uncertainties concerning earthquake accelerations are respected in the PSHA of Wiemer et al. (2016). Nevertheless, our approach still contains some limitations, including the following points:

- As already mentioned in Strupler et al. (2017), the assumption of the infinite-slope mode that the glide plane is planar, is not strictly valid for the slopes of Lake Zurich (Switzerland), which show an irregularly changing bathymetry. Also, using a pseudostatic approach, where a constant force acting only in one direction is applied to the sediment column does not consider the earthquake-shaking history (e.g. Jibson 2011). A strong shaking for a very short time does not necessarily need to cause failure, which is not considered in the here used pseudostatic approach, implying only first-order estimations of slope stability. As the constant pseudostatic force, represented by the peak ground acceleration, acts only briefly, a pseudostatic coefficient is selected. However, the selection of such a pseudostatic coefficient is difficult although critically important (Bray and Travasarou 2009; Jibson 2011). The coefficient also depends on the fundamental period (Ts) of the sliding mass, which is calculated by the division of four times the height of the sliding mass (H) by Vs_{30} of the sediment (e.g. Bray and Travasarou 2009, Eq. 4):

  $$Ts = \frac{4H}{Vs_{30}} \qquad \text{(Equation 4)}$$

  Due to missing information on the Vs_{30} of Lake Zurich's sediments, and because literature values for subaqueous and mainly silty-clayey soils show Vs_{30} values in the range between <100 and 400 m/s (e.g. Ewing et al. 1992; European Commitee for Standardization 2004; Hunter et al. 2007; Vessia et al. 2015), these values could not be calculated. The influence of the seismic coefficient and the PGA amplification on the PoF_{eo} is demonstrated in a sensitivity test (Appendix D, Fig. D.9), where it is assumed that *k* and *f* cancel each other out (*k***f*=1), thus PSA is assumed equal to PGA in that case and consequently, the PoF_{eo} is much higher. For example, while most of the slopes show a low PoF_{eo} (i.e. <0.4) for PGA forecasted for an EP_{50} of 10%, assuming k*f=0.5, most of the slopes show a high PoF_{eo} (i.e. >0.6) for k*f=1.
- A calculated high PoF, which implies slope failure, does not necessarily mean that a landslide will result immediately. As a first stage of unstable slopes, some local deformations of the sediment on the slopes may occur (e.g. Leroueil et al. 1996; Shillington et al. 2012).
- Another limitation is that our approach does not consider possible hydrological effects. However, as deltas are excluded in our SSA, and no fluid flow evidence can be found in the geoacoustic datasets, we consider such effects not relevant for Lake Zurich. The exclusion of deltas, however, may underestimate the landslide hazard, as delta failures can happen even without additional triggers (e.g. Girardclos et al. 2007), mainly because of high sediment input. Strasser and Anselmetti (2008) mapped a mass transport deposit at the base of the

Küsnacht Delta (Fig. 4.1), documenting such a delta collapse. In future studies, delta collapses should be included in subaqueous hazard assessments.

- The quality of the sedimentation model can be independently controlled with the thickness of the sediment-mechanical units from cores (Appendix D, Tab. D1; Strasser and Anselmetti 2008; Strupler et al. 2017). Due to positioning uncertainties during coring, vertical uncertainty in reflection seismic data and local sedimentation-rate variations, the sedimentation has some uncertainties. There is no clear trend identifiable, for which slope- and water-depth characteristics the error is greatest. The mean deviation between the calculated and the measured sediment thickness is smaller than 10% for both SMU3 and SMU4. Also, uncertainties in age intervals of the sediment-mechanical units (+/- ~200 years for the bottom of SMU4 and +/-400 years for the bottom of SMU3) affects their thickness. However, this uncertainty affects changes in the sediment column by variations of ~1 dm and is thus smaller than the influence of the above mentioned other uncertainties. We assume a constant sedimentation rate for the time intervals during SMU3 and SMU4. An age model from Strasser and Anselmetti (2008), however, indicates that while during deposition of SMU3, the sedimentation rate remained more or less constant, sedimentation rate was slightly greater in the last ~1000 cal. years BP This provides another uncertainty for the thickness of the sediment drape at the time ~2210 cal. years BP.
- Our model is not valid for slopes with gradients > 25°. However, as on most of these slopes gullies occur that inhibit sedimentation by directly transporting the sediment to the toe of the slope, these steep zones are regarded to remain stable, as no potentially mobile sediment is available.

In general, it is difficult to judge the quality of a hazard assessment, as a predicted hazard can only be verified or falsified by its occurrence or not-occurrence (Heinimann et al. 1998). However, the fact that the already failed slopes in the study area are surrounded by zones with a high slope-failure susceptibility motivates the usefulness of our approach. The results of the back-analysis at the case-study site ‘Oberrieden’ can be regarded as ‘proof of concept’, although they also show the limitations in predicting the exact lateral extent of landslides. The back-analysis as well as the slope-failure scenarios from the hazard assessment of the present-day situation, suggest that a PGA with an EP_{50} of 2% (i.e. mean recurrence time of ~2475) years characterize the ~2210 cal. years BP prehistorical event.

4.5.5 Outlook

Hazard assessments should be an ongoing process (Wang et al. 2005), which need updates if changes in the input parameters occur. Ongoing sedimentation will increase the hazard (by adding more sediment load on the slopes) whereas removal of sediment by future landslides will decrease the subsequent hazard. In a future work, it may be investigated whether the documented landslides on the

lateral slopes of Lake Zurich were capable of triggering tsunamis and, if that is the case, they could be quantified. Also, based on the here presented subaquatic earthquake-triggered landslide hazard map, a tsunami hazard assessment may be conducted.
Furthermore, the earthquake-triggered hazard may be assessed with the spectral acceleration as a function of the fundamental period of the soil, instead of PGA, to include resonance. To achieve this, knowledge of Vs_{30} of the sediments on the lateral slopes is required.
Regarding the mechanism of slope failures in near-shore areas, there is a general lack of knowledge. For assessing the shore-loading induced landslide hazard, an approach that combines onshore and offshore data is needed (L'Heureux et al. 2013). For example, small subsidences caused by shore loading may be detected by remote sensing techniques, such as differential SAR interferometry. As the shores of Lake Zurich are densely populated, potential shore collapses always pose a threat to infrastructure along the shore.

4.6 Conclusions

We present an approach for the basin-wide earthquake-induced subaquatic landslide hazard assessment, based on high-resolution sediment-mechanical and geophysical input data. Furthermore, we provide a first quantitative landslide-hazard estimation for the lateral slopes in Lake Zurich. To this end, a sedimentation model is calibrated from sediment cores and seismic data, to map the thicknesses of the sediment-mechanical units. Parts of the slopes in greater water depth and low slope gradients show the greatest thicknesses of the mechanical units. The mapped sediment-mechanical unit thicknesses were used in a spatial limit-equilibrium model on an infinite slope, with Monte Carlo sampled input values from log-normally distributed mechanical properties of the lateral slopes from a previous study (Strupler et al., 2017).
The following outcomes are highlighted:

- A back-analysis for the ~2210 cal. years BP Oberrieden landslide revealed pseudostatic critical accelerations in the range of 0.04 to 0.08 g (corresponding to PGA values between ~0.08 and 0.16 g). This acceleration is comparable to back-calculated values of the ~2220 cal. years BP in Lake Lucerne.
- In terms of hazard, the ~2210 cal. years BP event in Lake Zurich can be assigned to an earthquake with an exceedance probability of 2% in 50 years (median PGA values of ~0.1g). A similar earthquake happening for the present-day sediment drape is assumed to cause failure at zones that remained stable during the ~2210 cal. years BP event, due to a change stability conditions, caused by additional sediment loading.
- A hazard evaluation of the present-day sediment drape indicates, that an earthquake with a probability of 10% in 50 years (median PGA of ~0.05 g) may be sufficient to trigger multiple, yet minor subaqueous landslides on the lateral slopes of Lake Zurich. An earthquake with an exceedance probability of 2% in 50 years (median PGA of ~0.1 g) might cause major failures on the lateral slopes, where as an earthquake with an exceedance probability of 0.5% in 50 years

(median PGA of ~0.2 g) might be considered as 'worst case' scenario, where all slopes are supposed to fail (estimated volume ~70 Mio m^3).

- Generally, for earthquakes with ground accelerations forecasted for exceedance probabilities of 10 and 2 % in 50 years, the slopes most prone to failure have gradients between 10 and 25°. Such slopes can mostly be found i) between the villages of Thalwil and Rüschlikon with potential failure volumes of ~540'000 and 1'900'000 m^3 for an exceedance period of 10 and 2% in 50 years, respectively, ii) south of the 1875-Horgen slide (with potential failure volumes of ~ 490'000 and 1'900'000 m^3) and iii) between Meilen and Herrliberg with potential failure volumes of ~ 440'000 and 4'320'000 m^3).

It is obvious that subaqueous landslides in Lake Zurich will occur in the future. Hence, it is important to estimate where and when they will occur, and what threat they pose to society. While we cannot control most of the factors determining the landslide hazard (e.g. geological conditions and earthquakes; Mulder et al. 1994), we should take mitigation measures and be prepared where possible. For most of the land areas in Switzerland, well-established hazard maps exist (Heinimann et al. 1998; Lateltin 2002). However, subaquatic hazards are not included so far. This study emphasizes the need of including subaqueous earthquake-triggered landslide hazard also in the official hazard maps.

Acknowledgements

This work was supported by the Swiss National Foundation Grant Nr. 133481. Utsav Mannu is thanked for his help with speeding up the Matlab code. Andrea Wolter is thanked for the discussions on the interslice-forces.

References

Aleotti P and Chowdhury R (1999) Landslide hazard assessment: summary review and new perspectives. Bulletin of Engineering Geology and the Environment 58:21–44. doi: 10.1007/s100640050066

Bellugi D, Milledge DG, Dietrich WE, Perron JT and McKean J (2015) Predicting shallow landslide size and location across a natural landscape: Application of a spectral clustering search algorithm. Journal of Geophysical Research: Earth Surface 120:2552–2585. doi: 10.1002/ 2015JF003520

Bertoldi CE (1988) Computer simulation of progressive failure in soil slopes. Doctor of Philosophy thesis, Department of Civil and Mining Engineering, University of Wollongong.

Bollinger D (1996) Erfassung, Darstellung und Beurteilung von Naturgefahren - Sinn und Zweck. In: Oddson B (ed) Instabile Hänge und andere risikorelevante natürliche Prozesse - Nachdiplomkurs in angewandten Erdwissenschaften. Birkhäuser, Basel, pp 55–66

Bray JD and Travasarou T (2009) Pseudostatic Coefficient for Use in Simplified Seismic Slope Stability Evaluation. Journal of Geotechnical and Geoenvironmental Engineering 135:1336–1340. doi: 10.1061/(ASCE)GT.1943-5606.0000012

Chapron E, Beck C, Pourchet M and Deconinck JF (1999) 1822 earthquake-triggered homogenite in Lake Le Bourget (NW Alps). Terra Nova 11:86–92. doi: 10.1046/j.1365-3121.1999.00230.x

Dan G, Sultan N and Savoye B (2007) The 1979 Nice harbour catastrophe revisited: Trigger mechanism inferred from geotechnical measurements and numerical modelling. Marine Geology 245:40–64. doi: 10.1016/j.margeo.2007.06.011

Dimmock P, Mackenzie B and Mills a J (2012) Probabilistic Slope Stability Analysis in the West Nile Delta. In: Allan P (ed) Offshore site investigation and geotechnics. Proceedings of the 7th International Offshore site Investigation and Geotechnics Conference. London, pp 535–542

Dobry R, Borcherdt RD, Crouse CB, Idriss IM, Joyner WB, Martin GR, Power MS, Rinne EE and Seed RB (2000) New Site Coefficients and Site Classification System Used in Recent Building Seismic Code Provisions. Earthquake Spectra 16:41–67. doi: 10.1193/1.1586082

European Commitee for Standardization (2004) Eurocode 8: Design of structures for earthquake resistance - Part 1 : General rules, seismic actions and rules for buildings. European Committee for Standardization 1:231. doi: [Authority: The European Union per Regulation 305/2011, Directive 98/34/EC, Directive 2004/18/EC]

Ewing J, Carter JA, Sutton GH and Barstow N (1992) Shallow-Water Sediment Properties Derived From High-Frequency Shear and Interface Waves. Journal Of Geophysical Research-Solid Earth 97:4739–4762. doi: 10.1029/92jb00180

Fäh D, Giardini D, Kästli P, Deichmann N, Gisler M, Schwarz-Zanetti G, Alvarez-Rubio S, Sellami S, Edwards B, Allmann B, Bethmann F, Wössner J, Gassner-Stamm, G. Fritsche S and Eberhard D (2011) ECOS-09 Earthquake Catalogue of Switzerland Release 2011. Report and Database. Public catalogue, 17.4.2011. Zürich

Fedele JJ and García MH (2009) Laboratory experiments on the formation of subaqueous depositional gullies by turbidity currents. Marine Geology 258:48–59. doi: 10.1016/j.margeo.2008.11.004

Field ME, Gardner J V. and Prior DB (1999) Geometry and significance of stacked gullies on the northern California slope. Marine Geology 154:271–286. doi: 10.1016/S0025-3227(98)00118-2

Girardclos S, Schmidt OT, Sturm M, Ariztegui D, Pugin A and Anselmetti FS (2007) The 1996 AD delta collapse and large turbidite in Lake Brienz. Marine Geology 241:137–154. doi: 10.1016/j.margeo.2007.03.011

Grilli ST, Taylor ODS, Baxter CDP and Maretzki S (2009) A probabilistic approach for determining submarine landslide tsunami hazard along the upper east coast of the United States. Marine Geology 264:74–97. doi: 10.1016/j.margeo.2009.02.010

Hammond CJ, Prellwitz RW and Miller SM (1991) Landslide hazard assessment using Monte Carlo simulation. In: Bell DH (ed) Landslides. Balkema, Rotterdam, pp 959–964

Heim A (1876) Bericht und Expertengutachten über die im Februar und September 1875 in Horgen am Zürichsee vorgekommenen Rutschungen. Die Eisenbahn 4:191–196.

Heinimann HR, Hollenstein K, Kienholz H, Krummenacher B and Mani P (1998) Methoden zur Analyse und Bewertung von Naturgefahren. Umwelt-Materialien Naturgefahren 85:248.

Henriod S, Douard R, Ullmann D and Humbel R (2016) Statistik der Bevölkerung und Haushalte (STATPOP). Bundesamt für Statistik (BFS), Bern. BFS-Nummer: be-d-00.03-13-STATPOP-v16

Hilbe M and Anselmetti FS (2014) Signatures of slope failures and river-delta collapses in a perialpine lake (Lake Lucerne, Switzerland). Sedimentology n/a-n/a. doi: 10.1111/sed.12120

Hilbe M and Anselmetti FS (2015) Mass Movement-Induced Tsunami Hazard on Perialpine Lake Lucerne (Switzerland): Scenarios and Numerical Experiments. Pure and Applied Geophysics 172:545–568. doi: 10.1007/s00024-014-0907-7

Hoffmann G and Reicherter K (2016) Geohazards: Coastal Disasters. In: Harff J, Meschede M, Petersen S, Thiede Jö (eds) Encyclopedia of Marine Geosciences. Springer Netherlands, Dordrecht, pp 276–283

Hunter JA, Burns RA, Good RL, Aylsworth JM, Pullan SE, Perret D and Douma M (2007) Borehole shear wave velocity measurements of Champlain Sea sediments in the Ottawa-Montreal region, Open File 5345, CD ROM.

ISSMGE (2004) Glossary of Risk Assessment Terms - Version 1. TC32 - Technical Committee on Risk Assessment and Management 66:1–7.

Izumi N (2004) The formation of submarine gullies by turbidity currents. Journal of Geophysical Research 109:1–13. doi: 10.1029/2003JC001898

Jibson RW (2011) Methods for assessing the stability of slopes during earthquakes—A retrospective. Engineering Geology 122:43–50. doi: 10.1016/j.enggeo.2010.09.017

Jibson RW, Harp EL and Michael JA (2000) A method for producing digital probabilistic seismic landslide hazard maps. Engineering Geology 58:271–289.

Kelts K (1978) Geological and sedimentary evolution of Lakes Zurich and Zug, Switzerland. ETH Zurich, PhD Thesis, Nr.6146

Kelts K, Briegel U, Ghilardi K and Hsu K (1986) The limnogeology-ETH coring system. Swiss Journal of Hydrology 48:104–115. doi: 10.1007/BF02544119

Kelts K and Hsü KJ (1980) Resedimented facies of 1875 Horgen slumps in Lake Zurich and a process model of longitudinal transport of turbidity currents. Eclogae geol Helv 73:271–281.

Kramer SL (1996) Geotechnical Earthquake Engineering. Prentice-Hall, Upper Saddle River

Kremer K, Hilbe M, Simpson G, Decrouy L, Wildi W and Girardclos S (2015) Reconstructing 4000 years of mass movement and tsunami history in a deep peri-Alpine lake (Lake Geneva, France-Switzerland). Sedimentology 1305–1327. doi: 10.1111/sed.12190

Kremer K, Simpson G and Girardclos S (2012) Giant Lake Geneva tsunami in ad 563. 5:2011–2013.

Kuen E (1999) Der Uferabbruch im Kusen. In: Küsnachter Jahrheft. Ortsgeschichtliche Kommission der Kulturellen Vereinigung Küsnacht, pp 44–50

L'Heureux J-S, Hansen L, Longva O and Eilertsen RS (2013) Landslides Along Norwegian Fjords: Causes and Hazard Assessment. In: Margottini C, Canuti P, Sassa K (eds) Landslide Science and Practice. Springer Berlin Heidelberg, Berlin, Heidelberg, pp 81–87

Lateltin OJ (2002) Landslides , land-use planning and risk management : Switzerland as a case-study. In: McInnes, R.G. and Jakeways J (ed) Instability: Planning and Management. Thomas Telford, London, pp 89–96

Lee EM and Jones DKC (2014) Landslide Risk Assessment, 2nd edn. ICE Publishing, London

Leroueil S, Vaunat J, Picarelli L, Locat J, Lee H and Faure R (1996) Geotechnical characterisation of slope movements. In: Senneset K (ed) Landslides, 1st edn. Balkema, Rotterdam, pp 53–74

Melo C and Sharma S (2004) Seismic Coefficients for Pseudostatic slope analysis. Paper No. 369.

Micallef A and Mountjoy JJ (2011) A topographic signature of a hydrodynamic origin for submarine gullies. Geology 39:115–118. doi: 10.1130/G31475.1

Moernaut J and De Batist M (2011) Frontal emplacement and mobility of sublacustrine landslides: Results from morphometric and seismostratigraphic analysis. Marine Geology 285:29–45. doi: 10.1016/j.margeo.2011.05.001

Moernaut J, De Batist M, Charlet F, Heirman K, Chapron E, Pino M, Brümmer R and Urrutia R (2007) Giant earthquakes in South-Central Chile revealed by Holocene mass-wasting events in Lake Puyehue. Sedimentary Geology 195:239–256. doi: 10.1016/j.sedgeo.2006.08.005

Monecke K, Anselmetti FS, Becker A, Sturm M and Giardini D (2004) The record of historic earthquakes in lake sediments of Central Switzerland. Tectonophysics 394:21–40. doi: 10.1016/j.tecto.2004.07.053

Mueller C, Mountjoy J, Power W, Lane E and Wang X (2016) Towards a Spatial Probabilistic Submarine Landslide Hazard Model for Submarine Canyons. In: Lamarche G, Mountjoy J, Bull S, et al. (eds) Submarine Mass Movements and their Consequences. Cham, pp 589–597

Mulder T, Tisot JP, Cochonat P and Bourillet JF (1994) Regional assessment of mass failure events in the Baie des Anges, Mediterranean Sea. Marine Geology 122:29–45. doi: 10.1016/0025-3227(94)90203-8

Nadim F, Kalsnes B and Eide A (1996) Analysis of submarine slope stability under seismic action. In: Senneset K (ed) Landslides. Balkema, Rotterdam, pp 561–565

Nipkow F (1927) Über das Verhalten der Skelette planktischer Kieselalagen im geschichteten Tifenschlamm des Zürich- und Baldeggersees. ETH Zurich, PhD Thesis, Nr. 455

Praet N, Moernaut J, Van Daele M, Boes E, Haeussler PJ, Strupler M, Schmidt S, Loso MG and De Batist M (2016) Paleoseismic potential of sublacustrine landslide records in a high-seismicity setting (south-central Alaska). Marine Geology. doi: 10.1016/j.margeo.2016.05.004

Reusch A, Moernaut J, Anselmetti FS and Strasser M (2016) Sediment mobilization deposits from episodic subsurface fluid flow-A new tool to reveal long-term earthquake records? Geology 44:243–246. doi: 10.1130/G37410.1

Schnellmann M, Anselmetti FS, Giardini D, McKenzie JA and Ward SN (2002) Prehistoric earthquake history revealed by lacustrine slump deposits. Geology 30:1131–1134. doi: 10.1130/0091-7613(2002)030<1131:PEHRBL>2.0.CO;2

Shillington DJ, Seeber L, Sorlien CC, Steckler MS, Kurt H, Dondurur D, Çifçi G, Imren C, Cormier MH, McHugh CMG, Gürçay S, Poyraz D, Okay S, Atgin O and Diebold JB (2012) Evidence for widespread creep on the flanks of the sea of Marmara transform basin from marine geophysical data. Geology 40:439–442. doi: 10.1130/G32652.1

Smith SB, Karlin RE, Kent GM, Seitz GG and Driscoll NW (2013) Holocene subaqueous paleoseismology of lake tahoe. Bulletin of the Geological Society of America 125:691–708. doi: 10.1130/B30629.1

Strasser M and Anselmetti FS (2008) Mass-movement event stratigraphy in Lake Zurich; A record of varying seismic and environmental impacts. Beiträge zur Geologie der Schweiz 95:23–41.

Strasser M, Anselmetti FS, Fäh D, Giardini D and Schnellmann M (2006) Magnitudes and source areas of large prehistoric northern Alpine earthquakes revealed by slope failures in lakes. Geology 34:1005. doi: 10.1130/G22784A.1

Strasser M, Hilbe M and Anselmetti FS (2011) Mapping basin-wide subaquatic slope failure susceptibility as a tool to assess regional seismic and tsunami hazards. Marine Geophysical Research 32:331–347. doi: 10.1007/s11001-010-9100-2

Strasser M, Monecke K, Schnellmann M and Anselmetti FS (2013) Lake sediments as natural seismographs: A compiled record of Late Quaternary earthquakes in Central Switzerland and its implication for Alpine deformation. Sedimentology 60:319–341. doi: 10.1111/sed.12003

Strasser M, Stegmann S, Bussmann F, Anselmetti FS, Rick B and Kopf A (2007) Quantifying subaqueous slope stability during seismic shaking: Lake Lucerne as model for ocean margins. Marine Geology 240:77–97. doi: 10.1016/j.margeo.2007.02.016

Strupler M, Hilbe M, Anselmetti FS, Kopf AJ, Fleischmann T and Strasser M (2017) Probabilistic stability evaluation and seismic triggering scenarios of submerged slopes in Lake Zurich (Switzerland). Geo-Marine Letters 37:241–258. doi: 10.1007/s00367-017-0492-8

Strupler M, Hilbe M, Anselmetti FS and Strasser M (2015) Das neue Tiefenmodell des Zürichsees: Hochauflösende Darstellung der geomorphodynamischen Ereignisse im tiefen Seebecken. Swiss Bull angew Geol 20:71–83.

Sultan N, Cochonat P, Canals M, Cattaneo A, Dennielou B, Haflidason H, Laberg JS, Long D, Mienert J, Trincardi F, Urgeles R, Vorren TO and Wilson C (2004) Triggering mechanisms of slope instability processes and sediment failures on continental margins: A geotechnical approach. Marine Geology 213:291–321. doi: 10.1016/j.margeo.2004.10.011

Terlien MTJ (1996) Modelling spatial and temporal variations in rainfall triggered landslides: The Integration of Hydrologic Models, Slope Stability Models and Geographic Information Systems

for the Hazard Zonation of Rainfall-triggered Landslides with Examples from Manizal. PhD Thesis. International Institute for Aerospace Survey and Earth Sciences (ITC)

Terzaghi K (1951) Mechanisms of Landslides. Harvard University, Harvard

Urgeles R, Locat J, Lee HJ and Martin F (2002) The Saguenay Fjord, Quebec, Canada: integrating marine geotechnical and geophysical data for spatial seismic slope stability and hazard assessment. Marine Geology 185:319–340. doi: 10.1016/S0025-3227(02)00185-8

Vessia G, Rainone ML and Signanini P (2015) Vs and NSPT Measures for Seismic Characterization of Soils. In: Engineering Geology for Society and Territory. pp 1143–1147

Waldmann N, Anselmetti FS, Ariztegui D, Austin Jr J a., Pirouz M, Moy CM and Dunbar R (2011) Holocene mass-wasting events in Lago Fagnano, Tierra del Fuego (54°S): implications for paleoseismicity of the Magallanes-Fagnano transform fault. Basin Research 23:171–190. doi: 10.1111/j.1365-2117.2010.00489.x

Wang HB, Liu GJ, Xu WY and Wang GH (2005) GIS-based landslide hazard assessment: an overview. Progress In Physical Geography 29:548–567. doi: 10.1191/0309133305pp462ra

Wiemer S, Danciu L, Edwards B, Marti M, Fäh D, Hiemer S, Wössner J, Cauzzi C, Kästli P and Kremer K (2016) Seismic Hazard Model 2015 for Switzerland. 1–163. doi: 10.12686/a2

Wiemer S, Giardini D, Fäh D, Deichmann N and Sellami S (2009) Probabilistic seismic hazard assessment of Switzerland: best estimates and uncertainties. Journal of Seismology 13:449–478. doi: 10.1007/s10950-008-9138-7

Chapter 5

Subaqueous landslide-triggered tsunami hazard for Lake Zurich, Switzerland

This chapter was submitted to Swiss Journal of Geosciences as Strupler, M., Hilbe, M., Kremer, K., Danciu, L., Anselmetti, F.S., Strasser, M., and Wiemer, S. Subaqueous landslide-triggered tsunami hazard for Lake Zurich, Switzerland.

Abstract

Subaqueous landslides can induce tsunamis that may cause damage to society and infrastructure. Tsunamis are not restricted to the marine environment, but have also been documented on lakes in Switzerland and worldwide. For Lake Zurich (central Switzerland), previous work documented multiple, assumedly earthquake-triggered landslides. However, no information about past tsunamis is available for Lake Zurich. In a back-analysis, we model tsunami scenarios as a consequence of the earthquake-triggered landslides in the past. Furthermore, on the basis of a recent map of the earthquake-triggered subaqueous landslide hazard, we present results of a tsunami hazard assessment. The subaqueous landslide progression, wave propagation and run-up are calculated with a combination of open source codes. Results indicate that for a past landslide event that occurred at ~2210 cal. yr BP, a tsunami with peak wave heights of up to ~1.5 m may have occurred if all the assigned landslides of that event occurred simultaneously. Although no historic evidence of past tsunamis has been documented for Lake Zurich, a tsunami hazard exists. However, only earthquakes with long return periods are assumed to cause considerable tsunamis. An earthquake with an exceedance probability of 0.5 % in 50 years (corresponding to an earthquake with a return period of 9975 years) is assumed to cause tsunamigenic landslides on most lateral slopes of Lake Zurich. A hypothetical tsunami for such an event would create damage especially along the shores of the central basin of Lake Zurich with estimated peak flow depths of up to ~4.6 m. Our results suggest that for an earthquake with an exceedance probability of 10 % in 50 years (i.e. mean return period of 475 years), no considerable tsunami hazard is estimated. Even for a worst-case scenario, the cities of Zurich and Rapperswil, located at the northern and southern ends of the lake, respectively, are assumed to experience very little damage. The here presented estimated wave heights and inundated zones can be considered as first-order results, showing rather conservative values. However, the results provide valuable information on tsunami-prone areas that can be used for further investigations and mitigation measures.

5.1 Introduction

5.1.1 Background

Subaqueous landslides can be triggered by different mechanisms, e.g. earthquakes, wave loading, water-level changes, sediment overloading, or fluid escape (e.g. Locat and Lee 2002). In many cases, such subaqueous landslides occur without anybody's awareness (Lee et al. 1993). In some cases, however, subaqueous landslides may induce tsunamis (i.e. gravity-driven water waves), that potentially cause damage to civilisation and coastal infrastructure (e.g. Jiang and Leblond 1992; Tappin 2017). The height of landslide-generated waves depends primarily upon the volume of the mass movement, its initial acceleration, speed, water depth and coherence (Watts 1998; Tappin et al. 2008; Bornhold and Thomson 2012). A subaqueous landslide typically creates waves that travel both in the direction of the slide and opposite to the slide (Tinti and Bortolucci 2000). In general, tsunamis have much higher velocities, wave lengths and periods than wind-driven waves, resulting in different consequences on the shoreline (Ward 2011). The impact of tsunamis on the shores can be described by the run-up (i.e. the vertical distance between the sea-/lake level at rest and maximum height reached by the tsunami on the shore), the inundation distance and inundation area (i.e. horizontal distance and area that a tsunami penetrates inland, respectively) and flow depth (i.e. the water depth during inundation on land) (Pararas-Carayannis 1988; Intergovernmental Oceanographic Commission 2016). Most of the tsunami waves do not break, they rather flow like a river on the shores (Pelinovsky and Mazova 1992; Ward 2011).

Well-investigated examples of past tsunamis resulting from earthquake-triggered landslides include the 1929 AD Grand Banks landslide tsunami, triggered off the NE coast of the United States (Fine et al. 2005; ten Brink et al. 2009), and the 1998 Papua New Guinea tsunami (Tappin et al. 1999; Tappin et al. 2001; Synolakis et al. 2002). Modelling of assumedly earthquake-triggered subaqueous landslides also allowed the investigation of past tsunamis in New Zealand (Wang et al. 2016) and Puerto Rico (López-Venegas et al. 2008). Previous work suggested that earthquakes have repeatedly caused multiple subaqueous landslides on the slopes of Swiss perialpine lakes (e.g. Schnellmann et al. 2002; Strasser et al. 2013; Kremer et al. 2014; Reusch et al. 2016). Some of these slides were even related to historically reported tsunamis in Lake Lucerne (Siegenthaler et al. 1987; Schnellmann et al. 2002), which were reproduced with numerical modelling by Hilbe and Anselmetti (2015). The latter study combined publicly available codes for modelling mass movements, wave generation, propagation, and inundation to simulate historically reported and hypothetical tsunamis in Lake Lucerne. Peak wave heights and maximum run-up of several meters on the shores of Lake Lucerne were estimated.

For Lake Zurich, reflection seismic and bathymetric datasets (Schlund 1972; Strasser et al. 2013; Strupler et al. 2015) show fingerprints of many postglacial subaqueous mass movements affecting the lateral slopes. Three major basin-wide lateral slope-failure events (dated to ~2210, ~11600 and ~13760 cal. yr BP) were interpreted by Strasser et al. (2013) as earthquake-triggered, due to the synchronous occurrence of multiple slides in the lake basin (i.e. they appear on the same seismic stratigraphic horizon and are therefore considered coeval). It is not known whether tsunamis occurred as a consequence of these events, but it was hypothesized that the event ~13760 cal. yr BP might have triggered a tsunami (Strasser et al. 2008). For various human-triggered slides that occurred in

the last 150 years on the lateral slopes of Lake Zurich (Heim 1876; Nipkow 1927; Kelts and Hsü 1980; Kuen 1999), no tsunami waves have been reported. However, documented evidence of past landslides, as well as potentially unstable slopes that have been mapped for different earthquake hazard levels (Strupler et al. in press) highlight the need to assess the tsunamigenic potential of past and potential future subaqueous slope failures.

5.1.2 Objectives

This study presents a first-order tsunami-hazard assessment that follows up on the assessment of the earthquake-triggered subaqueous landslide hazard (Strupler et al. in press). The aims of this study are a) to investigate the tsunamigenic potential of past subaqueous landslides on the lateral slopes of Lake Zurich, and b) to assess the hazard of tsunamis related to potential future earthquake-triggered landslides in the study area. With the approach of Hilbe and Anselmetti (2015) and the model limitations described therein, the impact of different landslide scenarios are modelled in terms of peak wave height, onshore flow depth and inundation:

- The **past tsunamigenic potential** is investigated for an event of multiple basin-wide, assumedly earthquake-triggered landslides that occurred ~2210 cal. yr BP at the slopes of Lake Zurich (Strasser et al. 2013). From the three major events documented by Strasser et al. (2013), the ~2210 cal. yr BP event is selected for a back-analysis, as it occurred on the lateral slopes with the same lithostratigraphic succession as today's undisturbed slopes (due to its relatively younger age compared to the other events).
- The **current tsunami hazard** is assessed by simulating the consequences of basin-wide slope failures that are to be expected (Strupler et al. in press) for earthquake accelerations with a probability of exceedance in 50 years (EP_{50}) of 10%, 2% and 0.5% (i.e. mean return periods of 475, 2475 and 9975 years, respectively).

5.2 Setting of the study area and previous studies

5.2.1 Study area

Lake Zurich (~47° N, 8.5° E, 406 m a.s.l.) is located in a glacially overdeepened trough in northern Switzerland. Remnants of a recessional terminal moraine from the last glaciation separate Lake Zurich in two parts (e.g. Keller and Krayss 2005; Fig. 5.1). The part to the northwest of the moraine is termed Lake Zurich sensu stricto, and the part to the southeast of the moraine is termed Obersee. The northern part of Lake Zurich consists of a shallow zone near the city of Zurich, Switzerland's economic capital, followed by an up to 136 m deep, central basin and an again shallow (~25 m), flat southeastern basin, which hosts two islands 'Ufenau' and 'Lützelau' with highest elevations of 17 and 8 m above lake level, respectively. The central basin and the southeastern basin are connected via an escarpment structure with topographic steps in the Molasse bedrock. The main tributaries are the Linth, Jona and Wägitaler Aa rivers. The only outflow is the Limmat River at the northern end of the lake. Today, the lake level is managed and in the recent years, the mean monthly lake level fluctuated between ~405.6 and ~406.5 m a.s.l. (AWEL 2016).

The majority of the documented subaqueous landslides occurred on the lateral slopes surrounding Lake Zurich's central basin (Strasser et al. 2013; Strupler et al. 2015). Relatively recent subaqueous slides (i.e. in the last 150 years) occurred offshore the villages of Horgen, Oberrieden, Rüschlikon and Küsnacht (Fig. 5.1; Heim 1876; Nipkow 1927; Kelts and Hsü 1980; Kuen 1999). The shores of Lake Zurich are densely populated, approximately a quarter million people live within 1 km from the lakeshore, and ~57'000 of these live less than 10 m above lake level (Henriod et al. 2016).

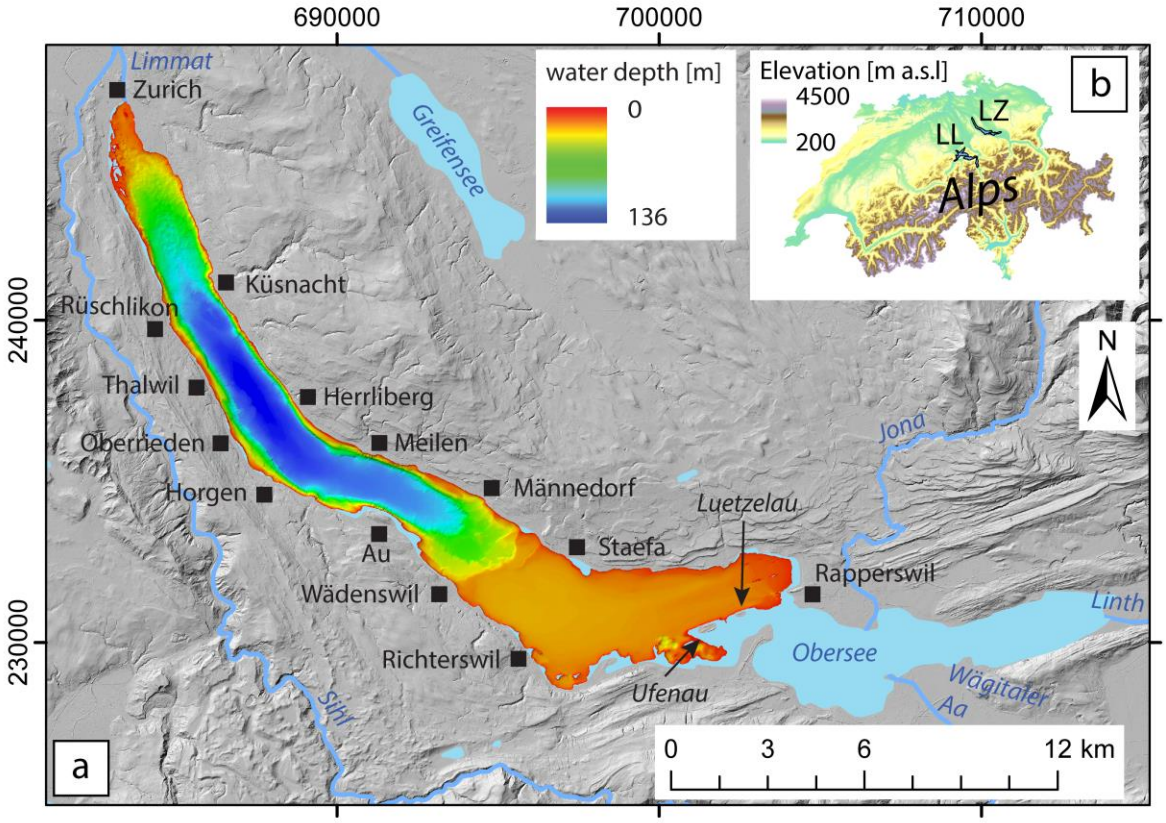


Figure 5. 1 a) Map of the study area. LiDAR digital elevation model and surface water data from Swisstopo. Bathymetric dataset from Strupler et al. 2015. Swiss coordinates (LV03). b) Location of the study lake within Switzerland. LZ= Lake Zurich, LL=Lake Lucerne.

5.2.2 Previous studies

Strupler et al. (2017) categorized the post-glacial lithological succession on the lateral slopes of Lake Zurich into four sediment-mechanical units, based on characteristic patterns of bulk density (ρ_{bulk}) and undrained shear strength (s_u). The same study investigated the glide planes of three subaqueous landslides, located offshore Oberrieden (Fig. 5.1), which are assumed to have occurred in water-saturated sediments under undrained conditions. All the glide planes lie within a sediment-mechanical unit with relatively high ρ_{bulk}, but low s_u, corresponding to a lithological unit consisting of Late Glacial plastic muds.

Strupler et al. (in press) assessed the earthquake-triggered, subaqueous landslide hazard by conducting a spatially distributed slope-stability analysis that considered earthquake accelerations

from a probabilistic seismic hazard assessment (Wiemer et al. 2016). Slope stabilities were calculated for all cells of an equally-spaced grid with a limit-equilibrium equation on an infinite slope. The thickness of the sediment-mechanical units at each pixel location was estimated as a function of water depth and slope gradient, calculated with a sedimentation model (Strupler et al. in press). Profiles of ρ_{bulk} and s_u vs. depth were adapted to the thickness of the sediment-mechanical units at each pixel. Random values from log-normally distributed ρ_{bulk} and s_u profiles were selected for each depth step with a Monte Carlo Simulation, to incorporate uncertainty due to the spatial variability of the sediment-mechanical data. Earthquake shaking was implemented as pseudostatic acceleration, which was assumed to represent 50% of the peak ground acceleration (PGA). For each pixel of the bathymetric dataset of Lake Zurich (Strupler et al. 2015), a probability of failure (conditional on earthquake shaking; PoF_{eo}) vs. depth profile was calculated. In the model, the glide plane was defined as the depth of the maximum PoF_{eo} (queried from the top of the PoF_{eo} vs. depth profile). Mean PGAs for earthquakes with EP_{50} of 10, 2 and 0.5% (corresponding to mean return periods of 475, 2475 and 9975 years, respectively) from a probabilistic seismic hazard analysis (Wiemer et al. 2016) were considered for the earthquake-triggered landslide hazard assessment. Strupler et al. (in press) mapped individual slopes with high PoF_{eo} (i.e > 0.6; Fig. 5.2). While for an earthquake with an EP_{50} of 10% (median PGA: ~0.05 g) only minor parts of the slopes are expected to fail (cumulative slide volume of ~3 Mio m^3; Fig. 5.2), for an earthquake with an EP_{50} of 2% (median PGA:~0.1g), larger parts are expected to slide downslope (cumulative slide volume of ~12 Mio m^3), and for an earthquake with an EP_{50} of 0.5% (median PGA:~0.2g), most of the yet unfailed, lateral slopes are expected to become unstable (i.e. cumulative slide volume of 48 Mio m^3, excluding slopes < 1°, to avoid large instable volumes on the terraces of the escarpment structure; Strupler et al. in press). Because the model of Strupler et al. (in press) defines the glide plane as the depth of the maximum PoF_{eo} (queried from the top of the PoF_{eo} vs. depth profile), the slide thickness is occasionally a few dm lower for a scenario of an EP_{50} of 0.5% compared to an EP_{50} of 2%. Hence, the higher earthquake acceleration for an EP_{50} of 0.5% causes the slope to fail a few dm higher (Fig. 5.2).

Hilbe and Anselmetti (2015) modelled the kinematics of subaqueous landslides in Lake Lucerne (Fig. 5.1b) as single-phase, fluid-like mass movements propagating on the lake floor with MassMov2D (Beguería et al. 2009), which is implemented in the free GIS package PCRaster (Wesseling et al. 1996). Hilbe and Anselmetti (2015) fed the output of MassMov2D (i.e. the changing bathymetry as a function of time) into GeoClaw (Berger et al. 2011) in order to calculate wave generateion, propagation and inundation, starting with a lake surface at rest. The results of the numerical experiments performed on Lake Lucerne showed a good agreement with historically reported tsunami effects. However, according to Hilbe and Anselmetti (2015), the model likely overestimates wave heights and run-up close to the tsunami source areas, which is an important limitation.

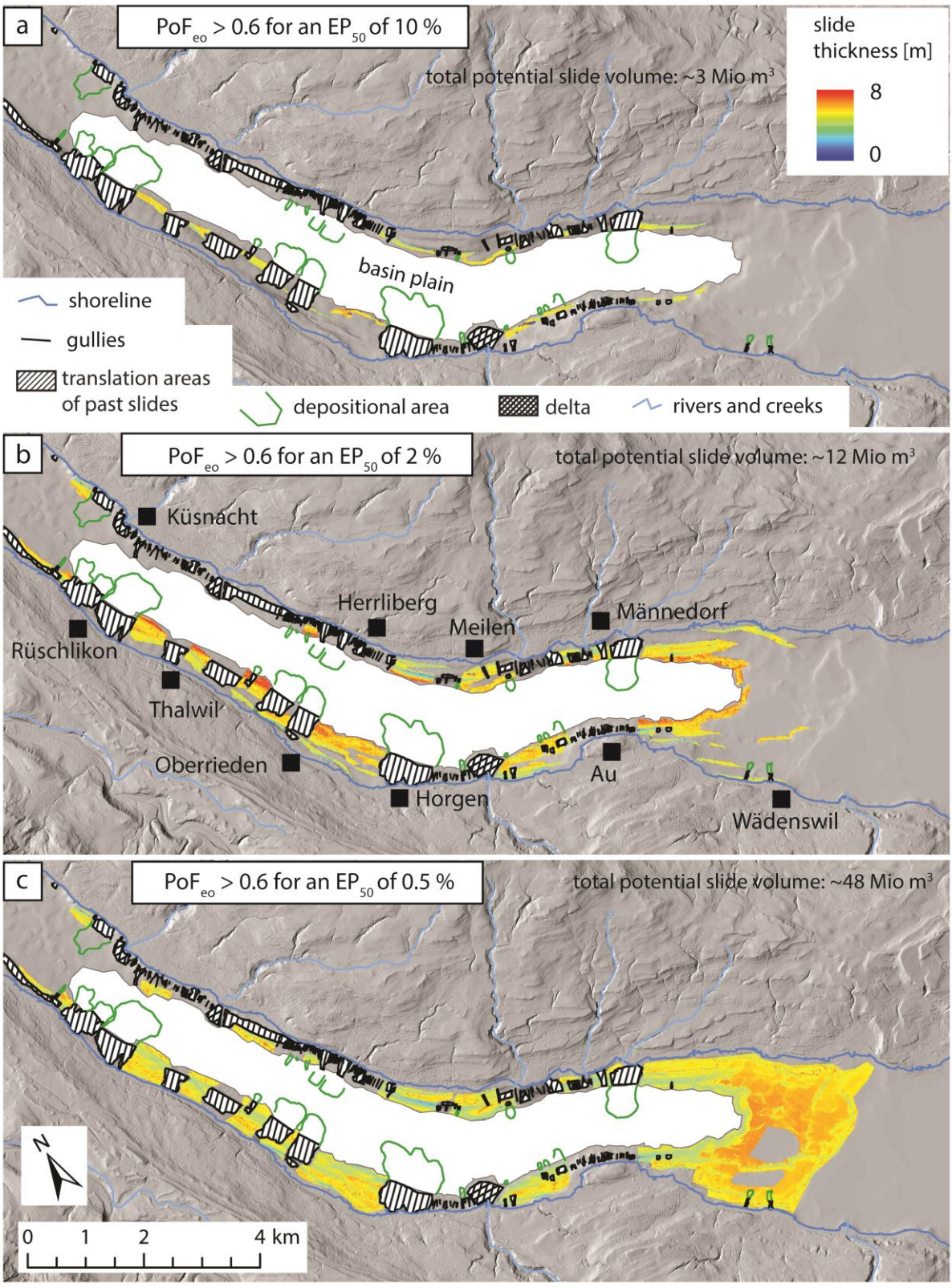


Figure 5. 2 Zones with a high failure probability upon earthquake occurrence (PoF_{eo}) and corresponding potential failure depths for peak ground accelerations with an exceedance period in 50 years of a) 10 %, b) 2% and c) 0.5 % (Strupler et al. in press). Slopes < 1° are here considered stable (to avoid large unstable volumes on the terraces of the escarpment structure), although the model of Strupler et al. (in press) considers such slopes (i.e. >0.01 -1°) as unstable for strong earthquake accelerations, such as assumed for an EP_{50} of 0.5%.

5.3 Data and Methods

The mass-movement propagation was simulated in a first step, followed by modelling the tsunami wave generation and propagation (Hilbe and Anselmetti 2015). Calculations were done with a grid resolution of 20 m. Previous sensitivity tests demonstrated that smaller grid sizes do not have a significant influence on runout distance, velocity and geometry of the deposit for the mobility analysis of the landslide, and the amplitudes of the free surface wave do not significantly change for a smaller grid size (Hilbe and Anselmetti 2015).

5.3.1 Simulation of the subaqueous landslide progression

The MassMov2D program code, used for the landslide simulation, needs a digital terrain model (DTM) as input. For the study area, this DTM was created by combining a digital elevation model (DEM), which was resampled from a grid resolution of 2 m (SwissAlti3D; swisstopo) to 20 m and a digital depth model (DDM), which was interpolated from DHM25 isobaths (swisstopo). For the modelling of landslides and tsunamis, we did not consider an available high-resolution DDM (Strupler et al. 2015) because all the calculations were conducted on a 20 m resolution.

5.3.1.1 Thickness of the mobile sediment drape and rheological input parameters

The back-calculated (in the case of the ~2210 cal.yr BP Oberrieden event) and estimated slide volumes for potential future earthquakes with their respective EP_{50} are taken from Strupler et al. (in press). In contrast to Hilbe and Anselmetti (2015), who assumed a constant thickness for the slides, we assume slightly varying slide thicknesses within the slides (as a function of varying sedimentation dependent on the slope gradient and water depth; see Strupler et al. in press).
After adding the initial slide thicknesses to the DDM, the subaqueous landslide is modelled with the Bingham plastic rheology, as mud-rich subaqueous sediments behave approximately as Bingham plastic fluids (e.g. Mei and Liu 1987; Skvortsov and Bornhold 2007). As rheological input parameters, submerged bulk density ρ' [kg m^{-3}], dynamic viscosity μ [Pa s], and yield strength τ [Pa] are required. We assumed a submerged bulk density of $\rho' = 600$ kg m^{-3}, which corresponds to the typical ρ_{bulk} of the Late Glacial plastic muds, the unit in which the glide plane is located (Strupler et al. 2017), minus the density of the ambient water. The parameters μ and τ were calibrated on the distinct slide deposit of the ~2210 cal. yr BP Oberrieden slide (Strupler et al. 2015) by matching the modelled landslide runout with the observed extent of the deposition lobe. Subsequently, these parameters were used for the calculation of all the slide scenarios (see section 5.4.1.1).

5.3.2 Tsunami wave propagation modelling and flow depth

The propagation of the tsunami wave, as well as the inundation, were calculated with the GeoClaw code (version 4.6.3; Berger et al. 2011). The peak wave height was recorded on virtual gauges that were defined in the study area (Table 5.1):

Table 5. 1 Gauge locations (Swiss grid coordinates LV03 in m) in the lake (see also Figs. 5.5, 5.6, and 5.8)

Gauge-Nr.	x-Coordinate	y-Coordinate	Location	Present-day water depth [m]
1	687315	237735	central deep basin	136
2	688572	237571	Herrliberg harbour	14
3	686406	237293	Oberrieden	3
4	690935	235857	Meilen harbour	15
5	687716	235268	Horgen harbour	8
6	685553	238880	Thalwil harbour	12
7	683287	246640	offshore Zurich Buerkliplatz	11
8	704081	231435	Rapperswil harbour	1
9	683819	244703	northern basin	32
10	697195	231070	southern basin	25

The DTM does not include buildings or vegetation, which could drag the tsunami wave and thus reduce the inundated area. Friction is implemented in the GeoClaw code by applying a Manning roughness coefficient. The Manning coefficient can vary from ~0.015 for very smooth terrain to ~0.07 very rough coastal areas (Bretschneider and Wybro 1977). Here, as Hilbe and Anselmetti (2015), we apply a coefficient of 0.03 (representing grass, roads, and scrubs; e.g. Kaiser et al. 2011). Previous lake-level reconstructions suggest a ~2 m higher lake level between the first millenium BC and the first century AD, caused by damming of the lake outflow by sediments of the Sihl River (Wild 2009). Therefore, the lake level was set to 408 m for the back-analysis of the free surface wave height, flow depth and inundated area of a potential ~2210 cal. yr BP tsunami. The present-day lake level of 406 m was used for the assessment of the current tsunami hazard.

5.4 Results

5.4.1 Mobility analysis of past and potential future mass movements

In this section, we provide results of landslide-mobility analyses for (i) the single ~2210 cal. yr BP subaqueous slide offshore Oberrieden (section 5.4.1.1), (ii) for the case of all ~2210 cal. yr BP slides occurring simultaneously (section 5.4.1.2), and (iii) for hypothesized landslides assumed to be triggered by PGAs with EP_{50} of 10, 2 and 0.5 % (section 5.4.1.3).

5.4.1.1 Back-analysed scenario Oberrieden ~2210 cal. yr BP

The following input parameters were back-analysed from the 2210 cal. yr. BP Oberrieden slide (Table 5.2):

Table 5. 2 Back-analysed parameters for the ~2210 cal. yr. BP Oberrieden slide, used to model the forward scenarios

rheological model	Bingham
submerged bulk density ρ' [kg m^{-3}]	600
yield strength τ [Pa]	5
dynamic viscosity μ [Pa s]	40
landslide propagation time [s]	120

The rheological parameters μ and τ were iteratively varied to match the slide extent. For μ = 40 Pa s and τ = 5 Pa, the modelled runout of the ~2210 cal. yr BP Oberrieden slide shows a relatively good agreement with the toe of the observed landslide deposit (Appendix E, Fig. E.1). Both the modelled runout distance (i.e. the distance from the toe of the slope to the maximal extension of the deposit) and the measured runout distance of the deposit are 490 m. The modelled maximum width of the deposition lobe, however, is 780 m, compared to measured 560 m. The slide reaches a maximum speed of 14 m/s. 30 s after slide initiation, the speed of the slide is ~5 m/s. After ~90 s, the maximum extent of the slide is reached, and only minor movements within the depocenter are occurring (~1 m/s). The modelled deposit at its final stage has a maximum thickness of ~3 m. As in Hilbe and Anselmetti (2015), a thin layer remains in the source area. The authors interpreted this as an effect of the used Bingham plastic rheology. The modelled deposit thickness is much lower than the measured maximum deposit thickness in the seismic reflection dataset (~15 m; Strasser et al. 2013; Strupler et al. 2015). However, a considerable percentage of the latter is composed of deformed basin-floor sediments, which have not been transported from the source area of the landslide, but deformed virtually in place. This process is obviously not included in the landslide-mobility model. Due to the fact that the slide is modelled as a Bingham fluid, some lateral spreading occurs, making the modelled deposition zone slightly wider than the mapped one from Strupler et al. (2015).

5.4.1.2 Back-analysed scenario of multiple landslides dated to ~2210 cal. yr BP slides

Strasser et al. (2013) assigned a total of ten individual landslide deposits to the assumedly earthquake-triggered ~2210 cal. yr BP event. For some of these deposits, the corresponding source and translation areas could not be distinguished clearly because they have been overprinted by human-triggered slides in the last 150 years (Heim 1876; Nipkow 1927; Kelts and Hsü 1980; Kuen 1999). Due to the overprinting and the fact that the back-calculated depth of the glide plane for the ~2210 cal. yr BP event is only available for the Oberrieden case-study site (Strupler et al. in press), a constant depth to the glide plane of 5 m was assigned for the other ~2210 cal. yr BP slides (mean headscarp heights ~3−7 m; Strupler et al. 2015). The translation area corresponding to the northernmost deposit with the smallest extent of the ~2210 cal. yr BP event could not be identified in

the bathymetric dataset (Strupler et al. 2015). It is assumed that this very small slide was draped by sediments from the Küsnacht Delta and is thus not included in the simulation of all ~2210 cal.yr BP slides. The total volume of the slides assigned to the ~2210 cal. yr BP event accounts to ~ 4 Mio m^3, which is five times larger than the single ~2210 cal. yr BP Oberrieden slide modelled above (section 5.4.1.1; 803'900 m^3; Strupler et al. in press).

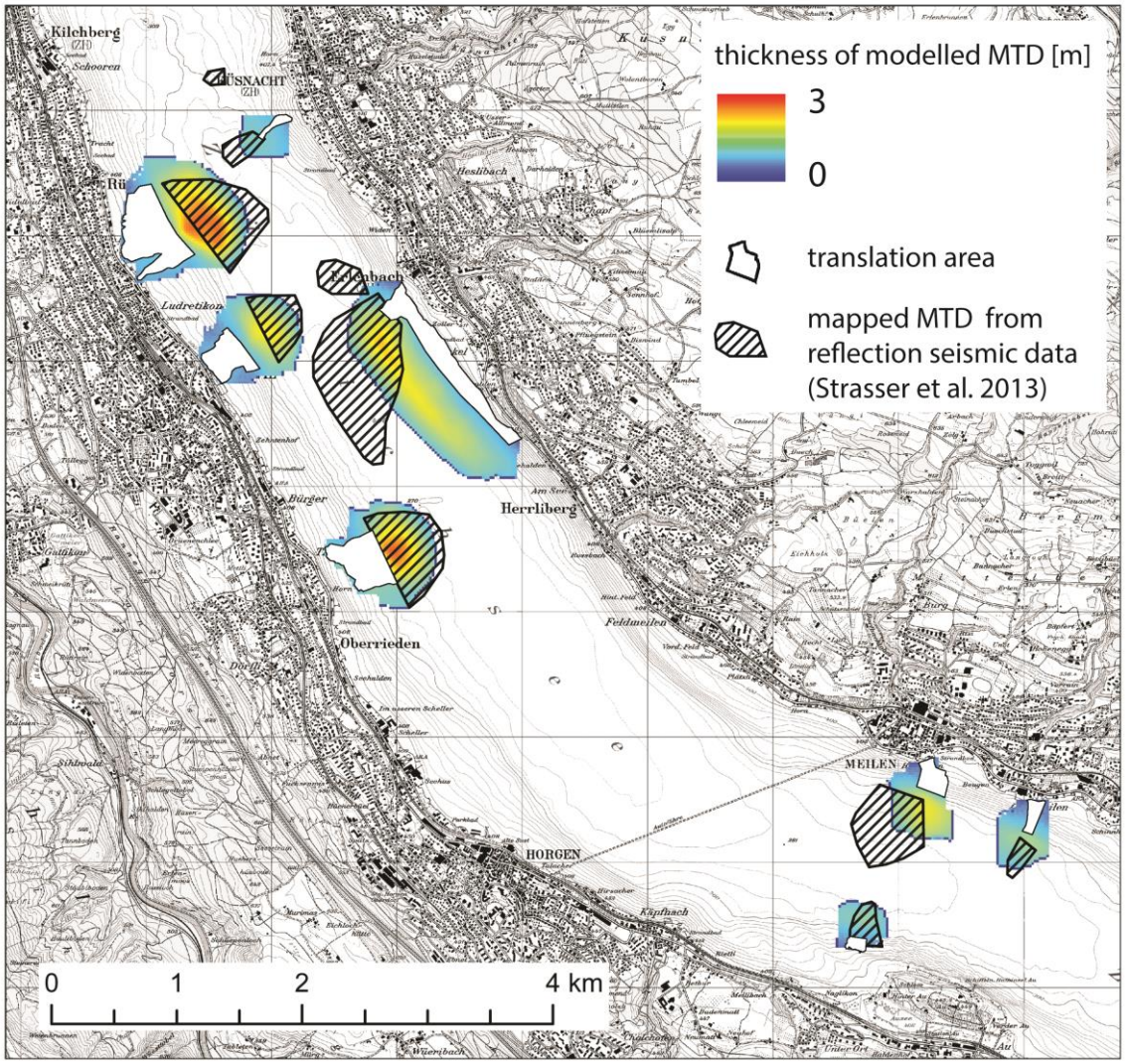


Figure 5. 3 Modelled Mass Transport Deposits (MTDs) from a mobility analysis of all ~2210 cal. yr BP slides mapped in Strasser et al. (2013).

The modelled MTDs of the ~2210 cal. yr BP event on the western slopes coincide well with the extents of the MTDs mapped in Strasser et al. (2013). On the eastern slope, the modelled slides correlate only partly with the mapped extent of the deposits (Fig. 5.3). There is a relatively large discrepancy between the modelled and mapped MTDs from the seismic reflection data between the villages of Erlenbach and Herrliberg, which may be related to mapping uncertainties on these steep zones, where also many gullies occur (Strupler et al. 2015). Instead of two distinct deposits, such as

mapped from the seismic reflection seismic data (Strasser et al. 2013), only one wider slide is modelled.

5.4.1.3 Potential future subaqueous slides for PGA of different EP_{50} scenarios

Results from a mobility analysis of subaqueous landslides that are assumed to occur as a consequence of different earthquake-hazard scenarios (Fig. 5.2; Strupler et al. in press) provide the backbone for the current hazard assessment. Using the rheological parameters from the back-analysis of the ~2210 cal. yr BP Oberrieden slide (Table 5.2), the distributions of the modelled basin-wide MTDs show greater runout distances for landslides triggered by stronger earthquakes (smaller EP_{50}) than for landslides triggered by weaker earthquakes (greater EP_{50}) (Fig. 5.4). Due to the fact that most failure-prone zones for earthquakes with an EP_{50} of 10% are located near the bottom of the slopes, the height drop is small and the slope angles are low, implying slow velocities and short runout distances. Modelled thicknesses of the landslide deposits vary between ~1 and ~1.5, between ~1 and ~4, and between ~1 and ~10 m for potential landslides triggered by an earthquake with PGAs for an EP_{50} of 10%, 2%, and 0.5%, respectively (Fig. 5.4).

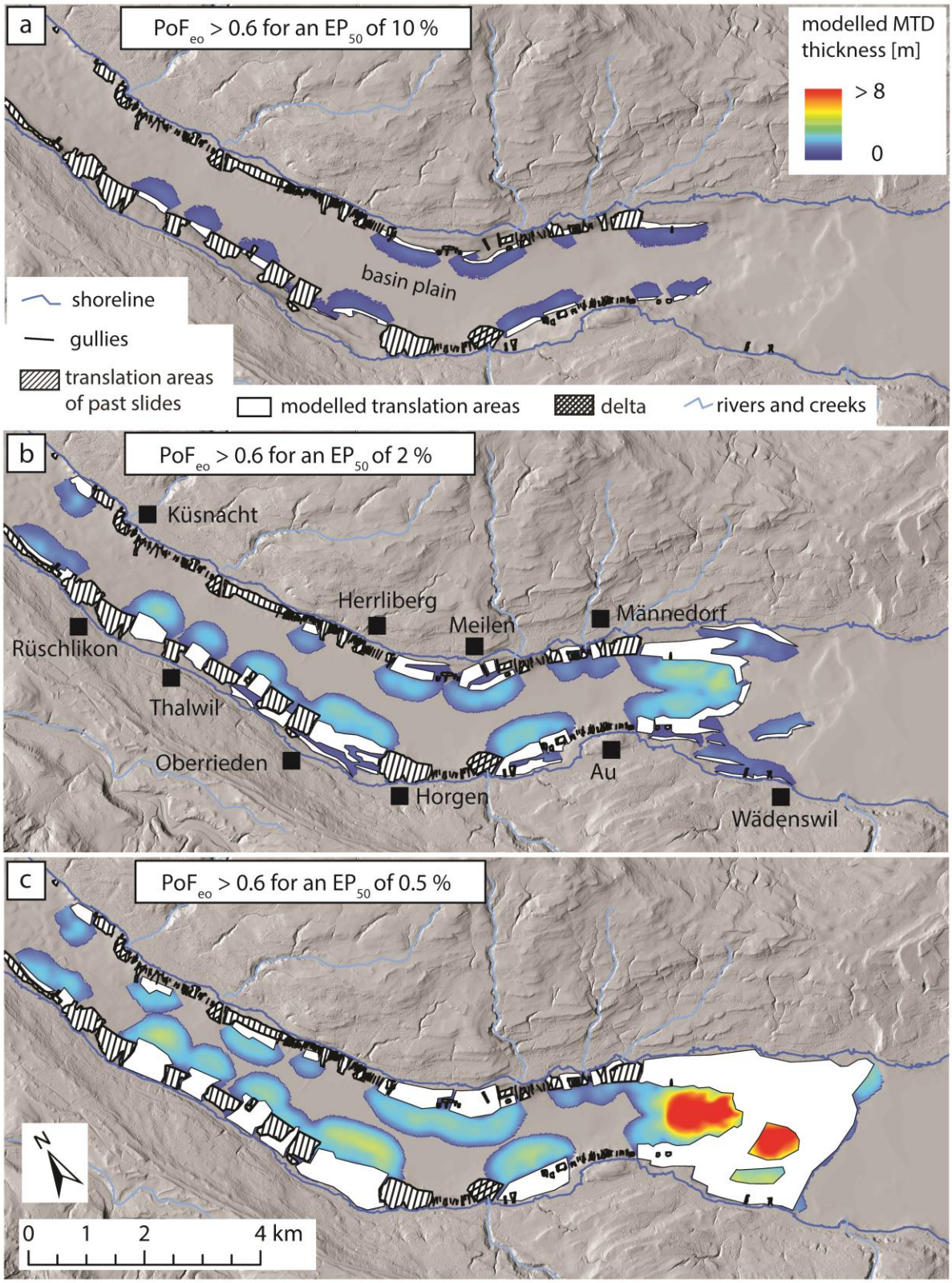


Figure 5. 4 Spatial distributions and thicknesses of mass transport deposits modelled for potential landslides expected for earthquake scenarios with different exceedance periods of a) 10 b) 2 and c) 0.5 % in 50 years.

5.4.2 Simulation of landslide-induced tsunami waves

5.4.2.1 Back analysed potential tsunami caused by earthquake-triggered landslides ~2210 cal. yr BP

The results of the modelling scenario assuming that all ~2210 cal. yr BP slides with a cumulative volume of ~4 km^3 occurred simultaneously indicate that the strongest tsunami effects are felt on the shorelines around the central basin, where the slides occur. At the gauge located behind the Oberrieden slide, a peak amplitude of ~1.5 m is recorded (~1 min after slide initiation; Fig. 5.5). After that, the wave oscillates with peak amplitudes of ~0.5 m for the following 10 minutes. In Thalwil, three successive waves of 0.5–1 m peak amplitude arrive within the first 3 min after the triggering of the slides. After that, the waves diminish to half of their size, continuing for another 15 min. The first wave peak arrives at the northern end of Lake Zurich (offshore today's location of Buerkliplatz) ~8 min after the triggering of the landslides, with a low peak amplitude of ~0.1 m (Appendix E, Fig. E4). At the gauge location Rapperswil, a wave of only ~1 cm can be detected after ~15 min. In such a case of a synchronous sliding of all the 2210 cal. yr BP events, the shorelines around the deep basin (mainly on the western lake shores in the near field of landslides; Fig. 5.5) may have experienced maximum flow depths of up to ~3 m under assumption of a paleolake level of 408 m a.s.l. with the present-day DTM (which may lead to overestimations of flow depths due to anthropogenic fillings along the shoreline).

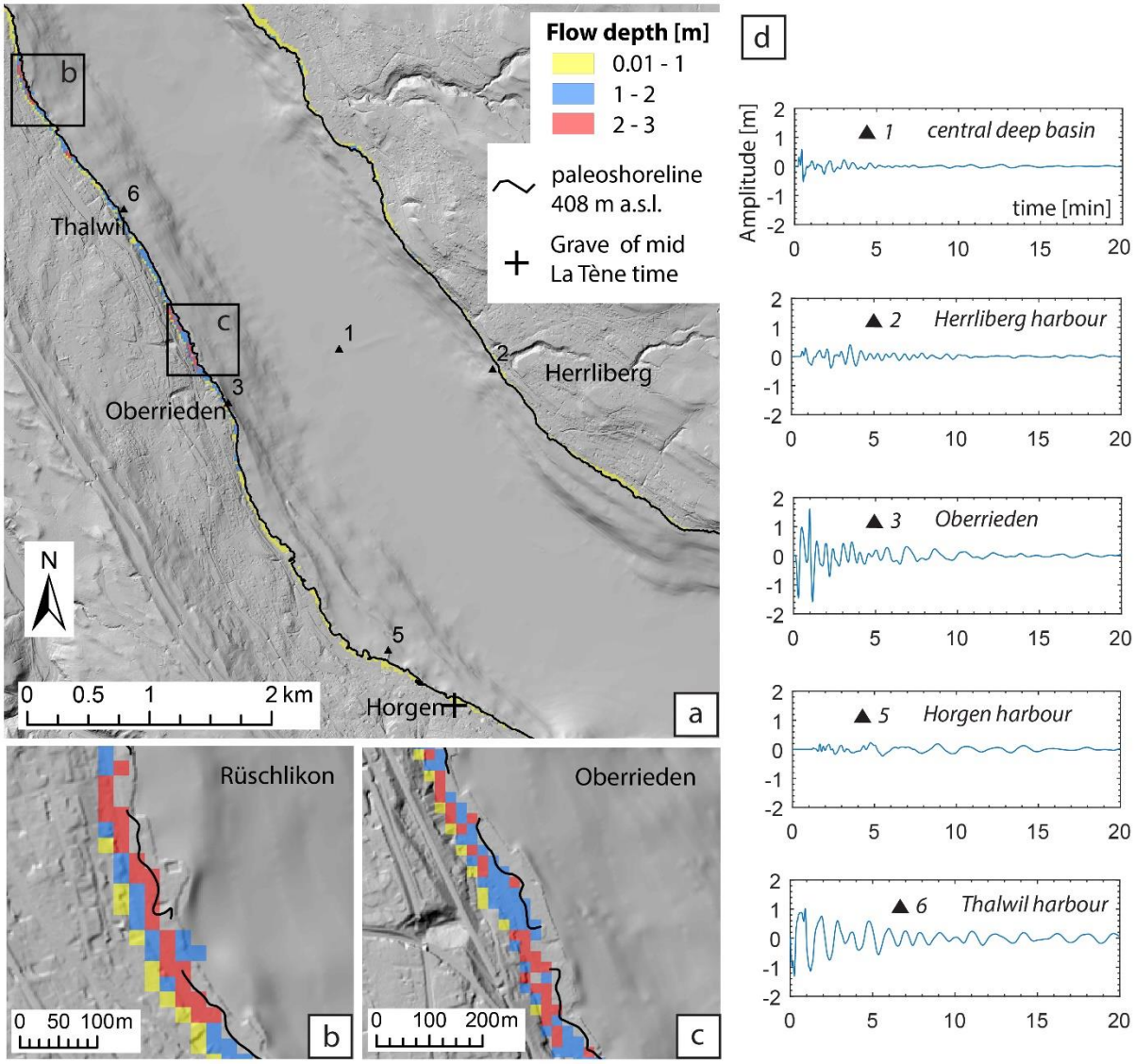


Figure 5. 5 a) Back-analysed inundation and flow depth on the shores of the deep basin for a scenario of a coeval failure of all slides assigned to the ~2210 cal. yr BP earthquake b) Zoom Rüschlikon c) Zoom Oberrieden d) Time series of wave amplitudes at different gauges

5.4.2.2 Scenario for tsunamis caused by hypothetical landslides that may be triggered by earthquakes with a median PGA for an EP_{50} of 10% and 2%.

The total slide volume of an earthquake with PGAs for an EP_{50} of 10% that was estimated by Strupler et al. (in press) to ~3 Mio m^3 (Fig. 5.2a), would cause free surface waves with maximum peak amplitudes of 0.4 m in the deep basin (Fig. 5.6a), given that all these slides occurred simultaneously. 5 min after slide initiation, the peak amplitudes do not exceed 0.2 m at all the gauges. This scenario does not cause any considerable inundation.

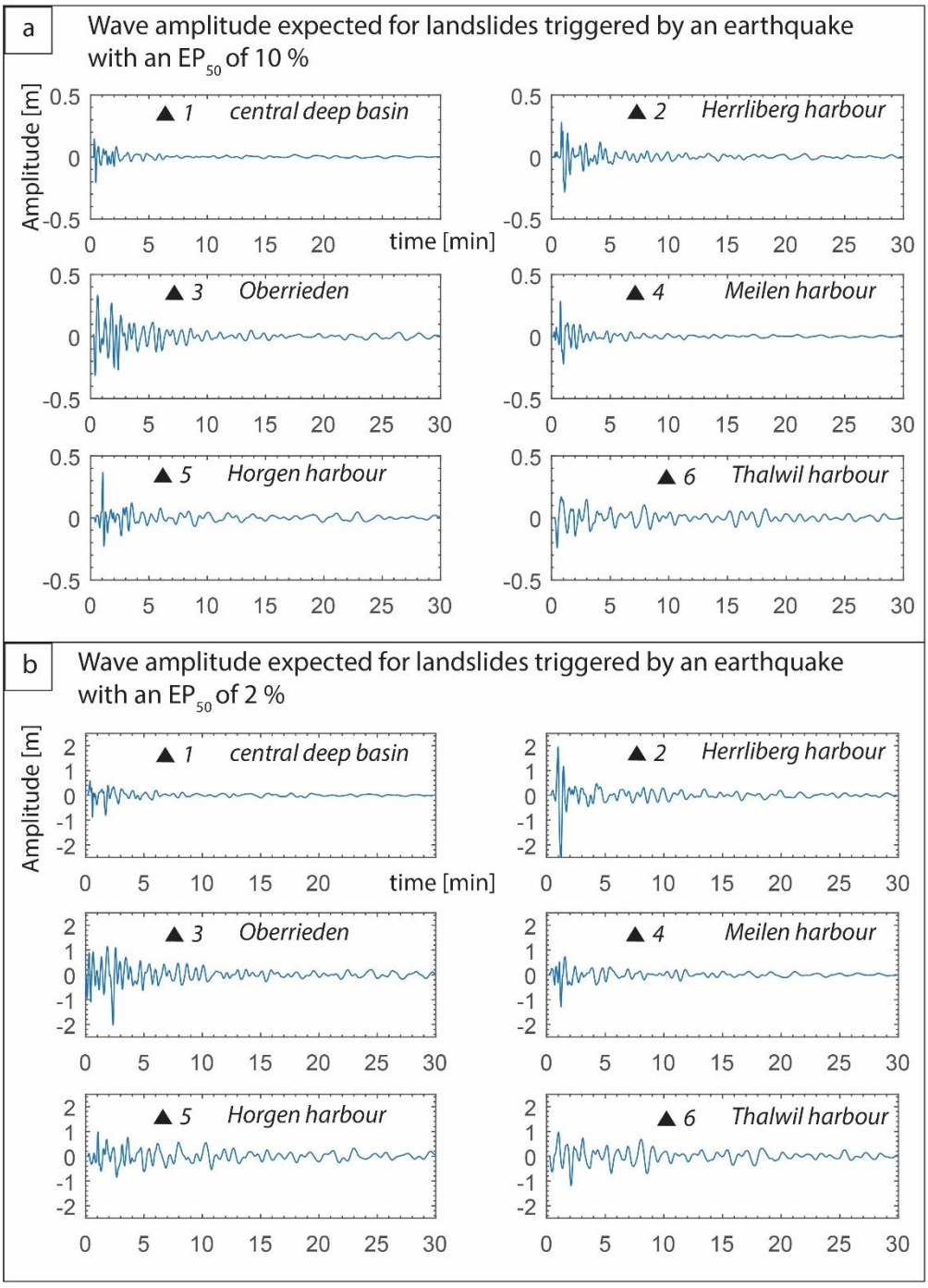


Figure 5. 6 Time series of wave amplitudes at different gauges for hypothetical landslides caused by an earthquake with a median PGA expected for an EP_{50} of 10 % (a) and 2 % (b).

Estimated slope failures triggered by an earthquake with an EP_{50} of 2% would lead to a similar pattern of tsunami occurrences as assumed for tsunamis caused by estimated slope failures triggered by earthquakes with an EP_{50} of 10%. The main difference is that the expected peak amplitudes are higher for an EP_{50} of 2% (instead of maximum peak amplitudes of ~0.4 m (Fig. 5.6a), they reach up to ~2 m, albeit in the near field of the landslides; Fig. 5.6b). The shores around the deep basin would be inundated, e.g. south of Au and around the village of Uetikon, the latter at the former location of the oldest Swiss chemical production site for fertilizer; Fig. 5.7; Geilinger-Schnorf 1993). However, the maximum flow depth would amount to less than 1 m for most zones.

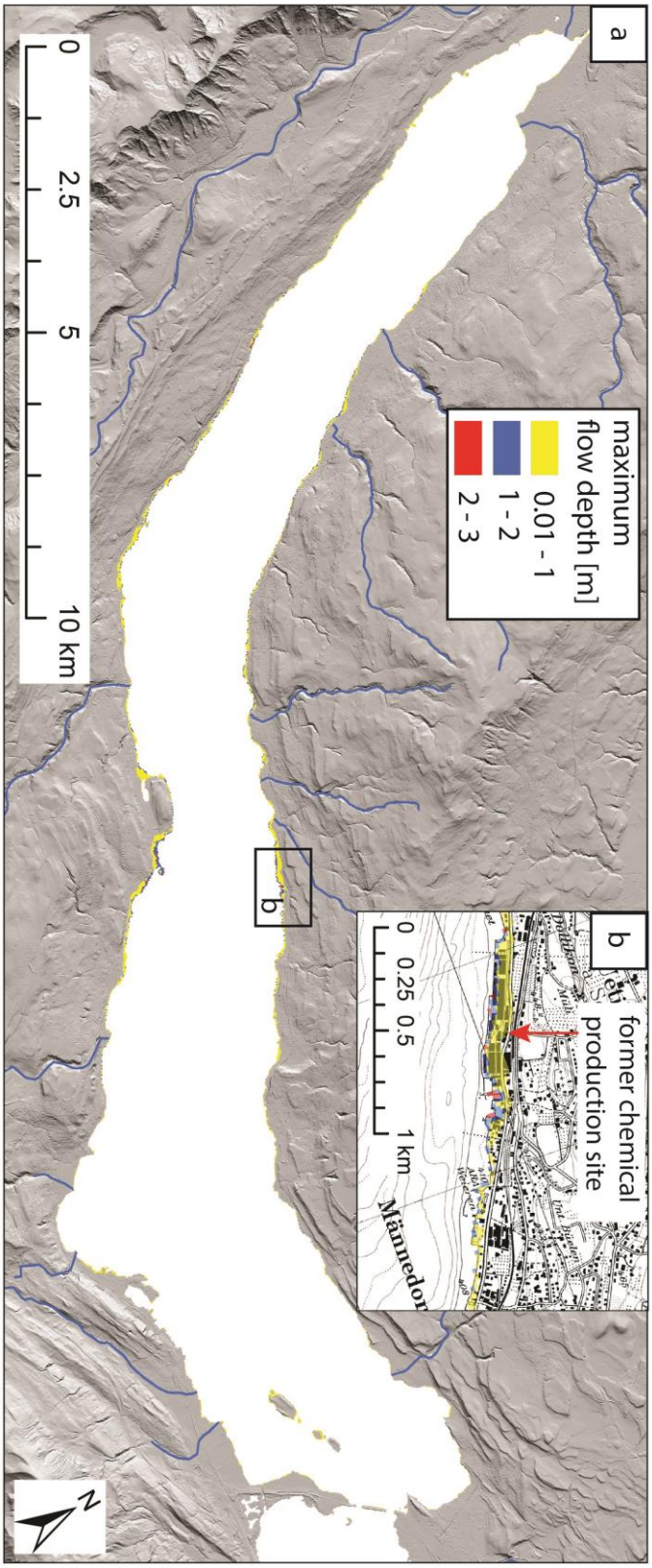


Figure 5. 7 Inundated areas for a tsunami as a consequence of an earthquake with a median PGA of an EP_{50} of 2%. a) Entire lake b) Zoom Uetikon

5.4.2.3 Scenario for tsunamis caused by hypothetical landslides that may be triggered by an earthquake with a median PGA expected for an EP_{50} of 0.5%

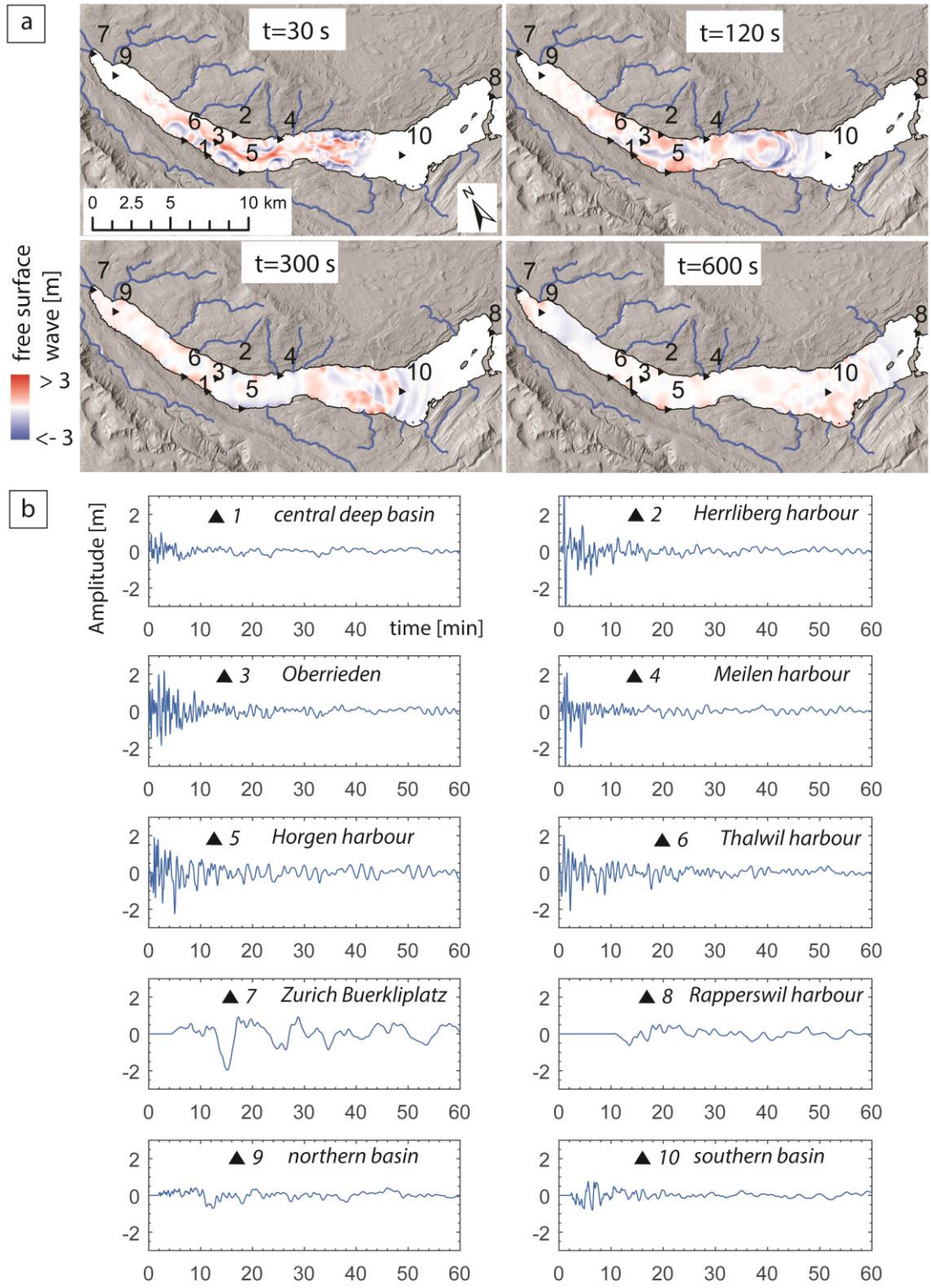


Figure 5. 8 Plotted time steps of wave amplitudes (a) and time series at the different gauges (b) for the hypothetical 'worst case scenario' of landslides occurring on all yet unfailed slopes (scenario for earthquake median PGA expected for an EP_{50} of 0.5%). Expected time of arrival of the first wave at the northern end of the lake is ~5 min (gauge 7) and at the southern end ~12 min (gauge 8).

For a worst-case scenario of all yet unfailed slopes sliding down simultaneously (as expected for an earthquake with an EP_{50} of 0.5%; Strupler et al. in press), the entire shoreline would be affected. The villages located around the central basin, where the majority of the slides occur, would especially be affected by inundations within the first 10 min after the occurrence of the slides. The most distal cities of Zurich and Rapperswil would be affected by the tsunami only ~5 and ~12 min after the slide occurrence, respectively. In Zurich, after two initial waves with a peak elevation of ~0.5 m, the lake level would lower during ~3 min by ~2 m and rise again for the succeeding 3 minutes (gauge 7, Fig. 5.8). This irregular wave pattern has been interpreted to be caused by interference of the waves. For an earthquake with a mean return period of ~9975 years, large landslides occur between Meilen and Herrliberg, causing initial peak amplitudes of more than ~2 m measured at the nearby virtual gauges 2 and 4 (Fig. 5.8).

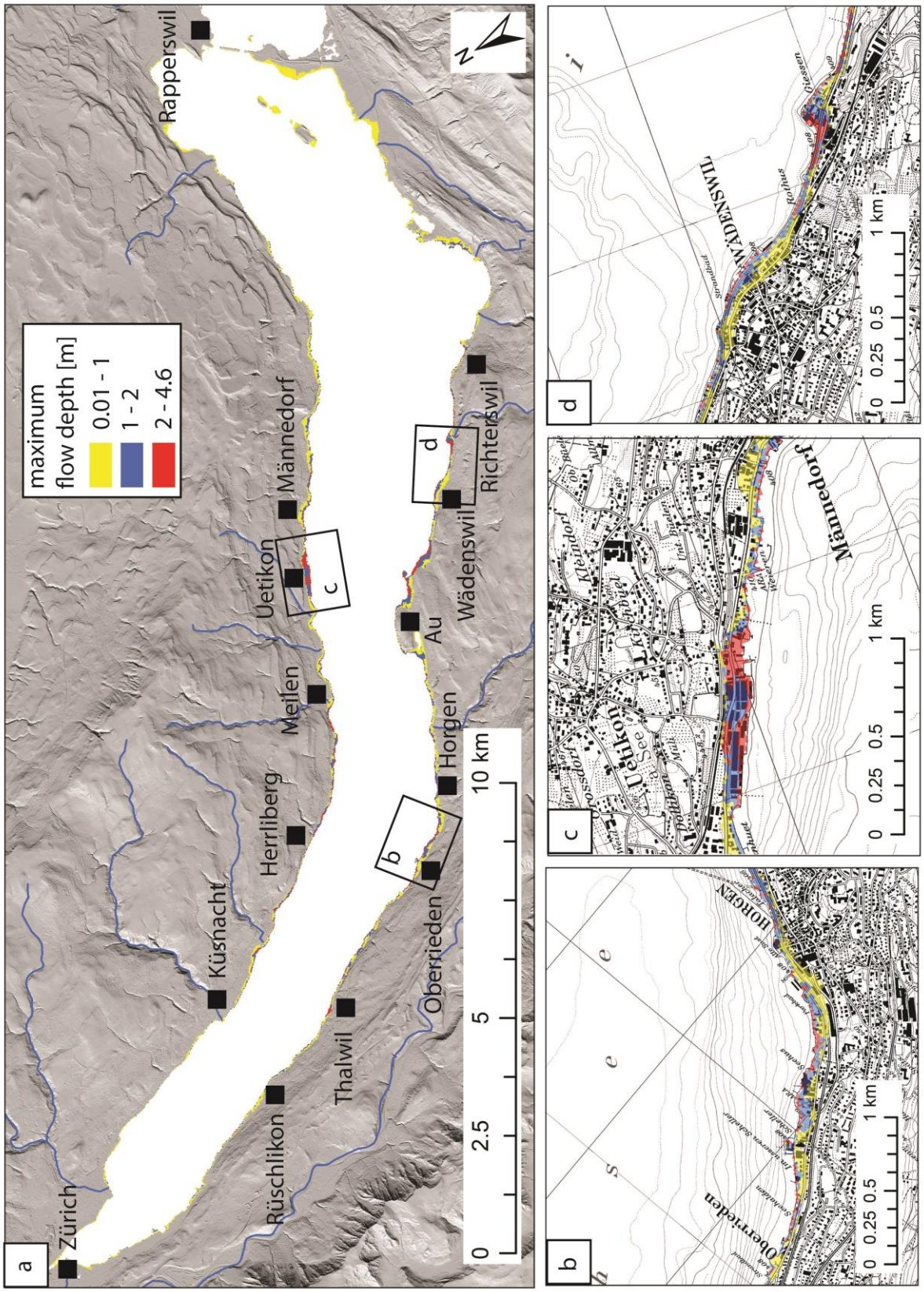


Figure 5. 9 Inundated areas with color-coded flow depth estimated for landslides triggered by an earthquake with an EP_{50} of 0.5% ('worst case scenario'). a) Overview map of the entire study area. b) Oberrieden c) Uetikon d) Wädenswil

The zones most affected by inundation on the western shores can be found between Oberrieden and Richterswil, where the maximum inundation distance reaches up to ~200 m, with flow depths exceeding 1 m mostly in the shore-proximal zones. The eastern shores of the deep basin show the highest flow depths, mostly in the range between 1 and 4 m. Most parts of the island of Lützelau would be inundated (Fig. 5.9).

5.5 Discussion

5.5.1 Quality and limitations of the applied model

The results of this study, i.e. the modelled wave heights and inundation, are based on various steps involving mapping, modelling, and interpretation. Each of these steps involves limitations and uncertainties, which are difficult to assess. Therefore, the here presented results can be considered as first-order results.

5.5.1.1 Mapped past and potential future translational areas

The mapped extents of the translation areas corresponding to the ~2210 cal. yr BP event may include some uncertainties, mostly due to overprinting by gullies and younger slide events (Strupler et al. 2015). However, in general, there is a relatively good agreement between the runout distances and areas of the modelled and mapped mass transport deposits. As a first simplification from the probabilistic assessment of the earthquake-triggered subaqueous landslide hazard, Strupler et al. (in press) arbitrarily considered all slopes with a failure probability of > 0.6 to fail for each hazard scenario. Also, the approach of using constant earthquake acceleration as input in the pseudostatic analysis in the study of Strupler et al. (in press) showed its limitation, especially for high earthquake accelerations, such as the ~0.2 g representing an earthquake with a return period of 9975 years in the study area, which would cause failure even on slopes with gradients < 1°. In this study, slopes < 1° were here considered stable, to avoid large instable volumes on the terraces of the escarpment structure. However, it needs to be tested if the slope-stability assessment of Strupler et al. (2017) is valid for the lateral slopes only or if it also applies for the escarpment structure.

5.5.1.2 Mobility analysis

The back-analysed subaqueous landslides modelled as a Bingham fluid may not represent the mechanism of translational subaqueous landslides correctly, as the modelled slides do not actually glide, but rather flow. However, Hilbe and Anselmetti (2015) showed that the resulting landslide-triggered tsunami wave height compared relatively well to historical reports of wave heights and inundation, indicating that the model provides realistic results. The fact that rheological parameters were back-analysed on the ~2210 cal. yr BP Oberrieden slide and used for the simulation of all scenarios may ignore varying sediment-mechanical and geomorphic influences on the slide velocities within the lateral slopes. Also, a potential dependency of the parameters on the slide volumes was not considered. However, the modelled extents match the mapped extents of the ~2210 cal. yr BP deposits relatively accurately, particularly on the western lateral slopes. On the eastern lateral slopes,

the modelled extents are slightly smaller than the mapped extents. The comparably steeper lateral slopes on the eastern part of the basin (Strupler et al. 2015) might cause faster slide velocities and hydroplaning, which increases the runout of landslides and may cause distal turbidites (e.g. Mohrig et al. 1998; Elverhoi et al. 2010). This process, however, is not considered in the model. A further simplification stems from the fact that no interaction with the underlying sediment occurs in the model. Compared to thicknesses of the MTDs measured in the seismic reflection dataset (Strasser et al. 2013), the modelled thicknesses of past slides are thus generally much lower. It may be tested in future work what the effect of the interaction between landslides and the underlying sediment is on the modelled tsunamis. Lastras et al. (2013) assume that the deformation of the lake floor by landslides also contributes to the tsunami generation.

5.5.1.3 Tsunami model

A typical weakness of the applied model, i.e. the overestimation of the wave height and flow depth in the near field of tsunami sources, needs to be considered for the data interpretation (Hilbe and Anselmetti, 2015). Thus, if an area with great inundation is close to a translation area of a landslide, the results (especially high values of single cells) need to be interpreted with caution. However, the wave heights and impacts on the shore at a certain distance from the landslide are assumed to be acceptably approximated.

As the height of the wave is mainly depending on the slide volumes, speed and depth of submergence (Watts 1998), uncertainties in these parameters contribute to the uncertainties in the tsunami height. The estimated cumulative volumes of all slides occurring coevally represent a worst-case scenario, thus maximum expected wave heights. Also, the here modelled scenarios all assume that sliding occurred at once, i.e. not retrogressively in multiple phases, as documented for the anthropogenically triggered Horgen slide (Heim 1876; Kelts and Hsü 1980). Sliding in multiple phases would result in smaller individual slide volumes, reducing the resulting tsunami wave height. The landslide hazard map (Strupler et al. in press) does not consider retrogressive failure implying that the volumes assumed to fail are derived from mapped zones with a high PoF_{eo}. However, because geomorphic data shows that most of the slides in Lake Zurich are initiated immediately at the upper end of a steep zone (Strupler et al. 2015), the mapped slides can be assumed to represent potential slide extents. Also, a potential retrogressive slide mechanism may be slower than failure initiating at the top of the slope, which would result in lower initial wave elevations (Tappin 2017).

The inundation area is strongly affected by the surface roughness represented by houses and other infrastructure (e.g. Shimazu 2016), which have been neglected in our approach. The arbitrary selection of a Manning roughness coefficient that is lower than values typically used for built-up areas, might thus lead to overestimation of the inundation area. Using a digital surface model that includes buildings and trees that limit inundated zones and using a significantly higher spatial resolution of the inundated area might be needed for an exact prediction of inundated zones. However, the here presented first assessment of potential tsunamis generated by earthquake-triggered landslides for Lake Zurich provides a first-order overview on which areas may be exposed to a tsunami hazard (and which areas may be less exposed). By assuming a 2 m higher lake level for the investigation of tsunami scenarios ~2210 cal. yr BP, the inundation at anthropogenically designed

near-shore zones might be overestimated as well, as human activity since industrialization flattened the shore morphology at many locations.
In summary, the here presented first-order results of wave heights and inundation provide valuable information about consequences of potential past and future tsunamis on Lake Zurich if interpreted with the necessary caution. Because of the above-mentioned factors, the results can be considered as conservative, representing worst-case scenarios.

5.5.2 Tsunamigenic potential of past subaqueous landslides on the lateral slopes of Lake Zurich ('paleotsunamis')

Compared to estimated volumes of past landslides for other lakes in Switzerland (up to ~250 Mio m^3; Kremer et al. 2015; Hilbe and Anselmetti 2015) the total volume of the slides assigned to ~2210 cal. yr BP (4 Mio m^3) is rather small. The mobility analysis of the ~2210 cal. yr BP Oberrieden slide, whose rheological parameters were calibrated in order to match the mapped extent of the depositional lobe (Strupler et al. 2015), resulted in maximum slide speeds of ~14 m/s. This value lies between the velocity of the modelled slides by Hilbe & Anselmetti (2015) in Lake Lucerne (~20 to 35 m/s), and velocities mentioned by Kremer et al. (2015) for Lake Geneva (6 to 11 m/s). Different slide volumes height drops and slope angles, together with the back-analysed dynamic viscosity of the slide material are likely responsible for these differences. For example, the volume of the ~2210 cal. yr BP Oberrieden slide (~0.8 Mio m^3) is much smaller than the Weggis slide in Lake Lucerne (~11.5 Mio m^3; Hilbe & Anselmetti, 2015). Also its height drop (i.e. elevation difference between headscarp and farthest extent of the deposit) is significantly lower (~94 vs. ~120 m). Additionally, we back-analysed a higher dynamic viscosity (40 vs. 8 Pa s). The confined frontal emplacement of the ~2210 cal. yr BP Oberrieden slide, showing very distinct frontal bulges (Strupler et al. 2015) may be interpreted as a geomorphic confirmation of a rather low slide speed. In contrast, slides with higher speeds may develop hydroplaning (i.e. the front of the slides glide on a water layer; Mohrig et al. 1998) and run out of their stratigraphic position, ending up in frontally emergent slides (De Blasio 2011; Moernaut and De Batist 2011).
The tsunami simulation of the ~2210 cal. yr BP Oberrieden slide (Appendix E, Figures E.2 and E.3) indicates no considerable inundated areas. Apart from the initial wave trough of ~1.5 m and subsequent crest of ~1 m immediately offshore behind the slide, possibly related to an overestimation of simulated wave heights close to landslide source areas (Hilbe and Anselmetti 2015), the peak amplitude remains very low (i.e. < 0.5 m). This result also coincides with the lack of tsunami observations during the 1875 Horgen slide, which had a comparable total slide volume (1–1.5 Mio m^3; Kelts 1978). However, the Horgen slide occurred in multiple slide phases (Heim 1876; Kelts and Hsü 1980), thus with lower sliding volumes for each phase than the total volume, reducing the tsunami potential.
If all the ten documented slides that were dated to ~2210 cal. yr BP (Strasser et al. 2013) occurred synchronously (total volume of ~4 Mio m^3), the zones close to the shores of today's villages of Oberrieden and Thalwil would have been affected by inundations with flow depths at single cells of up to 3 m. However, these maximum flow depths appear in the vicinity of landslide translation areas correlated to the 2210 cal. yr BP event (Strasser et al. 2013; Strupler et al. 2015) and may thus overestimate the values. The villages located around the shallower northern and southern basins are

less affected by tsunamis, as the wave experiences a greater drag in shallower waters (Berger et al. 2011). We conclude that the most slide-distal areas of the future cities of Zurich and Rapperswil were not directly affected by a potential tsunami triggered by a simultaneous failure of all the landslides assigned to a ~2210 cal. yr BP event (Strasser et al. 2013).

Only little is known about settlements located around the deep basin at the time of the assumed ~2210 cal. yr BP (i.e. ~200 B.C) earthquake, but it is assumed that the direct shorelines were not inhabited anymore, as they were earlier during lake dwellers epoch in the Neolithic and Bronze Age periods (Primas 1981; Ruoff 1981). In historical terms, the earthquake and related landslides have occurred in the La Tène epoch (~500 B.C to 0; Wells 2011) of the Iron age. Among the few archaeological findings along the shorelines is a grave, dated to the mid La Tène epoch, that was found in Horgen (Swiss LV03 Coordinates: 688250/234825; Fig. 5.5). The grave is located at 410 m a.s.l., thus only 2 m above the paleo-lake level estimated for that time (Müller et al. 1999; Wild 2009). Additional historical information on occupation gaps along the lake shores may provide helpful insight on potentially disastrous tsunamis, such as discussed in Kremer et al. (2014). These authors suggested a causal relationship between an occupation gap of lake dwellers settlements on the shores of Lake Geneva and a reconstructed tsunami event dated to 1758 BC.

Our simulations represent the 'worst-case', where all slides were triggered simultaneously. An important question is whether the ~2210 cal. yr BP slides (Strasser et al. 2013) occurred within the exactly same time (i.e. within same seconds to few minutes). Some of these slides, for example, could also have been triggered by an aftershock of an earthquake event, thus a few min to days later, which cannot be distinguished within reflection seismic data resolution. In such a case, the potential wave height and inundation may have been smaller, mainly due to the smaller cumulative slide volume. However, it has to be further investigated, what the effect of multiple slides on the wave interference is.

5.5.3 Tsunami hazard from earthquake-triggered landslides in Lake Zurich

The modelled consequences of potential slope failures expected for PGAs with EP_{50} of 10, 2 and 0.5% indicate that the occurrence of future tsunamis on Lake Zurich cannot be excluded. The presented first-order results help predicting where and how much time after a potential landslide tsunami waves reach the shores of Lake Zurich, providing crucial data for measures such as potential evacuation planning. The results of all three EP_{50} scenarios for tsunamis following earthquake-triggered landslides show that the run-up is mainly dependent on the bathymetric features close to the shoreline (e.g. Grilli et al. 2009; De Blasio 2011). On relatively steep transitions from the nearshore area to the shore (i.e. around the central basin), the run-up is greater than in extended relatively shallow zones such as the northern and southern lake-basins (Fig. 5.1a). Due to their protection by extensive shallow-water areas and their distal location with respect to the tsunami sources, the cities of Zurich and Rapperswil are barely affected by tsunamis for all modelled scenarios. The most tsunami-prone zones have a low elevation above lake level and are located around the deep basin. Most affected are the nearshore zones of the villages Thalwil, Oberrieden, Horgen, Wädenswil, Richterswil, Uetikon and Meilen. Results showed that the first wave arrives at these locations ~1 min after an earthquake has triggered the slides, implying a very short warning and reaction time. The peak wave amplitudes (excluding the values in the near field of tsunami source and single cells with

high values, which were assessed to be unreliable; Hilbe and Anselmetti 2015) for an EP_{50} of 0.5% (~2 m) are twice as high as for an EP_{50} of 2% (~1 m), and four times higher than for an EP_{50} of 10 % (~0.5 m), mainly as a consequence of the higher slide volumes expected for stronger earthquakes. Similarly, expected flow depths and inundation areas are also greater for earthquakes with a lower EP_{50}.

Although the lake level is also fluctuating up to ~1 m (AWEL 2016), a hypothetical lake level rise of ~1 m cannot be compared to a wave with an amplitude of ~1 m, for the following reasons: First, the lake level would rise much slower (i.e. hours to days), whereas a tsunami wave on Lake Zurich would arrive at the shores within seconds to minutes after being generated by a subaqueous landslide. Second, a tsunami wave of 1 m amplitude would shoal on the shore, i.e. increasing its amplitude, which would result in greater inundation areas and flow depths. Whereas for a lake-level rise, the movement of the water is only in the vertical direction, for a tsunami, there is a horizontal component in the movement of the water in the shallow areas, i.e. the tsunami waves flow "like rivers" on the shores (Ward 2011).

Quantifying the absolute tsunami hazard caused by earthquake-triggered landslides seems difficult, as the subaqueous landslide hazard is also dependent on transient conditions of the sediment drape (e.g. Strupler et al. in press). An earthquake with a certain return period does not automatically imply that a tsunami will occur. For example, if most of the potentially mobile sediment drape has been removed by landslides as a consequence of a strong earthquake, a subsequent earthquake with the same intensity may not cause landslides of considerable sediment volumes, and as a consequence no tsunami would occur. In contrast to simulations from Lake Geneva, where a tsunami that was caused by a delta collapse propagated as relatively simple wave train along the lake axis (Kremer et al. 2012), the here modelled coeval slides at the lateral slopes cause interference between the waves, resulting in a complex interference pattern.

5.5.4 Outlook

The simulation of tsunamis generated by different hypothetical earthquake-triggered landslides allows an estimation of zones affected by tsunami impacts. Due to the more alpine-proximal setting of Lake Lucerne, its topography is more complex and thus, large parts of the shore are not inhabited. In contrast, the shores of Lake Zurich are densely inhabited. As a consequence, a potential tsunami causing a similar flow depth and inundation area may create much greater damage on the shores of Lake Zurich than of Lake Lucerne, e.g. in the Gersau-basin; Hilbe and Anselmetti (2015). A quantitative tsunami-risk analysis, based on the here presented results, would be a step towards quantifying the economic impact of potential tsunamis. To this end, as risk is defined as the product of hazard, exposure and vulnerability, additional information on the latter two factors needs to be included.

The here presented tsunami hazard assessment also allows for hazard mitigation measures: Knowing which zones are endangered, the authorities could for example install an early warning system that is activated by strong earthquake and design some evacuation areas. However, the relatively short travel times of waves (due to the limed basin sizes) in lakes compared to marine settings are challenging (Kremer et al. 2015). Land-use planning authorities may consider the here presented first-order results for zonation.

To our knowledge, no clear evidence of paleotsunamis has been described in the geological records at the shores of Lake Zurich. The here mapped zones that would have been affected by a potential tsunami following the ~2210 cal. yr BP event may define investigation areas for paleotsunami deposits.

5.6 Conclusions

In this study, we modelled the tsunamigenic potential of documented earthquake-triggered Holocene landslide events occurring on the lateral slopes of Lake Zurich. Furthermore, we presented the first assessment of tsunamis that may be triggered by future earthquake-triggered landslides at a basin-wide scale. For that purpose, we used volumes of potential landslides from a probabilistic earthquake-triggered subaqueous landslide hazard map (Strupler et al. in press). The here presented estimated flow depths and inundation areas around the entire basin of Lake Zurich can be considered as first-order, rather conservative results. However, our results provide valuable information that may be used for a more detailed simulation at a more local level.

We conclude that a coeval occurrence of all the landslides assigned to the ~2210 cal. yr BP earthquake event may have triggered a tsunami with peak free surface wave heights of up to ~1.5 m. The shorelines around the deep basin may have experienced flow depths of up to ~3 m. A single slide assigned to the same earthquake-event, such as the well-described Oberrieden slide, may have caused a wave with a maximal free surface height of ~0.5 m, and thus no serious inundations on the lakeshores.

Despite the missing evidence of past tsunamis on Lake Zurich, a future tsunami hazard exists, as shown in our modelled scenarios. The zones most affected by potential tsunamis are the shore-proximal zones of the villages located around the deep, central basin, especially, where the greater water depths exist close to the shore. However, a considerable tsunami hazard caused by landslides only exists for earthquakes with very low exceedance probabilities in 50 years (i.e. large return periods).

For selected landslide-hazard levels, the following consequences may be expected:

- According to our model, an earthquake with PGAs of ~0.05 g (as expected for an exceedance probability of 10% in 50 years) would generate a total expected slide volume of ~3 Mio m^3, causing waves with peak amplitudes less than 0.5 m and no considerable inundations on the shorelines of Lake Zurich.
- Expected PGAs of ~0.1g (exceedance probability of 2% in 50 years) cause failure on most slopes steeper than ~10° (Strupler et al. in press), leading to total slide volumes of ~12 Mio m^3. This may cause tsunamis with peak wave amplitudes of ~1 m and inundations on the shores around the central basin. However, the flow depth on most of these zones is calculated to amount only to a few dm.
- A ‘worst case scenario’ of all yet unfailed slopes sliding simultaneously, that is assumed for PGAs with an exceedance period of 0.5% in 50 years, may cause tsunami waves of up to 2 m peak free surface amplitude. Inundation can be expected on all shorelines, with greatest

impact around the central basin, where maximum flow depths of up to ~4.6 m and maximum inundation-distances of the water up to ~200 m are modelled

The cities of Zurich and Rapperswil, located on the northern and southern ends of the lake, respectively, are assumed to experience very little damage, even for a worst-case scenario (i.e. simultaneous triggering of all the yet unfailed slopes), because they are protected by large, relatively shallow zones, that decelerate the tsunami wave.

Acknowledgements

This work was supported by the Swiss National Foundation Grant Nr. 133481. Swisstopo geodata was reproduced with the authorisation (JA100120). We would like to thank the developers of MassMov2D and GeoClaw for providing the open-source codes.

References

AWEL (2016) Wasserstand Zürichsee - Oberrieden 2010-2016. http://www.hw.zh.ch/hochwasser/jahrbuch/0502w016.PDF. Accessed 16 Apr 2017

Beguería S, Van Asch TWJ, Malet J-P and Gröndahl S (2009) A GIS-based numerical model for simulating the kinematics of mud and debris flows over complex terrain. Natural Hazards and Earth System Science 9:1897–1909. doi: 10.5194/nhess-9-1897-2009

Berger MJ, George DL, LeVeque RJ and Mandli KT (2011) The GeoClaw software for depth-averaged flows with adaptive refinement. Advances in Water Resources 34:1195–1206. doi: 10.1016/j.advwatres.2011.02.016

Bornhold BD and Thomson RE (2012) Tsunami hazard assessment related to slope failures in coastal waters. In: Clague JJ, Stead D (eds) Landslides. Cambridge University Press, Cambridge, pp 108–120

Bretschneider CL and Wybro PG (1977) Tsunami inundation prediction. In: Proceedings of the Fifteenth coastal Engineering Conference. Am. Soc. of Civil Engineers, New York, pp 1006–1024

De Blasio FV (2011) Subaqueous Landslides. In: Introduction to the Physics of Landslides. Springer Netherlands, Dordrecht, pp 295–351

Elverhoi A, Breien H, De Blasio F V., Harbitz CB and Pagliardi M (2010) Submarine landslides and the importance of the initial sediment composition for run-out length and final deposit. Ocean Dynamics 60:1027–1046. doi: 10.1007/s10236-010-0317-z

Fine I V., Rabinovich AB, Bornhold BD, Thomson RE and Kulikov EA (2005) The Grand Banks landslide-generated tsunami of November 18, 1929: Preliminary analysis and numerical modeling. Marine Geology 215:45–57. doi: 10.1016/j.margeo.2004.11.007

Geilinger-Schnorf U (1993) 175 Jahre Chemie Uetikon: Die Geschichte der Chemischen Fabrik Uetikon von 1818 bis 1993. UBV Uetikon Betriebs- und Verwaltungs _AG, Uetikon

Grilli ST, Taylor ODS, Baxter CDP and Maretzki S (2009) A probabilistic approach for determining submarine landslide tsunami hazard along the upper east coast of the United States. Marine Geology 264:74–97. doi: 10.1016/j.margeo.2009.02.010

Heim A (1876) Bericht und Expertengutachten über die im Februar und September 1875 in Horgen am Zürichsee vorgekommenen Rutschungen. Die Eisenbahn 4:191–196.

Henriod S, Douard R, Ullmann D and Humbel R (2016) Statistik der Bevölkerung und Haushalte (STATPOP). Bundesamt für Statistik (BFS), Bern. BFS-Nummer: be-d-00.03-13-STATPOP-v16

Hilbe M and Anselmetti FS (2015) Mass Movement-Induced Tsunami Hazard on Perialpine Lake Lucerne (Switzerland): Scenarios and Numerical Experiments. Pure and Applied Geophysics 172:545–568. doi: 10.1007/s00024-014-0907-7

Intergovernmental Oceanographic Commission (2016) Tsunami Glossary. IOC Technical Series 85. UNESCO, Paris

Jiang L and Leblond PH (1992) The Coupling of A Submarine Slide and The Surface. Journal of Geophysical Research 97:12731–12744.

Kaiser G, Scheele L, Kortenhaus A, Løvholt F, Römer H and Leschka S (2011) The influence of land cover roughness on the results of high resolution tsunami inundation modeling. Natural Hazards and Earth System Science 11:2521–2540. doi: 10.5194/nhess-11-2521-2011

Keller O and Krayss E (2005) Der Rhein-Linth-Gletscher im letzten Hochglazial. 1. Teil: Einleitung, Aufbau und Abschmelzen des Rhein-Linth-Gletschers im Oberen Würm. Verteljahrsschrift der Naturforschenden Gesellschaft in Zürich 150:19–32.

Kelts K (1978) Geological and sedimentary evolution of Lakes Zurich and Zug, Switzerland. ETH Zurich, PhD Thesis, Nr.6146

Kelts K and Hsü KJ (1980) Resedimented facies of 1875 Horgen slumps in Lake Zurich and a process model of longitudinal transport of turbidity currents. Eclogae geol Helv 73:271–281.

Kremer K, Hilbe M, Simpson G, Decrouy L, Wildi W and Girardclos S (2015) Reconstructing 4000 years of mass movement and tsunami history in a deep peri-Alpine lake (Lake Geneva, France-Switzerland). Sedimentology 1305–1327. doi: 10.1111/sed.12190

Kremer K, Marillier F, Hilbe M, Simpson G, Dupuy D, Yrro BJF, Rachoud-Schneider A-M, Corboud P, Bellwald B, Wildi W and Girardclos S (2014) Lake dwellers occupation gap in Lake Geneva (France–Switzerland) possibly explained by an earthquake–mass movement–tsunami event during Early Bronze Age. Earth and Planetary Science Letters 385:28–39. doi: 10.1016/j.epsl.2013.09.017

Kremer K, Simpson G and Girardclos S (2012) Giant Lake Geneva tsunami in ad 563. 5:2011–2013.

Kuen E (1999) Der Uferabbruch im Kusen. In: Küsnachter Jahrheft. Ortsgeschichtliche Kommission der Kulturellen Vereinigung Küsnacht, pp 44–50

Lastras G, Amblas D, Calafat AM, Canals M, Frigola J, Hermanns RL, Lafuerza S, Longva O, Micallef A, Sepúlveda S a, Vargas G, Batist M De, Daele M Van, Azpiroz M, Bascuñán I, Duhart P, Iglesias O, Kempf P, Rayo X and Effects E (2013) Landslides Cause Tsunami Waves: Insights From Aysén Fjord, Chile. Eos, Transactions American Geophysical Union 94:297–298. doi: 10.1002/2013EO340002

Lee H, Schwab W and Booth J (1993) Submarine Landslides: An Introduction. In: Schwab WC, Lee HJ, Twichell DC (eds) Submarine Landslides: Selected Studies in the US Exclusive Economic Zone. US Geological Survey Bulletin 2002, pp 1–11

Locat J and Lee HJ (2002) Submarine landslides: advances and challenges. Canadian Geotechnical Journal 39:193–212. doi: 10.1139/t01-089

López-Venegas AM, ten Brink US and Geist EL (2008) Submarine landslide as the source for the October 11, 1918 Mona Passage tsunami: Observations and modeling. Marine Geology 254:35–46. doi: 10.1016/j.margeo.2008.05.001

Mei CC and Liu K-FF (1987) A Bingham-plastic Model For A Muddy Seabed Under Long Waves. Journal of Geophysical Research-oceans 92:14581–14594. doi: 10.1029/JC092iC13p14581

Moernaut J and De Batist M (2011) Frontal emplacement and mobility of sublacustrine landslides: Results from morphometric and seismostratigraphic analysis. Marine Geology 285:29–45. doi: 10.1016/j.margeo.2011.05.001

Mohrig D, Whipple KX, Hondzo M, Ellis C and Parker G (1998) Hydroplaning of subaqueous debris flows. Bulletin of the Geological Society of America 110:387–394. doi: 10.1130/0016-7606(1998)110<0387:HOSDF>2.3.CO

Müller F, Kaenel G and Lüscher G (1999) Eisenzeit = Age du Fer. Die Schweiz vom Paläolithikum bis zum frühen Mittelalter. SPM IV. Schweizerische Gesellschaft für Ur- und Frühgeschichte, Basel

Nipkow F (1927) Über das Verhalten der Skelette planktischer Kieselalagen im geschichteten Tifenschlamm des Zürich- und Baldeggersees. ETH Zurich, PhD Thesis, Nr. 455

Pararas-Carayannis G (1988) Risk Assessment of the Tsunami Hazard. In: El-Sabh MI, Murty TS (eds) Natural and Man-Made Hazards. Springer Netherlands, Dordrecht, pp 183–191

Pelinovsky EN and Mazova RK (1992) Exact analytical solutions of nonlinear problems of tsunami wave run-up on slopes with different profiles. Natural Hazards 6:227–249. doi: 10.1007/BF00129510

Primas M (1981) Urgeschichte des Zürichseegebietes im Überblick: Von der Steinzeit bis zur Früheisenzeit. In: Degen R (ed) Zürcher Seeufersiedlungen - Von der Pfahlbau-Romantik zur modernen archäologischen Forschung. Basel, pp 5–18

Reusch A, Moernaut J, Anselmetti FS and Strasser M (2016) Sediment mobilization deposits from episodic subsurface fluid flow-A new tool to reveal long-term earthquake records? Geology 44:243–246. doi: 10.1130/G37410.1

Ruoff U (1981) Die Ufersiedlungen an Zürich- und Greifensee. In: Degen R (ed) Zürcher Seeufersiedlungen - Von der Pfahlbau-Romantik zur modernen archäologischen Forschung. Basel, pp 19–61

Schlund RA (1972) Zürichsee: topogr. Plan 1:5 000. Meliorations- und Vermessungsamt des Kt. Zürich.

Schnellmann M, Anselmetti FS, Giardini D, McKenzie JA and Ward SN (2002) Prehistoric earthquake history revealed by lacustrine slump deposits. Geology 30:1131–1134. doi: 10.1130/0091-7613(2002)030<1131:PEHRBL>2.0.CO;2

Shimazu H (2016) Relationships Between Coastal and Fluvial Geomorphology and Inundation Processes of the Tsunami Flow Caused by the 2011 off the Pacific Coast of Tohoku

Earthquake. In: Natural Disaster and Coastal Geomorphology. Springer International Publishing, Cham, pp 65–92

Siegenthaler C, Finger W, Kelts K and Wang S (1987) Earthquake and seiche deposits in Lake Lucerne, Switzerland. Eclogae Geologicae Helvetiae 80:241–260.

Skvortsov A and Bornhold B (2007) Numerical simulation of the landslide-generated tsunami in Kitimat Arm, British Columbia, Canada, 27 April 1975. Journal of Geophysical Research: Earth Surface 112:1–12. doi: 10.1029/2006JF000499

Strasser M, Monecke K, Schnellmann M and Anselmetti FS (2013) Lake sediments as natural seismographs: A compiled record of Late Quaternary earthquakes in Central Switzerland and its implication for Alpine deformation. Sedimentology 60:319–341. doi: 10.1111/sed.12003

Strasser M, Schindler C and Anselmetti FS (2008) Late Pleistocene earthquake-triggered moraine dam failure and outburst of Lake Zurich, Switzerland. Journal of Geophysical Research: Earth Surface 113:1–16. doi: 10.1029/2007JF000802

Strupler M, Hilbe M, Anselmetti FS, Kopf AJ, Fleischmann T and Strasser M (2017) Probabilistic stability evaluation and seismic triggering scenarios of submerged slopes in Lake Zurich (Switzerland). Geo-Marine Letters 37:241–258. doi: 10.1007/s00367-017-0492-8

Strupler M, Hilbe M, Anselmetti FS and Strasser M (2015) Das neue Tiefenmodell des Zürichsees: Hochauflösende Darstellung der geomorphodynamischen Ereignisse im tiefen Seebecken. Swiss Bull angew Geol 20:71–83.

Strupler M, Danciu L, Hilbe M, Kremer K., Danciu L., Anselmetti F.S., Strasser M. and Wiemer S. (in press) A subaqueous hazard map for earthquake-triggered landslides in Lake Zurich, Switzerland. Natural Hazards. doi: 10.1007/s11069-017-3032-y

Synolakis CE, Bardet J-P, Borrero JC, Davies HL, Okal EA, Silver EA, Sweet S and Tappin DR (2002) The slump origin of the 1998 Papua New Guinea Tsunami. Proceedings of the Royal Society A: Mathematical, Physical and Engineering Sciences 458:763–789. doi: 10.1098/rspa.2001.0915

Tappin DR (2017) The Generation of Tsunamis. In: Encyclopedia of Maritime and Offshore Engineering. John Wiley & Sons, Ltd, Chichester, UK, pp 1–10

Tappin DR, Matsumoto T, Watts P, Satake K, McMurtry GM, Matsuyama M, Lafoy Y, Tsuji Y, Kanamatsu T, Lus W, Iwabuchi Y, Yeh H, Matsumotu Y, Nakamura M, Mahoi M, Hill P, Crook K, Anton L and Walsh JP (1999) Sediment slump likely caused 1998 papua new Guinea Tsunami. Eos. doi: 10.1029/99EO00241

Tappin DR, Watts P and Grilli ST (2008) The Papua New Guinea tsunami of 17 July 1998: anatomy of a catastrophic event. Nat Hazards Earth Syst Sci 8:243–266.

Tappin DR, Watts P, McMurtry GM, Lafoy Y and Matsumoto T (2001) The Sissano, Papua New Guinea tsunami of July 1998 - Offshore evidence on the source mechanism. Marine Geology 175:1–23. doi: 10.1016/S0025-3227(01)00131-1

ten Brink US, Lee HJ, Geist EL and Twichell D (2009) Assessment of tsunami hazard to the U.S. East Coast using relationships between submarine landslides and earthquakes. Marine Geology 264:65–73. doi: 10.1016/j.margeo.2008.05.011

Tinti S and Bortolucci E (2000) Energy of Water Waves Induced by Submarine Landslides. Pure and Applied Geophysics 157:281–318. doi: 10.1007/s000240050001

Wang X, Mountjoy J, Power WL and Lane EM (2016) Coupled Modelling of the Failure and Tsunami of a Submarine Debris Avalanche Offshore Central New Zealand. Springer International Publishing, Cham

Ward SN (2011) Tsunami. In: Gupta HK (ed) Encyclopedia of Solid Earth Geophysics. Springer Netherlands, Dordrecht, pp 1473–1493

Watts P (1998) Wavemaker curves for tsunamis generated. Journal of Waterway, Port, Coastal, and ocean engineering 127–137.

Wells PS (2002) The Iron Age. In: Milisauskas S (ed) European Prehistory: A Survey. Springer US, Boston, MA, pp 335–383

Wesseling CG, Karssenberg D-J, Burrough P and Van Deursen WPA (1996) Integrating dynamic environmental models in GIS: The development of a Dynamic Modelling language. Transactions in GIS 1:40–48. doi: 10.1111/j.1467-9671.1996.tb00032.x

Wiemer S, Danciu L, Edwards B, Marti M, Fäh D, Hiemer S, Wössner J, Cauzzi C, Kästli P and

Kremer K (2016) Seismic Hazard Model 2015 for Switzerland. 1–163. doi: 10.12686/a2

Wild D (2009) Lindenhof, Sihl und Zürichsee-Fragen zu Geologie und Topographie zwischen Spätlatène und Frühmittelalter. In: Zürich in der Spätlatène- und frühen Kaiserzeit - Vom keltischen Oppidum zum römischen Vicus Turicum. Hochbaudepartment der Stadt Zürich, Zürich, pp 14–17

Chapter 6

Conclusions and Outlook

6.1 Overall conclusions

This PhD thesis aimed at i) conceptually advancing the assessment of the earthquake-related subaqueous landslide hazard and at ii) quantifying and mapping these hazards on a basin-wide scale in Lake Zurich, Switzerland. A combined approach of geophysical, sedimentological, geotechnical, Geo Information Science (GIS), and numerical modelling methods was used to investigate subaqueous hazards. As a first step of the hazard-assessment process, a high-resolution bathymetric dataset (1 m grid resolution) of Lake Zurich was acquired. Based on the novel bathymetric dataset (Chapter 2), the morphometric parameters related to subaqueous landslides were identified, quantified, and characterised. Subsequently, a concept for flexibly assessing the sediment-mechanical properties of the lateral slopes and their spatial variability was presented and tested at a case-study site offshore Oberrieden (Chapter 3). Based on the resulting sediment-mechanical stratigraphy of the lateral slopes, the first basin-wide probabilistic assessment of the subaqueous seismic landslide-hazard in Lake Zurich was conducted (Chapter 4). Finally, potential past and future tsunamis in Lake Zurich were simulated (Chapter 5).
The main outcomes of this thesis are i) the development of a cost- and time-efficient probabilistic assessment of subaqueous slope stabilities and landslide hazard and ii) the first quantitative assessment of the subaqueous earthquake-triggered landslide and tsunami hazard for Lake Zurich based on probabilistic input data. Furthermore, this PhD thesis demonstrates the need for interdisciplinarity, e.g. between the fields of limnogeology and earthquake-engineering, to improve our understanding and management of geohazards.

6.2 Specific conclusions

The specific conclusions, based on the results of this PhD thesis are listed in the following subsections:

6.2.1 Quantitative characterisation of subaqueous landslides based on a high resolution DDM

- "A high spatial resolution matters": the high-resolution (1 m) digital depth model (DDM), which shows the geomorphic features on the lake floor in a yet unprecedented detail, allowed the extraction of quantitative information concerning the causes, processes and timing of the subaqueous mass movements (Chapter 2). Fingerprints of subaqueous landslides that date back to ~5000 cal. yr BP and small-scale gullies could be detected, which were not identifiable in a previous dataset (Schlund 1972) with a lower spatial resolution (expressed by constant isobath values 5 m in the deep zones and 2.5 m in the shallow areas, respectively). However, the morphological features of slides older than ~5000 cal. yr BP have been smoothed by sedimentation and other slope processes and can only be investigated with seismic reflection analyses.
- Quantitative analyses of subaqueous landslides with GIS allow for a rapid characterisation of mass-movement processes in lake basins, given an existing bathymetric dataset. The total of 50 mapped landslide-translation areas in Lake Zurich show similar frequency distributions concerning area and slope angles as described for marine slopes: most of the slides are relatively small (this study: < 0.05 km^2), and slides occur on a broad variety of slope angles (this study: 5-35°, with a majority of slides occurring on slopes gradients between 10-25°). Such

commonalities between lacustrine and marine systems highlight the comparability between these settings and thus the importance of studying lakes as 'model oceans'.

- The surface roughness of individual translation areas is represented by the standard deviation of a Topographic Position Index (TPI). It was found that it can be correlated to ages of past landslides and used as relative dating tool. Translation areas with a great surface roughness correspond to recent landslides (i.e. younger than ~150 years, whereas translation areas with a low surface roughness correspond to sub-recent landslides. A surface-roughness analysis of translational areas may become a routine procedure for subaqueous landslide-hazard analyses, allowing for a first-order dating without expensive laboratory analyses.

6.2.2 Concept of a flexible sediment-mechanical stratigraphy and its application in Lake Zurich

- The comparison of geotechnical profiles versus sediment depth from core logs and in situ cone penetration testing (CPT) data suggest that a linear increase of geotechnical parameters with depth may represent an oversimplification. This appears to be especially the case where multiple different mechanical units appear on a relatively small (i.e. decimetre to metre) scale. Hence, we proposed a concept for an adaptable sediment-mechanical stratigraphy of the lateral slopes. Our concept is based on the fact that the geotechnical profiles of each sediment core's lithological units show a similar pattern but different sediment thicknesses (due to different sedimentation at the different coring locations).
- The here presented approach allows an efficient probabilistic assessment of basin-wide slope stability along a depth-profile incorporating the spatial variability of the geotechnical input parameters. The concept of a flexible sediment-mechanical stratigraphy, tested at the well-studied site in Oberrieden with a dense spacing of sediment cores and CPT sites may be transferred to other lacustrine and marine settings. Applied at a larger scale, in a first step, geotechnical profiles may be taken at a low spatial sampling resolution (e.g. one core per km^2) to detect general commonalities and differences in sediment-mechanical patterns. In a further step, the spatial sampling resolution may be increased in order to construct mechanical stratigraphies for different zones.
- The post-glacial sediment drape on the lateral slopes of Lake Zurich could be classified in four mechanical units with distinct characteristics. Results from slope-stability analyses and sedimentological groundtruthing showed that the glide plane of the investigated slides is located in a lithostratigraphic unit of Late Glacial plastic muds, the same unit as documented for nearby Lake Lucerne (Strasser et al. 2007). Our results suggest that future slides originating from the sediment-charged lateral slopes of Lake Zurich are also expected to occur in the same lithostratigraphic unit.
- Results from a one-dimensional limit equilibrium equation on an infinite slope supported previously hypothesized earthquake-triggers for landslide events occurring ~2210 and 640 cal. yr BP in the study area (Strasser and Anselmetti 2008) from a geotechnical perspective. A spatial back-analysis of the ~2210 cal. yr BP event assigned pseudostatic earthquake acceleration values in the range between 0.04 and 0.08 g to that event. In this study, back-analyses were used as 'proof of concept' as the pseudostatic earthquake accelerations are in the range of similar events (e.g. Strasser et al. 2011), and the modelled slide volumes of past events are in the same range as estimations with other methods.

6.2.3 Subaqueous earthquake-triggered landslide and tsunami hazard assessment

- Based on sediment-mechanical and geophysical input data, we presented a grid-based approach to assess the basin-wide earthquake-triggered subaqueous landslide hazard. Peak ground accelerations (PGAs) from an existing probabilistic seismic hazard assessment (Wiemer et al. 2016) were included in a limit-equilibrium equation on an infinite slope, which was applied on a spatial scale. Our result is one of the first sublacustrine earthquake-triggered landslide hazard maps and revealed 'hotspot areas' prone to slope failure and tsunami impact. In general, the shorelines around the central, deep basin of Lake Zurich are most prone to subaqueous earthquake related hazards.
- Results suggest that an earthquake with a mean return period of 475 years in the Lake Zurich area (representing PGAs of ~0.05 g) may trigger multiple, yet minor subaqueous landslides, with a total volume of ~3 Mio m^3. These hypothesized landslides are expected to induce waves with a maximum free surface height of ~0.5 m, however, not causing any damage. An earthquake with a mean return period of 2475 years, representing PGAs of ~0.1 g, is expected to trigger landslides on most slopes steeper than ~10° with an estimated total volume of ~12 Mio m^3. Such an event may cause tsunamis with peak amplitudes of ~1 m and flow depths around the central basin of mostly a few decimetres. An earthquake with a mean return period of 9975 years may trigger landslides on all lateral slopes, representing a 'worst case scenario'. Inundation can be expected on all shorelines with maximum flow depths of up to ~4.6 m in the near field of the subaqueous landslides. However, our results showed that for this scenario, large parts of the shorelines experience a flow depth of less than 1 m. Although a hazard for tsunamis triggered by earthquake-induced landslides exists for Lake Zurich, our findings suggested that the consequences can be considered as rather low. The cities of Zurich and Rapperswil, located at the northern and southern ends of Lake Zurich, respectively, are expected to experience very little damage because they are protected by extensive shallow zones.
- It still remains unknown whether an assumed ~2210 cal. yr BP earthquake (Strasser and Anselmetti 2008; Strasser et al. 2013) has caused a tsunami. First-order results suggested that such an event may have triggered a tsunami with free surface wave heights of up to ~1.5 m.

6.3 Outlook

6.3.1 Public applications of the datasets

The high resolution digital depth model of Lake Zurich may be further highly important for various applied aspects such as environmental planning, hazard management, fishery, and off- and alongshore civil engineering. The gap between the bathymetric dataset and digital elevation model may be filled by an airborne LiDAR survey, similar to the case of Lake Constance (North-eastern Switzerland; Wessels et al. 2015). The resulting seamless digital terrain model (DTM) may lead to a better understanding of the processes transferring from land to lake (e.g. subaerial slope failures) or vice versa (e.g. inundation or high-resolution wave impact modelling). Furthermore, the mapped subaqueous landslides on the slopes of Swiss lakes may be integrated in publicly accessible, official online maps of the Swiss Confederation, including their main characteristics such as area, volume, water depth and lithological characteristics of glide plane. Such a publically available database may be used for regional analyses of subaqueous landslide-characteristics, land use planning and catastrophe responses.

6.3.2 Scientific outlook and recommendations for future research

Apart from the conceptual and site-specific knowledge gain on earthquake-induced subaqueous hazards resulting from this study, some problems remained unsolved and many new questions arose. In the following subsections, the major challenges and research strategies for future studies based on the presented outcomes are described.

6.3.2.1 Analyses based on high-resolution bathymetric data

A repeated acquisition of a bathymetric dataset is recommended if an earthquake occurs in the Lake Zurich region with peak ground accelerations > 0.05 g (corresponding to a mean return period of 475 years; Wiemer et al. 2016). This would allow for the creation of a differential bathymetric dataset that shows 'hotspots' of sediment-dynamic changes related to earthquakes and / or sediment charging processes in the lake basins. Moreover, a monitoring of subaqueous landslides with repeated multibeam surveys at short time intervals can contribute to a better understanding of the preconditioning and triggering of slope failures and turbidity currents (e.g. Clare et al. 2016). A regular investigation of the gullies that appear on the steep slopes (i.e. > 25°) may lead to a better quantification of their hypothesized role of downslope sediment-transport compared to subaqueous landslides. Specific monitoring of the slope-transversal undulations that were discovered may also provide information on the process behind their morphologic expression. We hypothesized that these transversal undulations may be a geomorphic expression of a local instability as the undulations occur in the neighbouring area of subaqueous landslides on a steep part of the slope. Unpublished bathymetric data of perialpine Lake Zug, located ~15 km from Lake Zurich (courtesy of Prof. Flavio Anselmetti, University of Bern) showed similar slope-transversal undulations. Detailed multi-method investigations on such undulations may give better insights on the mechanics of subaqueous landslides. Finally, an ultimate vision of the approach that correlates the surface roughness of a landslide to an age, is to be able to estimate an absolute age range of subaqueous landslides just based on a high-resolution bathymetric dataset and knowledge about the sedimentation rate.

6.3.2.2 Mechanics of the subaqueous landslides in perialpine lakes

In order to advance the understanding of the mechanisms and kinematics of subaqueous landslides additional in situ and laboratory tests are needed:

- The presented approach of a sediment-mechanical stratigraphy (Chapter 3) may be extended with other geotechnical variables. In particular, pore pressure may be included for locations where this variable is a key player. Therefore, long-term measurements of the pore pressure would be needed. Generally, also for monitoring of other slope parameters, it needs to be tested if geotechnical in situ measuring methods (e.g. inclinometers) similarly used for the monitoring of the subaerial slopes may be adapted to the subaqueous environment.
- In addition, further research needs to be undertaken towards increasing the understanding of the small-scale geotechnical behaviour of different mechanical units, especially on the Late Glacial clays, which act as weak layers in Lake Zurich and Lake Lucerne. Such efforts may involve oedometer-tests or X-ray micro-CT investigations (e.g. Cnudde and Boone 2013) of the sediment. However, oedometer trial tests showed that this may be quite complicated due to measuring difficulties related to the behaviour of the lake-sediment samples.
- Measurements of the average shear-wave velocity of the uppermost 30 m of the sediment (Vs_{30}) of the lateral slopes may also be conducted. Information on the Vs_{30} allows calculating the earthquake-triggered hazard with the spectral acceleration as a function of the fundamental

period of the soil instead of PGA. This would include the resonance of the slopes for stability analyses, which was ignored in this study.

6.3.2.3 Hazard zonation and construction of risk maps

This study identified landslide-prone areas on the subaqueous slopes of Lake Zurich (Chapter 4) and gave first-order quantitative estimations of the tsunami impact along the shorelines (Chapter 5). This is an important basis for a further hazard zonation. In zones with a high hazard, additional, more detailed investigations on a greater spatial resolution may be conducted. Also, more sophisticated, site-specific methods for the assessment of slope stabilities such as a stress-deformation analysis (e.g. Jibson 2011) may be applied.

If the hazard map is completed by information on vulnerability and exposure, risk maps may be constructed (as risk is the product of hazard, vulnerability and elements at risk). These factors may be derived from publically accessible databases (e.g. Henriod et al. 2016) and mapped as individual layers that can be multiplied in GIS. Areas with high risk may be identified for mitigation measures and considered in a decision support system (e.g. Strunz et al. 2011) on a cantonal or national level (e.g. at the National Emergency Operations Centre).

The mapped zones that would have been affected by a potential tsunami following the ~2210 cal. yr BP event may be used to look for paleotsunami deposits. The existence of such deposits might confirm a modelled inundation of such a tsunami.

6.3.2.4 Probabilistic landslide-triggered tsunami hazard and risk assessment

Future studies may conduct a probabilistic hazard assessment of landslide-induced tsunamis that considers the volume-distribution of potential landslides. Such an approach could provide probabilities of exceeding given tsunami wave amplitudes (e.g. “what is the probability of waves arriving in Zurich with an amplitude greater than 1 m?”) and inundation areas (e.g. Sørensen et al. 2012; Intergovernmental Oceanographic Commission 2016). For a probabilistic analysis, other models and codes may be used, and collaboration with modelling experts is recommended. Also, in future studies, a way to assess delta failures, which may also contribute to tsunamis but have different failure mechanisms, needs to be implemented.

References

Clare MA, Hughes Clarke JE, Talling PJ, Cartigny MJB and Pratomo DG (2016) Preconditioning and triggering of offshore slope failures and turbidity currents revealed by most detailed monitoring yet at a fjord-head delta. Earth and Planetary Science Letters 450:208–220. doi: 10.1016/j.epsl.2016.06.021

Cnudde V and Boone MN (2013) High-resolution X-ray computed tomography in geosciences: A review of the current technology and applications. Earth-Science Reviews 123:1–17. doi: 10.1016/j.earscirev.2013.04.003

Henriod S, Douard R, Ullmann D and Humbel R (2016) Statistik der Bevölkerung und Haushalte (STATPOP). Bundesamt für Statistik (BFS), Bern. BFS-Nummer: be-d-00.03-13-STATPOP-v16

Intergovernmental Oceanographic Commission (2016) Tsunami Glossary. IOC Technical Series 85. UNESCO, Paris

Jibson RW (2011) Methods for assessing the stability of slopes during earthquakes—A retrospective. Engineering Geology 122:43–50. doi: 10.1016/j.enggeo.2010.09.017

Schlund RA (1972) Zürichsee: topogr. Plan 1:5 000. Meliorations- und Vermessungsamt des Kt. Zürich.

Sørensen MB, Spada M, Babeyko A, Wiemer S and Grünthal G (2012) Probabilistic tsunami hazard in the Mediterranean Sea. Journal of Geophysical Research: Solid Earth. doi: 10.1029/2010JB008169

Strasser M and Anselmetti FS (2008) Mass-movement event stratigraphy in Lake Zurich; A record of varying seismic and environmental impacts. Beiträge zur Geologie der Schweiz 95:23–41.

Strasser M, Hilbe M and Anselmetti FS (2011) Mapping basin-wide subaquatic slope failure susceptibility as a tool to assess regional seismic and tsunami hazards. Marine Geophysical Research 32:331–347. doi: 10.1007/s11001-010-9100-2

Strasser M, Monecke K, Schnellmann M and Anselmetti FS (2013) Lake sediments as natural seismographs: A compiled record of Late Quaternary earthquakes in Central Switzerland and its implication for Alpine deformation. Sedimentology 60:319–341. doi: 10.1111/sed.12003

Strasser M, Stegmann S, Bussmann F, Anselmetti FS, Rick B and Kopf A (2007) Quantifying subaqueous slope stability during seismic shaking: Lake Lucerne as model for ocean margins. Marine Geology 240:77–97. doi: 10.1016/j.margeo.2007.02.016

Wessels M, Anselmetti F, Artuso R, Baran R, Daut G, Gaide S, Geiger A, Groeneveld JD, Hilbe M, Möst K, Klauser B, Niemann S, Roschlaub R, Steinbacher F, Wintersteller P and Zahn E (2015) Bathymetry of Lake Constance - A high-resolution survey in a large, deep lake. ZFV - Zeitschrift fur Geodasie, Geoinformation und Landmanagement 140:203–210. doi: 10.12902/zfv-0079-2015

Wiemer S, Danciu L, Edwards B, Marti M, Fäh D, Hiemer S, Wössner J, Cauzzi C, Kästli P and Kremer K (2016) Seismic Hazard Model 2015 for Switzerland. 1–163. doi: 10.12686/a2

Appendix A

Bathymetric dataset and sediment cores

A1 Bathymetric dataset

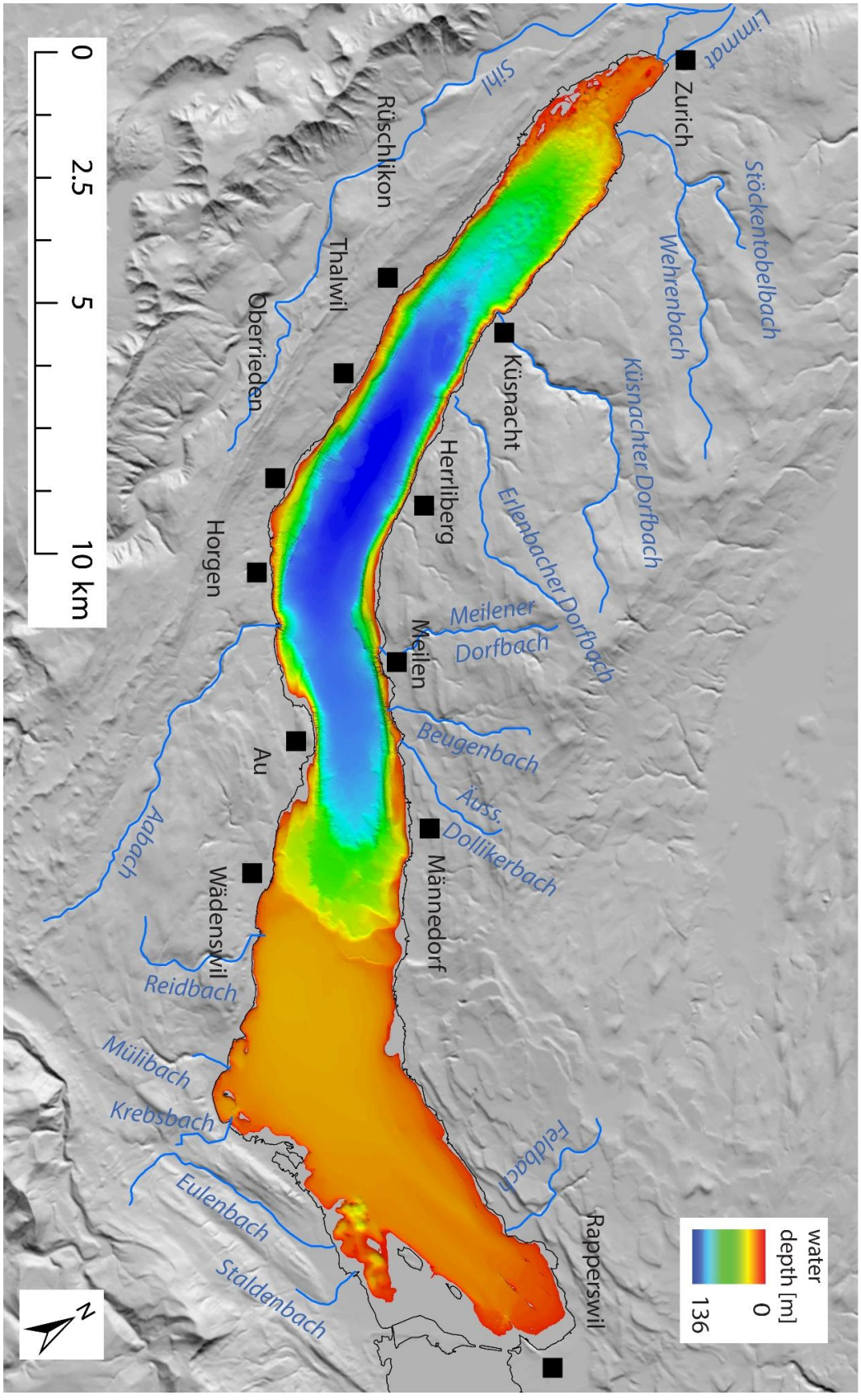


Figure A. 1 *New high-resolution bathymetric dataset of Lake Zurich. LiDAR hillshade data: Swisstopo*

A2 Sediment coring locations and photos

Sediment coring locations

Table A. 1 Locations of the sediment cores

Corename	x-coordinate	y-coordinate	slope gradient [°]	Depth below lake level [m]
ZH15-S01	237911	686442	18.6	72
ZH15-S02	237955	686569	8.4	117
ZH15-S03	237472	686473	10.8	56
ZH15-S04	237471	686568	11.3	65
ZH15-S05	237558	686708	17.3	99
ZH15-S06	237431	686807	12.9	108
ZH15-S07	237297	686760	5.7	99
ZH15-S08	236912	686736	12.6	70
ZH15-S09	236903	686809	14.7	82
ZH15-S10 (I)	236930	686887	17.0	99
ZH15-S10 (II)	236936	686885	18.6	100
ZH15-S11	237000	686998	2.6	118
ZH15-S12	236807	686972	20.5	103
ZH15-S13	236849	687073	2.1	118
ZH15-S14	237334	686879	19.6	112
ZH15-S15	237411	686695	16.4	88
ZH15-S16	237764	686604	19.9	94
ZH15-S17	237155	686892	5.5	107
ZH16-S01	237913	686521	22.6	97
ZH16-S02	237934	686517	21.4	100
ZH16-S03	237970	686509	23.7	105
ZH14-S11	236737	686857	12.9	66
ZH14-S12	236763	686893	20.2	82
ZH14-S15	237167	686757	10.9	94
ZH14-S16	237262	686919	18.2	114
ZH15-K01	237848	686300	8.1	40
ZH15-K03	237902	686441	19.5	69
ZH15-K04	237067	686721	10.1	74
ZH15-K05	237101	686809	10.6	97
ZH15-K06	236639	687233	14.8	111
ZH15-K07	236454	687019	12.0	57
ZH15-K13	237422	686644	10.7	76

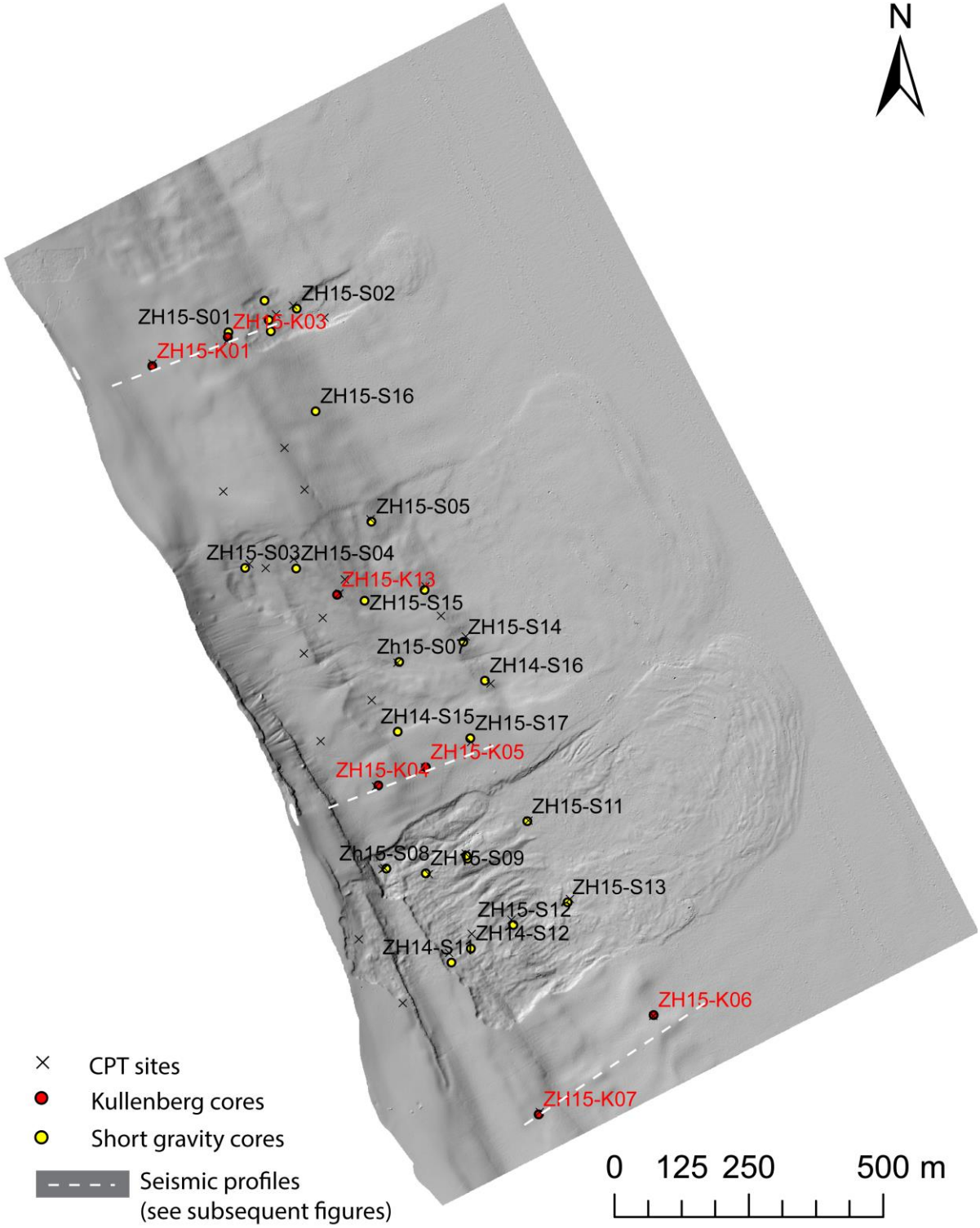


Figure A. 2 Map with location of sediment cores and CPT

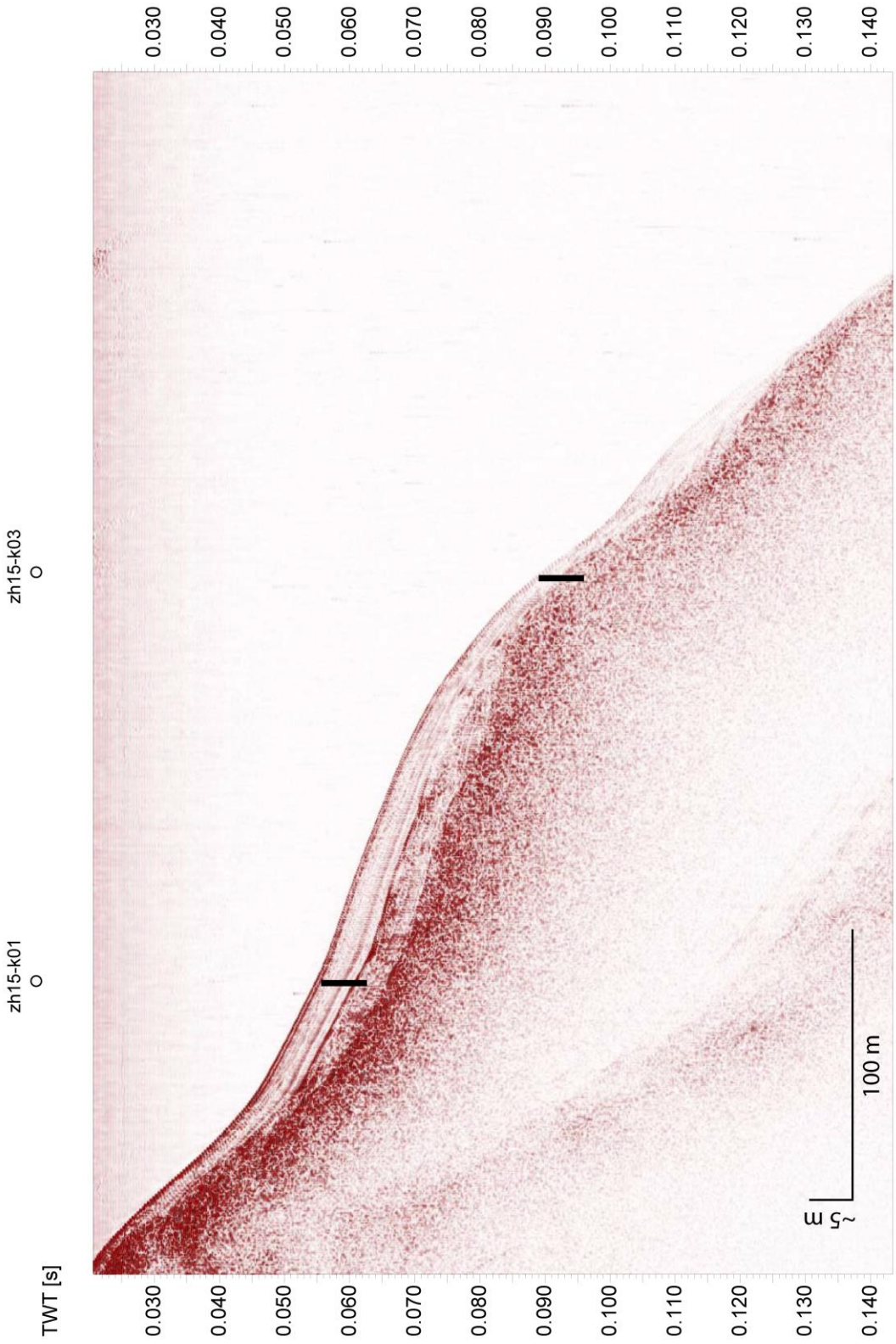


Figure A. 3 Location of Kullenberg cores ZH15-K01 and K03 (seismic reflection data from Strasser and Anselmetti 2008)

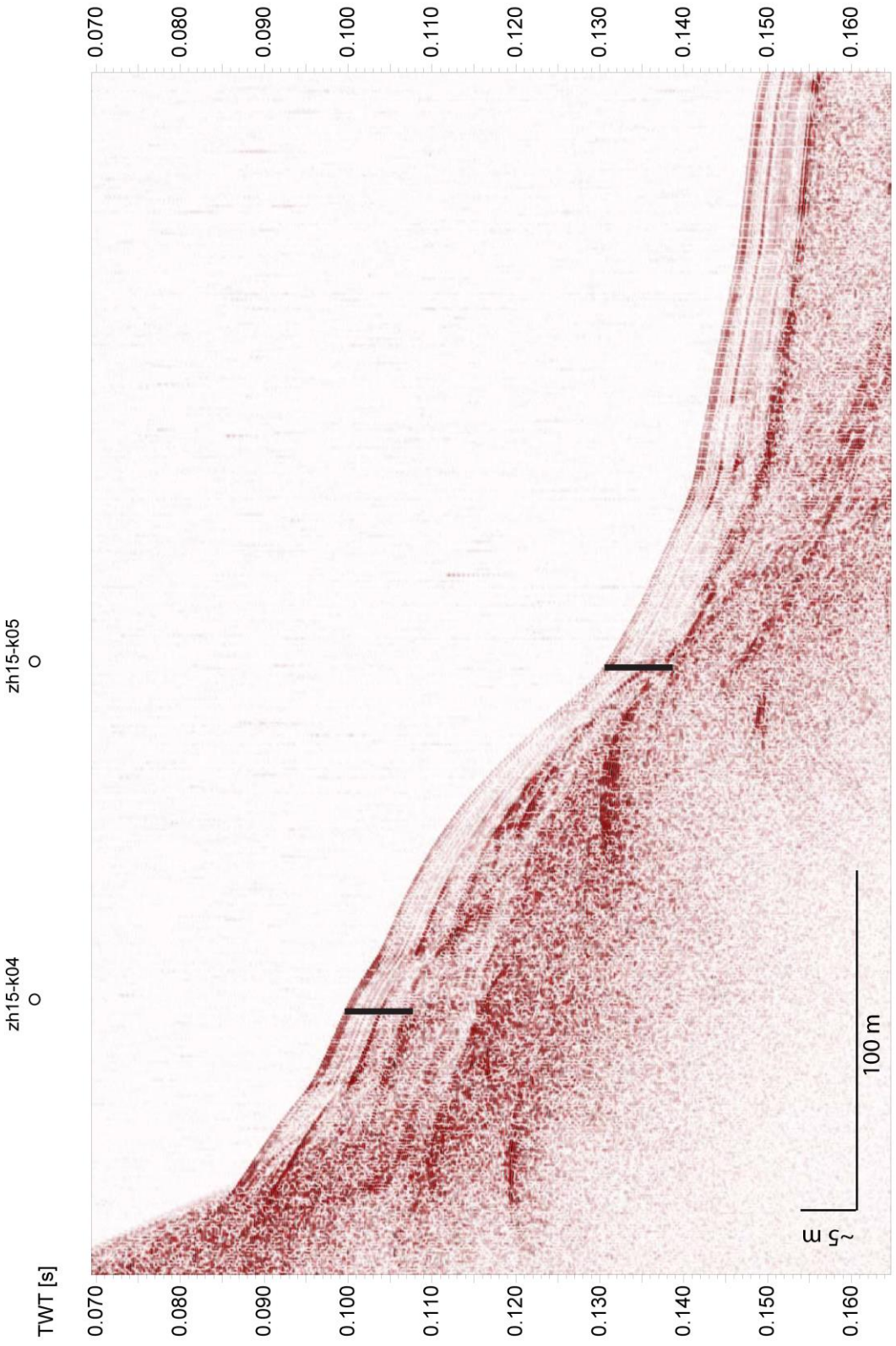


Figure A. 4 Location of Kullenberg cores ZH15-K04 and K05 (seismic reflection data from Strasser and Anselmetti 2008)

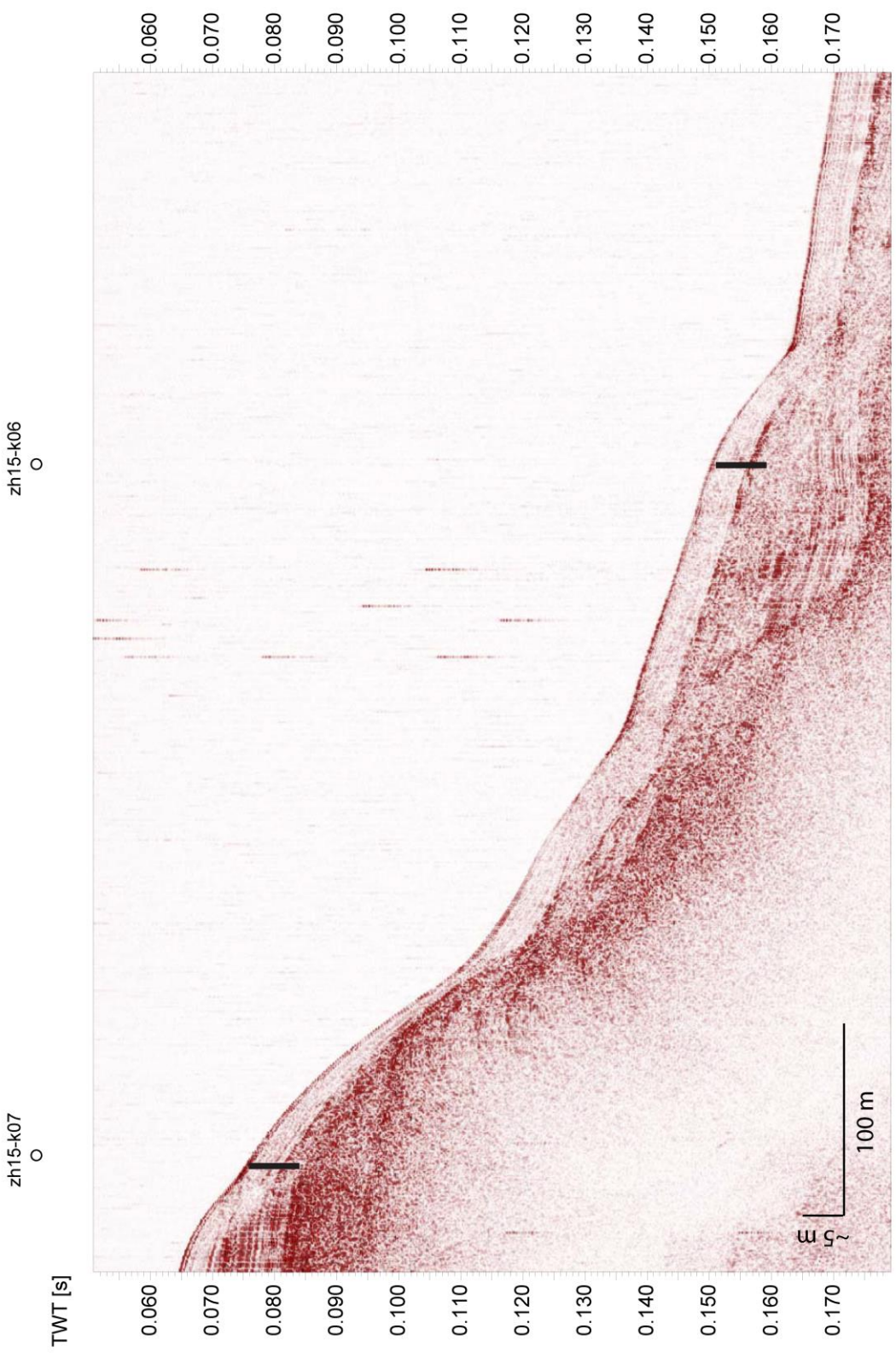


Figure A. 5 Location of Kullenberg cores ZH15-K06 and K07 (seismic reflection data from Strasser and Anselmetti 2008)

Photos of the lengthwise split sediment cores

Kullenberg type cores



Figure A. 6 Core ZH15-K01

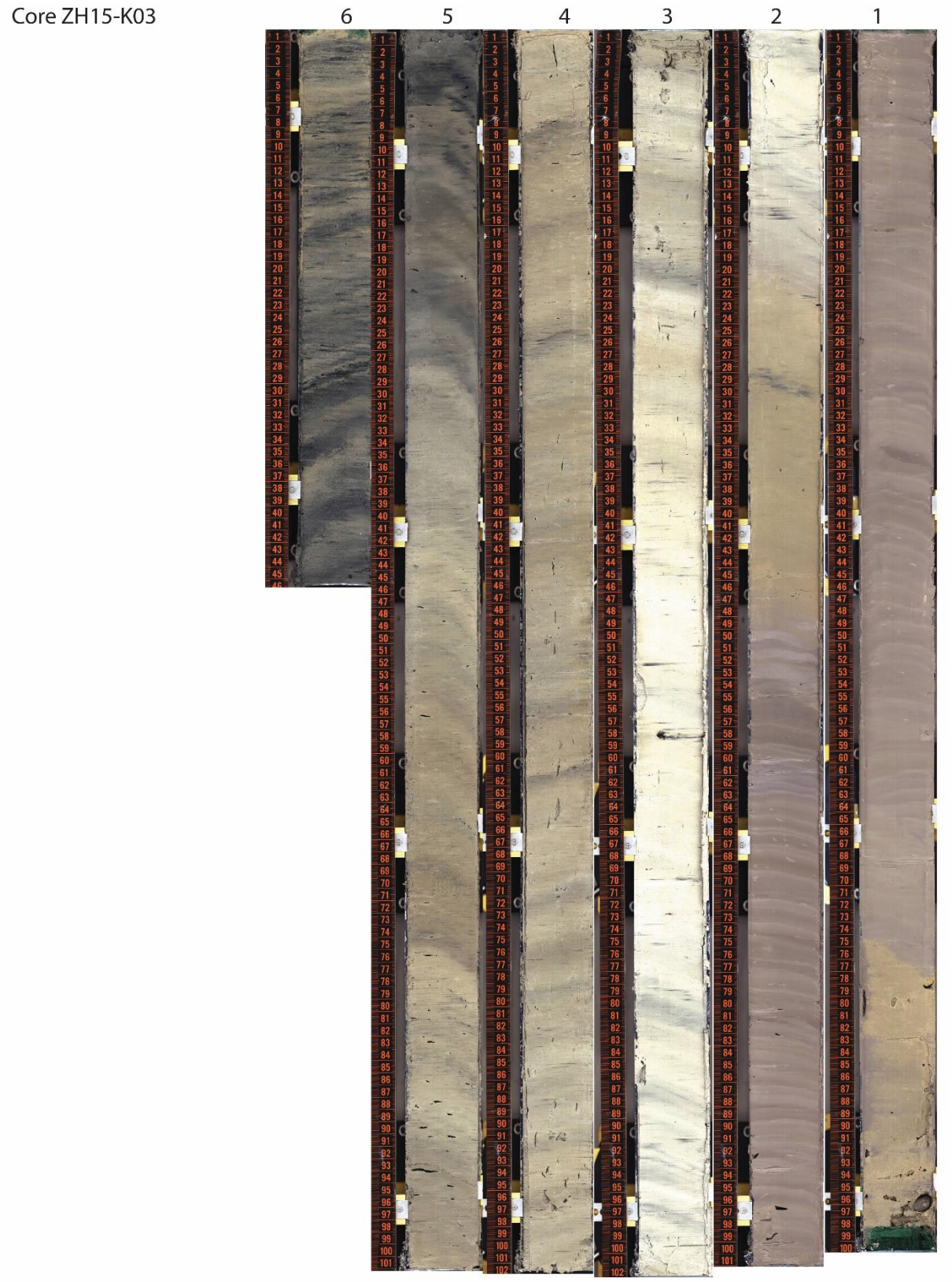


Figure A. 7 Core ZH15-K03

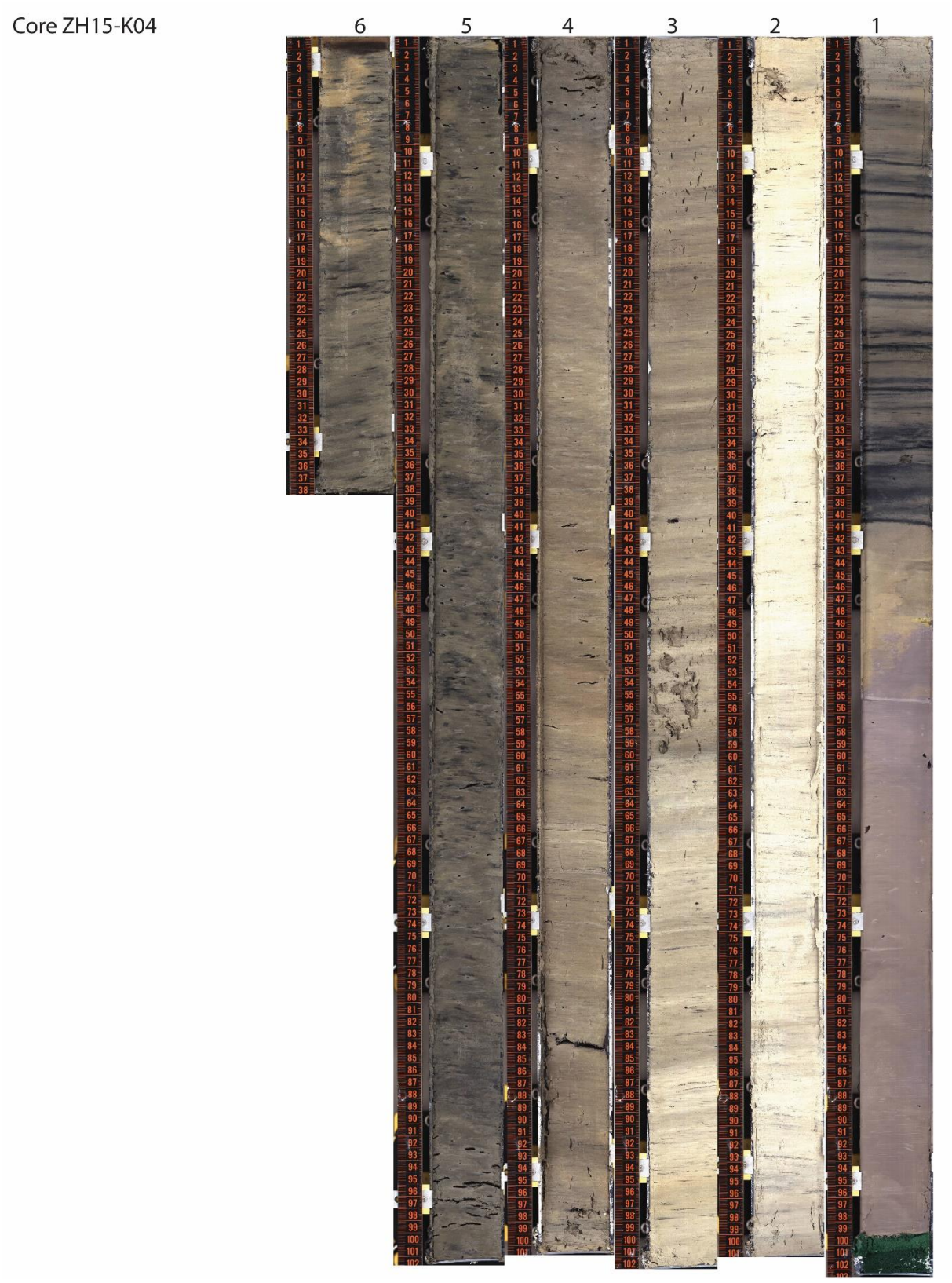


Figure A. 8 Core ZH15-K04



Figure A. 9 Core ZH15-K05

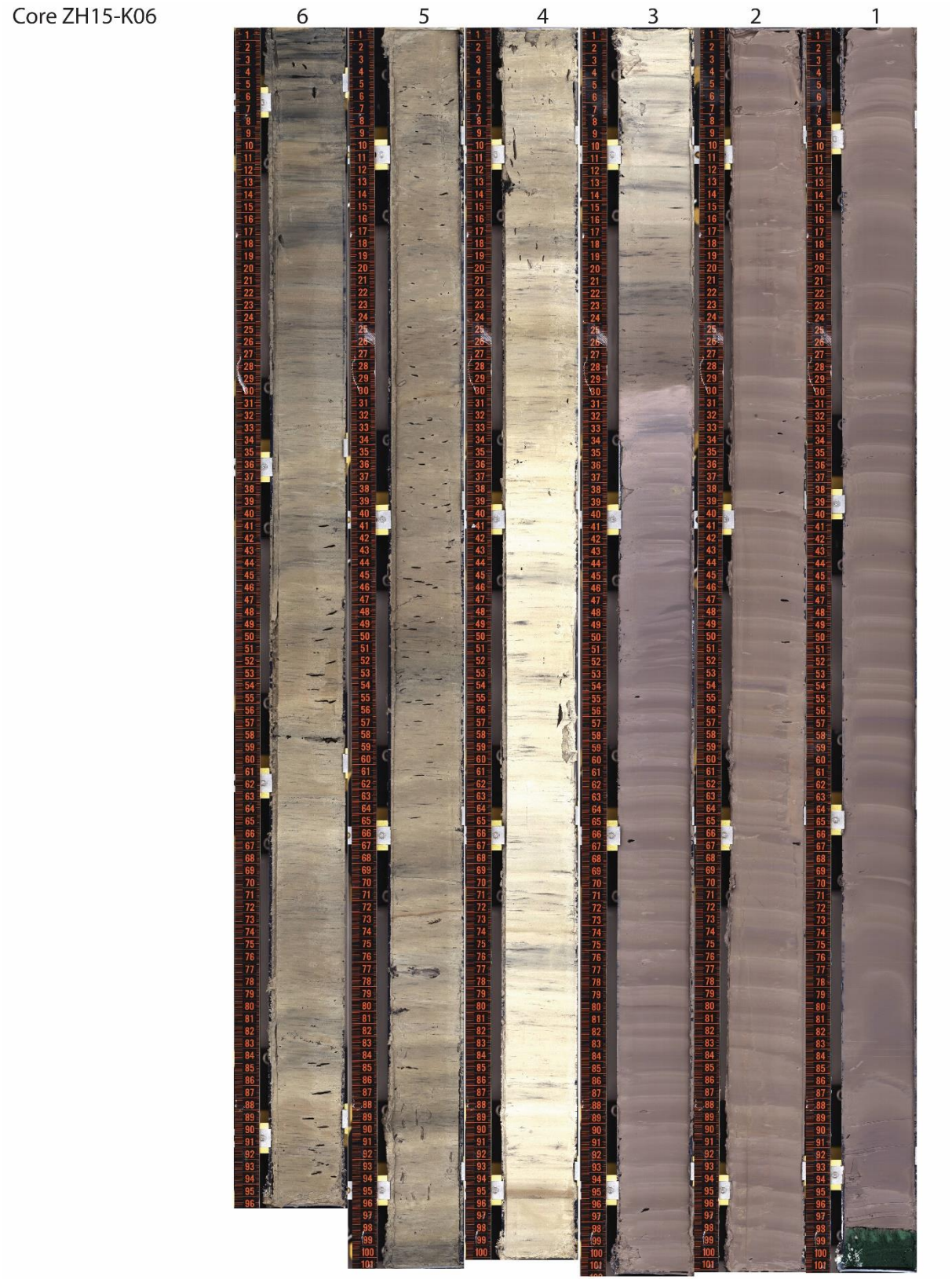


Figure A. 10 Core ZH15-K06

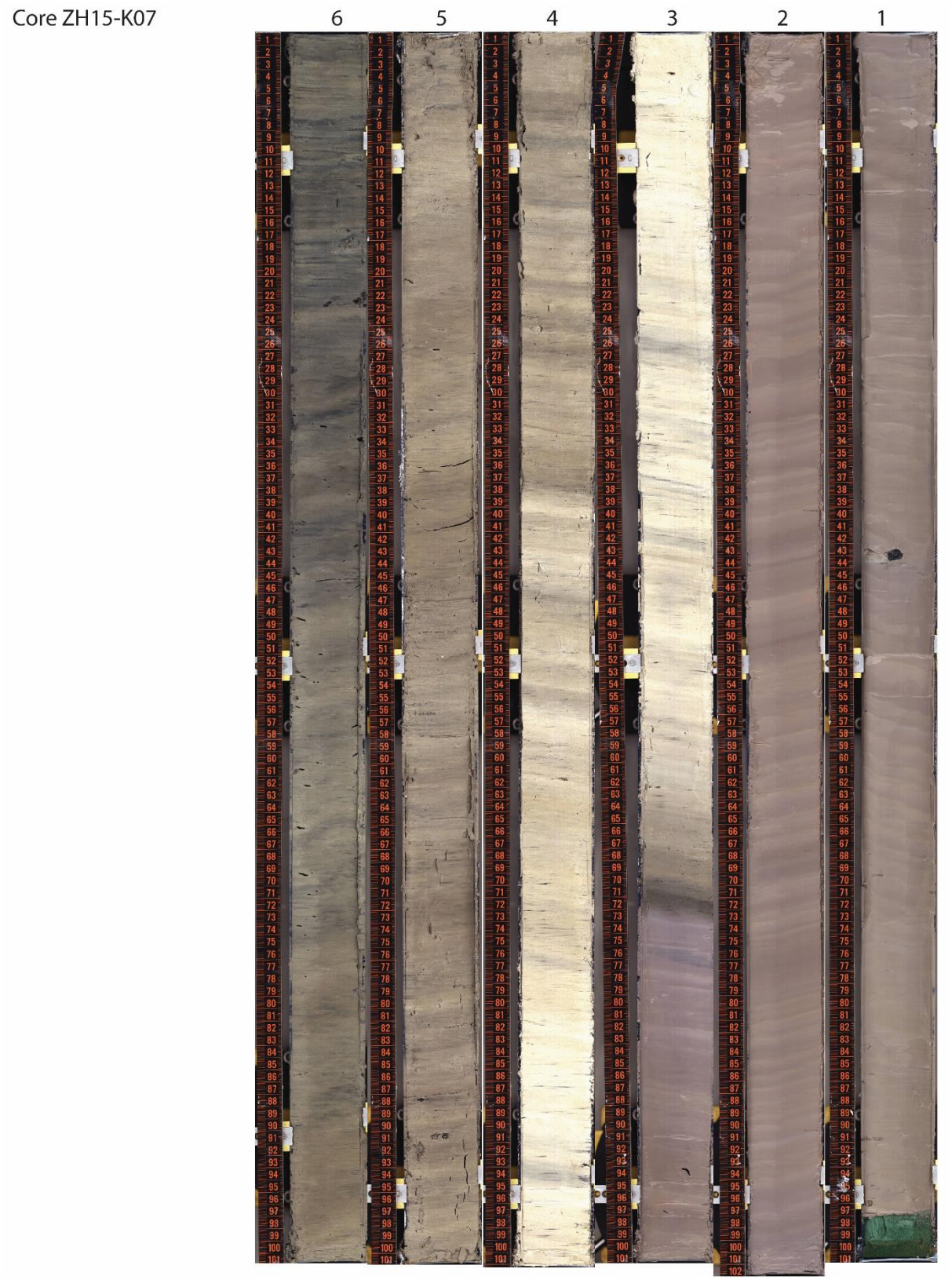


Figure A. 11 Core ZH15-K07



Figure A. 12 Core ZH15-K13

Short gravity cores

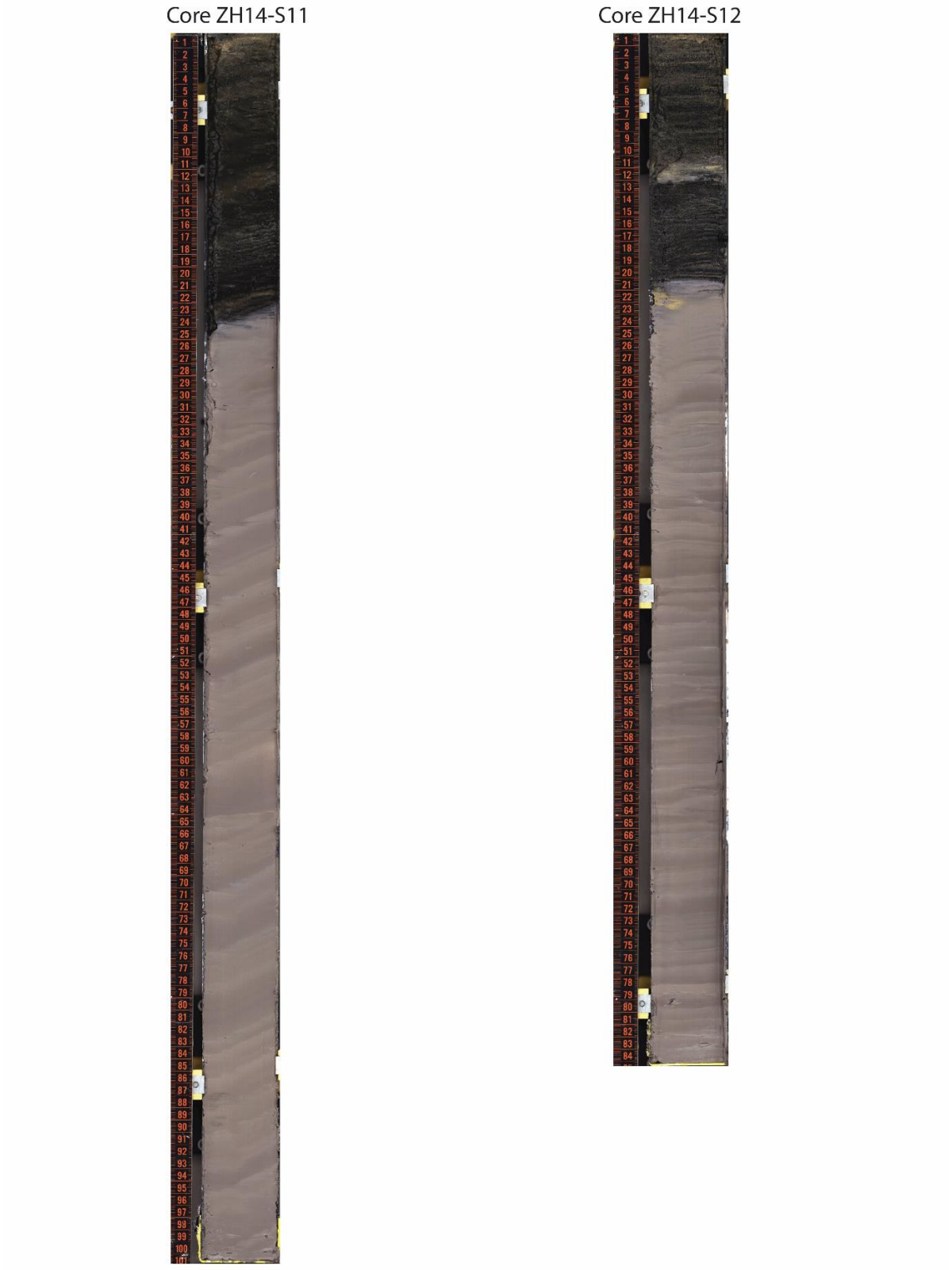


Figure A. 13 Core ZH14-S11 and S12



Figure A. 14 Core ZH14-S15 and S16



Figure A. 15 Core ZH15-S01 and S02



Figure A. 16 Core ZH15-S03 and S04



Figure A. 17 Core ZH15-S05 and S06

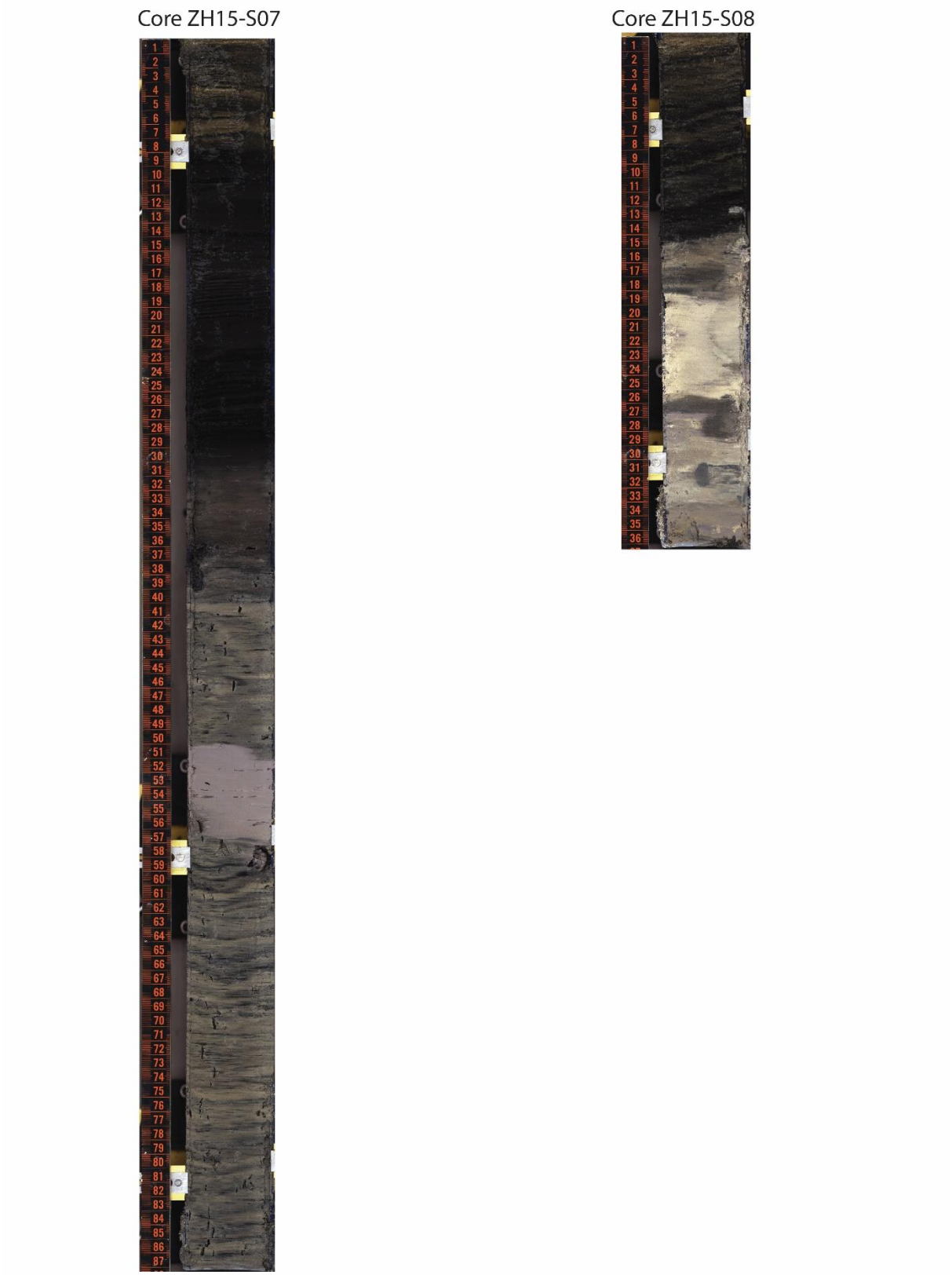


Figure A. 18 Core ZH15-S07 and S08



Figure A. 19 Core ZH15-S09, S10(I), and S10(II)



Figure A. 20 Core ZH15-S11 and S12



Figure A. 21 Core ZH15-S13 and S14



Figure A. 22 Core ZH15-S15, S16, and S17



Figure A. 23 Core ZH16-S01, S02, and S03

Appendix B

Supplementary material chapter 2

B1 Uncertainty map of the bathymetric data

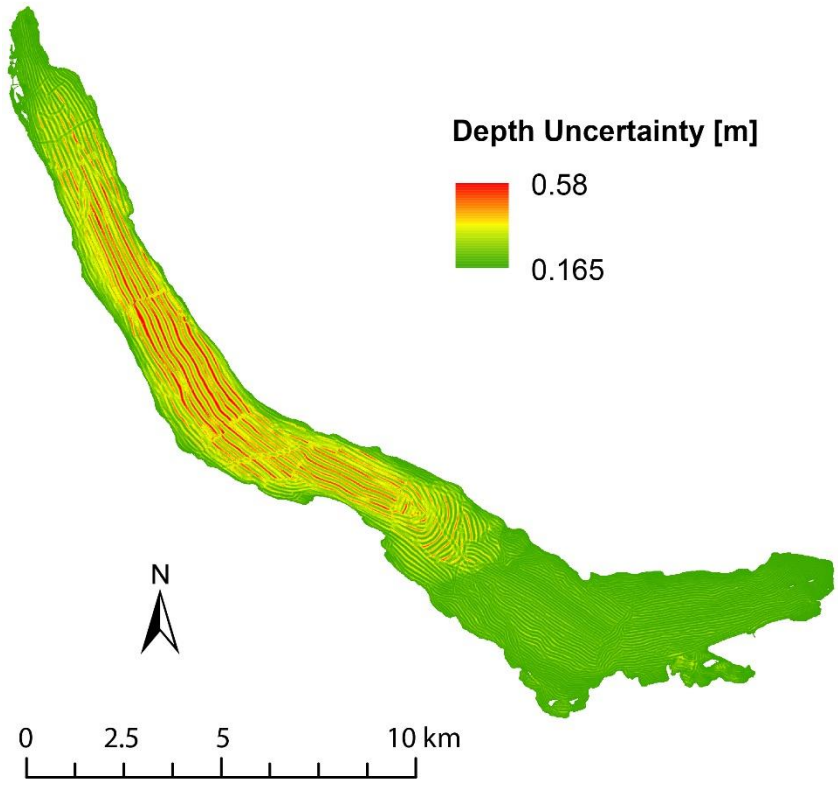


Figure B. 1 Depth uncertainties calculated with Caris HiPS/SIPS

Appendix C

Supplementary material chapter 3

C1 Metadata of sediment cores and in-situ CPT

Table C. 1 Core names, Swiss Coordinates (CH1903/LV03), slope gradient and depth below lake level

Corename	x-coordinate	y-coordinate	slope Gradient [°]	Depth below lake level [m]
ZH15-S01	237911	686442	18.6	72
ZH15-S02	237955	686569	8.4	117
ZH15-S03	237472	686473	10.8	56
ZH15-S04	237471	686568	11.3	65
ZH15-S05	237558	686708	17.3	99
ZH15-S06	237431	686807	12.9	108
ZH15-S07	237297	686760	5.7	99
ZH15-S08	236912	686736	12.6	70
ZH15-S09	236903	686809	14.7	82
ZH15-S10 (I)	236930	686887	17.0	99
ZH15-S10 (II)	236936	686885	18.6	100
ZH15-S11	237000	686998	2.6	118
ZH15-S12	236807	686972	20.5	103
ZH15-S13	236849	687073	2.1	118
ZH15-S14	237334	686879	19.6	112
ZH15-S15	237411	686695	16.4	88
ZH15-S16	237764	686604	19.9	94
ZH15-S17	237155	686892	5.5	107
ZH16-S01	237913	686521	22.6	97
ZH16-S02	237934	686517	21.4	100
ZH16-S03	237970	686509	23.7	105
ZH14-S11	236737	686857	12.9	66
ZH14-S12	236763	686893	20.2	82
ZH14-S15	237167	686757	10.9	94
ZH14-S16	237262	686919	18.2	114
ZH15-K01	237848	686300	8.1	40
ZH15-K03	237902	686441	19.5	69
ZH15-K04	237067	686721	10.1	74
ZH15-K05	237101	686809	10.6	97
ZH15-K06	236639	687233	14.8	111
ZH15-K07	236454	687019	12.0	57
ZH15-K13	237422	686644	10.7	76

Table C. 2 CPT locations, water depth, slope gradient and CPT Profile length

CPT name	x-coordinate	y-coordinate	water depth [m]	slope gradient [°]	profile length [cm]
CPT01	686658	237451	78	14.8	210
CPT02	686648	237425	76.9	13.2	239
CPT03	686706	237563	98.7	17.6	257
CPT04	686883	236940	100	19.1	248
CPT05	686766	236662	23.2	17.9	307
CPT06	687077	236856	117.7	1.9	212
CPT07	686968	236817	103.8	21.2	n.a.*
CPT08	686894	236791	84.8	10.4	376
CPT09	686852	236755	68.1	17.4	291
CPT10	687000	237002	118.2	2.6	260
CPT11	686814	236902	82.8	14.9	262
CPT12	686732	236913	69.1	13.5	n.a.*
CPT13	686728	236911	67.2	13.1	n.a.*
CPT14	686807	237101	96.6	10.8	605
CPT15	686716	237065	72.9	10.3	605
CPT16	686583	237618	65.1	23.7	n.a.*
CPT16-take2	686546	237696	65.6	24.5	n.a.*
CPT17	686432	237615	42.1	7.1	408
CPT18	686300	237853	40	7.9	143
CPT19	686441	237898	68.6	19.6	540
CPT31	687232	236638	111	14.2	499
CPT32	687021	236459	57.5	12.5	363
CPT37	686620	237939	121.1	5.6	n.a.*
CPT38	686562	237961	114.5	11.3	n.a.*
CPT39	686530	237945	107.1	21.7	n.a.*
CPT40	686511	237472	60.8	8.5	136
CPT41	686837	237383	106.8	13.2	336
CPT42	686480	237480	56.7	6.8	484
CPT43	686563	237489	62.1	9.7	418
CPT44	686808	237438	109.3	15.4	433
CPT45	686883	237345	116.1	19.5	327
CPT46	686929	237257	115.4	17.9	353
CPT47	686756	237296	98.2	6.1	244
CPT48	686617	237379	80.2	5.5	342
CPT49	686582	237313	64.1	8.5	413
CPT50	686893	237148	106.8	4.8	399
CPT51	686708	237226	89.4	12.2	445
CPT52	686613	237150	60.4	9.6	n.a.
CPT53	686684	236781	20.9	18.9	n.a.

*for CPT with Profile length ‘n.a.’ a disturbance during testing happened; the profiles are not to be used. Blue shaded profiles are representing CPT profiles used for the construction of the sediment-mechanical stratigraphy.

C2 Sedimentation model

Horizon overlap ages (Strasser & Anselmetti, 2008):
~2210 cal. yr. BP: 2157-2267 cal. yr. BP
~640 cal. yr. BP: 590-699 cal. yr. BP
B.P.=1950 → for 2014,2015,2016 ages, add 64,65,66 yrs
To account for the age uncertainty, the thickness (d) of the drape on the glide plane for each core was considered in the multivariate linear regression analysis with both the minimum and maximum horizon overlap age (e.g. core ZH15-K13 shows a sediment drape on the glide plane i) since 2157 cal. yr. B.P (B.P = until 1950) and ii) since 2267 cal. yr. B.P.) To have the same weighting, the cores from the 1918 A.D, were also accounted twice in the regression analysis (both with the exact known age).

Table C. 3 Thickness (d) of sedimentary drape on the glide plane, slope gradient, water depth and age of glide plane

Core	d drape on glide plane [cm]	slope gradient [°]	Water depth [m]	Age [years since core recovery]
ZH15-K13	135	10.7	76	2222
ZH15-S05	112	17.3	99	2222
ZH15-S14	125	19.6	112	2222
ZH14-S16	90	18.2	114	2221
ZH15-K13	135	10.7	76	2332
ZH15-S05	112	17.3	99	2332
ZH15-S14	125	19.6	112	2332
ZH14-S16	90	18.2	114	2331
ZH16-S01	70	22.6	97	656
ZH16-S02	65	21.4	100	656
ZH16-S01	70	22.6	97	765
ZH16-S02	65	21.4	100	765
ZH14-S11	23	12.9	66	96
ZH14-S12	20	20.2	82	96
ZH15-S09	12	14.7	82	97
ZH15-S10(I)	10	17	99	98
ZH15-S10(II)	7	18.6	100	97
ZH15-S12	26	20.5	103	97
ZH14-S11	23	12.9	66	96
ZH14-S12	20	20.2	82	96
ZH15-S09	12	14.7	82	97
ZH15-S10(I)	10	17	99	98
ZH15-S10(II)	7	18.6	100	97
ZH15-S12	26	20.5	103	97
Not included in model because of sediment-redistribution, no continuous sedimentary drape on glide plane:				
ZH15-S08		12.6	70	97
ZH15-S11		2.6	118	97
ZH15-S13		2.1	118	97

Table C. 4 SPSS Output for sedimentation model

Variables Entered/Removed[a]

Model	Variables Entered	Variables Removed	Method
1	age, wd[b]	.	Enter

a. Dependent Variable: drape

b. All requested variables entered.

Model Summary

Model	R	R Square	Adjusted R Square	Std. Error of the Estimate
1	.955[a]	.913	.904	14.48816

a. Predictors: (Constant), age, wd

ANOVA[a]

Model		Sum of Squares	df	Mean Square	F	Sig.
1	Regression	46121.790	2	23060.895	109.863	.000[b]
	Residual	4408.043	21	209.907		
	Total	50529.833	23			

a. Dependent Variable: drape

b. Predictors: (Constant), age, wd

Coefficients[a]

Model		Unstandardized Coefficients		Standardized Coefficients	t	Sig.
		B	Std. Error	Beta		
1	(Constant)	44.476	20.715		2.147	.044
	wd	-.310	.227	-.094	-1.367	.186
	age	.046	.003	.985	14.283	.000

a. Dependent Variable: drape

C3 Sediment-mechanical stratigraphy

Table C. 5 Thicknesses (d) of the lithologic units of the Kullenberg cores used to construct the sediment-mechanical stratigraphy

Corename	d unit 3b [cm]	d unit 3a [cm]	d unit 2 [cm]	d unit 1 down to clasts [cm]
ZH15-K01	112	68	44	290
ZH15-K03	249	121	-	130
ZH15-K04	300	140	49	11
ZH15-K05	250	130	49	176
ZH15-K06	190	110	28	171
ZH15-K07	240	120	14	224

Table C. 6 Mean coefficients of variation for ρ_{bulk} and s_u per sediment-mechanical unit

	SMU1	SMU2	SMU3	SMU4
Mean unit CV ρ_{bulk}	0.03	0.04	0.03	0.02
Mean unit CV s_u CPT	0.14	0.16	0.11	0.51

C4 Thicknesses of stratigraphic units converted from two-way-traveltime (TWT)

Table C. 7 TWT and converted thicknesses of the stratigraphic units for model locations on transect U. Thicknesses in italics are interpolated from neighbouring sediment cores.

TWT thickness [s]	U1	U2	U3	U4	U5
SMU4	0.00547	0.00381	0.00465	0.00495	0.00433
SMU3 + SMU2	0.00227	0.00145	0.00145	0.00196	0.00165
TWT thickness in cm [1500 m/s sonic speed]					
SMU4	410	286	349	371	325
SMU3+SMU2	170	109	109	147	124
SMU3	156	95	95	119	96
SMU2	*14*	*14*	*14*	28	28
SMU1	*224*	*224*	*224*	*171*	*171*

Table C. 8 TWT and converted thicknesses of the stratigraphic units for model locations on transect V. Thicknesses in italics are interpolated from neighbouring sediment cores.

TWT thickness [s]	**V1**	**V2**	**V3**	**V4**	**V5**	**V6**	**V7**	**V8**
SMU4	0.00430	0.00431	0.00442	0.00399	0.00343	0.00251	0.00283	0.00267
SMU3 + SMU2	0.00403	0.00303	0.00283	0.00259	0.00211	0.00252	0.00239	0.00443
Thickness in cm [1500 m/s sonic speed]								
SMU4	323	323	331	299	257	188	212	200
SMU3+SMU2	302	227	212	194	158	189	179	332
SMU3	257	182	167	149	113	144	134	287
SMU2	*45*	*45*	*45*	*45*	*45*	*45*	*45*	*45*
SMU1	*50*	*50*	*50*	*175*	*175*	*175*	*175*	*175*

Table C. 9 TWT and converted thicknesses of the stratigraphic units for model locations on transect U. Thicknesses in italics are interpolated from neighbouring sediment cores.

TWT thickness [s]	**W1**	**W2**	**W3**	**W4**	**W5**	**W6**
SMU4	0.00442	0.00443	0.00323	0.00299	0.00411	0.00380
SMU3 + SMU2	0.00156	0.00182	0.00151	0.00189	0.00162	0.00205
Thickness in cm [1500 m/s sonic speed]						
SMU4	332	332	242	224	308	285
SMU3+SMU2	117	137	113	142	122	154
SMU3	77	97	73	102	81	114
SMU2	*40*	*40*	40	40	40	40
SMU1	*290*	*290*	*290*	*130*	*130*	*130*

C5 Slope stability analysis

Table C. 10 Model locations, swiss coordinates (CH 1903/LV03), corresponding slope gradient, depth below lake level and thickness (d) of the sediment-mechanical units.

Location	**x-coordinate**	**y-coordinate**	**Water depth [m]**	**Slope gradient [°]**	**d SMU4 [cm]**	**d SMU3 [cm]**	**d SMU2 [cm]**	**d SMU1 [cm]**
U1	686927	236477	47	4.2	410	156	14	224
U2	686972	236502	53	11.2	286	95	14	224
U3	687014	236528	66	18	349	95	14	224

U4	687088	236570	91	10.1	371	119	28	171
U5	687168	236619	104	5.2	325	96	28	171
V1	686699	237056	70	9.1	322	257	45	50
V2	686722	237065	74	10	323	182	45	50
V3	686735	237072	77	10	331	167	45	50
V4	686755	237083	81	18.2	299	149	45	175
V5	686774	237095	88	19.9	257	113	45	175
V6	686790	237104	94	12	188	144	45	175
V7	686803	237113	96	9.8	212	134	45	175
V8	686818	237122	99	8.3	200	287	45	175
W1	686372	237678	39	8.1	332	77	40	290
W2	686406	237694	45	5.2	332	97	40	290
W3	686465	237711	51	6	242	73	40	290
W4	686531	237740	69	20.5	224	102	40	130
W5	686583	237760	87	18.3	308	81	40	130
W6	686626	237779	105	20.4	285	114	40	130

Table C. 11 Thicknesses to substract from the present-day sediment drape (calculated with the sedimentation model)

Location	**Thickness to substract from the present-day sediment drape [cm]**	
	~2210 cal. yr. BP. Scenario	*~640 cal. yr. BP. Scenario*
U1	135	62
U2	133	61
U3	129	56
U4	121	49
U5	117	45
V1	127	55
V2	126	54
V3	125	53
V4	124	52
V5	122	50
V6	120	48
V7	119	47
V8	118	46
W1	137	65
W2	135	63
W3	133	61
W4	128	56
W5	122	50
W6	117	44

Table C. 12 Minimum deterministic FS at the model locations

Location	**minimum deterministic FS in the FS-depth profile**		
	~2210 cal. yr. BP. scenario	*~640 cal. yr. BP. scenario*	*Present-day scenario*
U1	3.46	3.16	2.94
U2	1.79	1.62	1.48
U3	1.06	0.95	0.88
U4	1.74	1.56	1.46
U5	3.80	3.37	3.15
V1	1.73	1.55	1.43
V2	1.90	1.66	1.52
V3	1.95	1.70	1.55
V4	1.03	0.92	0.86
V5	1.11	0.98	0.91
V6	1.82	1.60	1.48
V7	2.17	1.92	1.78
V8	2.03	1.83	1.73
W1	1.98	1.82	1.70
W2	2.98	2.76	2.56
W3	2.94	2.69	2.51
W4	1.36	1.16	1.05
W5	1.31	1.15	1.05
W6	1.13	1.00	0.93

Table C. 13 Max PoF at the model locations

Location	**maximum PoF in the PoF-depth profile**		
	~2210 cal. yr. BP. scenario	*~640 cal. yr. BP. scenario*	*Present-day scenario*
U1	0.02	0.04	0.06
U2	0.05	0.13	0.18
U3	0.38	0.63	0.82
U4	0.14	0.22	0.27
U5	0.01	0.04	0.06
V1	0.06	0.12	0.17
V2	0.08	0.15	0.20
V3	0.07	0.15	0.21
V4	0.43	0.66	0.83
V5	0.33	0.59	0.75
V6	0.01	0.04	0.09
V7	0.01	0.05	0.08
V8	0.01	0.02	0.05

W1	0.04	0.10	0.15
W2	0.01	0.04	0.07
W3	0.00	0.02	0.04
W4	0.06	0.23	0.42
W5	0.21	0.34	0.45
W6	0.28	0.55	0.73

C6 Slope-stability assessment with SLIDE

To construct the slope model in SLIDE, the thicknesses of the sediment mechanical units at the model locations were imported into ArcGIS and interpolated along a transect. The resulting profile of each mechanical unit top was then imported into SLIDE as material boundary. As SLIDE can only handle constant values for ρ_{bulk} for each lithologic units and gradients for s_u, mean values and gradients for geotechnical values were calculated from the sediment-mechanical stratigraphy stretched to the location of core ZH15-K04 (Fig. C.1).

#	Material Name	Property	Distribution	Mean	Std. Dev.	Rel. Min	Rel. Max
1	SMU4	Cohesion	Lognormal	1	0.82	0	2.46
2	SMU4	Unit Weight	Lognormal	12.76	0.25	0.75	0.75
3	SMU4	Cohesion Change	Lognormal	1.16	0.82	0	2.46
4	SMU2	Unit Weight	Lognormal	13.9989	0.59	1.77	1.77
5	SMU2	Cohesion	Lognormal	6.98	1.11	3.33	3.33
6	SMU1	Unit Weight	Lognormal	16.3435	0.47	1.41	1.41
7	SMU1	Cohesion	Lognormal	5.21	1.2142	3.6426	3.6426
8	SMU1	Cohesion Change	Lognormal	7.71	1.2142	3.6426	3.6426
9	SMU3-upper	Cohesion	Lognormal	4.42	0.5863	1.7589	1.7589
10	SMU3-upper	Unit Weight	Lognormal	13.655	0.43733	1.31199	1.31199
11	SMU3-upper	Cohesion Change	Lognormal	1.09	0.5863	0	1.7589
12	SMU3-lower	Unit Weight	Lognormal	14.597	0.3104	0.9312	0.9312
13	SMU3-lower	Cohesion	Lognormal	5.15	0.5119	1.5357	1.5357

Figure C. 1 Geotechnical material statistics for probabilistic analysis in SLIDE

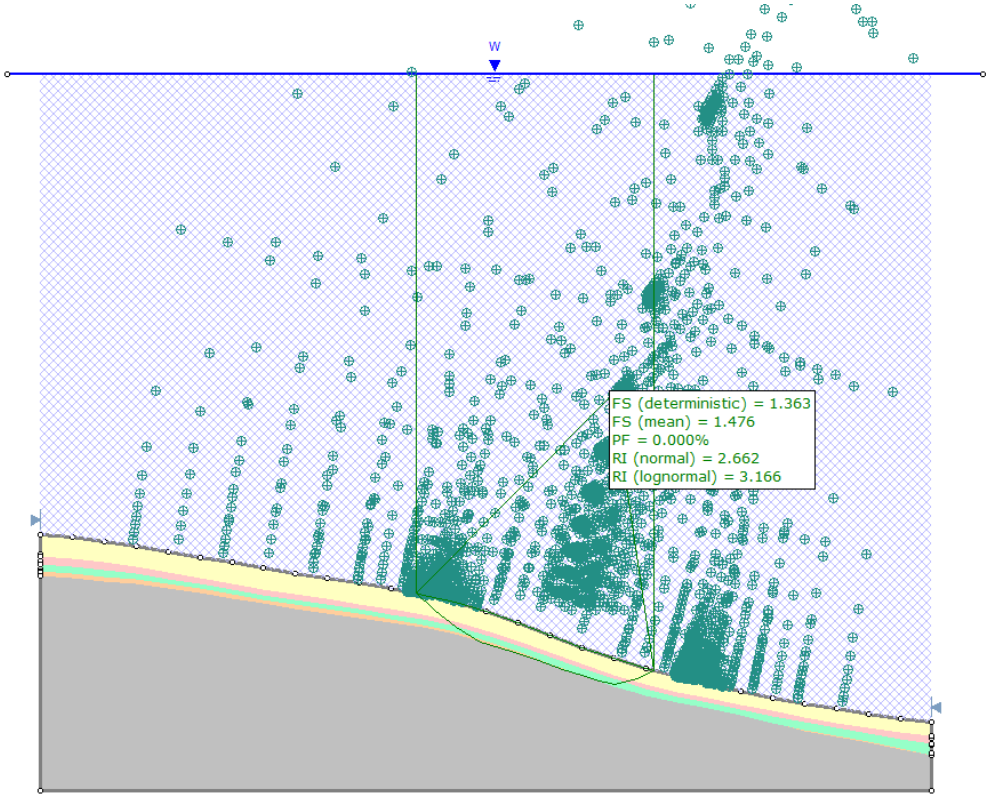


Figure C. 2 Global minimum FS Surface with deterministic and mean probabilistic FS

Appendix D

Supplementary material chapter 4

D1 Sedimentation model

Two seismic profiles showing varying water depths and slope angles, but few terraces (which disturb the sedimentation model due to temporary deposition) were selected (ZH16-417 and Z20-5q; Figs. D.1 and D.2). The thickness of SMU4 and the combined thickness of SMU2 and SMU3 were sampled at a regular distance of ~30 m. The thickness of SMU3 was calculated by subtracting a constant thickness of SMU2 = 40 cm (estimated from sediment cores). The sedimentation rate [cm/yr] per mechanical unit was then calculated by known ages from Strasser and Anselmetti (2008; ~7000 yr for SMU4 and ~5000 yr for SMU3). Then, a linear regression was done to calculate the sedimentation rate as a function of the water depth and slope gradient:

$$sr(i)[cm/yr] = a(i)\,[cm/yr] + b^{*}\,wd(i)\,[m] - c^{*}\alpha\,(i)\,[°]$$

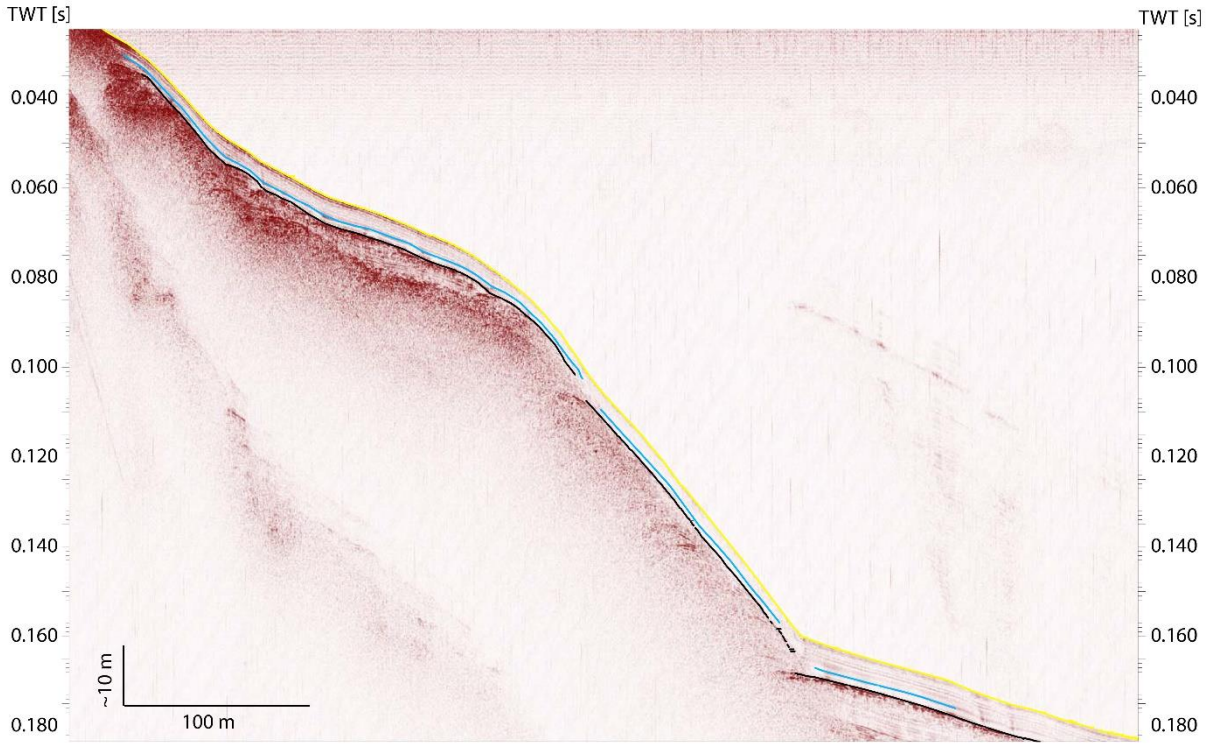


Figure D. 1 3.5 kHz Pinger seismic reflection profile ZH16-417 with interpreted sediment-mechanical unit (SMU) boundaries. Yellow horizon: lake bottom. Black and blue horizons: strong reflection between SMU1 and 2 as well as SMU3 and 4 respectively. Details see Strupler et al. 2017.

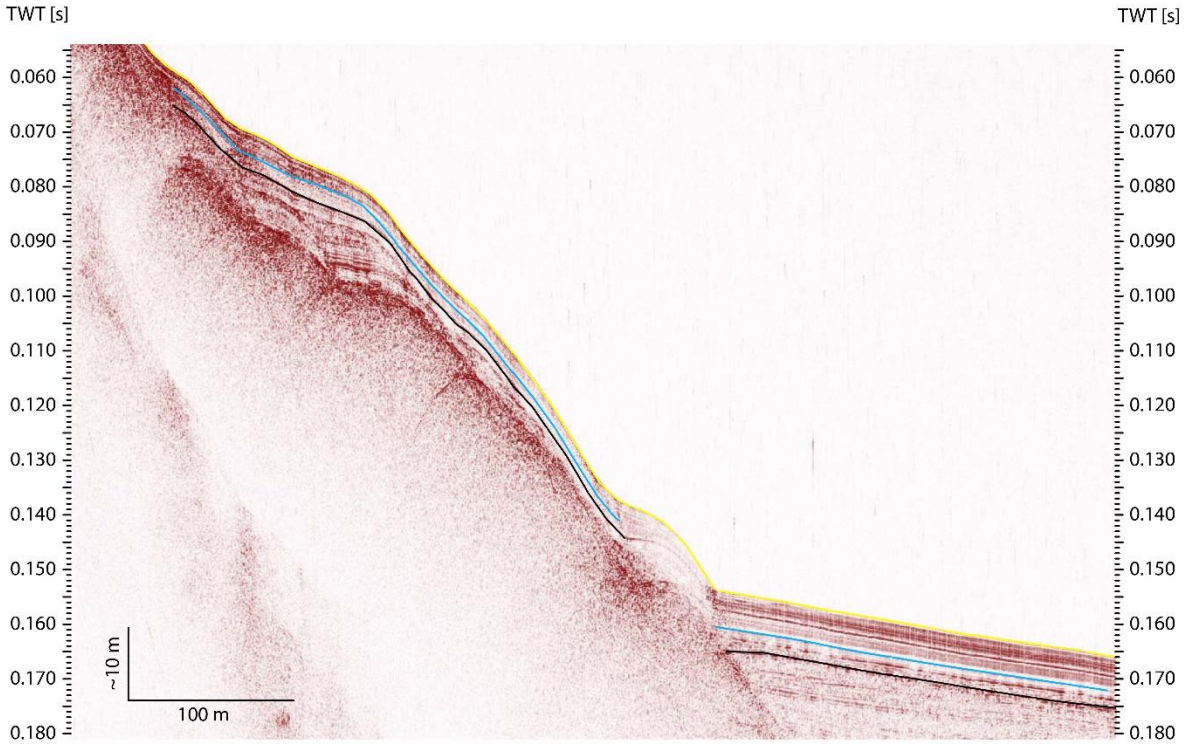


Figure D. 2 3.5 kHz Pinger seismic reflection profile Z20-5q (Strasser and Anselmetti 2008) with interpreted sediment-mechanical unit (SMU) boundaries. Yellow horizon: lake bottom. Black and blue horizons: strong reflection between SMU1 and 2 as well as SMU3 and 4 respectively. Details see Strupler et al. 2017.

The quality of the sedimentation model was assessed with data from sediment cores (Table D.1; Strasser and Anselmetti 2008; Strupler et al. 2017).

Table D. 1 Comparison of SMU thicknesses derived from sediment cores with SMU-thicknesses derived from sedimentation model.=Cores from Strasser & Anselmetti, 2008, which have no disturbance in lithologic units LU3c*

Sediment core	Swiss coordinates (LV03)		slope gradient [°]	water depth [m]	Thickness SMU4 [cm]			difference calculated from measured in %	Thickness SMU3 [cm]		difference calculated from measured in %
					calculated	measured LU3b	incl.~ 50 cm LU3c (lost by coring)		calculated	measured	
ZH15-K01	686300	237848	8.1	40	304	112	162	46.71	99	68	31.53
ZH15-K03	686441	237902	19.5	69	235	249	299	-27.02	77	121	-56.91
ZH15-K04	686721	237067	10.1	74	327	300	350	-6.91	110	140	-26.75
ZH15-K05	686809	237101	10.6	97	351	250	300	14.53	121	130	-7.64
ZH15-K06	687233	236639	14.8	111	330	190	240	27.22	114	110	3.78
ZH15-K07	687019	236454	12	57	289	240	290	-0.27	95	120	-25.79
ZHK04-4*	693095	233887	1.23	108	450	375	375	16.68	157	100	36.36
ZHK04-5*	699687	230486	0.18	22	354	325	325	8.27	116	75	35.26
ZHK04-6*	693969	233029	0.58	64	402	400	400	0.52	136	80	41.34
			mean difference measured/calculated (+/-)					8.86			3.47

Basin-wide thicknesses of SMU3 and SMU4 vary between 0 and 1.8m cm and 0 and 4.8 m, respectively (Figure D.3).

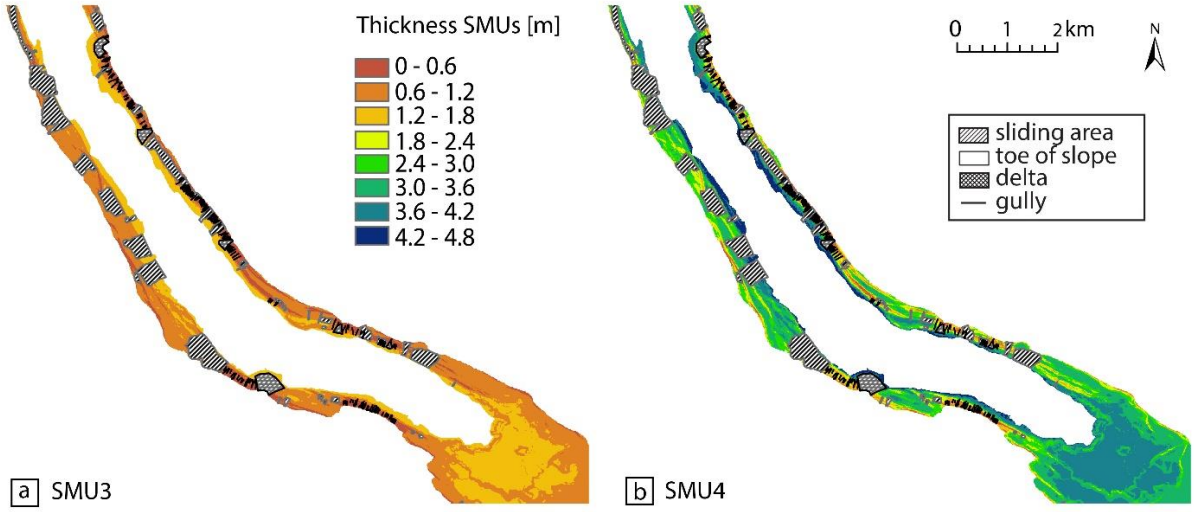


Figure D. 3 basin-wide thicknesses of SMU3 (a) and SMU4 (b) for the present-day scenario as function of water depth and slope gradient, calculated with the sedimentation model.

Up to ~1.5 m sediment was deposited on the Oberrieden slopes since the ~2210 cal. yr. B.P. event (Fig. D.4).

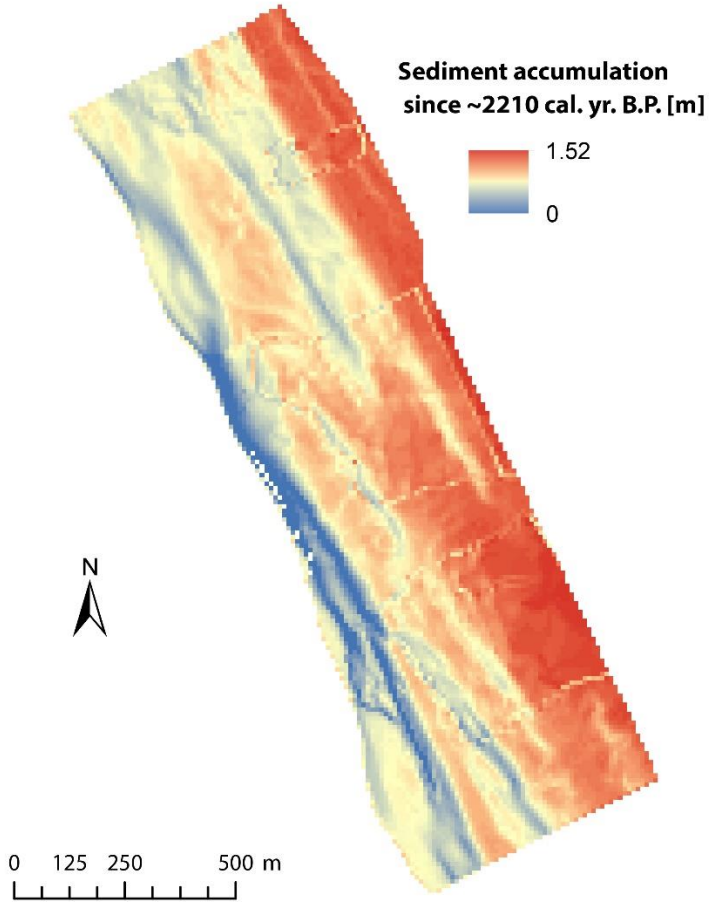


Figure D. 4 Sediment accumulation since the occurrence of the ~2210 cal. yr. B.P. Oberrieden slide

D2 Geotechnial data for core ZH15-K09 (Eastern lateral slopes)

The geotechnical data of core ZH15-K09 shows the same characteristics as found in the data used for the sediment-mechanical stratigraphy, calibrated at the Oberrieden study site (see Figs. 4.1 and 4.3 in manuscript).

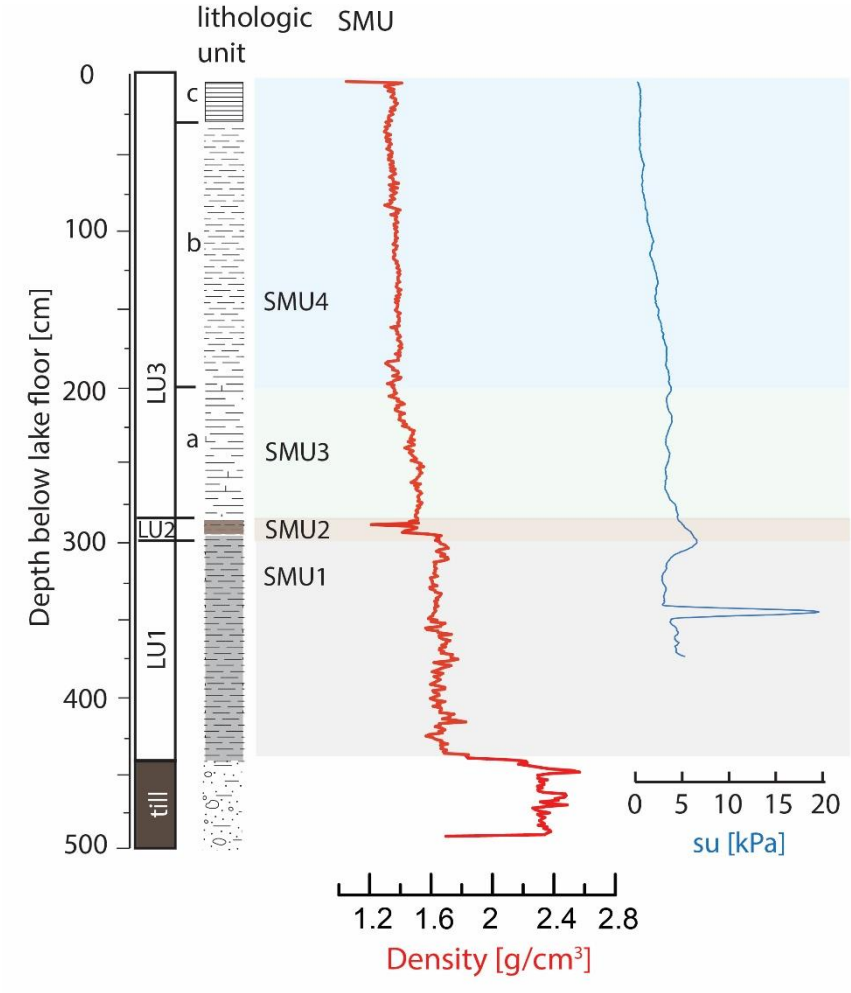


Figure D. 5 Density profile of sediment core ZH15-K09 (location shown in Figure 4.1 in chapter 4 of this thesis) and in situ free fall CPT profile CPT24 (located ~50m west of ZH15-K09)

D3 Depth of maximum PoF maps

A multiplication of the sum of the depth of the maximum PoF_g of all pixels (Figure D.6) with the cell size (10 m) leads to a mobilized slide volume of the ~2210 cal. yr. BP slide in the range between ~583'000 and ~818'000 m^3.

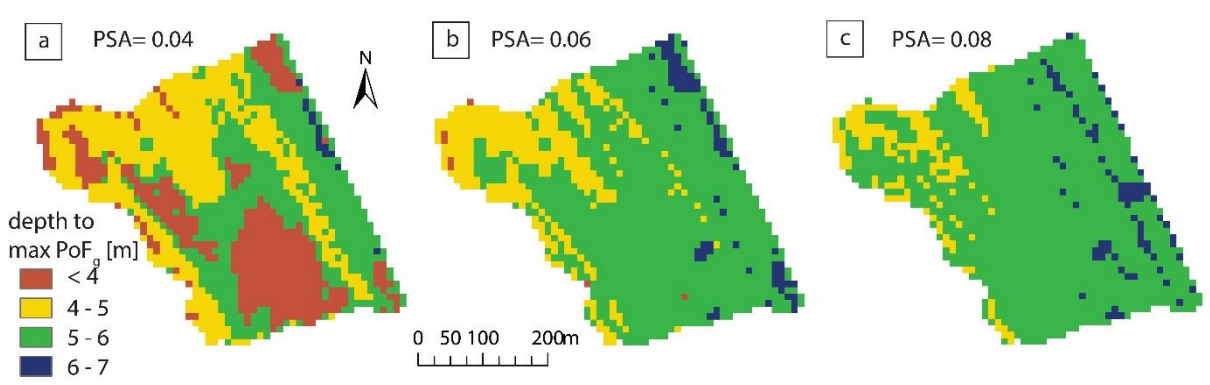


Figure D. 6 Back-analysed depths of the maximum PoF_g for the Oberrieden slide (~2210 cal.yr B.P.) with respect to different pseudostatic accelerations. a: PSA=0.04g, b: PSA=0.06g; c: PSA=0.08g. The sum of the max. PoF_g of all the pixels are 5829, 8039 and 8175 m, for PSA of 0.04, 0.06 and 0.08, respectively.

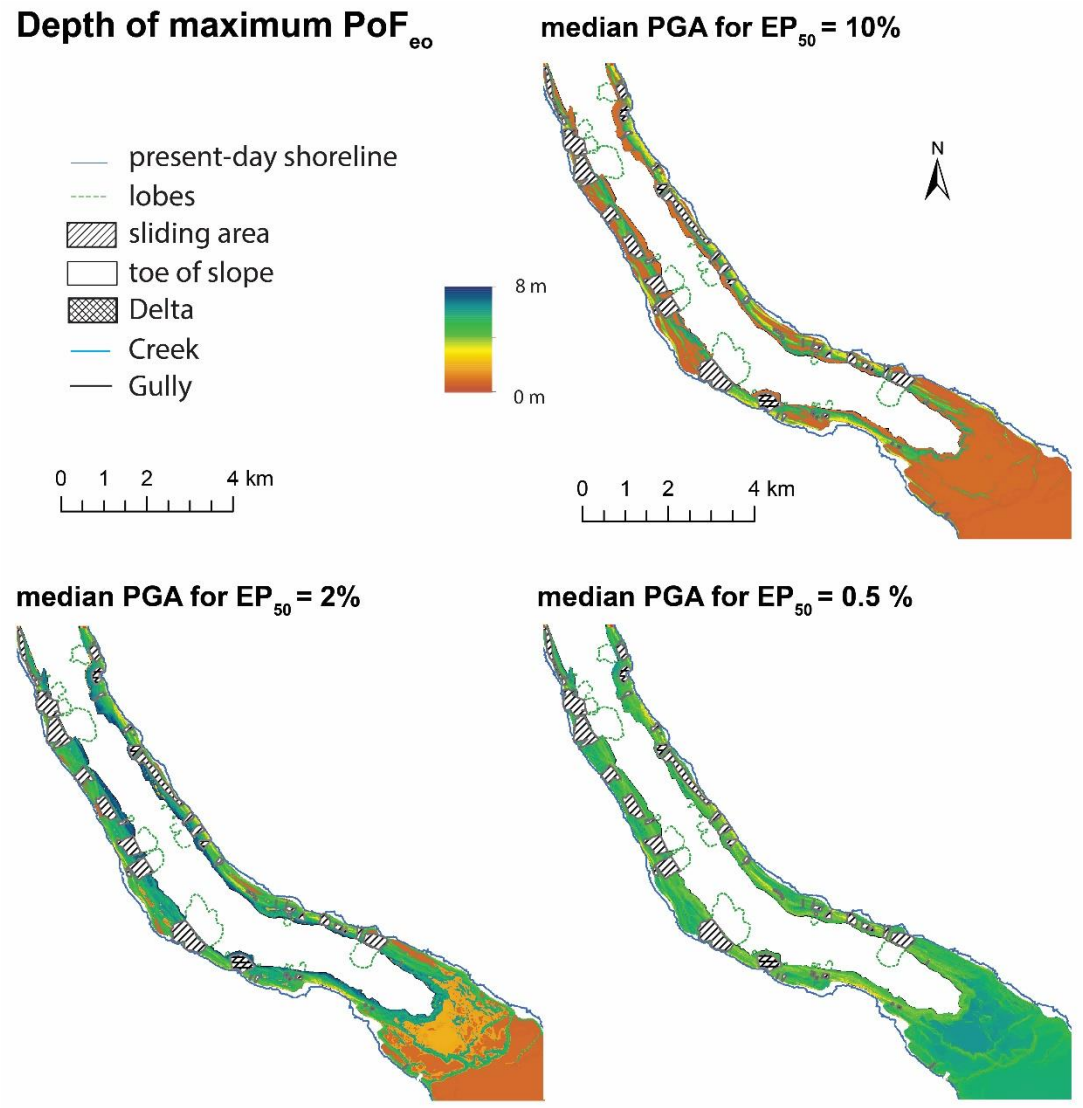


Figure D. 7 Depth of maximum PoF_{eo} for the different PGA expected for EP50 of 10, 2 and 0.5 %.

D4 Mapped most probable slide areas and volumes

The mapped most probable slide scenarios for different EP_{50} are displayed in Fig. D.8. Tables D.2 and D.3 show the individual areas and volumes of the mapped slides in Fig. D.8.

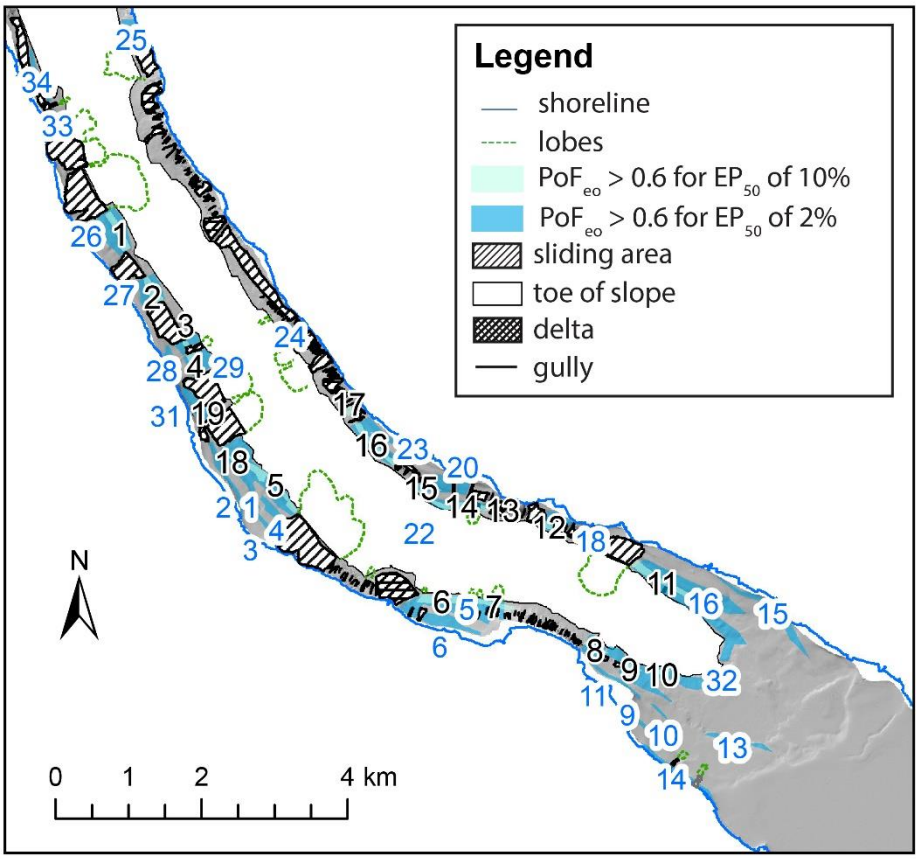


Figure D. 8 Mapped most probable slide scenarios for EP_{50} of 10% (labelled in black) and 2% (labelled in blue).: PoF_{eo} >0.6 for EP_{50} of 0.5% is not mapped for illustrating reasons, as it covers all the slopes.

Table D. 2 Most probable slide scenarios for a median PGA with an EP_{50} of 10% (PoF_{eq} >0.6). Obj. Id Numbers are displayed in Fig. D.8.

Obj.Id. (black labels in ESM Fig. 8)	**Area [m2]**	**Volume [m3]**
1	60841	325117
2	45440	215849
3	5121	23441
4	40025	197408
5	72199	376720
6	65552	310483

minimum translation area [m2]	2672
maximum translation area [m^2]	82028
cumulative translation area [m^2]	608360
minimum slide volume [m^3]	12917
maximum slide volume [m^3]	394499

7	34169	181809
8	14183	67218
9	16770	82584
10	12163	64211
11	82028	394499
12	10055	49600
13	11240	53045
14	47904	258427
15	14686	68477
16	50132	249341
17	10548	51676
18	12631	58800
19	2672	12917

cumulative slide volume [m^3]	3041621
control: average slide height : (total slide volume / slide area)	4.999706
potential landslide volume between Rüschlikon and Thalwil [m^3] Sum of black Obj-Nr. 1 and 2	540966
potential landslide volume between S-Horgen and Au Sum of black Obj-Nr. 6 and 7 [m^3]	492292
potential landslide volume between Herrliberg and Männedorf Sum of black Obj-Nr.11 and 12 [m^3]	444099

Table D. 3 Most probable slide scenarios for a median PGA with an EP50 of 2% (PoF_{eq} >0.6). Obj. Id Numbers are displayed in Fig. D.8.

Obj.Id. (blue labels in ESM Fig. 8)	**Area [m2]**	**Volume [m3]**
1	357871	2150370
2	69571	318320
3	19409	99120
4	41009	236603
5	164818	929338
6	92492	452945
7	91035	509292
8	73660	391023
9	301261	1784450
10	41576	210111
11	37015	155288
12	9440	49884
13	51467	282460
14	54819	238974
15	129047	613455
16	561059	3222660

minimum translation area [m^2]	9440
maximum translation area [m^2]	561059
total translation area [m^2]	2195459
minimum slide volume [m^3]	49884
maximum slide volume [m^3]	3222660
total slide volume [m^3]	12137669
control: average slide height : (total slide volume / slide area)	5.528532
potential landslide volume between rüschlikon and thalwil: Sum of blue Obj. Nr. 26 and 27	1878770

17	16344	83370
18	32438	164611
19	51130	245395
20	99729	522369
21	32930	170431
22	90663	518789
23	189430	927637
24	35706	226900
25	79393	413504
26	207919	1222070
27	117140	656700
28	38743	185404
29	92975	596471
30	38003	237333
31	81967	436327
32	35999	214669
33	33205	184711
34	47630	269108

potential landslide volume between S-Horgen and Au

Sum of blue Obj. Nr. 5, 6 and 7 1891575

potential landslide volume between Herrliberg and Männedorf

Sum of blue Obj. Nr. 15-19 4329491

D5 Sensitivity test of the k*f coefficients

Fig. D.9 shows the effect of using a k (pseudostatic coefficient) *f (soil amplification) = 1 (i.e. PSA=PGA) instead of k*f=0.5, as used in our study. Illustrated are median PGA values expected for EP_{50} of 10, 2 and 0.5 %, respectively.

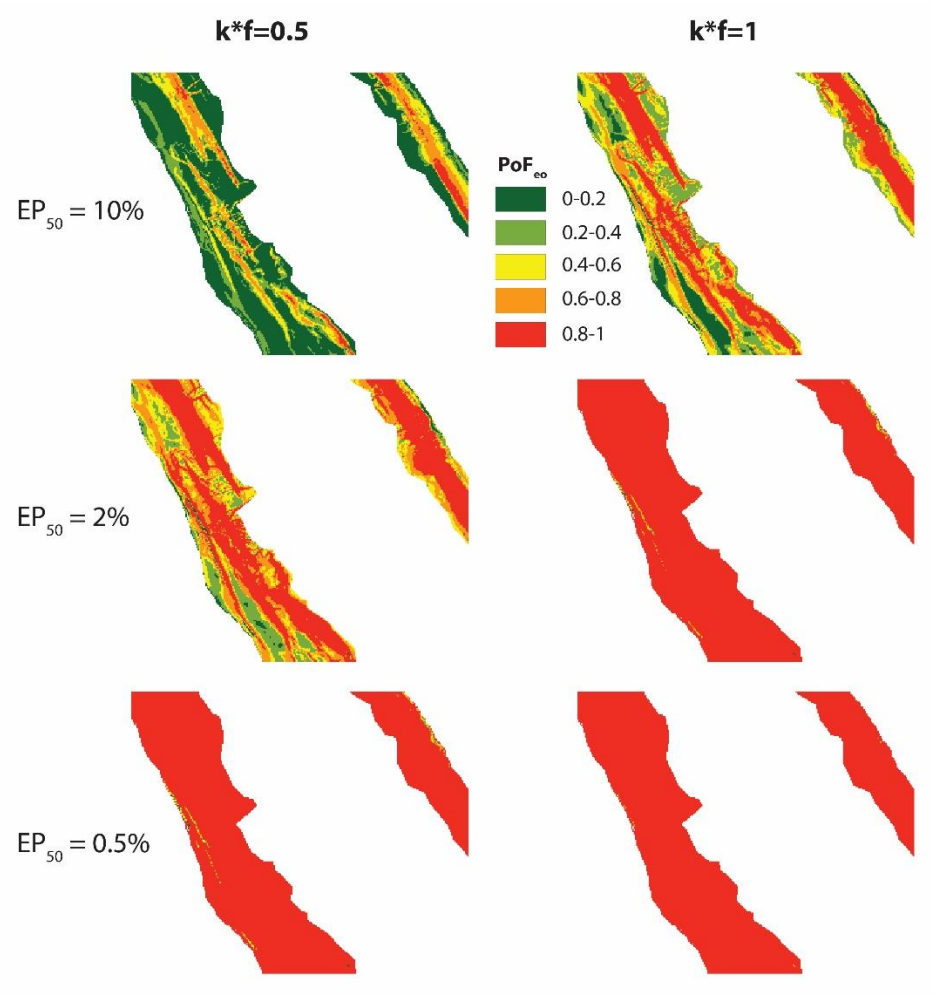


*Figure D. 9 Sensitivity test with k*f =0.5 (left column) and k*f=1.*

D6 Disaggregation plots for identifying predominant earthquake scenarios

As the exceedance probabilities (here: EP_{50}) computed in a PSHA are not associated with any particular earthquake magnitude or source-site distance, but rather represent the combined hazard from different earthquakes occurring at different source-site distances (Kramer 1996), disaggregation plots were constructed. The controlling (i.e. most likely) scenarios - defined by Mw and distance (R) in km, are: M_w = 4.7 and R 12.5 km for a mean return period of 475 years, Mw = 4.7 and R 7.5 km for a mean return period of 2475 years, and Mw = 5.1 and R 7.5 km for a mean return period of 9975 years (Figs. D.10-D.12).

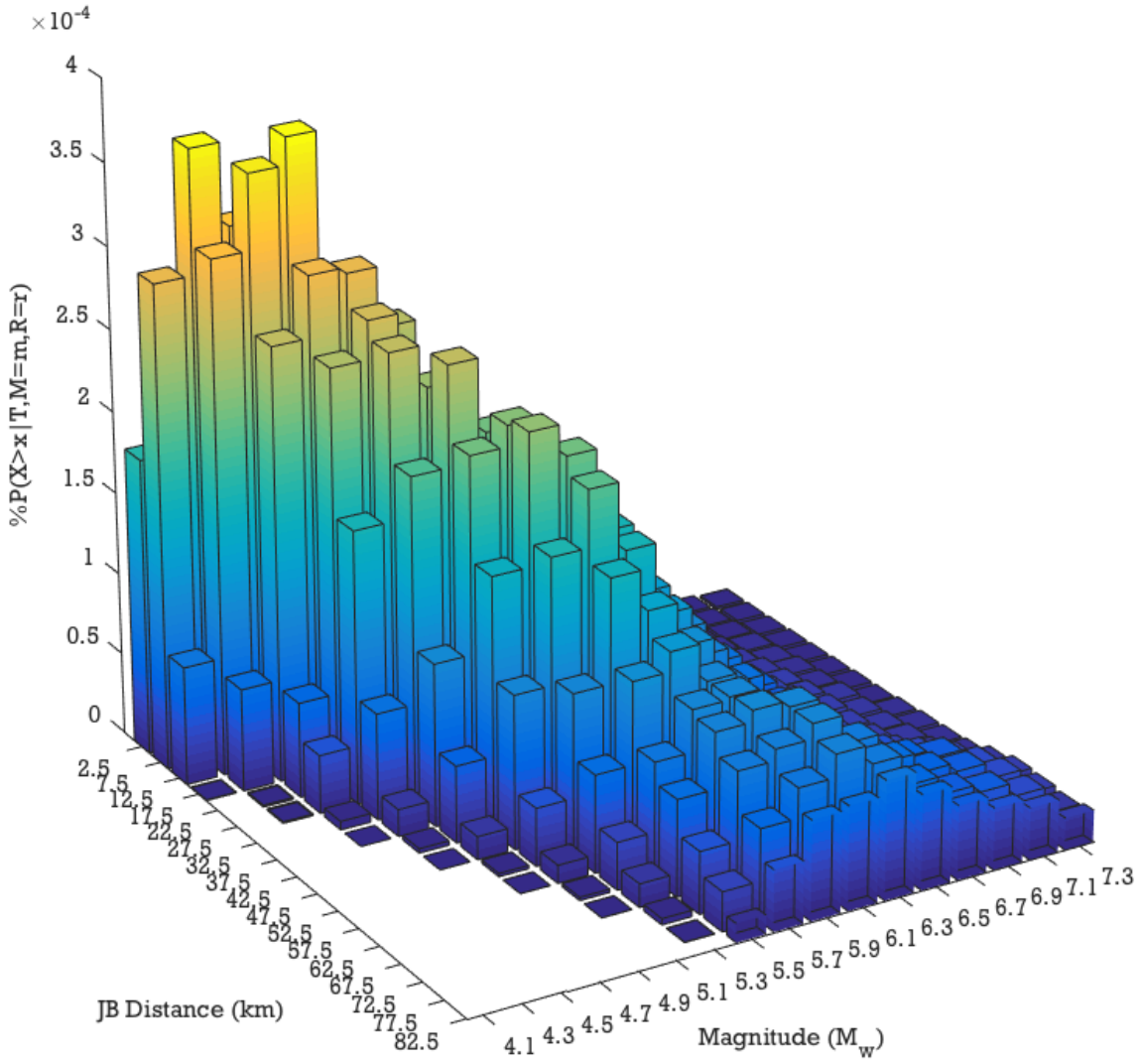


Figure D. 10 Disaggregation plot for PGA with an intensity measure level (IML~0.04g) corresponding to a mean return period (RP) of 475 yrs (i.e. EP50 of 10%). The controlling scenario of the IML is defined by 4.7 Mw and R=12.5km. Data: Wiemer et al. 2016. Location: deepest point ofcentral basin; 687196/ 237734, SwissGrid (LV03)

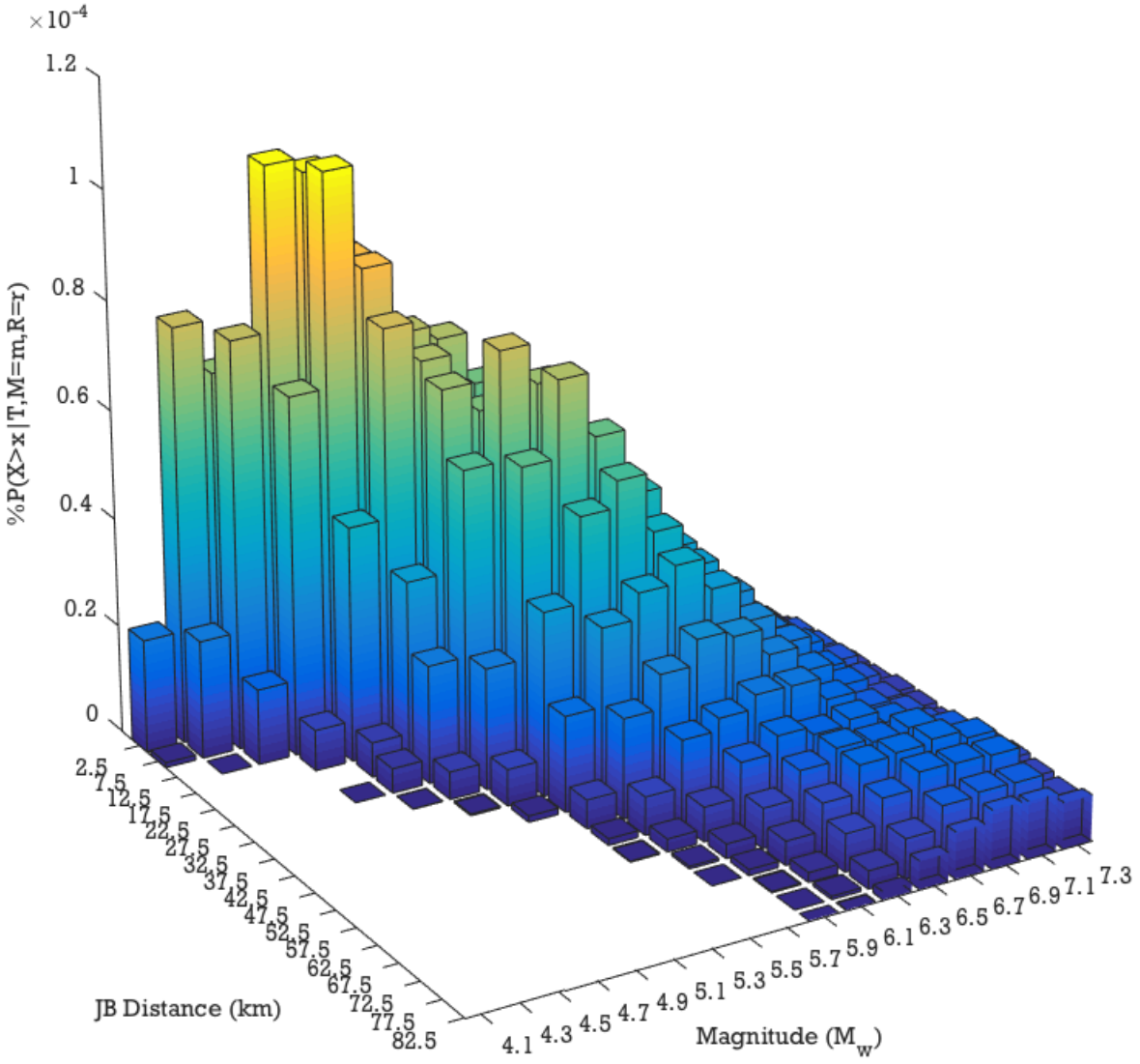


Figure D. 11 Disaggregation plot for PGA with an intensity measure level (IML~0.10g) corresponding to a mean return period (RP) of 2475 yrs (i.e. EP50 of 2%). The controlling scenario of the IML is defined by 4.7Mw and R=7.5km. Data: Wiemer et al. 2016. Location: deepest point of central basin; 687196/ 237734, SwissGrid (LV03)

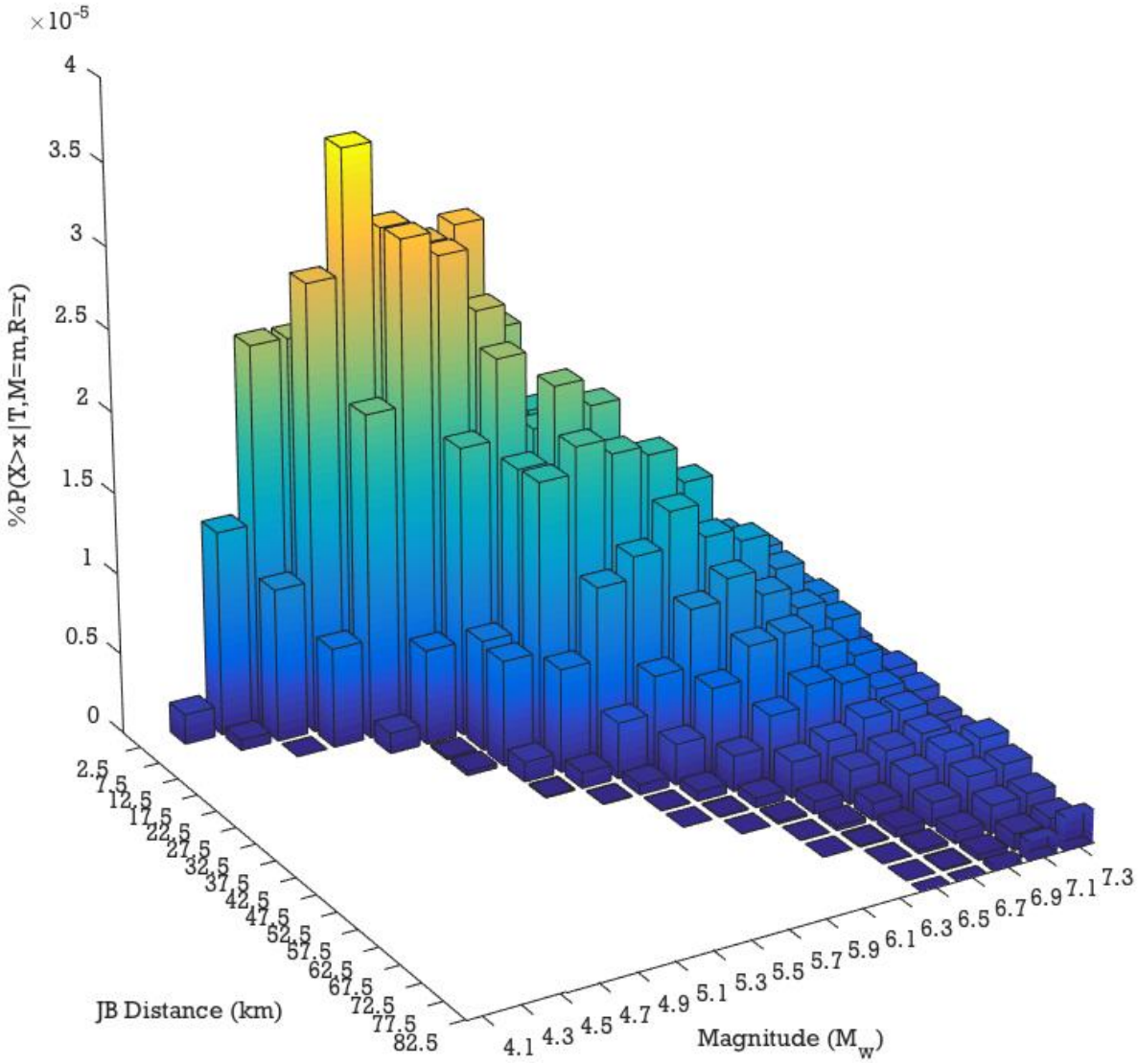


Figure D. 12 Disaggregation plot for PGA with an intensity measure level (IML~0.19g) corresponding to a mean return period (RP) of 9975 yrs (i.e. EP50 of 0.5%). The controlling scenario of the IML is defined by 5.1Mw and R=7.5km. Data: Wiemer et al. 2016. Location: deepest point of central basin; 687196/ 237734, SwissGrid (LV03)

References

Kramer SL (1996) Geotechnical Earthquake Engineering. Prentice-Hall, Upper Saddle River

Strasser M and Anselmetti FS (2008) Mass-movement event stratigraphy in Lake Zurich; A record of varying seismic and environmental impacts. Beiträge zur Geologie der Schweiz 95:23–41.

Strupler M, Hilbe M, Anselmetti FS, Kopf AJ, Fleischmann T and Strasser M (2017) Probabilistic stability evaluation and seismic triggering scenarios of submerged slopes in Lake Zurich (Switzerland). Geo-Marine Letters 37:241–258. doi: 10.1007/s00367-017-0492-8

Appendix E

Supplementary material chapter 5

E1 Back-analysed scenario Oberrieden ~2210 cal. yr BP landslide and tsunami

Landslide mobility analysis

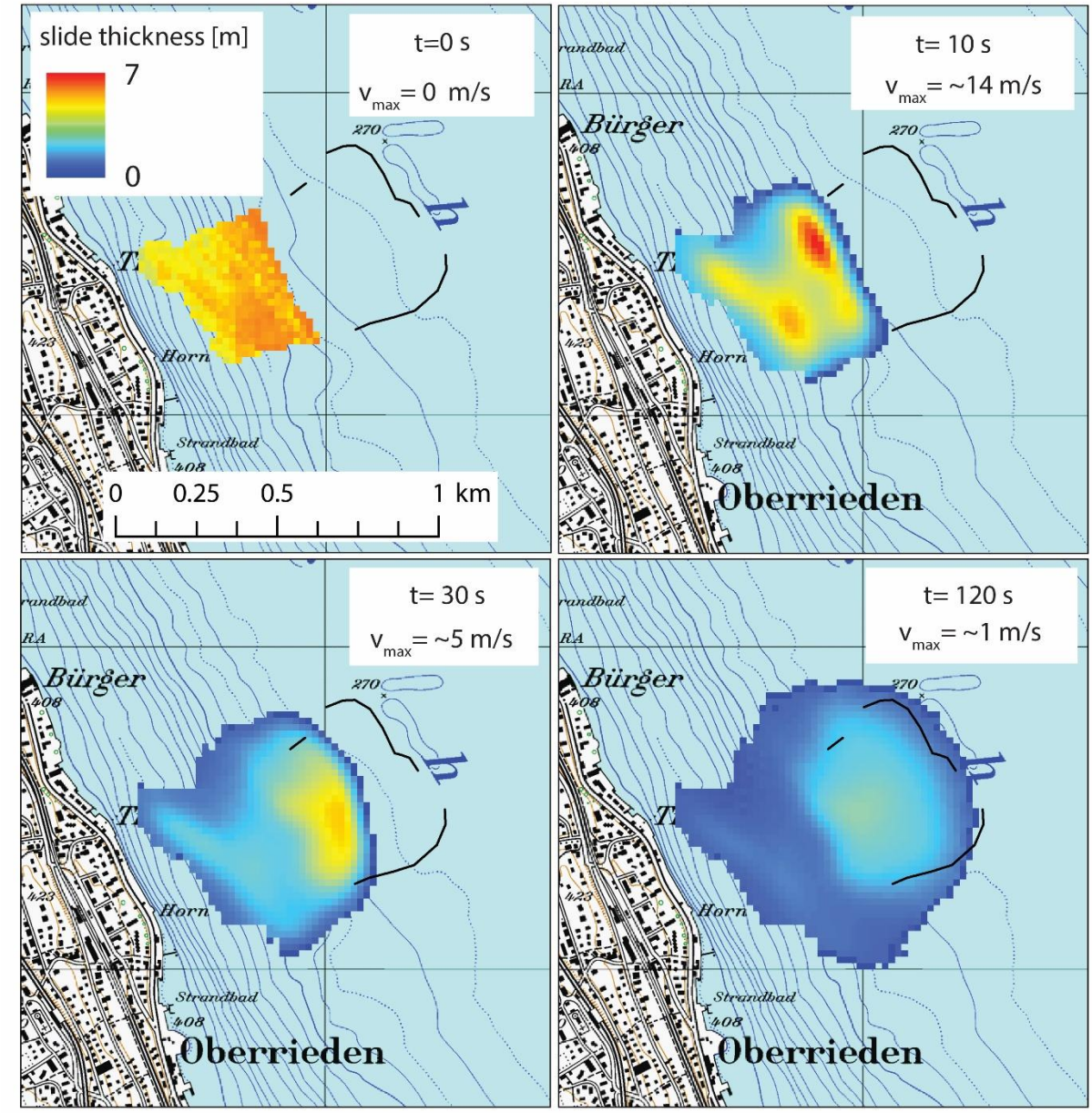


Figure E. 1 Modelled mass-movement at different time steps for the Oberrieden ~2210 cal. yr BP slide. Black dashed line indicates the extent of the deposit, mapped on the high-resolution digital depth model (Strupler et al. 2015).

Back-analysed potential tsunami caused by the ~2210 cal. yr BP Oberrieden landslide

Wave amplitudes on the free lake surface as a function of time after the Oberrieden ~2210 cal. yr BP slide are shown in Fig. E.2. The maximum trough (-1.3 m) appears at the location of Oberrieden, immediately behind the slide, ~15 sec after the initiation of the landslide. The first wave reaches the opposite shore at Herrliberg harbour (~2 km apart; Fig. 1 in manuscript) ~1 min after the slide initiation, with a peak amplitude of ~0.5 m. The period T of the wave (i.e. time between the passing of two wave crests; Ward 2011) is ~1 min. The wave first arrives offshore the present-day location 'Buerkliplatz' after ~10 min, with a height of only a few cm (Gauge 7; Table 1 in manuscript and Figure E.2). At the southern end of the basin, the peak wave amplitude is only a few mm. The ~2210 cal.yr BP Oberrieden slide does not cause any considerable inundated areas, only affecting some single pixels along the shoreline with a maximum flow depth of a few dm.

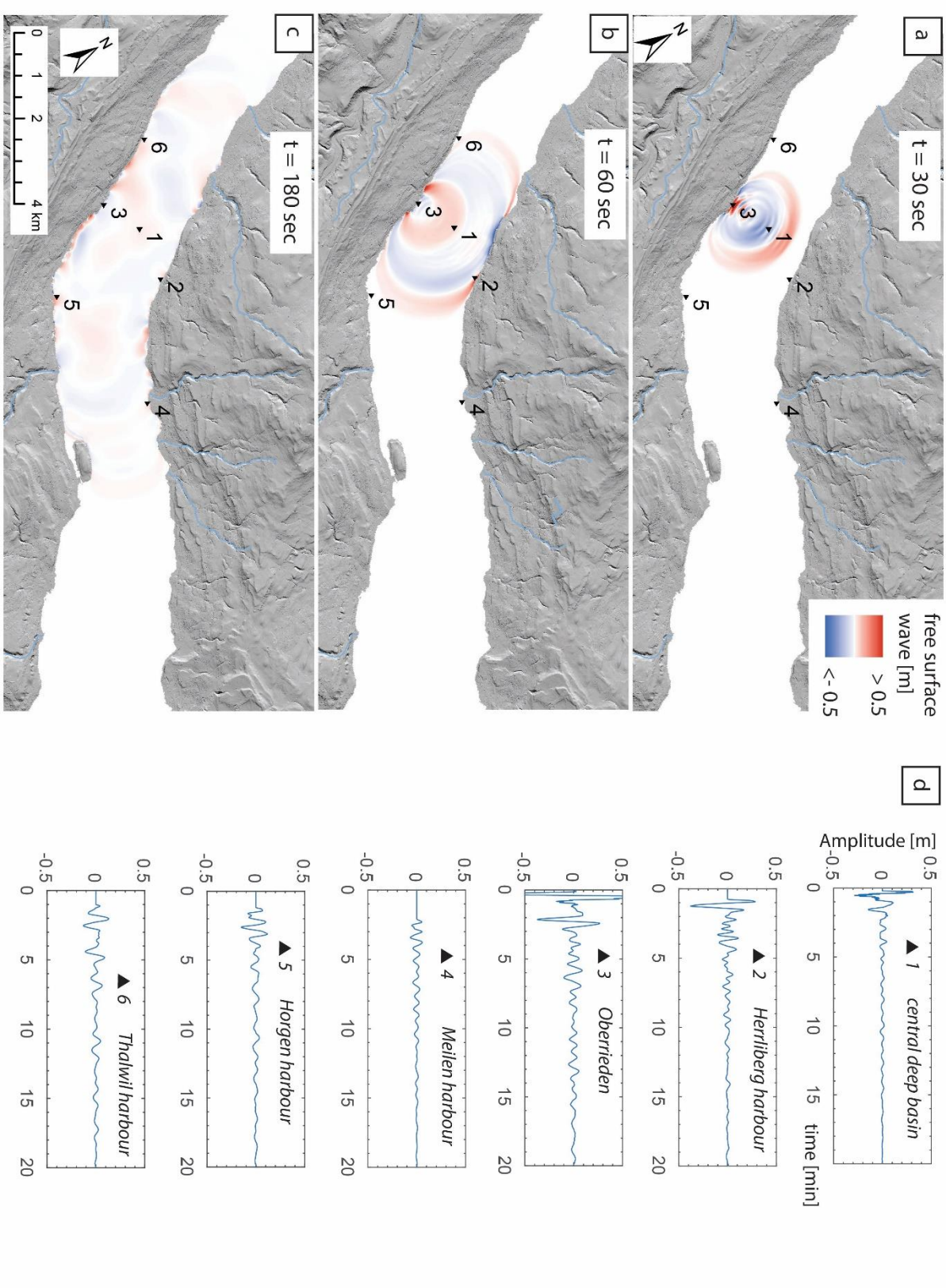


Figure E. 2 Peak wave amplitude at different time steps for a free surface wave induced by the ~2210 cal. yr. BP Oberrieden event. a) t=30 sec, b) t=60 sec, c) t=180 sec d) Time series of wave amplitudes for the Oberrieden ~2210 cal. yr. BP event at the different gauges.

E2 Gauge plots

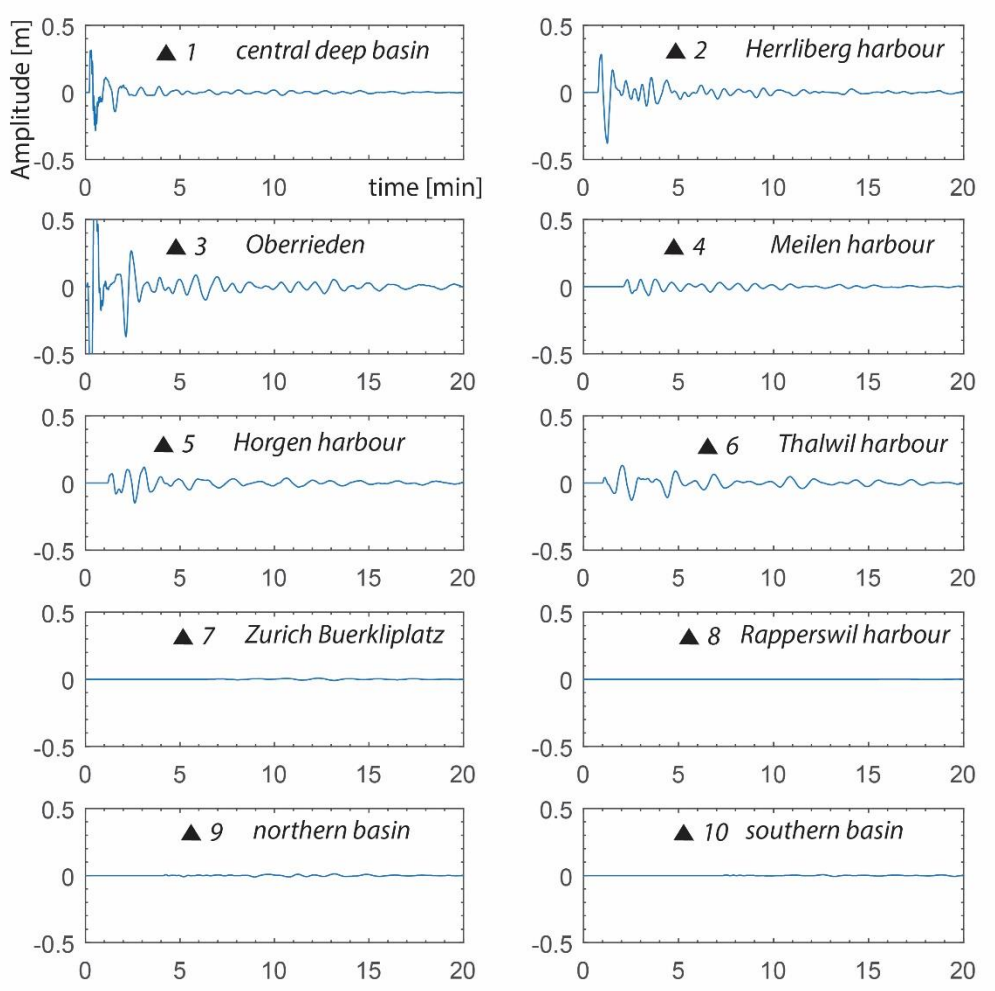


Figure E. 3 Gauge plots for a potential tsunami caused by the Oberrieden ~2210 cal. yr. BP slide

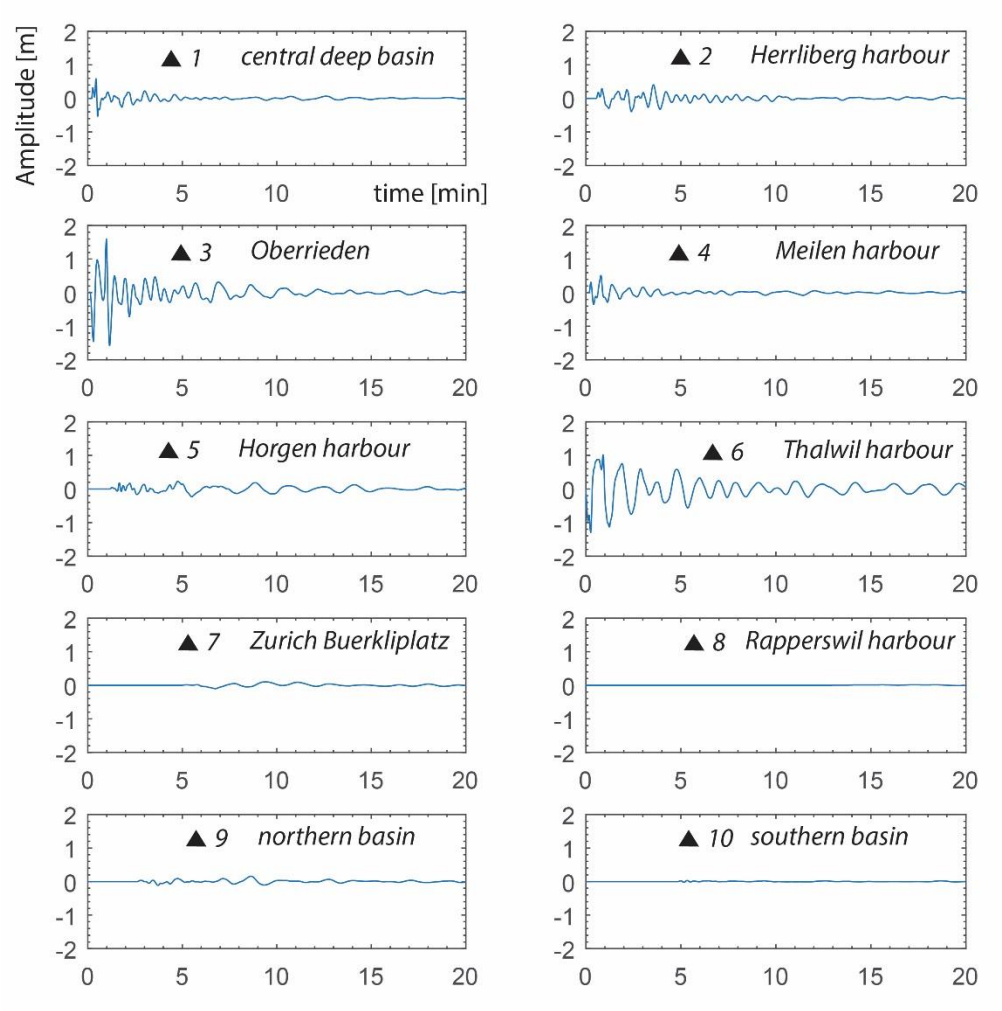


Figure E. 4 Gauge plots for a potential tsunami caused by a coeval occurrence of all ~2210 cal. yr. BP slides

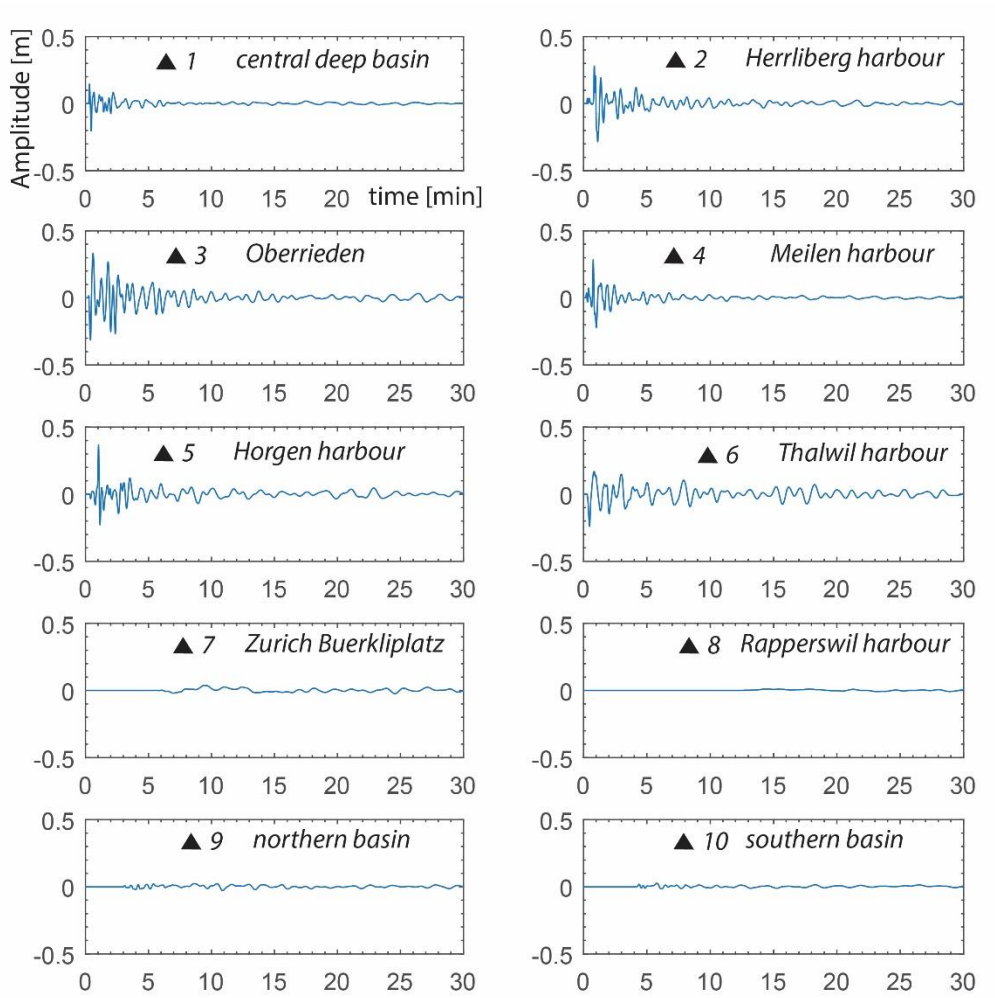


Figure E. 5 Gauge plots for a hypothetical tsunami caused by an earthquake with an exceedance period of 10% in 50 yrs (i.e. mean return period of 475 yrs)

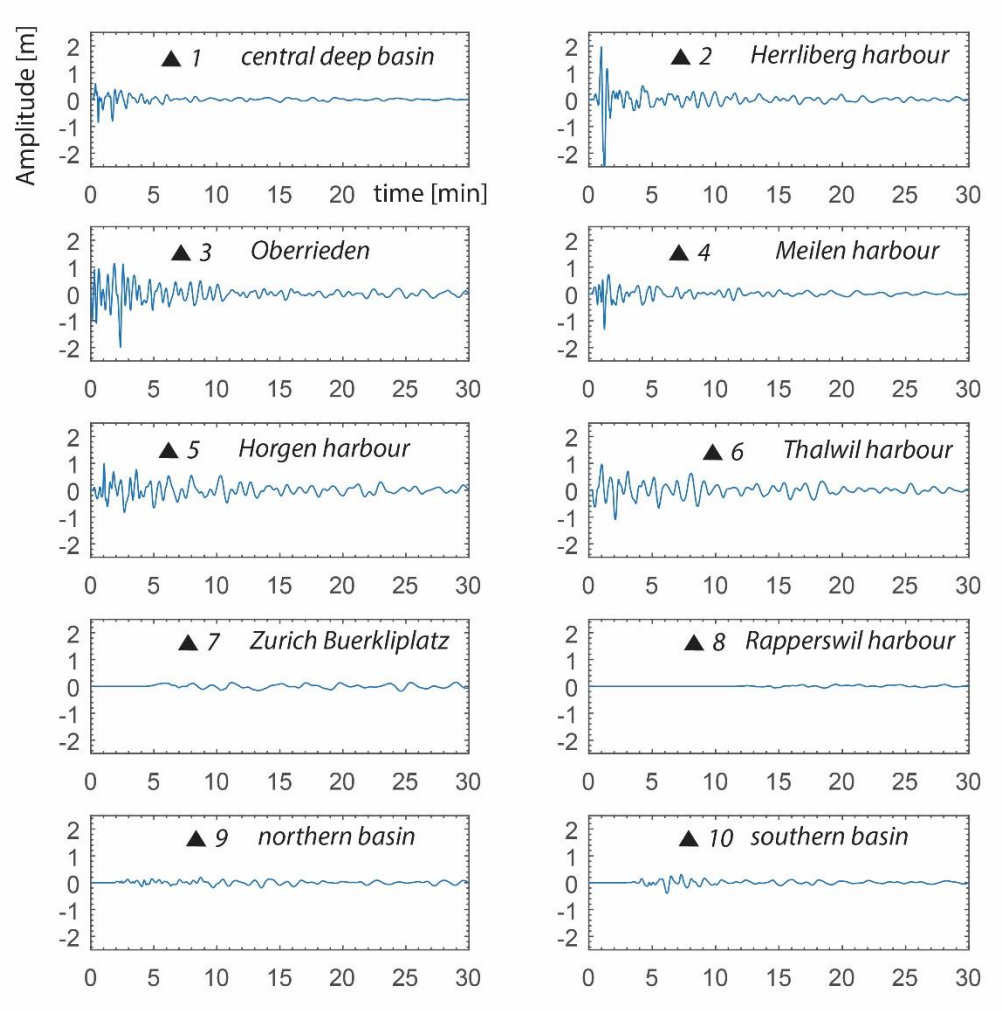


Figure E. 6 Gauge plots for a hypothetical tsunami caused by an earthquake with an exceedance period of 2% in 50 yrs (i.e. mean return period of 2475 yrs)

CURRICULUM VITAE

Michael M.Strupler

Date of Birth	22.02.1985
Place of Birth	Winterthur, Switzerland
Nationality	Swiss citizen

Jan. 2014 – Jun. 2017	**Doctoral studies** at the Geological Institute and Swiss Earthquake Service at ETH Zurich: «Basin-wide assessment of the earthquake-triggered landslide- and tsunami hazard: A conceptual approach and its application, tested in perialpine Lake Zurich (Switzerland)» Supervisors: Prof. M. Strasser, Prof. S. Wiemer, and Prof. F.S. Anselmetti
May 2012 – Dec. 2012	Work at Renard Centre of Marine Geology, Ghent University, Ghent, Belgium
2010 –2012	**Master of science (MSc) studies in physical geography** in the Glaciology, Geomorphodynamics, Geochronology group of the University of Zurich, Switzerland. Minor in Earth sciences (ETH Zurich, Switzerland) MSc Thesis: «Mapping and interpreting subaquatic moraines in Lake Lucerne» Supervision: Prof. F. Anselmetti (EAWAG), Prof. W. Haeberli (University of Zurich)
Jul. 2009 – Sep. 2009	**Traineeship Remote Sensing / GIS** with IAESTE (International Association for the Exchange of Students for Technical Experience) at the Institute of Informatics and Remote Sensing, Mongolian Academy of Sciences, Ulaanbaatar, Mongolia. *Radar backscatter analysis and satellite-image land cover analysis*
2006 –2009	**Bachelor of science (BSc) studies in geography** at the University of Zurich, Switzerland. Minors in Physics (University of Zurich) and Atmosphere and Climate (ETH Zürich), Switzerland BSc Thesis: «Erstellung und Anwendung von Digitalen Höhenmodellen für die Analyse von topographischen Veränderungen in steilem und alpinem Gelände». Supervisor: Dr. Luzia Fischer (University of Zurich)
1998 - 2005	Kantonsschule Zürcher Unterland (Latin), Bülach, Switzerland
1992 - 1998	Primary School, Seuzach / Bachenbülach, Switzerland